The role of infectious bronchitis virus accessory proteins 3a, 3b and 4b

Thesis submitted in accordance with the requirements of the University of Liverpool for the degree of Doctor of Philosophy by Mr Ross Howden Hall

September 2017

Abstract

The role of infectious bronchitis virus accessory proteins 3a, 3b and 4b

Mr Ross Howden Hall

Infectious bronchitis (IB) is a respiratory disease in domestic fowl caused by the gammacoronavirus infectious bronchitis virus (IBV). Current approaches to combat this disease are hindered due to vaccines unable to cross-protect against the many different strains of IBV. To develop novel therapies or more cross-protective vaccines, a better understanding of IBV molecular biology is required. IBV is known to express four accessory proteins, 3a, 3b, 5a, and 5b, as well as a sub-genomic RNA that has the potential to code for an additional 11 kDa protein, referred to as 4b. The role of this sub-genomic RNA is not known, as is whether this transcript is translated during infection. IBV accessory proteins are dispensable for replication and are thought to play a role in virulence or pathogenicity. The functions of 3a and 3b are unknown, although they have been shown to play a part in the interferon response in a yet unknown manner. Using *in vitro* assays and mass spectrometry, the mechanism of action of 3a on the interferon response was determined. IBV 3a inhibits and stimulates interferon expression in a dose-dependent manner by regulating the turnover of interferon signalling proteins, MAVS and IRF7. Flow cytometry has identified a role for IBV 3b in inducing apoptosis during infection, possibly by interacting with apoptotic proteins VDAC2 or BAG6. Lastly, using an antibody raised against the predicted 4b peptide sequence, 4b was detected during infection, confirming it as the fifth IBV accessory protein. Furthermore, mass spectrometry was utilised to identify a role for 4b in regulating cellular translation and the stress granule response. Accessory proteins are highly conserved in the many different strains of IBV and are usually pathogenicity factors making them potential targets for novel therapies. Researching the role of these accessory proteins is essential to understand how IBV causes IB and for the development of more targeted therapies
or more cross-protective vaccines.

Acknowledgements

First and foremost, I would like to thank my PhD supervisors, Dr Helena Maier and Prof. Julian Hiscox for allowing me to undertake this research. To Helena, I will be forever grateful for your time, patience and guidance that you have shown me over the past four years. I could not imagine having a more understanding and supportive supervisor. I would also like to thank the people in the Avian Endemic Virus group that have guided me through the highs and lows of doing a PhD, with a special thank you to Dr Erica Bickerton, Sarah Keep and Phoebe Stevenson-Leggett, it has truly been a pleasure to feel part of the lab family. I would also like to thank Weining Wu and Stuart Armstrong for their help with the complicated field of mass spectrometry. I would also like to reserve a special thank you to my friends, who never doubted I could become a doctor, even if I did. Finally, I would like to thank my mum and dad, who have strived to give me every opportunity to excel and succeed, thank you.

Declaration

I declare this is my own work and the use of all material from other sources has been properly and fully acknowledged.

Table of Contents

Abstract 1

Acknowledgements 2

Declaration 3

Table of Contents 4

List of Figures 11

List of Tables 14

Abbreviations 17

Publications 24

1. Introduction 26

1.1 Infectious Bronchitis Disease 26

1.2 Infectious Bronchitis Virus 26

1.3 Coronavirus Replication 30

1.3.1 Attachment and Entry 30

1.3.2 Replication, Transcription and Translation 31

1.3.3 Coronavirus-induced membrane rearrangement 36

1.3.4 Assembly and Budding 38

1.4 Structural Proteins 39

1.4.1 Membrane (M) 40

1.4.2 Envelope (E) 40

1.4.3 Nucleocapsid (N) 41

1.4.4 Spike (S) 42

1.5 Non-structural Proteins 43
1.6 Accessory proteins from other Coronaviruses 45
1.6.1 Alphacoronaviruses 45
1.6.2 Betacoronaviruses 47
1.6.3 Gammacoronaviruses 48
1.6.4 Deltacoronaviruses 49
1.7 IBV Accessory Proteins 51
1.7.1 Gene 3 accessory proteins 52
1.7.2 Transcript 4b 54
1.7.3 Gene 5 accessory proteins 55
1.8 Coronavirus–Host Interaction 55
1.8.1 Interferon response to viral infection 55
1.8.2 Viruses and the interferon response 58
1.8.3 Stress Granule pathway 61
1.8.4 Viruses and the stress granule pathway 62
1.8.5 Apoptosis 66
1.8.6 Viruses and Apoptosis 67
1.9 Aims 70
Objective 1 70
Objective 2 70
Objective 3 70
Objective 4 70
2. Materials and Methods 71
2.1 Cells and Media 71
2.1.1 Baby Hamster Kidney 21 (BHK-21) cells 71

2.1.2 Chicken Kidney (CK) cells....71
2.1.3 DF-1 Cells....71
2.1.4 Human embryonic kidney 293T (HEK-293T) Cells....72
2.1.5 Vero cells....72
2.1.6 Cell Media....72
2.2 Virological methods....74
2.2.1 Viruses....74
2.2.2 IBV titration....75
2.2.3 Growth curves....76
2.3 Reagents....77
2.3.1 Expression vectors....77
2.3.2 Antibodies....78
2.4 Cloning....81
2.4.1 Primers and DNA fragments....81
2.4.2 Reverse transcription....83
2.4.3 Polymerase chain reaction....84
2.4.4 Site-directed mutagenesis....85
2.4.5 Agarose gel electrophoresis....86
2.4.6 Restriction digest....87
2.4.7 Gel extraction/ PCR purification....87
2.4.8 PCR purification....88
2.4.9 DNA dephosphorylation....88
2.4.10 Ligation....88
2.4.11 Transformation....89
2.4.12 DNA miniprep....89
2.4.13 DNA maxiprep....90

2.4.14 Sequencing 90
2.5 Transfection 92
2.6 Western blotting 93
2.6.1 Proteasome inhibitor 93
2.6.2 Cell lysis 93
2.6.3 SDS-PAGE 94
2.6.4 Western Blotting 95
2.7 Indirect Immunofluorescence 96
2.7.1 Fixation 96
2.7.2 Labelling 96
2.7.3 Image Analysis 97
2.8 Immunoprecipitation 98
2.8.1 Cell lysis 98
2.8.2 Immunoprecipitation (IBV 4b) 99
2.9 Reverse genetics system 100
2.9.1 pGPT vectors 100
2.9.2 Transfection and infection 101
2.9.3 Transient dominant selection 101
2.9.4 BHK stocks 102
2.9.5 Ministocks 103
2.9.6 Purification and DNA extraction 105
2.9.7 Recombinant IBV rescue 107
2.10 Liquid Chromatography-Mass Spectrometry/Mass Spectrometry 109
2.10.1 Transfection 109
2.10.2 GFP capture 109
2.10.3 LC-MS/MS 110

2.10.4 Analysis 111
2.11 Interferon methods 113
2.11.1 Interferon luciferase reporter assay 113
2.11.2 Chicken interferon MxA reporter assay 114
2.12 Apoptosis methods 116
2.12.1 Caspase 3/7 activity assay 116
2.12.2 Annexin-V-FITC FACS assay 116
2.13 Stress granule methods 118
2.13.1 SG induction 118
2.13.2 Cellular translation rate 118
2.14 Bioinformatics analysis 119
2.14.1 Sequence Alignment 119
2.14.2 Eukaryotic Linear Motif Search 119

3. The role of accessory protein 3a 120

3.1. Introduction 120
Results 121
3.2. Generation of GFP-tagged 3a expression vectors 121
3.3. Testing anti-3a (JH3480) 124
3.4. Characterisation of IBV 3a effect on IFNβ expression 126
3.4.1. IBV 3a both inhibits and stimulates IFNβ expression 126
3.4.2. IBV 3a from Beau-R and M41 have the same effect on IFNβ expression 130
3.5. Mass spectrometry analysis of GFP-3aM IPs 133
3.6. IBV 3a interaction with RNF5 and CAND1 144
3.7. Characterisation of IBV 3a interaction with MAVS 146
3.7.1. IBV 3a increases levels of MAVS 146

3.7.2. IBV 3a localises with MAVS 147
3.7.3. IBV 3a agonises IFNβ expression by interfering with MAVS 150
3.8. Characterisation of IBV 3a interaction with IRF3/IRF7 153
3.8.1. IBV 3a degrades IRF3/7 153
3.8.2. IBV 3a colocalises with IRF7 156
3.9. Effect of 3a levels on IFNβ during infection 158
3.10. Discussion 161

4. The role of Accessory Protein 3b 171

4.1. Introduction 171
Results 172
4.2. Bioinformatic analysis of 3b 172
4.3. Generation of 3b-GFP expression vectors 176
4.4. Mass spectrometry analysis of 3b-GFP pull-downs 178
4.5. Effect of protein 3b on apoptosis 188
4.5.1. IBV induces apoptosis 188
4.5.2. IBV 3b induces caspase-dependent apoptosis 192
4.6. Discussion 194

5. The role of Accessory Protein 4b 199

5.1. Introduction 199
Results 200
5.2. Bioinformatic analysis of IBV and TCoV 4b 200
5.3. Generation of GFP-tagged 4b expression vectors 208
5.4. Detection of 4b during infection 210
5.4.1. Validation of anti-4b 210
5.4.2. Detection of 4b during M41 infection 213

5.5. Effect of 4b on viral replication 218
5.6. Mass spectrometry analysis of GFP-tagged 4b Co-IPs 219
5.7. IBV 4b interaction with RPS25 and LAP2 232
5.8. Effect of 4b on stress granule assembly 236
5.9. Effect of 4b on cellular translation 241
5.10. Role of RVxF and SILK on 4b function 242
5.11. Discussion 245

6. Discussion 256

6.1. Accessory protein 3a 256
6.2. Accessory protein 3b 258
6.3. Accessory protein 4b 259
6.4. IBV accessory proteins 261
6.5. Implications for vaccine design and novel therapies 265

7. Appendix 267

8. References 298

List of Figures

Figure 1.1 Schematic diagram of the IBV genome/ virion, and an electron micrograph of IBV. 29

Figure 1.2 Schematic diagram of the lifecycle of IBV. 34

Figure 1.3 Schematic diagram of IBV transcription. 36

Figure 1.4 Schematic diagram of IBV-induced membrane rearrangement. 38

Figure 1.5 Schematic diagram of the interferon signalling cascade in chickens. 58

Figure 1.6 Schematic diagram of the stress granule pathway. 65

Figure 1.7 Schematic diagram of the intrinsic apoptosis pathway. 69

Figure 2.1 Schematic diagram of the M41-K reverse genetics system 105

Figure 3.1 Plasmid map and confirmation of expression of the GFP-tagged 3a expression vectors. 123

Figure 3.2 Anti-3a can label both 3aB and 3aM 125

Figure 3.3 IBV 3a protein induces and inhibits IFNβ expression in a dose-dependent manner. 130

Figure 3.4 IBV 3a from M41-CK and Beau-R have the same effect on IFNβ signalling. 132

Figure 3.5 Confirmation of GFP-3aM transfection and IP. 133

Figure 3.6 Scatter plot representing results from the GFP-3aM co-IP. 141

Figure 3.7 GO cellular component annotations of cellular proteins that interact with GFP-3aM. 143

Figure 3.8 IBV 3a partially colocalises with RNF5 and CAND1. 145

Figure 3.9 IBV 3a increases levels of MAVS. 147

Figure 3.10 IBV 3a localises with MAVS..... 149

Figure 3.11 IBV 3a agonises IFNβ expression by interfering with MAVS, only after stimulation with poly(I:C). 152

Figure 3.12 IBV 3a induces degradation of IRF7 in a dose-dependent, proteasome-dependent manner. 155

Figure 3.13 IBV 3a colocalises with IRF7. 157

Figure 3.14 IBV 3a induces IFNβ expression during infection, coinciding with a decrease in 3a levels..... 160

Figure 3.15 Proposed model for the mechanism of action of IBV 3a on IFNβ expression. 170

Figure 4.1 Sequence alignment and sequence identity of 3b isoforms. 173

Figure 4.2 Expression maps and confirmation of expression of GFP-tagged 3b vectors..... 177

Figure 4.3 Western blot analysis of 3bM-GFP, GFP-3bM expression and immunoprecipitation. 179

Figure 4.4 Scatter plot representing results from the GFP-3bM co-IP. 183

Figure 4.5 Scatter plot representing results from the 3bM-GFP co-IP. 185

Figure 4.6 IBV 3b induces apoptosis. 191

Figure 4.7 Protein 3b induces caspase-dependent apoptosis. 193

Figure 5.1 Peptide sequence alignment of 4b. 207

Figure 5.2 Plasmid map and confirmation of expression of the GFP-tagged 4b expression vector. 209

Figure 5.3 Anti-4b can detect the presence of GFP-tagged 4bM.....212

Figure 5.4 Anti-4b can label GFP-4bM. 213

Figure 5.5 M41-K expresses an 11 kDa protein known as 4b during infection.216

Figure 5.6 Anti-4b can detect 4b during infection. 217

Figure 5.7 Protein 4b is not required for in vitro viral replication.....218

Figure 5.8 Confirmation of GFP-4bM/4bM-GFP transfection and IP.....220

Figure 5.9 Scatter plot representing results from the GFP-4bM co-IP. 226

Figure 5.10 Scatter plot representing results from the 4bM-GFP co-IP. 228

Figure 5.11 IBV 4b interacts with a higher proportion of ribonucleoproteins....231

Figure 5.12 RPS25 partially colocalises with GFP-tagged 4b. 233

Figure 5.13 LAP2 partially colocalises with GFP-tagged 4b.....234

Figure 5.14 RPS25 interacts with 4b during M41-CK infection.....235

Figure 5.15 IBV induces stress granule assembly.....238

Figure 5.16 IBV 4b induces and colocalises with stress granules. 239

Figure 5.17 GFP-4bM does not colocalise or inhibit sodium arsenite-induced stress granules.....240

Figure 5.18 IBV 4b increases cellular translation. 242

Figure 5.19 Protein 4b effect on cellular translation is dependent on SILK and/or RVxF.....244

Figure 7.1 IBV 3b induces apoptosis.....282

List of Tables

Table 1.1 Viruses within the coronavirinae subfamily 28

Table 1.2 Summary of non-structural protein (nsp) functions 44

Table 1.3 The role of coronavirinae accessory proteins 50

Table 2.1 GMEM for BHK-21 cell culture 72

Table 2.2 1x CK cell maintenance media (1x BES) 73

Table 2.3 CK cell maintenance media (2x BES) for IBV plaque assays 73

Table 2.4 List of plasmids used for immunofluorescence, western blot and mass spectrometry. 77

Table 2.5 Primary antibodies used for immunofluorescence and western blot. . 78

Table 2.6 Primers and DNA fragments for accessory protein expression plasmids. 81

Table 2.7 Reagent mix for first strand cDNA synthesis (I) 83

Table 2.8 Reagent mix for first strand cDNA synthesis (II) 83

Table 2.9 Reverse transcription thermal cycle 84

Table 2.10 Reagent concentrations for PCR 84

Table 2.11 PCR thermal cycle 85

Table 2.12 Reagent concentrations for SDM 85

Table 2.13 SDM thermal cycle 86

Table 2.14 Recipe for DNA loading buffer 87

Table 2.15 Reagent mix for ligation 88

Table 2.16 Reagent concentrations for Lysogeny broth 89

Table 2.17 Primers used for sequencing of expression vectors and IBV cDNA. 91

Table 2.18 Reagent composition of RIPA lysis buffer 94

Table 2.19 SDS Running Buffer..... 94

Table 2.20 Reagent composition of Pierce lysis buffer 98

Table 2.21 Reagent composition of RNA RIPA buffer 99

Table 2.22 Reagent composition of IP wash buffer..... 99

Table 2.23 DNA fragments and primers for the synthesis of pGPT expression vectors..... 100

Table 2.24 MXH selection media for TDS..... 102

Table 2.25 Recipe for TE buffer 107

Table 2.26 Recipe for proteinase K buffer (2x) 107

Table 2.27 Co-IP lysis buffer..... 109

Table 2.28 1x Dilution buffer 110

Table 3.1 Cellular proteins identified my LC-MS/MS that significantly interact with GFP-3aM..... 135

Table 4.1 Eukaryotic linear motifs (ELM) identified in the 3b peptide sequence. 175

Table 4.2 Cellular proteins that significantly interact with GFP-3bM 181

Table 4.3 Function and localisation of proteins classified as significant interacting partners for GFP-3bM 187

Table 5.1 Bioinformatic analysis of the ORF4b predicted peptide sequence in IBV/TCoV strains..... 202

Table 5.2 Eukaryotic linear motifs identified in 4b (M41) peptide sequence. ... 203

Table 5.3 Cellular proteins identified by LC-MS/MS that significantly interact with GFP-4bM.....222

Table 5.4 Cellular proteins detected by LC-MS/MS that significantly interact with 4bM-GFP. 223

Table 5.5 Function and localisation of proteins classified as significant that interact with GFP-4bM and/or 4bM-GFP. 229

Table 7.1 Cellular proteins identified my LC-MS/MS that significantly interact with GFP-3aM.....267

Table 7.2 Panther GO Cellular component of GFP-3aM interacting partner....276

Table 7.3 Cellular proteins that have a higher chance of interacting with GFP-3bM 277

Table 7.4 Cellular proteins that have a higher chance of interacting with 3bM-GFP 280

Table 7.5 Cellular proteins identified by LC-MS/MS that interact with 4bM-GFP 283

Table 7.6 Cellular proteins identified by LC-MS/MS that interact with GFP-4bM. 290

Abbreviations

+ssRNA – Postive-Sense Single-Stranded RNA

AIF – Apoptosis-Inducing Factor

Apaf-1 – Apoptotic Protease Activating Factor 1

ATP – Adenosine Triphosphate

Bad – Bcl-2 Lymphoma 2

Bak – Bcl-2 Homologous Antagonist Killer

Bax – Bcl-2-Associated X protein

BcL-X_L – B-cell Lymphoma-Extra Large

Beau-CK – Beaudette-CK

Beau-R – Beaudette Recombinant

BeCoV – Beluga whale coronavirus SW1

Bcl-2 – B-cell Lymphoma 2

BCoV – Bovine Coronavirus

BES – N, N-Bis(2-hydroxyethyl)-2-Aminoethanesulfonic Acid

BSA – Bovine Serum Albumin

BuCoV – Bulbul Coronavirus

C – Cytosine

CAND1 – Cullin-Associated NEDD8-Dissociated protein 1

CCoV – Canine Coronavirus

cDNA – Complementary DNA

CK Cells – Chicken Kidney Cells

CoV – Coronavirus

CpG – 5′-C-Phosphate-G-3′

CUL1 – Cullin 1

DAPI – 4’,6-Diamidino-2-Phenylindole

DMEM – Dulbecco’s Minimum Essential Medium

DMSO – Dimethyl Sulfoxide

DMV – Double Membrane Vesicle

DNA – Deoxyribonucleic Acid

dNTP – Deoxyribonucleotide

dsDNA – Double-Stranded DNA

dsRNA – Double-Stranded RNA

E – Viral Envelope Protein

E.coli – Escherichia coli

EDTA – Ethylenediaminetetraacetic Acid

eGFP – Enhanced Green Fluorescent Protein

EMEM – Eagle’s Minimum Essential Medium

eIF2α – Eukaryotic Translation Initiation Factor 2α

eIF2B – Eukaryotic Translation Initiation Factor 2B

EndoG – Endonuclease G

EBV – Epstein-Barr Virus

ER – Endoplasmic Reticulum

ER-GIC – Endoplasmic Reticulum-Golgi Intermediate Compartment

FCS – Foetal Calf Serum

FIPV – Feline Infectious Peritonitis Virus

FITC – Fluorescein Isothiocyanate

FPV – Fowlpox Virus

G3BP1 – Ras GTPase-activating protein-Binding Protein 1

G – Guanine

GCN2 – General Control Non-Derepressible 2

GFP – Green Fluorescent Protein

GO – Gene ontology

Gp78 – Glycoprotein 78

GPT – Guanine-xanthine Phosphoribosyltransferase

HBV – Hepatitis B Virus

HCV – Hepatitis C Virus

HCoV – Human Coronavirus

HIV – Human Immunodeficiency Virus

H.p.i – Hours Post Infection

HRI – Heme-Regulated eIF2α Kinase

IAV – Influenza A Virus

IB – Infectious Bronchitis

IBDV – Infectious Bursal Disease Virus

IBV – Infectious Bronchitis Virus

IFN – Interferon

IFNAR – Interferon Receptor

IFNα – Interferon-alpha

IFNβ – Interferon-beta

IM – Inner Mitochondrial Membrane

IR – Intergenic Region

IRES – Internal Ribosomal Entry Site

IRF 3/7 – Interferon Regulatory Factor 3/7

ISG – Interferon Stimulated Gene

JAK – Janus kinase

Kb – Kilobases

kDa – Kilodaltons

KPNA2 – Karyopherin Alpha 2

KSHV - Kaposi's Sarcoma-associated Herpesvirus

LB – Luria Broth

LC-MS/MS – Liquid Chromatography-Mass Spectrometry/Mass Spectrometry

LPS – Lipopolysaccharide

M41 – Massachusetts 41

M – Viral M Protein

MAM – Mitochondrial-Associated Membrane

MAVS – Mitochondrial Antiviral Signalling Protein

MDA-5 – Melanoma Differentiation-Associated Protein 5

MEM – Minimum Essential Medium

MERS-CoV – Middle East Respiratory Syndrome Coronavirus

MHV – Mouse Hepatitis Virus

MMP – Mitochondrial Membrane Permeabilisation

MOI – Multiplicity of Infection

MPA – Mycophenolic Acid

mRNA – Messenger RNA

MS – Mass spectrometry

MunCoV – Munia Coronavirus

N – Viral Nucleocapsid Protein

Nemo – NF-kappa-B Essential Modulator

NF-κB – Nuclear Factor - kappa B

NS1 – Influenza A Virus Non-Structural Protein 1

Nsp – Non-structural protein

OM – Outer Mitochondrial Membrane

ORF – Open Reading Frame

PABP – Poly-A Binding Protein

PAMP – Pathogen-Associated Molecular Pattern

P-Body – Processing-Body

PBSa – Phosphate Buffered Saline a

PCR – Polymerase Chain Reaction

PEDV – Porcine Epidemic Diarrhoea Virus

PDCoV – Porcine Deltacoronavirus

p-eIF2α – Phosphorylated-eIF2α

PERK – Protein Kinase R-Like ER Kinase

PFU – Plaque Forming Unit

PI – Propidium Iodide

PIC – Protease Inhibitor Cocktail

PKR – Protein Kinase R

pp1a/1ab – Polyprotein 1a/1ab

PP1c – Protein Phosphatase 1c

PRRSV – Porcine Respiratory and Reproductive Syndrome Virus

RBD – Receptor Binding Domain

RdRp – RNA-dependent RNA polymerase

rIBV – Recombinant IBV

RIG-I – Retinoic Acid-Inducible Gene I

RLR – RIG-I-Like Receptor

RNA – Ribonucleic Acid

RNF5 – RING Finger Protein 5

RNP – Ribonucleoprotein

ROS – Reactive Oxygen Species

RSV – Respiratory Syncytial Virus

RT – Reverse Transcription

RTC – Replication-Transcription Complex

rVV – Recombinant Vaccinia Virus

S – Viral Spike Protein

SARS-CoV – Severe Acute Respiratory Syndrome Coronavirus

SDS-PAGE – Sodium Dodecyl Sulphate-Polyacrylamide Gel Electrophoresis

SG – Stress Granule

sgRNA – Sub-genomic RNA

STAT1/3/7 – Signal Transducer and Activator of Transcription 1/3/7

TCoV – Turkey Coronavirus

TBK1 – TANK-Binding Kinase 1

TDS – Transient Dominant Selection

TGEV – Transmissible Gastroenteritis Virus

TIA-1 – T-Cell-Restricted Intracellular Antigen-1

TIAR – TIA-1-Related Protein

TLR3/7 – TOLL-Like Receptor 3/7

TNF – Tumour necrosis factor

TRAF3 – TNF Receptor-Associated Factor 3

TRIM25 – Tripartite Motif-Containing Protein 25

TRS – Transcription Regulatory Sequence

TRS-B – TRS-Body

TRS-L – TRS-Leader

UPR – Unfolded Protein Response

UTR – Untranslated Region

VDAC – Voltage-dependent Anion Channel

VLP – Virus-Like Particle

WT – Wild-type

Publications

Paper Publications

Maier HJ, Neuman BW, Bickerton E, et al. Extensive coronavirus-induced membrane rearrangements are not a determinant of pathogenicity. Scientific Reports. 2016;6:27126. doi:10.1038/srep27126.

Infectious bronchitis virus accessory protein 3a interferes with interferon expression by regulating the turn-over of interferon signalling proteins (In progress)

Ross Hall, Julian A. Hiscox, Weining Wu, Selma Rayon, Helena J. Maier

Infectious bronchitis virus accessory protein 4b plays a role in regulating cellular translation (In progress)

Ross Hall, Sarah Keep, Julian A. Hiscox, Erica Bickerton, Stuart Armstrong, Helena J. Maier

Poster Presentations

The role of IBV accessory protein 3a

SGM Conference 2015, Birmingham, UK

The role of IBV accessory protein 3a

Positive-strand RNA virus symposium 2016,

Austin, Texas, US

IBV accessory protein 4b and stress granules

SGM Conference 2017, Edinburgh, UK

Oral Presentations

IBV 3a, dsRNA and innate immunity

SGM 2016, Liverpool, UK

IBV and the role of accessory proteins

COST Meeting 2016, Istanbul, Turkey

The discovery of IBV accessory protein 4b

DTP conference 2017, Oxford, UK

IBV accessory protein 4b and stress granules

Nidovirus Symposium 2017, Kansas City, US

1. Introduction

1.1 Infectious Bronchitis Disease

Infectious bronchitis (IB) is a highly contagious globally endemic disease that infects domestic fowl (*Gallus gallus*). Symptoms of this respiratory disease include snicking, coughing, red eyes, and rales. Infected fowl can also suffer from poor weight gain and lower/poorer egg production (Chen et al. 1996, Cavanagh 2003). Due to these symptoms, the disease causes a significant economic loss to the British poultry industry of around £24 million per year (Defra 2002). The etiological agent, infectious bronchitis virus (IBV), mainly infects the epithelial cells of the respiratory tract but can also infect the epithelial cells of the kidneys; where it can cause nephrotoxicity, as well as the ovaries and oviduct. Current vaccine strategies against IBV rely on the use of live attenuated and inactivated vaccines. These vaccines offer poor cross-protection against the many different strains of IBV and are resource intensive to manufacture. There is thus a growing need to better understand IBV molecular biology to develop more novel therapies (Tomley et al. 1987, Koch et al. 1990).

1.2 Infectious Bronchitis Virus

IBV belongs to the *gammacoronavirinae* genus, of the *coronavirinae* subfamily, in the *Nidovirales* order. The coronavirinae subgroup is split into four genera, alpha-, beta-, gamma- and deltacoronaviruses, summarised in **Table** 1.1. Coronaviruses contain a single-stranded positive-sense RNA genome (+ssRNA), which are among the largest RNA genomes found in viruses. Coronavirus genomes are

around 26 – 32Kb in length and have both a 5′-end methylated cap and 3′-end polyadenylated tail (Masters 2006). The genome of IBV is around 26.7Kb and is currently organised into six regions, expressed as six messenger RNAs (mRNA). Messenger RNA 1 contains two open-reading frames (ORFs); 1a and 1b, which comprises two-thirds of the genome at the 5′-end. ORF 1b overlaps with 1a and is only translated after a -1 ribosomal frameshift (Brierley et al. 1987) (**Figure 1.1A**). Polyproteins 1a (pp1a) and 1ab (pp1ab) are cleaved by two virus-encoded proteases (Lim et al. 1998, Lim et al. 1998) into 15 non-structural proteins (nsps) (Ziebuhr et al. 2000). The 3′-end of the genome encodes the structural and accessory proteins. Four structural mRNAs are expressed from the genome in the order spike (S) – envelope (E) – membrane (M) – nucleocapsid (N) along with two mRNAs that express four known accessory proteins, 3a, 3b, 5a, and 5b. Structural protein E is expressed from the same mRNA as 3a and 3b and is regulated by an internal ribosome entry site (IRES) (Liu et al. 1992). A recently identified transcript, known as mRNA 4b, is expressed from the intergenic region (IR) between M and 5a (Bentley et al. 2013). It is not known whether mRNA 4b is translated during infection. Untranslated regions (UTRs) are present at both the 5′- and 3′-end of the genome and have been shown to be involved in RNA replication and viral translation (Dalton et al. 2001). The viral genome is encapsulated by protein N to form a ribonucleoprotein (RNP). This RNP is in turn encased by a lipid envelope containing the three other structural proteins, S, E and M. A single virion is pleomorphic and approximately 120 nm in diameter (**Figure 1.1B,C**) (Masters 2006). There are many different strains of IBV, amongst

the most studied strains are Beaudette-CK (Beau-CK) and Massachusetts 41-CK (M41-CK). Beau-CK is an apathogenic lab strain that was obtained by serial passage in eggs, while M41-CK is a pathogenic lab strain (Beaudette 1937, Van Roekel 1950, Casais et al. 2003).

Table 1.1 Viruses within the coronavirinae subfamily

Coronavirinae		
Alphacoronavirus	**Betacoronavirus**	**Gammacoronavirus**
Transmissible gastroenteritis coronavirus (TGEV)	**Murine Hepatitis Virus (MHV)**	**Infectious bronchitis virus (IBV)**
Canine coronavirus (CCoV)	Bovine coronavirus (BCoV)	Beluga whale coronavirus SW1 (BeCoV)
Feline coronavirus (FCov)	Human coronavirus HKU1 (HCoV-HKU1)	Turkey coronavirus (TCoV)
Human coronavirus 229E (HCoV-229E)	Human coronavirus OC43 (HCoV-OC43)	**Deltacoronavirus**
Human coronavirus NL63 (HCoV-NL63)	Middle-East Respiratory coronavirus (MERS-CoV)	**Porcine deltacoronavirus (PDCoV)**
Porcine epidemic diarrhoea virus (PEDV)	Severe acute respiratory syndrome coronavirus (SARS-CoV)	Bulbul coronavirus HKU11 (BuCoV)
		Munia coronavirus HKU13 (MunCoV)

Prototype viruses in the respective genera are labelled in bold

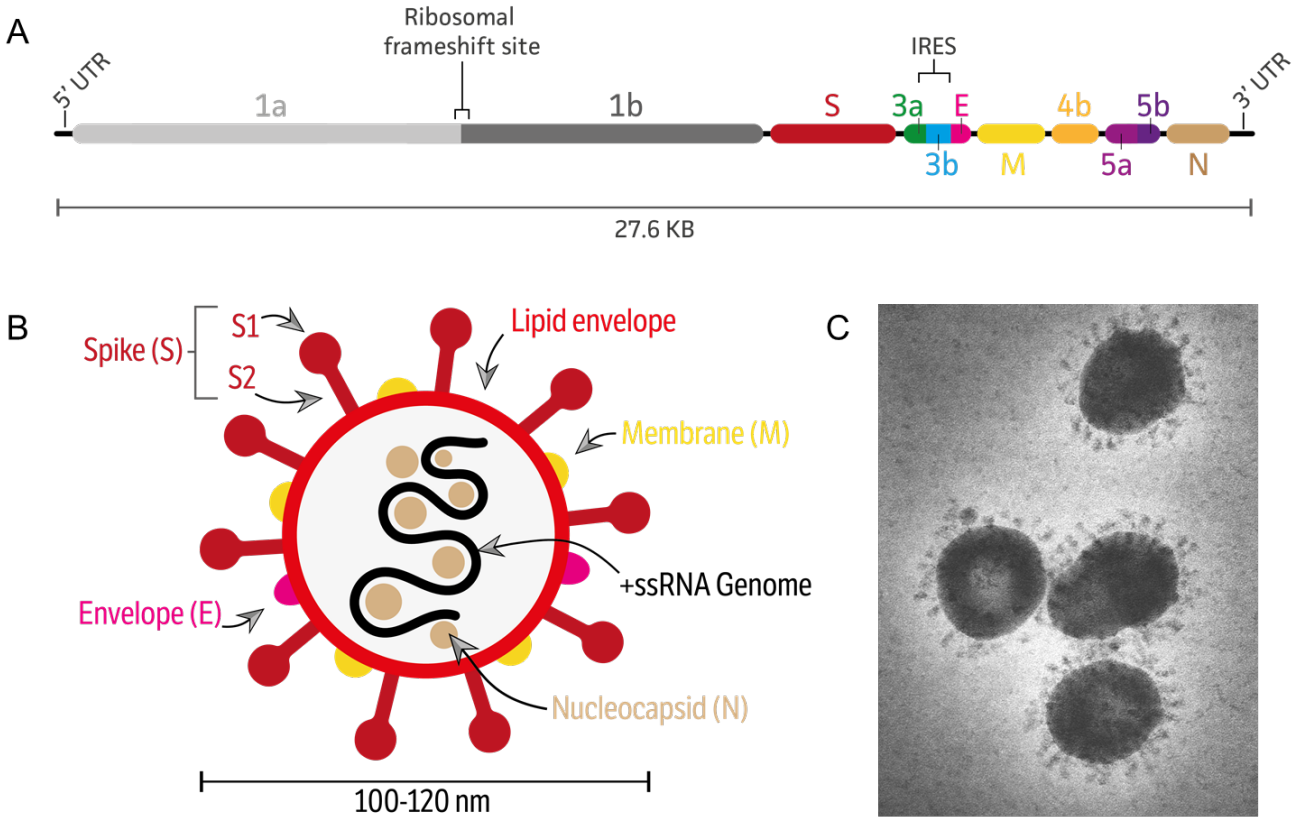

Figure 1.1 Schematic diagram of the IBV genome/ virion, and an electron micrograph of IBV.

(A) IBV genome expresses six mRNAs and one putative mRNA known as 4b and is flanked by untranslated regions at the 5′- and 3'-end. A pseudoknot and slippery sequence are responsible for mediating the -1 frameshift during pp1ab translation, while an IRES mediates translation of E. (B) The IBV lipid envelope contains three structural proteins, spike (S), envelope (E) and membrane (M) and encapsulates the positive-sense single-stranded RNA (+ssRNA) genome bound to nucleocapsid (N) protein. (C) Transmission electron micrograph of IBV virions (Dr Fred Murphy; Sylvia Whitfield, Centers for Disease Control).

1.3 Coronavirus Replication

1.3.1 Attachment and Entry

Coronavirus cell entry is mediated by the S protein, a large type I transmembrane protein. The IBV S protein is around 1,160 amino acids and is cleaved by furin, a cellular protease, into two functional domains, S1 and S2 (Yamada et al. 2009). The gammacoronavirus spike protein is cleaved between domains S1 and S2 during assembly but is rarely cleaved in alpha- and beta- coronaviruses (Belouzard et al. 2012). The S1 domain contains the receptor binding domain (RBD) and mediates cell attachment (Promkuntod et al. 2014). IBV attachment and entry into cells is dependent on α-2,3-linked sialic acid, a cell surface molecule (Winter et al. 2006). Due to the ubiquitous nature of sialic acid, it is believed that another unknown cell receptor is required for cell entry, as IBV has restricted cellular tropism (Schultze et al. 1992, Winter et al. 2006). IBV may enter the cell by clathrin-mediated endocytosis, although alternative mechanisms have not been disproved (Yamada et al. 2009) (**Figure 1.2A**). The mechanism of coronavirus cell entry and fusion differs between coronaviruses and strains (Belouzard et al. 2012). In the case of IBV, fusion is pH dependent. After endocytosis, IBV-cellular fusion is initiated by an acidic environment, which causes a conformational change in the S protein, exposing the class I viral fusion peptide residing in the S2 domain. The coronavirus fusion peptide is inserted into vesicle membranes and mediates fusion with the viral lipid envelope (Bosch et al. 2003). Fusion releases the ribonucleoprotein (RNP) and thus the viral genome into the cytoplasm (**Figure 1.2B**).

1.3.2 Replication, Transcription and Translation

After entry of the RNP into the cell cytoplasm, ORF1a and ORF1ab are translated by host-cellular machinery into pp1a and pp1ab. Translation of pp1ab occurs after a -1 frameshift (Brierley et al. 1989). The -1 ribosomal frameshift occurs when the ribosome encounters a slippery site sequence in the coronavirus RNA. This site induces ribosomal and mRNA unpairing and then repairing but in the -1 reading frame. A downstream pseudoknot called the stimulatory element is responsible for the pause in translation allowing the frameshift to occur. After the frameshift, the pseudoknot is unwound by the ribosome allowing translation to continue, resulting in a protein with an extended C-terminus, known as pp1ab (Brierley et al. 1987, Inglis et al. 1990). These polyproteins are cleaved by the virally encoded proteases; nsp3 and nsp5, into individual nsps, of which some assemble into the replication-transcription complex (RTC) (**Figure 1.2C**) (Ziebuhr et al. 2001). The RTC produces negative-sense sub-genomic (sg)RNAs by discontinuous transcription, and negative-sense full-length genome templates by continuous transcription (Sawicki et al. 2007) (Sawicki et al. 1995) (**Figure 1.3**). The mechanism of transcription is not fully understood but is dependent on a conserved transcription regulatory sequence (TRS) (Hiscox et al. 1995). There is a TRS-leader (TRS-L) present at the 5′-end of the genome, and a TRS-body (TRS-B) found upstream of each gene block to regulate the transcription of negative-sense sgRNA. The sequence of the TRSs are conserved in both IBV and the closely related Turkey Coronavirus (TCoV) (CUUAACAA), except IBV

mRNA 3 and S, which are regulated by a slightly altered TRS (CUGAACAA). The recently discovered 4b transcript is regulated by a non-canonical TRS (CAA) (Bentley et al. 2013). Transcription is initiated by the RTC at the 3′-end of the full-length genome and continues upstream until a TRS-B is encountered, at which point transcription pauses (Pasternak et al. 2001). Transcription can either continue until the next TRS-B or can jump to the 5′-end due to complementary base pairing between TRS-B and TRS-L. Transcription continues resulting in an anti-leader sequence at the 3′-end of the negative-sense sgRNA (van Marle et al. 1999) (Zuniga et al. 2004). This discontinuous transcription creates a collection of negative-sense sgRNAs of varying length. The abundance of these sgRNAs is in part dependent on proximity to the 3′-end of the genome, with shorter sgRNA more abundant than longer sgRNA (van der Most et al. 1995). The negative-sense sgRNA and full-length transcripts are used as templates for synthesis of positive-sense viral sgRNA and full-length genomes. Each viral sgRNA is capped at the 5′-end and polyadenylated at the 3′-end (**Figure 1.2D**) (Masters 2006). Viral sgRNA are translated into the structural proteins, S, E, M, and N, and the accessory proteins 3a, 3b, 5a, and 5b. ORFs at the 5′-end are translated by host-cell machinery. Translation is believed to occur in a cap-dependent manner due to the presence of a 5′-end M^7G cap (Nakagawa et al. 2016). The translation of downstream ORFs; 3b in mRNA 3 and 5b in mRNA 5, are translated by leaky ribosomal scanning (Liu et al. 1992). Expression of E; the third ORF in mRNA 3, is regulated by an IRES present upstream in the 3a/3b RNA secondary structure (**Figure 1.2E**) (Liu et al. 1992, Le et al. 1994). A feature of coronavirus replication

is the production of double-stranded RNA (dsRNA), which occurs at around 3-5 hours post infection (h.p.i) (Hagemeijer et al. 2012, Maier et al. 2016). While historically dsRNA was believed to be an intermediate of ssRNA synthesis, this has recently been questioned as dsRNA does not colocalise with the RNA-dependent RNA polymerase or nascent RNA (Maier et al. 2013) (Hagemeijer et al. 2012) (Knoops et al. 2008). The role of this dsRNA is unknown.

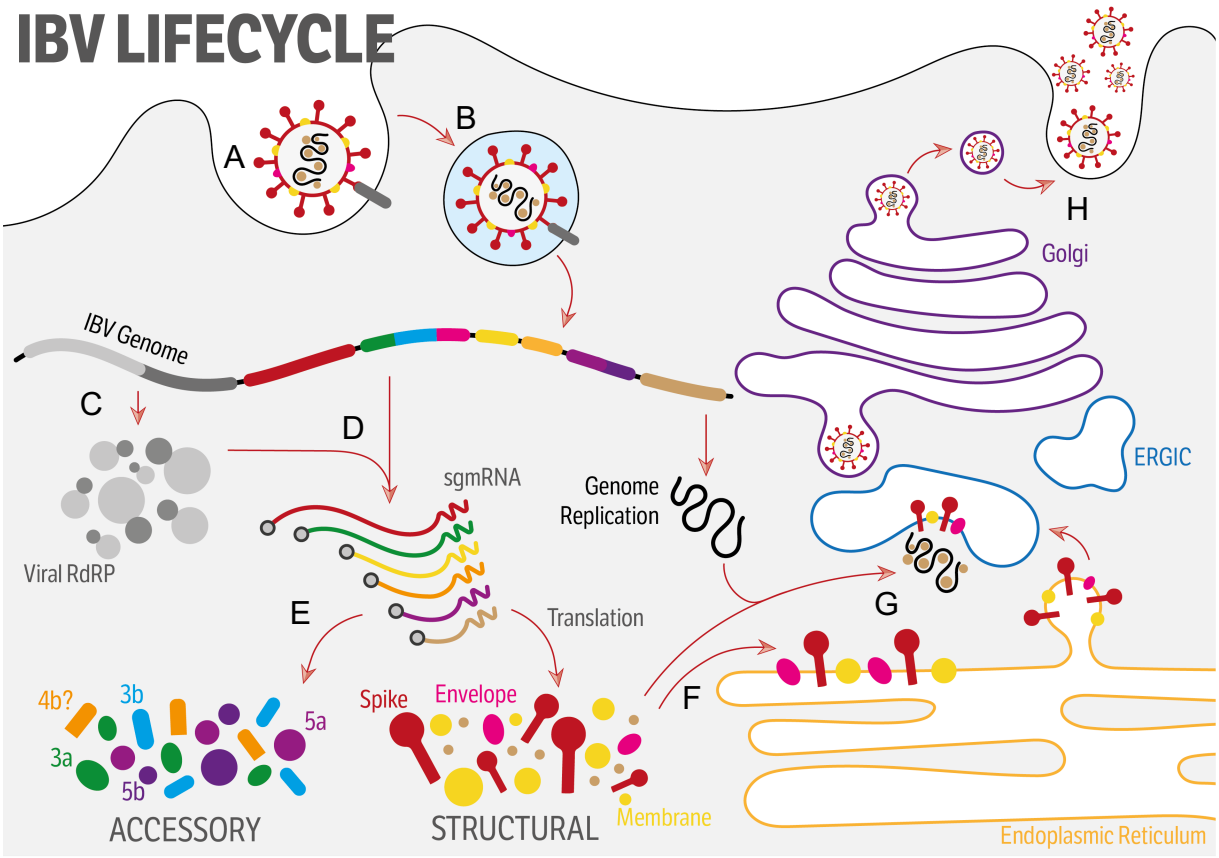

Figure 1.2 Schematic diagram of the lifecycle of IBV.

(A) IBV S protein attaches to an unknown cell surface receptor and enters the cell by endocytosis. (B) Virions fuse with the cell membrane and release the RNP into the cytoplasm. (C) Replicase proteins pp1a and pp1ab are translated by host-cell machinery and once cleaved assemble to form the viral RTC. (D) The RTC transcribes sgRNA and full-length genomes. (E) SgRNAs are translated into structural proteins and accessory proteins. (F) Structural proteins are translated at the ER and translocate to the Golgi or ER-GIC. Protein N binds to newly synthesised full-length genomic RNA. (G) New virions bud into the ER-GIC lumen. (H) The cell secretory pathway releases viral progeny by exocytosis at around 6-8 h.p.i.

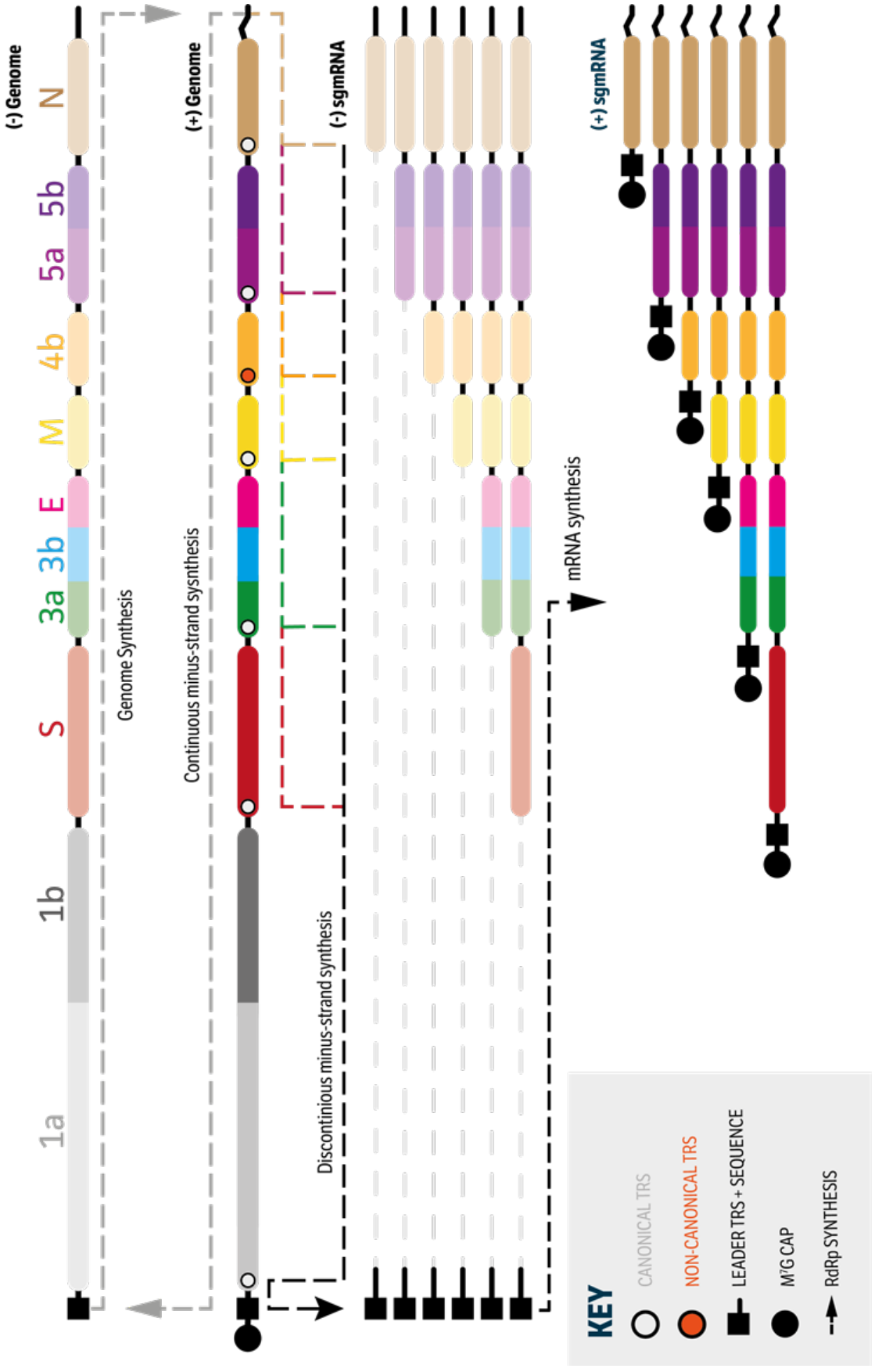
(-) Genome
1a
1b
S
3a
3b
E
M
4b
5a
5b
N
Genome Synthesis
(+) Genome
Continuous minus-strand sysnthesis
(-) sgmRNA
Discontinious minus-strand synthesis
mRNA synthesis
(+) sgmRNA
KEY
CANONICAL TRS
NON-CANONICAL TRS
LEADER TRS + SEQUENCE
M7G CAP
RdRp SYNTHESIS

Figure 1.3 Schematic diagram of IBV transcription.
RNA transcripts are transcribed by continuous and discontinuous transcription of the genomic RNA. Continuous and discontinuous transcription is initiated at the 3′-end of the genome by the viral RTC and moves upstream until a TRS-body (TRS-B) is encountered, at which point transcription can either continue or jump to the TRS-leader (TRS-L). Discontinuous transcription creates a nested set of 3′-co-terminal negative-sense sgRNA of varying length each with a common sequence at the 5′- and 3′-end. These sgRNA act as templates for the synthesis of positive-sense sgRNA, which are later translated into viral proteins. Continuous transcription occurs when transcription is not halted at a TRS-B, creating a negative-sense full-length genome, which is used as a template for synthesis of new +ssRNA genomes.

1.3.3 Coronavirus-induced membrane rearrangement

Positive-sense RNA viruses induce membrane rearrangement during infection; this provides a platform for viral replication and/or assembly, while also allowing compartmentation of viral PAMPs (Denison 2008, van Hemert et al. 2008). Coronaviruses have been extensively studied for their ability to induce membrane rearrangement. Betacoronaviruses; SARS-CoV and MHV, generate double-membrane vesicles (DMVs) as well as complex membranous structures known as convoluted membranes (CM) during infection (Gosert et al. 2002, Goldsmith et al. 2004, Knoops et al. 2008). IBV has also been shown to induce DMVs (**Figure 1.4A**), as well as a novel structure known as zippered ER which has attached vesicles (**Figure 1.4D**). These vesicles are termed spherules and are dispersed along the zippered ER structure with a small channel connecting the interior of the spherule to the cytoplasm (**Figure 1.4C**) (Maier et al. 2013). The exact site of IBV or coronavirus RNA synthesis is unknown, although a possible site are these spherules. The observed pores would allow the transfer of viral

RNA and proteins to and from the cytoplasm, while also providing protection from cellular detection. Historically, dsRNA produced during +ssRNA infection was thought to be an intermediate component of ssRNA synthesis. However, the role of dsRNA during IBV and indeed coronavirus infection is unclear and does not necessarily suggest the site of RNA synthesis. Early during MHV infection, dsRNA has been shown to colocalise with newly synthesised RNA but at later time points this colocalisation declines (Hagemeijer et al. 2012). In addition, during SARS-CoV infection, dsRNA has been shown to localise to the interior of DMVs. Unlike IBV induced spherules, DMVs lack pores or any connection to the cytoplasm, further questioning if these are the site of RNA synthesis (Knoops et al. 2008). In the case of IBV, only 1.5% of dsRNA colocalises with Nsp12; the RNA-dependent-RNA polymerase, suggesting that the location of dsRNA is not the primary site of RNA synthesis (Maier et al. 2013). IBV-induced membrane rearrangement appears not to be a determinant of pathogenicity, as M41, a pathogenic lab strain produces fewer spherules than the apathogenic strain, Beau-R (Maier et al. 2016), although it is possible that other virus-induced double membrane structures compensate, and it is structure, rather than shape that is an important determinant of viral pathogenicity. IBV and other coronaviruses further manipulate membranous structures to compartmentalise and release progeny virions by exocytosis, utilising the host-cell secretory pathway (Ruch et al. 2011) (**Figure 1.4B**).

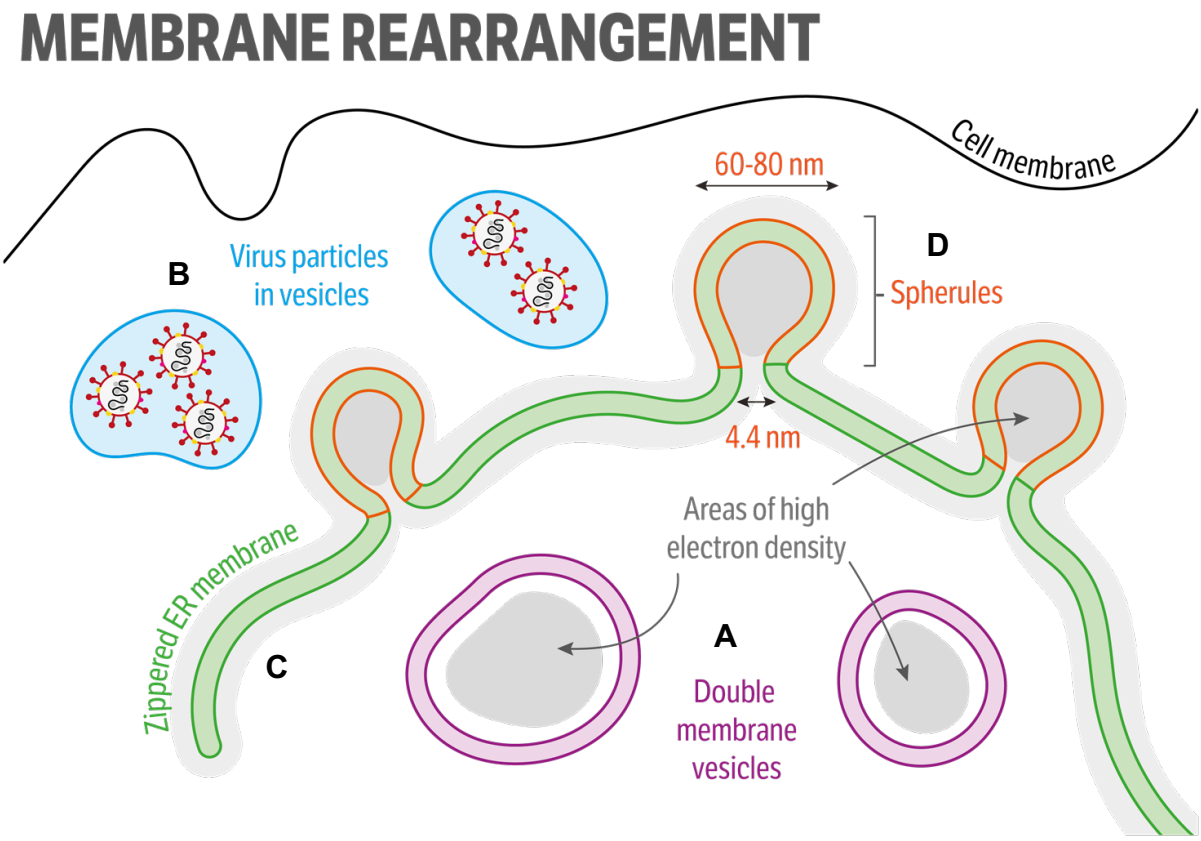

Figure 1.4 Schematic diagram of IBV-induced membrane rearrangement.
During infection, IBV induces four types of membrane rearrangement, (A) double-membrane vesicles (DMVs), (B) vesicles for the export of progeny viruses and (C) zippered-ER structures with (D) spherules.

1.3.4 Assembly and Budding

Structural proteins S, E, and M are translated and inserted into the ER (**Figure 1.2F**) (Krijnselocker et al. 1994) and are shuttled to the ER-GIC via the cell secretory pathway. Full-length genomic RNA, produced during replication, associates with newly synthesised N protein into a helical RNP structure (Zhou et al. 2000). RNPs bud into the ER-GIC lumen to form new virions by binding to M (**Figure 1.2G**) (Tooze et al. 1987) (Klumperman et al. 1994) (Narayanan et al.

2000). The S protein is first glycosylated at the ER and is then incorporated into virions at the ER-GIC by interacting with M (Hurst et al. 2005, Youn et al. 2005). Nascent virions are transported in vesicles to the cell surface and released by exocytosis (Emmott et al. 2013). IBV begins to release progeny virions by 6-8 hours post infection in a non-lytic manner (Maier et al. 2013) (**Figure 1.2H**). IBV E has been shown to be essential for virion egress by altering the host-cell secretory pathway, as well as inducing viral membrane curvature and viral particle scission (Ruch et al. 2011). IBV E protein is post-translationally modified with the addition of palmitic acid onto cysteine residues. In MHV this modification has been shown to increase VLP yield and production of infectious virions (Boscarino et al. 2008) (Corse et al. 2002). Expression of M and E is sufficient for coronavirus VLP assembly, but when co-expressed with N, VLP yield is significantly higher (Corse et al. 2000) (Vennema et al. 1996).

1.4 Structural Proteins

Coronaviruses express four structural proteins, S, E, M, and N. These proteins form part of the virus particle and are essential for the synthesis of infectious virions (Sturman et al. 1980, Delmas et al. 1990, Vennema et al. 1996). Most of the research on structural proteins are collated from other coronaviruses, and although some differences do occur, the primary role of these proteins is conserved within the coronavirinae family.

1.4.1 Membrane (M)

The M protein is 25 kDa and the most abundant viral protein (Stern et al. 1982). M protein is a type III transmembrane protein that transverses the lipid envelope three times and interacts with N through its C-terminal cytoplasmic domain (Rottier et al. 1984). The IBV M protein accumulates at the *cis*-Golgi membrane when expressed alone, but accumulates at the ER-GIC during infection due to its interaction with N (Klumperman et al. 1994, Narayanan et al. 2000). The M protein has also been shown to interact with the S protein during SARS-CoV infection, which results in spike retention at the ER-GIC (McBride et al. 2007). Expression of IBV M and E alone is enough for the synthesis of VLPs (Corse et al. 2000, Corse et al. 2003)

1.4.2 Envelope (E)

The smallest coronavirus structural protein, E, is 12 kDa and the least abundant component of the viral envelope. Most of the protein remains within the cell (Liu et al. 1992). The protein transverses the IBV lipid envelope once and has a single hydrophobic membrane domain flanked by two hydrophilic domains (Corse et al. 2000, Ruch et al. 2011). Protein E is a viroporin and forms a cation-selective ion channel in lipid bilayers, thought to aid membrane permeability and curvature (Wilson et al. 2004, Wilson et al. 2006). During IBV infection, E localises to the Golgi membrane due to a signalling motif in the cytoplasmic tail (Corse et al. 2000). The coronavirus E protein is thought to play a role in membrane curvature or virion

scission as well as virus assembly and egress (Fischer et al. 1997, Fischer et al. 1998, Raamsman et al. 2000).

1.4.3 Nucleocapsid (N)

The IBV N protein has a molecular weight of 45 kDa. The N protein contains a high ratio of serine residues, which are phosphorylated during infection, and a high basic residue content (Lomniczi et al. 1981). The N-terminal domain of N binds to and packages nascent full-length genomes into new virions as a helical RNP structure and interacts with M through its C-terminal domain (Calvo et al. 2005, Yu et al. 2006, McBride et al. 2014) (Fan et al. 2005). The N protein also interacts with genomic RNA through the leader sequence at the 5′-end and the UTR at the 3′-end. As these regions have a role in transcription, N is believed to play a role in sgRNA production (Zhou et al. 1996). During infection, IBV N protein localises to both the cytoplasm and nucleolus. Due to this distribution, it has been suggested that N may play a role in regulating host-cellular translation by interfering with ribosome assembly and rRNA synthesis (Tahara et al. 1994, Wurm et al. 2001). Furthermore, mass spectrometry analysis of IBV N pull-downs have identified a high number of cellular proteins involved in translation and RNA modification/processing (Emmott et al. 2013). Lastly, N protein has been shown to have a role in viral budding, and immune suppression (Denison et al. 1999, Siu et al. 2008, Zhou et al. 2008) (Lu et al. 2011).

1.4.4 Spike (S)

The IBV spike protein is a 180 kDa glycoprotein and protrudes from the virus envelope as a homotrimer (Delmas et al. 1990). The coronavirus S protein is a type I glycoprotein and the largest viral protein composed of two main domains, S1 and S2. The S1 subunit binds to host-cell receptors, including α-2,3-linked sialic acid, through its RBD. The spike protein from Beaudette also contains a putative heparan sulfate binding domain, and it has been suggested that heparan sulfate may be an attachment factor (Madu et al. 2007). The S2 subunit is responsible for viral–cell fusion resulting in entry of the RNP (Degroot et al. 1987). During infection, the S protein is translated as a single polypeptide and due to a signal motif localises to the ER, where it oligomerises (Delmas et al. 1990). The IBV S protein is cleaved into two subunits by furin proteases which target a rich basic sequence present in between the two domains (Abraham et al. 1990) (Luytjes et al. 1987). The protein is further processed at the Golgi where oligosaccharides are added (Cavanagh 1983). The coronavirus S protein is the primary target for neutralising antibodies and plays a role in cell tropism (Kubo et al. 1994, Casais et al. 2003). The Beaudette strain of IBV has broad cell tropism and can infect primary and secondary cell lines, while M41-CK can only infect primary chicken cells. Replacement of the Beaudette S gene with the S gene from M41 restricts cell tropism to primary chicken cells, suggesting the S protein is a major determinant of cell tropism (Casais et al. 2003). The extended cell tropism of IBV Beaudette has been linked to the presence of the heparan sulfate binding site. Vaccination against IBV relies on the induction of neutralising antibodies

against the S1 domain, but due to frequent mutations and recombination events in this domain, which generates a large number of serotypes, vaccines are rarely cross-protective (Britton 2007).

1.5 Non-structural Proteins

The 5′-end of the IBV genome encodes two large polyproteins pp1a and pp1ab. Expression of pp1ab occurs after a -1 frameshift, which occurs in roughly 30% of translation events (Brierley et al. 1989). These polyproteins are proteolytically cleaved by the virally encoded proteases, nsp3 and nsp5, into 15 nsps. Alpha-, beta- and delta- coronaviruses encode 16 nsps, while gammacoronaviruses only encode 15 nsps (Ziebuhr et al. 2000, Ma et al. 2015). Gammacoronaviruses do not encode nsp1, instead expressing a larger nsp2 due to the lack of a cleavage site (Lim et al. 1998). IBV ORF1a encodes nsp 2-11 while ORF1b encodes nsp 12-16. The function of some IBV nsps have not been confirmed but can be inferred by their similarity to other coronaviruses. Their function is summarised in **Table 2**.

Table 1.2 Summary of non-structural protein (nsp) functions

Nsp	Activity
1	Host mRNA degradation, translation inhibition, cell cycle arrest, inhibition of IFN signalling (Kamitani et al. 2006)
2	Unknown, dispensable for replication in MHV and SARS-CoV (Graham et al. 2005)
3	Papain-like proteases, polyprotein processing, IFN antagonist, DMV formation (Putics et al. 2005) (Lim et al. 1998, Oostra et al. 2008)
4	DMV formation (Oostra et al. 2007)
5	Cysteine-like protease, polyprotein processing (Lu et al. 1996)
6	DMV formation, induce autophagy (Oostra et al. 2008) (Maier et al. 2013)
7	Single stranded RNA binding, forms a complex with nsp8 (Velthuis et al. 2012)
8	Primase (RNA polymerase) (Imbert et al. 2006) (Velthuis et al. 2012)
9	Replicase complex protein (Egloff et al. 2004, Sutton et al. 2004)
10	Replicase complex protein (Decroly et al. 2008) (Chen et al. 2011)
11	Unknown
12	RNA-dependent RNA polymerase (RdRp) (Imbert et al. 2006)
13	Helicase, nucleoside triphosphate activity (Ivanov et al. 2004, Ivanov et al. 2004)
14	3′ – 5′ exonuclease, RNA cap formation, methyltransferase (Chen et al. 2009)
15	Endonuclease (Bhardwaj et al. 2012)
16	RNA cap formation (2 'O-methyltransferase) (Decroly et al. 2008)

1.6 Accessory proteins from other Coronaviruses

All coronaviruses encode accessory proteins. These accessory proteins are considered non-essential for replication *in vitro* but may play a role in virulence or pathogenicity (Hodgson et al. 2006, Narayanan et al. 2008). Even though accessory proteins are present in all coronaviruses, they share little or no sequence homology, and no functional information can be derived from their genome location or name (Hodgson et al. 2006, Cavanagh et al. 2007, McBride et al. 2012, Liu et al. 2014, Fang et al. 2016). Nonetheless, IBV as with other coronaviruses will be subject to similar host-cell pressures. For example, several coronavirus accessory proteins function as interferon (IFN) antagonists (Liu et al. 2014). The role of coronavirus accessory proteins is summarised in **Table** 1.3, highlighting the range of roles these proteins have.

1.6.1 Alphacoronaviruses

The alphacoronavirus genus in the coronavirinae subfamily includes transmissible gastroenteritis virus (TGEV), feline and porcine viruses and human coronaviruses, NL63 (HCoV-NL63) and 229E (HCoV-229E). Viruses within this genus encode two or three accessory proteins between the structural genes, S and M. Some viruses within this genus also encode an extra ORF downstream of N, known as ORF7. TGEV expresses three known accessory proteins, 3a and 3b, encoded between gene S and E, and protein 7 encoded downstream of gene N. Deletion of 3a and 3b had a limited effect on replication and cell tropism *in vitro* (Hodgson et al. 2006), while deletion of protein 7 from TGEV resulted in increased

cytopathic effect (CPE) and cell death compared to wild-type. Furthermore, recombinant viruses lacking ORF7 were more pathogenic and caused earlier death in piglets (Cruz et al. 2011). This result suggested that protein 7 is involved in host-cell antiviral responses essential to prevent extensive tissue damage. Feline infectious peritonitis virus (FIPV) expresses five accessory proteins, 3a, 3b, 3c, 7a, and 7b. Deletion of ORF3, which encodes 3abc, did not affect viral titres *in vitro*, although it severely restricted pathogenicity and cell tropism *in vivo* (Dedeurwaerder et al. 2013), while ORF7 has been shown to be essential for efficient replication *in vitro* and important for virulence *in vivo* (Dedeurwaerder et al. 2013). Studies have shown that recombinant FIPV lacking ORF7a rendered the virus more susceptible to IFN-α treatment. Complementing the virus with ORF7a only restored resistance to IFN-α, in the presence of ORF3, suggesting ORF7a is dependent on ORF3 for functionality (Annelike Dedeurwaerder 2014). Porcine Respiratory coronavirus (PRCoV) ORF3 and ORF7 both play a role in virulence (Tung et al. 1992, Paul et al. 1997). HCoV-229E clinical isolates contain a single ORF in gene 4, resulting in a single polypeptide. Conversely, lab-adapted strains of HCoV-229E contain either a truncation, resulting in a smaller ORF4, or two ORFs corresponding to ORF4a and ORF4b. Transcription of ORF4b in these lab-adapted strains has not been shown, and no mechanism of ribosome entry for ORF4b has been postulated. Protein 4 from clinical isolates is highly conserved and has been identified as a viroporin, with deletions of this protein causing a reduction in viral titres (Zhang et al. 2014).

1.6.2 Betacoronaviruses

Betacoronaviruses are an important coronavirus genus regarding human health and include human coronavirus HKU1 (HCoV-HKU1), severe acute respiratory syndrome coronavirus (SARS-CoV) and Middle East respiratory syndrome coronavirus (MERS-CoV) along with the mouse hepatitis coronavirus (MHV) (**Table** 1.1) (To et al. 2013). These viruses can encode numerous accessory proteins with a variety of functions. SARS-CoV encodes eight known accessory proteins, 3a, 3b, 6, 7a, 7b, 8a, 8b, and 9 (Narayanan et al. 2008), while MERS-CoV expresses four accessory proteins, 3, 4a, 4b, and 5, encoded between gene S and gene E. SARS-CoV accessory proteins have been studied extensively and have been implicated in a wide variety of functions. SARS-CoV 3a is a minor structural protein and has been detected in VLPs by electron microscopy (Ito et al. 2005). Deletion of ORF3a caused a log reduction in viral titres compared to wild-type suggesting that although 3a is non-essential for replication, it may be beneficial (Yount et al. 2005). SARS-CoV 3b is also expressed from mRNA3 and localises to both the nucleus and mitochondria where it inhibits MAVS signalling and IRF3 activation, respectively (Spiegel et al. 2005, Freundt et al. 2009). Protein 3b has an apoptotic phenotype when expressed alone and further modulates the immune response by binding to the transcription factor, Runt Related Transcription Factor 1b (RUNX1b) (Khan et al. 2006, Kopecky-Bromberg et al. 2007). SARS-CoV protein 6 is not required for replication but does play a role in virulence (Zhao et al. 2009). GFP-tagged protein 6 was shown to localise to the ER and Golgi apparatus (Geng et al. 2005, Pewe et al. 2005). Overexpression of

protein 6 inhibits interferon-beta (IFNβ) expression and prevents signal transducer and activator of transcription 1 (STAT1) nuclear translocation in IFN treated cells by sequestering the STAT1 nuclear import factor karyopherin alpha 1 (KPNA1) (Zhao et al. 2009). Deletion of SARS-CoV 7a did not effect *in vitro* and *in vivo* replication (Pekosz et al. 2006). Overexpression of protein 7a was also shown to induce cell-cycle arrest and induce caspase-dependent apoptosis as well as inhibit cellular translation (Tan et al. 2004, Kopecky-Bromberg et al. 2006, Tan et al. 2007). Protein 7b is also dispensable for viral replication *in vitro* (Yount et al. 2005, Schaecher et al. 2007). Conversely, recombinant virus lacking ORF7b resulted in higher titres *in vivo* suggesting this protein may play a role in attenuation (Pfefferle et al. 2009). MERS-CoV encodes four accessory proteins, 3, 4a, 4b, and 5 encoded between gene S and gene E. Proteins 3 and 5 localise to the ER-GIC while proteins 4a and 4b have a diffuse cytoplasmic distribution as well as a nuclear localisation. Proteins 4a, 4b, and 5 are all IFN antagonists (Liu et al. 2014). Protein 4a binds to dsRNA to prevent detection by MDA-5 and RIG-I (Niemeyer et al. 2013) and has been shown to inhibit the stress granule pathway, increasing cellular translation (Rabouw et al. 2016). MERS-CoV also contains an ORF known as 8b in gene N that has not been characterised (van Boheemen et al. 2012, Raj et al. 2014).

1.6.3 Gammacoronaviruses

IBV is the prototype coronavirus within this genus, with TCoV considered a close relative (Guy 2000). IBV is known to express four accessory proteins during

infection, 3a, 3b, 5a, and 5b (Liu et al. 1991, Casais et al. 2005, Hodgson et al. 2006). TCoV also expresses these four accessory proteins which all have a high sequence identity with IBV (Britton 2007).

1.6.4 Deltacoronaviruses

Deltacoronaviruses are the most recently described genus within the coronavirinae subfamily and as such little is known about this genus of coronaviruses, including the function of the accessory proteins. These viruses mainly infect wild birds and pigs (Woo et al. 2012). The prototype virus, porcine deltacoronavirus (PDCoV), is predicted to express four accessory proteins, ORF6 located between gene M and gene N, and ORF7, encoding 7a, 7b, and 7c, located downstream of N (Woo et al. 2012, Fang et al. 2016). Currently, only accessory proteins 6 and 7a have been shown to be translated during infection. Production of sgRNA7a is regulated by a non-canonical TRS (Fang et al. 2017).

Table 1.3 The role of coronavirinae accessory proteins

Coronavirus	Name	Role
FIPV	3a, b, c	Restricts cell tropism to the intestine (Adam Balint 2014)
	7a, 7b	IFN antagonist (dependent on ORF3) (Annelike Dedeurwaerder 2014)
TGEV	3a	Limited role in virulence and cell tropism (Kim et al. 2000)
	3b	Limited role in virulence and cell tropism (Galan et al. 2009)
	7	Deletion decreases cell death and cytopathic effect. Interacts with phosphatase protein 1c (Ortego et al. 2003, Cruz et al. 2011)
HCoV 229E	4a	Viroporin (Zhang et al. 2014)
PRCoV	3a, 3b	Unknown
MERS-CoV	3	Unknown
	4a	IFN antagonist(Siu et al. 2014) Stress granule inhibitor (Rabouw et al. 2016)
	4b	IFN antagonist (Yang et al. 2015)
	5	IFN antagonist (Yang et al. 2013)
	8b	Unknown
MHV	HE	Sialate-O-acetylesterase (Siddell et al. 1983) Non-essential structural protein (Lissenberg et al. 2005)
	2a	Cleaves 2'-5′-oligoadenylate synthase (OAS) (Zhao et al. 2012)
	4a	Role in pathogenicity (de Haan et al. 2002) IFN antagonist Stress granule inhibitor (Raaben et al. 2007)
	5a	IFN antagonist (Koetzner et al. 2010)
SARS-CoV	3a	Induces cellular membrane rearrangement (Ito et al. 2005) Activates the PERK pathway (Minakshi et al. 2009)
	3b	IFN antagonist by inhibiting IRF3 activity Interacts with activator protein 1 (AP-1) Interacts with runt-related transcription factor 1b (RUX1b) (McBride et al. 2012)
	6	IFN antagonist Interacts with N-Myc and karyopherin α2 Essential for replication and present in virions Induces cellular DNA synthesis(McBride et al. 2012)
	7a	Induces apoptosis in a caspase-3 and p38 MAPK dependent manner Interacts with virions (McBride et al. 2012) (Tan et al. 2007)
	7b	Non-essential for replication Role in apoptosis (Schaecher et al. 2007)

	8a	Forms an ion-channel in lipid bilayers (Chen et al. 2011)
	8b	Inhibits expression of the E viral protein (McBride et al. 2012)
	9b	Apoptosis inducer Interacts with chromosomal maintenance (CRM1) Associated with virions (McBride et al. 2012)
IBV	3a,3b	No role in replication *in vitro* (Kint et al. 2015) Regulates expression of IFNβ (Casais et al. 2005, Hodgson et al. 2006)
	5a	No role in replication *in vitro* (Casais et al. 2005, Hodgson et al. 2006)
	5b	Host-cell translational shut-off (Kint et al. 2016)
PDCoV	6	Detected during infection (Fang et al. 2016)
	ORF7	Potentially encodes three accessory proteins, only 7a has been detected (Woo et al. 2012, Fang et al. 2017)

Alphacoronavirinae (red), Betacoronavirinae (blue), Gammacoronavirinae (green), Deltacoronavirinae (yellow), FIPV (feline infectious peritonitis virus), FCoV (feline coronavirus), TGEV (transmissible gastroenteritis coronaviruses), MERS-CoV (Middle East respiratory syndrome coronavirus), MHV (mouse hepatitis virus), SARS-CoV (serve acute respiratory syndrome coronavirus), IBV (infectious bronchitis virus), PRCoV (porcine respiratory coronavirus), PDCoV (Porcine deltacoronavirus)

1.7 IBV Accessory Proteins

The 3′-end of the coronavirus genome encodes accessory proteins as well as the structural proteins. IBV expresses four known accessory proteins during infection, 3a, 3b, 5a, and 5b. These accessory proteins are dispensable for replication *in vitro* (Britton et al. 2006). Along with these four proteins, IBV also expresses an additional transcript referred to as 4b, although the translation of this transcript has not yet been demonstrated (Bentley et al. 2013). Coronavirus accessory proteins are non-essential for *in vitro* replication but are usually highly conserved and often play a role in regulating IFN expression, cellular translation and apoptosis (**Table** 1.3) (Liu et al. 2014). While coronavirus accessory proteins may share similar functions, they have limited sequence homology to one another.

1.7.1 Gene 3 accessory proteins

Messenger RNA 3 is polycistronic and encodes three proteins, accessory proteins 3a and 3b and structural protein E. IBV 3a and 3b have been detected during IBV infection in chicken kidney (CK) cells utilising antibodies raised against the predicted peptide sequence (Liu et al. 1991). Recombinant IBVs that do not express 3a and 3b due to a scrambled start codon grew to similar titres *in vitro*, *in ovo,* and in *ex vivo* organ culture, suggesting these proteins are not required for *in vitro* replication (Hodgson et al. 2006).

IBV 3a is a 6 kDa protein and the first protein expressed from mRNA 3. IBV 3a is highly conserved among the many different IBV strains, with an 81 – 86.2% similarity in polypeptide sequences (Jia et al. 1997). The relatively high degree of sequence preservation suggests an important role for this protein. IBV 3a contains a signal peptide which directs 3a to the ER membrane, but due to the small size of 3a, this signal peptide sequence is not effectively recognised by signal recognition particles (Pendleton et al. 2005). This explains the dual localisation pattern seen for 3a during infection and transfection in Vero cells, which is either membrane-bound at the smooth ER or diffuse in the cytoplasm (Pendleton et al. 2005). This theory is further supported as the extension of 3a with a GFP-tag resulted in more membrane-bound 3a, compared to 3a expression alone. During infection in Vero cells, membrane-bound 3a has been shown to span the membrane once, with the C-terminus exposed to the cytoplasm and the N-terminus to the lumen of the smooth ER (Pendleton et al. 2005). IBV 3a has

also been shown to closely localise with MxA, which is a small GTPase that has antiviral activity (Pendleton et al. 2005, Haller et al. 2011). Protein 3a has also been shown to inhibit IFNβ mRNA transcription at 24 h.p.i, while also inducing IFNβ protein expression at 36 h.p.i (Kint et al. 2015). The mode of action of IBV 3a on IFN expression is unknown.

IBV 3b is a 7.4 kDa protein and the second protein translated from sgRNA 3 via leaky ribosomal scanning (Liu et al. 1992). IBV 3b predominantly localises to the nucleus in mammalian cells while in avian cells appears predominantly in the cytoplasm (Pendleton et al. 2006). Furthermore, IBV 3b turnover is proteasome-dependent in mammalian cells and proteasome-independent in avian cells. The differences seen in avian and mammalian cells highlight the importance of using an appropriate cell line for experiments. In addition, the half-life of 3b is short, making it very difficult to detect this protein during infection and transient expression (Pendleton et al. 2006). A truncated form of 3b has been detected in a strain of Beau-CK serially passaged in Vero cells. This truncation was an advantageous mutation that conferred higher growth kinetics *in vitro* and higher virulence *in ovo* (Shen et al. 2003). Interestingly, this truncation changed the localisation of 3b from the nucleus to a diffuse cytoplasmic pattern in Vero cells, suggesting the C-terminal proportion is responsible for nuclear localisation in mammalian cells (Pendleton et al. 2006). There is little understanding of the function and mechanism of this small protein, although previous work has shown

that 3b plays a role in conferring IBV resistance to IFN expression (Kint et al. 2015).

1.7.2 Transcript 4b

Positioned between the gene M and gene 5 is the intergenic region (IR), which contains a putative ORF known as 4b. Due to the lack of an upstream TRS, this ORF was previously thought to be a pseudogene (Stern et al. 1980). However, Bentley *et al.* (2013) showed by northern blot that a sgRNA is expressed from the intergenic region during Beau-R infection, referred to as sgRNA 4b (Bentley et al. 2013). The presence of sgRNA 4b was also identified in RNA extracted from M41 infected avian trachea. While other proteins have an upstream canonical TRS (CUUAACAA), gene 4b is regulated by a non-canonical TRS (CAA). This non-canonical TRS resulted in transcription of mRNA 4b at a lower level than expected for its genome location. Furthermore, the related coronavirus, TCoV, also expresses this previously unidentified 4b transcript. The 4b transcript is not required for *in vitro* replication, suggesting if a protein is translated, it is most likely an accessory protein (Bentley et al. 2013). Replacement of ORF4b with GFP did result in GFP expression, suggesting that the transcript can act as a mRNA. The gene is also present in the Beau-R strain of IBV, although the potential protein is truncated to 5 kDa due to a stop codon present in the middle of the ORF (Bentley et al. 2013). Whether this transcript is translated during IBV infection is not known, nor is the function of this putative protein.

1.7.3 Gene 5 accessory proteins

Messenger RNA 5 is dicistronic and encodes two accessory proteins, 5a and 5b, 8 kDa and 9 kDa respectively (Liu et al. 1992). These proteins have been detected during IBV infection in CK cells using antibodies raised against the predicted amino acid sequences (Liu et al. 1992). Recombinant IBV lacking 5a or 5b grew to similar titres to wild-type virus *in vitro*, *in ovo* and *ex vivo* organ culture suggesting they are non-essential for replication (Casais et al. 2005). Protein 5a displays a diffuse pattern throughout the whole cell while 5b displays a more perinuclear granular pattern (Davies 2009). Kint *et al.* (2014) showed that protein 5b is involved in host translational shut-off. Wild-type Beau-R inhibited cellular translation while recombinant IBV lacking 5b expression did not. Translation of IBV proteins was not affected, suggesting 5b may target host-cell translation specifically. This reduction in host-cell translation can explain, in part, why there are high levels of IFNβ mRNA but low levels of IFNβ protein during IBV infection (Kint et al. 2016).

1.8 Coronavirus–Host Interaction

1.8.1 Interferon response to viral infection

The IFN signalling cascade is a cellular response to infection and is one of the first lines of defence against invading pathogens. The innate immune response detects ‘non-self’ signals known as pathogen-associated molecular patterns (PAMPs). These PAMPs include dsRNA, 5′-C-phosphate-G-3′ (CpG), lipopolysaccharides and dsDNA, among others, and are recognised by specific

pathogen recognition receptors (PRRs) (Thompson et al. 2011). Detection of PAMPs by the cell activates the IFN signalling cascade to induce the expression of IFNs, cytokines, and chemokines (Wu et al. 2014). IFN induces the expression of IFN stimulated genes (ISGs), which induces an antiviral state in the cell and neighbouring cells to prevent further viral replication (Stark et al. 2012). PRRs responsible for the detection of viral PAMPs such as dsRNA include RIG-I-like receptors (RLRs), and TOLL-like receptors (TLRs). So far 10 TLRs and 2 RLRs have been identified in domestic fowl compared to 11 and 3 in humans, respectively (Kannaki et al. 2010). While chickens express the membrane-bound PPRs, TLR3 and TLR7, used to detect dsRNA and ssRNA, respectively, chickens do not express the cytosolic dsRNA sensing PRR, RIG-I (Zou et al. 2009). However, the other dsRNA sensing RLRs in humans, MDA-5 and Laboratory of Genetics and Physiology 2 (LGP2) are expressed (Barber et al. 2013). MDA-5 detects and binds to dsRNA, and subsequently interacts with and activates the mitochondrial antiviral signalling protein (MAVS) (**Figure 1.5A**). MAVS is a membrane-bound protein that localises to the mitochondria, mitochondrial-associated membrane (MAM) structures and peroxisomes (Seth et al. 2005). MDA-5 activation induces MAVS aggregation, which then recruits downstream signalling proteins including TANK-binding kinase 1 (TBK1), NF-kappa-B essential modulator (NEMO) and TNF receptor-associated factor 3 (TRAF3) (**Figure 1.5B**) (Kawai et al. 2005). Mitochondria remodelling results in mitofusion and aggregation of signalling proteins, enhancing antiviral signalling (**Figure 1.5C**) (Castanier et al. 2010). Phosphorylation of TBK1 leads to the

phosphorylation of interferon regulatory factor 3 (IRF3) and 7 (IRF7) (**Figure 1.5D, E**). Phosphorylated IRF3/7 dimerises and translocates to the nucleus where it transcribes IFNβ mRNA (**Figure 1.5F, G**). Chickens express an IRF that closely resembles IRF7 but appear to have selectively lost IRF3 (Grant et al. 1995, Cormican et al. 2009). After translation, IFNβ is secreted from the cell and binds to IFN receptors (IFNAR) on the same cell and neighbouring cells, activating the JAK-STAT pathway (Stark et al. 2012). This pathway leads to the dimerisation of STAT3 and STAT7 which mediates expression of ISGs. ISGs include a wide variety of proteins involved in creating an antiviral state within the cell leading to viral suppression along with immunomodulation. Overexpression of IFN can induce a hyperimmune state which can be deleterious to the body. For this reason, the IFN signalling cascade is highly regulated after activation by controlling levels of IFN signalling proteins including MAVS and RIG-I (Lin et al. 2006, Castanier et al. 2012, Fuchs 2012, Hu et al. 2016). MAVS, as the gateway protein of the IFN signalling cascade, is targeted for degradation in a negative-feedback loop by the E3-ligases, Tripartite motif-containing protein 25 (TRIM25), glycoprotein 78 (gp78), and RING finger protein 5 (RNF5) to prevent further downstream signalling. This helps to turn off the IFN signalling cascade after infection (Zhong et al. 2010, Castanier et al. 2012, Jacobs et al. 2013).

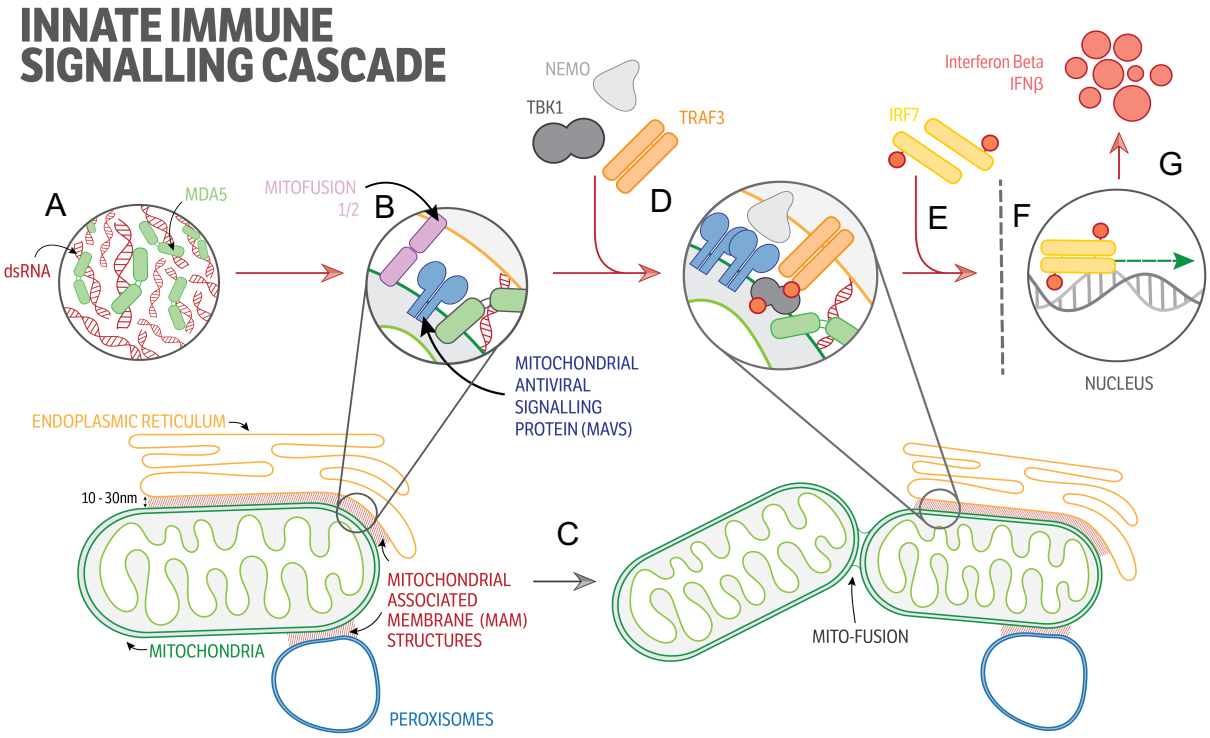

Figure 1.5 Schematic diagram of the interferon signalling cascade in chickens. (A) Viral dsRNA is detected by MDA-5. (B) MDA-5 is then recruited to MAVS at the mitochondria, peroxisome or mitochondrial-associated membrane (MAM) structures. (C) Mitochondrial remodelling concentrates IFN signalling proteins. (D) MAVS activation leads to aggregation and recruitment of downstream signalling proteins including TBK1, NEMO and TRAF3. (E) Phosphorylated TBK1 leads to the dimerisation and phosphorylation of IRF7. (F) Activated IRF7 translocates to the nucleus where it mediates transcription of IFNβ. (G) Once translated, IFNβ is released from the cell and induces antiviral states in the same and neighbouring cells.

1.8.2 Viruses and the interferon response

The innate immune response represents a significant barrier to viral replication. The selective pressure of the IFN response has created an evolutionary arms race, with viruses that inhibit this pathway having an advantage. Many viruses

express proteins that antagonise IFN expression, with the aim to prevent the cell inducing an antiviral state. These proteins can target the signalling cascade at any point, from the detection of PAMPs to nuclear translocation of IRFs, to the expression of IFN. A classic example of this is the multi-functional NS1 protein of Influenza A virus (IAV), which shields dsRNA from RLR detection, preventing MAVS activation and thus IFN expression (Hatada et al. 1992). Coronavirus accessory proteins, nsps and structural proteins have been shown to inhibit IFN expression. For example, SARS-CoV N is a potent IFN antagonist and inhibits IFN expression by interfering with TRIM25-mediated RIG-I ubiquitination (Hu et al. 2017). MERS-CoV proteins M and 4b inhibit IFN expression by inhibiting TBK1 phosphorylation and MDA-5 dsRNA sensing, respectively (Niemeyer et al. 2013, Lui et al. 2016). Nsp3 from SARS-CoV and HCoV-NL63 have been shown to antagonise IFN expression independent of its normal protease activity (Clementz et al. 2010, Sun et al. 2012). Alpha- and betacoronaviruses nsp1 have been shown to induce host translation shut-off, limiting translation of IFN (Kamitani et al. 2006) (Tohya et al. 2009) (Huang et al. 2011) (Wang et al. 2010). IBV lacks nsp1, but most likely expresses multiple proteins that target the IFN signalling cascade. The innate immune response to IBV is important for the pathogenicity and outcome of the disease in domestic fowl, with resistant and susceptible chicken lines showing a different initial innate immune response (Smith et al. 2015). Type I interferon response are upregulated in the trachea during IBV infection at around 3 days post infection. Increased levels of pro-inflammatory cytokines are associated with viral lesions and high viral load (Kameka et al. 2014,

Okino et al. 2014). IL-6 is considered a marker for poor outcome, with susceptible lines expressing 20 times more IL-6 compared to resistant line (Asif et al. 2007, Chhabra et al. 2015). Immunopathology is an important factor in disease progress and outcome, with strong innate responses associated with serve symptoms (Smith et al. 2015, Okino et al. 2017). The arming of the adaptive immune response is crucial for clearance of the virus, with local cell-mediated immune (CMI) response mediated by an influx of CD3+, CD8+ and CD4+ cells to the trachea at 3 to 7 days post infection (Okino et al. 2014). The IFN response to IBV infection has been investigated extensively (Kint 2015). MDA-5 is an essential PPR for the recognition of IBV-induced dsRNA and is required for the initiation of the IFN signalling cascade (Kint et al. 2015). IFNβ expression is the main IFN subtype produced during IBV infection, with interferon-α (IFNα) undetectable (Kint 2015). IBV fails to induce IFNβ expression until 24 h.p.i, suggesting IBV actively inhibits the IFN cascade during early infection. Interestingly, treatment of IBV infected cells with poly(I:C) during early infection resulted in a higher IFN response, compared to poly(I:C) treatment alone, suggesting that IBV can agonise IFN expression once stimulated upstream. IBV accessory proteins 3b have been shown to inhibit IFNβ mRNA expression during infection at 24 and 36 h.p.i. IBV 3a has also been shown to inhibit IFN mRNA transcription but only significantly at 24 h.p.i compared to the wild-type. Recombinant IBV lacking 3a was also shown to induce higher levels of IFN expression at 36 h.p.i, suggesting that 3a can also induce IFN expression and appears to have a dual effect on the

IFN cascade. The mechanism of action for 3a and 3b is not known (Kint et al. 2015).

1.8.3 Stress Granule pathway

The stress granule (SG) pathway is a cellular response to external and internal stimuli that induce cellular stress. The SG pathway is induced to preserve resources and energy until a return to cellular homeostasis is achieved (Buchan et al. 2009). A range of stimuli can activate the SG pathway including ER stress, through the protein kinase R (PKR)-like ER kinase (PERK) pathway, nutrient starvation through the General control non-derepressible 2 (GNC2) pathway, and heme deficiency and oxidative stress through the Heme-regulated eIF2α kinase (HRI) pathway (Beckham et al. 2008, Lian et al. 2009, Narayanaswamy et al. 2009, Moutaoufik et al. 2014). The SG pathway can also be activated during infection to inhibit viral protein translation. During infection, viral dsRNA can be detected by protein kinase R (PKR) (**Figure 1.6A**), which in turn phosphorylates the serine residue in eukaryotic inhibition factor 2α (eIF2α) at position 51 (**Figure 1.6B**) (Nanduri et al. 2000, Dauber et al. 2009). Compared to the unphosphorylated form, the phosphorylated form of eIF2α has a higher affinity for the eukaryotic initiation factor 2B (eIF2B). This higher affinity binding to eIF2B prevents eIF2α from exchanging GDP for GTP, which is essential for recruitment of the initiator methionine transfer RNA (tRNA) (**Figure 1.6C**). Protein phosphatase 1 (PP1) is the primary regulatory protein of eIF2α-induced translational arrest and can directly bind to and dephosphorylate eIF2α to return

the protein to its active state (**Figure 1.6G**). Stalled initiation complexes aggregate forming large granular structures within the cytoplasm referred to as SGs (Kedersha et al. 1999). SGs contain stalled mRNAs, translation initiation factors and small ribosomal subunits along with SG regulatory proteins, such as T cell intracellular antigen-1 (TIA-1) and TIA-1 related protein (TIAR) (**Figure 1.6D**). SG regulatory proteins play an integral role in SG formation and the shuttling of mRNA in and out of SGs (Kedersha et al. 2000). The Ras-GTPase activating protein-binding protein-1 (G3BP1) is essential for SG formation and is activated during cellular stress (Tourriere et al. 2003). SGs are highly dynamic structures that can respond quickly to changes in the cellular environment. The precise composition of SGs varies depending on the stress stimulus (Kedersha et al. 2005). Viruses lack their own translational system and are thus dependent on the host-cell machinery for production of viral proteins (Beckham et al. 2008). Stress-induced translational shut-off by the host, in theory, prevents translation of both cellular and viral proteins, preventing further viral replication. If the infection is not resolved mRNA within SGs can be shuttled to processing-bodies (p-bodies) where they can be targeted for degradation (**Figure 1.6E**) (Balagopal et al. 2009). If the infection is cleared, SGs can disassemble and translation can be reinitiated (**Figure 1.6F**) (Mollet et al. 2008).

1.8.4 Viruses and the stress granule pathway

Host triggered translational-shutoff and SGs are a significant barrier to viral infection, preventing synthesis of viral proteins required for replication and

assembly. For this reason, several viruses express proteins that modulate SG formation and eIF2α phosphorylation. Sendai virus inhibits SG formation by interacting with TIA-1/TIAR through an AU-rich domain in viral RNA transcripts (Iseni et al. 2002). While poliovirus (PV) 3c protease cleaves G3BP1 disrupting SG formation (White et al. 2007). Semliki Forest virus (SFV) and Mammalian orthoreovirus (MRV) inhibit SG formation in a time-dependent manner, with SGs only detectable early in infection (Qin et al. 2009, Qin et al. 2011). Other viruses have been shown to target PKR and eIF2α. Indeed, the African swine fever virus (ASFV) DP71L protein can bind to and recruit PP1c to eIF2α to induce dephosphorylation, while IAV NS1 can bind to dsRNA preventing detection by PKR (Bergmann et al. 2000, Zhang et al. 2010). Alternatively, viruses can also induce SGs to inhibit cellular protein translation and to facilitate viral replication. Respiratory syncytial virus (RSV) replication benefits from the presence of SGs, while Newcastle disease virus (NDV) induces SGs to reduce global host-translation while maintaining viral protein translation by a yet unknown mechanism (Sun et al. 2017).

Within the coronavirinae subfamily MERS-CoV, TGEV and MHV have been investigated for their ability to manipulate the SG pathway. MERS-CoV accessory protein 4a inhibits dsRNA-mediated PKR-dependent SG formation by binding to dsRNA directly. Conversely, MHV has been shown to induce eIF2α phosphorylation and SG formation (Raaben et al. 2007, Rabouw et al. 2016). SGs also appear during TGEV infection with the occurrence of SGs linked to

decreased viral replication (Sola et al. 2011). IBV accessory protein 5b has been shown to inhibit host-cell translation (Kint et al. 2016). Furthermore, previous work has shown that Beau-R infection can induce assembly of SGs, although this was independent of 5b (Kint 2015). Simultaneously, Beau-R infected cells could strongly inhibit sodium arsenite-induced SG formation, suggesting that while IBV infection can induce SGs, the virus also expresses an as yet unknown protein or proteins that can also inhibit their formation (Kint 2015). Collectively, this highlights the dynamic and responsive nature of mRNA movement between active ribosomes, SGs and P-bodies during the IBV life-cycle (Decker et al. 2012).

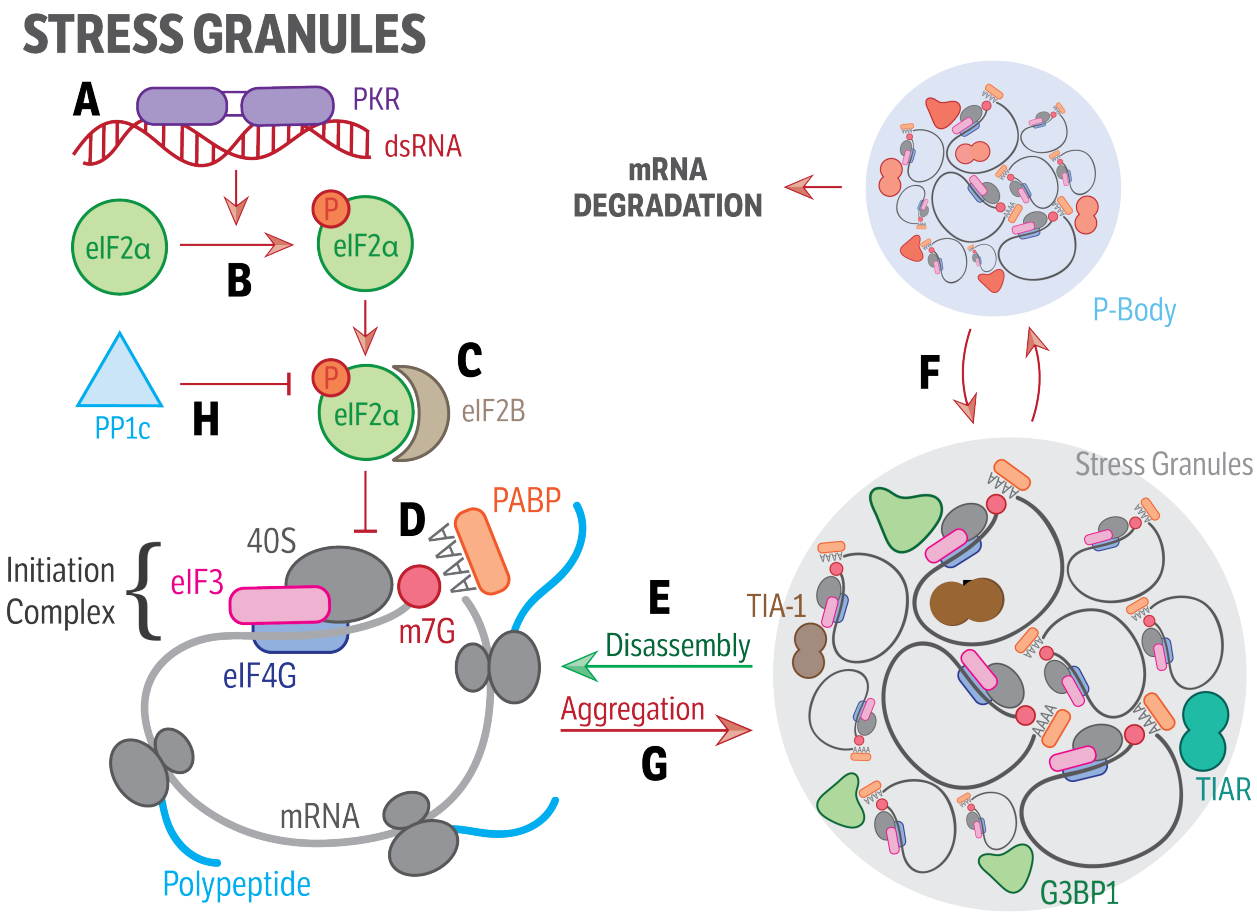

Figure 1.6 Schematic diagram of the stress granule pathway.

(A) Viral dsRNA is detected by the cytosolic sensor, protein kinase R (PKR). (B) PKR mediates phosphorylation of eIF2α (p-eIF2α). (C) When p-eIF2α is recruited to the translation initiation complex, translation is inhibited. (D) Multiple stalled initiation complexes aggregate with stress granule (SG) regulatory proteins such as G3BP1/TIA-1/TIAR to form an SG. (E) If viral infection is cleared, translation can be reinitiated. (F) Alternatively, mRNA can be shuttled to processing bodies (p-bodies) where they can be further stored or degraded. (G) Phosphatase protein 1c (PP1c) dephosphorylates eIF2α, inhibiting translational arrest.

1.8.5 Apoptosis

Apoptosis or programmed cell death (PCD) is a cellular response to extreme stress, wherein cellular homeostasis is no longer viable, and cell death is preferable. During viral infection, the cell can induce apoptosis to reduce viral progeny release, reducing disease outcome in the host. Apoptosis is regarded as the last resort for infected cells, although can be favourable to prevent viral spread and to activate other parts of the immune system (Campisi et al. 2014). Apoptosis is a highly-regulated system that can be triggered by two main pathways; the extrinsic and intrinsic pathways, which are triggered by the activation of the death receptor and through mitochondrial damage, respectively (Thorburn 2004). Each cascade leads to the cleavage of caspase-3, which results in DNA and protein degradation and irreversible apoptosis (**Figure 1.7**) (Cohen 1997). Although both pathways have a role in the immune response to infection, the intrinsic pathway is the primary cellular response to viral infection, for which mitochondria play an important role (Benedict et al. 2002). Mitochondria are the powerhouse of the cell and contain a matrix surrounded by an inner membrane (IM), and an intermembrane space surrounded by an outer membrane (OM). Under normal conditions, these membranes help to protect the cell from catabolic enzymes while also creating an electrical imbalance for adenosine triphosphate (ATP) production (Bertram et al. 2006, Kroemer et al. 2007). The integrity of the mitochondrial membrane is maintained by a balance of anti-apoptotic and pro-apoptotic regulatory factors, including members of the B-cell lymphoma 2 (Bcl-2) protein family. Viral infection can cause a shift in balance from anti- to pro-

apoptotic factors through a range of cellular pathways, including Ca^{2+} release from ER stress and dsRNA detection, while production of reactive oxygen species (ROS) can directly affect mitochondrial membrane integrity (**Figure 1.7A**). ROS and pro-apoptotic factors lead to mitochondrial membrane permeabilisation (MMP) (**Figure 1.7B**), which causes the release of intermembrane proteins including cytochrome C. These factors are released through mitochondrial pores composed of Bcl-2-associated X (Bax) and Bcl-2 homologous antagonist killer (Bak) proteins, as well as mitochondrial channels such as the Voltage-dependent anion channel (VDAC) (**Figure 1.7C**). Once released into the cytoplasm, cytochrome C can recruit apoptosis protease-activating factor 1 (apaf-1) and pro-caspase 9 to form the apoptosome (**Figure 1.7D**). This multiprotein complex leads to stimulation of the apoptosis cascade resulting in activation of cysteine proteases such as caspase 3 and 7. These proteases induce a range of cellular modifications, including membrane blebbing, DNA fragmentation, cellular shrinkage and finally cell death. Mitochondria can also release endonuclease G (EndoG) and apoptosis-inducing factor (AIF) to induce caspase-independent apoptosis (Li et al. 2001, Cande et al. 2004).

1.8.6 Viruses and Apoptosis

Viruses can express both anti-apoptotic proteins and/or pro-apoptotic proteins. Anti-apoptotic proteins increase the length of time that the cell is viable for viral replication, while pro-apoptotic proteins can aid viral release and pathogenicity (Barber 2001, McLean et al. 2008). Indeed, many oncogenic viruses encode anti-

apoptotic proteins to establish persistent infections aiding disease progression and the formation of tumours (Fuentes-Gonzalez et al. 2013). Epstein-Barr virus (EBV) expresses a viral Bcl-2 homologue, BHRF1, which localises to mitochondrial membranes and stabilises membrane integrity by binding to and thus inhibiting pro-apoptotic factors (Kvansakul et al. 2010). While apoptosis is a cellular response to infection and stress, viruses do not necessarily solely inhibit this pathway. Influenza A virus (IAV), protein PB1-F2 and infectious bursal disease virus (IBDV) protein VP5 bind to the outer mitochondrial membrane-bound proteins VDAC1 and VDAC2, respectively. This induces MMP resulting in cytochrome C release and caspase-3 activation (Zamarin et al. 2005, Li et al. 2012). SARS-CoV accessory protein 7a induces caspase-dependent apoptosis by binding to the anti-apoptotic protein B-cell lymphoma extra-large (BcL-X_L). However, the role of SARS-CoV protein 7a during infection is unknown as deletion of 7a does not affect replication or pathogenicity (Tan et al. 2004) (Tan et al. 2007). No anti-apoptotic proteins have been identified for coronaviruses to date, although SARS-CoV has been shown to activate the anti-apoptotic AKT pathway (Mizutani et al. 2004). Caspase-dependent apoptosis has been observed during IBV infection in Vero cells. However, inhibition of apoptosis had no significant effect on IBV titres suggesting that apoptosis is not required for replication *in vitro* (Liu et al. 2001). Furthermore, IBV-induced apoptosis is, in part, inhibited and modulated by the pro-survival IRE1α-XBP1 ER stress pathway, suggesting IBV actively induces apoptosis during infection (Fung et al. 2014).

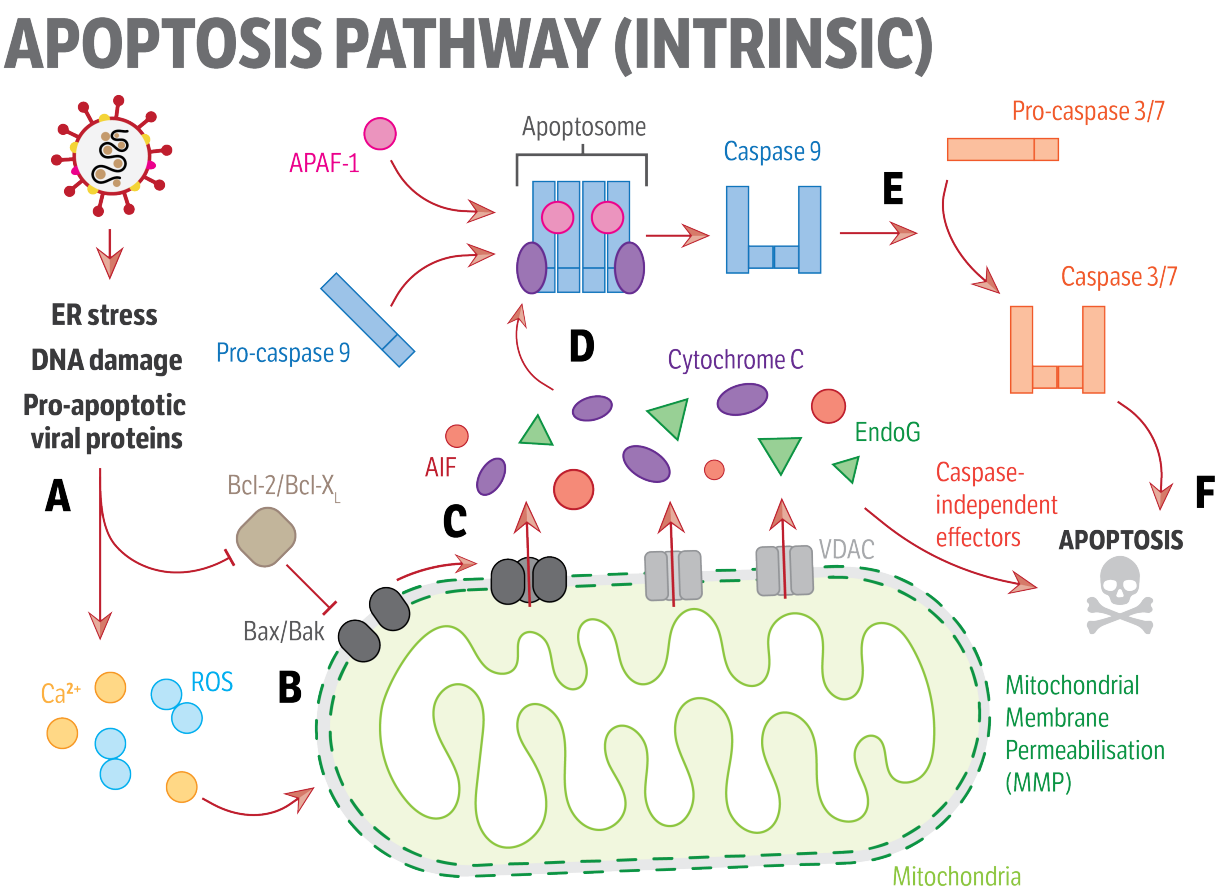

Figure 1.7 Schematic diagram of the intrinsic apoptosis pathway.

(A) Internal stimuli including ER stress, DNA damage or viral pro-apoptotic proteins can increase levels of cytosolic Ca^{2+} and ROS levels or inactivate anti-apoptotic proteins. (B) ROS and Ca^{2+} can permeabilise the mitochondrial membrane directly, while pro-apoptotic proteins can form pores. (C) Permeabilisation releases apoptosis effector proteins including cytochrome C, AIF and EndoG. (D) Cytochrome C assembles with pro-caspase 9 and APAF-1 leading to the formation of the apoptosome. (E) The apoptosome leads to activation of pro-caspase 3/7. (F) Caspase 3/7 along with caspase-independent effectors (AIF, EndoG) mediate a range of cellular changes including DNA fragmentation and membrane blebbing resulting in cellular apoptosis.

1.9 Aims

The aim of this project is to identify any host-cell interaction partners for IBV accessory proteins 3a and 3b that may allude to their function and to determine the role of ORF4b. A series of objectives were established to accomplish this aim.

Objective 1

The first objective is to utilise mass spectrometry to determine any cellular proteins that interact with IBV 3a and 3b that may allude to function.

Objective 2

The second objective is to characterise the role of 3a on the IFN response utilising IFN assays and mass spectrometry data.

Objective 3

To determine if ORF4b is translated into a protein during infection by optimising an antibody raised against the predicted peptide sequence or by using mass spectrometry.

Objective 4

To determine the role of ORF4b or the putative 4b protein using reverse genetics and/or mass spectrometry.

2. Materials and Methods

2.1 Cells and Media

All cell stocks were maintained by the Central Services Unit (Pirbright) or Microbiology Services department (Compton) at The Pirbright Institute and grown at 37 °C and 5% CO_2.

2.1.1 Baby Hamster Kidney 21 (BHK-21) cells

Continuous fibroblast cell line derived from the kidneys of five 1-day-old hamsters (Meager et al. 1977). BHKs were maintained in Glasgow Minimum Essential Media (GMEM) (**Table** 2.1).

2.1.2 Chicken Kidney (CK) cells

Primary CK cells were prepared using a combination of manual and trypsin disaggregation of kidneys collected from 2-3-week-old specific pathogen free (SPF) Rhode Island Red chicks (Oct 14 - Feb 16) or clean VALO chickens (March 16 – March 17) (Maier et al. 2015). CK cells were grown in CK growth media, and experiments performed using 1x N,N-bis[2-hydroxethyl]-2-Aminoethanesulfonic acid (BES) (**Table** 2.2).

2.1.3 DF-1 Cells

DF-1 cells are a continuous cell line of chicken embryo fibroblasts derived from 10-day old East Lansing strain eggs (Himly et al. 1998). DF-1 cells were

maintained in Dulbecco's Modified Eagle's Medium (DMEM) with 10% foetal calf serum (FCS).

2.1.4 Human embryonic kidney 293T (HEK-293T) Cells

A continuous cell line of human embryonic kidney cells stably expressing the SV40 large T-antigen (Shaw et al. 2002). HEK-293Ts were grown and maintained in DMEM with 10% FCS.

2.1.5 Vero cells

A continuous kidney epithelial cell line derived from the African Green monkey (C*hlorocebus spp*.) (Yasumura 1963). Vero cells were maintained in Eagle's Minimum Essential Medium (EMEM) with 10% FCS.

2.1.6 Cell Media

Table 2.1 GMEM for BHK-21 cell culture

Reagent	Final Concentration
GMEM	1x
FCS (Sigma)	1% v/v
Tryptose Phosphate Broth (TPB)	0.29% v/v
Nystatin (Sigma)	250,000 U/L
Penicillin/Streptomycin (Sigma)	100,000 U/L

Table 2.2 1x CK cell maintenance media (1x BES)

Reagent	Final Concentration
10X EMEM (Sigma)	1x
TPB	10% v/v
Bovine serum albumen (BSA) (Sigma)	1% v/v
N,N-bis[2-hydroxethyl]-2-Aminoethanesulfonic acid (BES) (Sigma)	20 mM
Sodium bicarbonate	0.2% w/v
L-glutamine (Gibco)	2 mM
Nystatin (Sigma)	250,000 U/L
Penicillin and streptomycin (Sigma)	100,000 U/L

Table 2.3 CK cell maintenance media (2x BES) for IBV plaque assays

Reagent	Final Concentration
10x EMEM	2x
TPB	20% v/v
BSA (Sigma)	2% v/v
BES	40 mM
Sodium bicarbonate	0.4% w/v
L-glutamine (Gibco)	4 mM
Penicillin/Streptomycin (Sigma)	200,000 U/L
Nystatin (Sigma)	500,000 U/L

2.2 Virological methods

2.2.1 Viruses

IBV Beau-R: A molecular clone of the IBV strain, Beaudette-CK (Beau-CK). Beau-CK has been serially passaged in embryonated eggs to adapt the virus to grow in CK, BHK-21, DF-1 and Vero cells. Beau-R is apathogenic in domestic fowl (Casais et al. 2001).

M41-CK: A pathogenic strain of IBV that has been adapted to grow in CK cells. M41-CK is unable to grow in BHK-21, DF-1 or Vero cells.

M41-K/M41-R: Molecular clones of M41-CK. M41-K is pathogenic, while M41-R is non-pathogenic.

BeauR-Sc3aAUG: Beau-R with the 3a AUG start codon scrambled (ATG>AAC) (Hodgson et al. 2006).This virus is unable to express IBV 3a.

BeauR-Sc3bAUG: Beau-R with the 3b AUG start codon scrambled (ATG>AAC). This virus is unable to express IBV 3b.

M41K-del4b: M41-K with ORF4b deleted. The non-canonical TRS is still present, so a shorter sgRNA is expressed that does not contain ORF4b. This virus was designed and generated by Sarah Keep.

M41K-BeauR(S): M41-K virus containing the S gene from Beau-R instead of M41-K. This virus can grow in Vero cells, unlike M41-K due to extended host range of Beau-R spike.

BeauR (M41R-IR): Recombinant IBV based on Beau-R with the intergenic region (IR) from the M41-K strain of IBV. The IR is the region in-between gene M and gene 5 and contains ORF4b.

2.2.2 IBV titration

Plaque assays were performed in CK cells in a 12-well plate (70-80% confluence). Virus samples were serially diluted in 1x BES by a factor of 10, up to 10^{-7}. Three wells were inoculated for each dilution. Cells were washed twice with Phosphate Buffered Saline a (PBSa) and 250 µl of inoculum added to the cells. Cells were incubated at 37 °C and 5% CO_2 for 1 hour. Viral inoculum was then removed and 2 ml of 1% agar,1x BES was added to each well. Cells were incubated for three days at 37 °C and 5% CO_2. To fix the cells, 10% paraformaldehyde (PFA) in PBSa was overlaid onto to the agar and incubated for 15 minutes. Agar was removed from each well and cells stained with 0.1% crystal violet (w/v) for 10 minutes. Single defined plaques were counted for the lowest serial dilution and averaged from three wells. The number of plaques is expressed as viral plaque forming units (PFU) per ml of viral inoculum.

2.2.3 Growth curves

The M41K-del4b growth curve virus was completed by Sarah Keep, as part of the quality control for synthesis of recombinant IBV. CK cells were seeded in a 12-well plate (70-80% confluency) and infected at an MOI of 0.1, diluted in 1x BES. After 1 hour at 37 °C, the inoculum was removed and fresh 1x BES added. The cell media was harvested at 1, 24, 48, 72 and 96 h.p.i. Viral titre was calculated by CK plaque assay (**2.2.2**). Growth titres were averaged from three biological replicates.

2.3 Reagents

2.3.1 Expression vectors

Expression vectors were either cloned or a gift and were used in western blotting and/or immunofluorescence experiments (**Table** 2.4). Construction of vectors is described in 2.4 below and confirmed by Sanger sequencing (Source Bioscience) (**Table** 2.17).

Table 2.4 List of plasmids used for immunofluorescence, western blot and mass spectrometry.

Plasmid	Expression	Tag/ reporter	Source
pEGFPC2-3aB	Beau 3a	GFP N-terminal	Cloned
pEGFPN1-3aB	Beau 3a	GFP C-terminal	Cloned
pEGFPC2-3aM	M41 3a	GFP N-terminal	Cloned
pEGFPN1-3aM	M41 3a	GFP C-terminal	Cloned
pEGFPC2-3bB	Beau 3b	GFP N-terminal	Cloned
pEGFPN1-3bB	Beau 3b	GFP C-terminal	Cloned
pEGFPC2-3bM	M41 3b	GFP N-terminal	Cloned
pEGFPN1-3bM	M41 3b	GFP C-terminal	Cloned
pEGFPC2-4bB	Beau 4b	GFP N-terminal	Cloned
pEGFPC2-4bM	M41 4b	GFP N-terminal	Cloned
pEGFPN1-4bM	M41 4b	GFP C-terminal	Cloned
pFLAG-CMV2-3aB	Beau 3a	FLAG N-terminal	Mark Davis (Davies 2009)

Plasmid	Expression	Tag/ reporter	Source
pCAGGS-NS1	IAV NS1	N/A	Gift from Joe James
peIF-V5-chIRF7	chIRF7-V5	V5 N-terminal	Gift from Steve Goodbourne
pRL-CMV vector	Renilla	N/A	Promega, gift from Jess Purcell
pEF1a-FLAG-chMAVS	chMAVS-FLAG	FLAG	Gift from Steve Goodbourne
pLUC-chIFNβ-promoter	chIFNβ promoter - luciferase	Luciferase C-terminal	Gift from Steve Goodbourne

2.3.2 Antibodies

Antibodies were used for labelling of cellular or viral targets for western blotting and/or immunofluorescence (**Table** 2.5). Antibodies were diluted in blocking buffer at the specified concentration.

Table 2.5 Primary antibodies used for immunofluorescence and western blot.

Antibody	Target	Application	Dilution	Source
Anti-dsRNA (J2)	dsRNA	IF	1:1000	Scicons
Anti-3a (JH3480)	IBV 3a	IF/WB	1:1000/1:5,000	Gift from Carolyn Machamer (Pendleton et al. 2005)

Antibody	Target	Application	Dilution	Source
Anti-N (48.8)	IBV N	IF/WB	1:500/1:1000	Acris Antibodies
Anti-4b	4b (M41)	IF/WB	1:50/1:100	Cambridge Research Biochemicals
Anti-GFP	GFP			Santa Cruz
Anti-V5	V5 Tag	IF/WB	1:200/1:500	Santa Cruz
Anti-FLAG (M2)	FLAG tag	IF/WB	1:500/1:1000	Sigma
Anti-MDA5	huMDA5	WB	1:200	Sigma
Anti-MAVS (E-3)	huMAVS	IF/WB	1:200	Santa Cruz
Anti-IRF3 (C-20)	huIRF3	IF/WB	1:500	Santa Cruz
Anti-IRF7 (C-20)	huIRF7	IF/WB	1:500	Santa Cruz
Anti-CANDI (48)	CANDI	IF/WB	1:1000	Santa Cruz
Anti-RNF5 (G-15)	RNF5	IF	1:100	Santa Cruz
Anti-RPS25 (C-16)	RPS25	IF/WB	1:250	Santa Cruz
Anti-G3BP1 (611126)	G3BP1	IF	1:500	Invitrogen
Anti-G3BP1	G3BP1	IF	1:200	Abcam
Anti-eIF2α	P-eIF2α	WB	1:500	GeneTex
Anti-LAP2 (Y-20)	LAP2	IF	1:200	Santa Cruz
Anti-β-Actin	β-Actin	IF/WB	1:10,000	Cell Signalling technology
Anti-FNDC3a	FNDC3a	IF	1:200	Santa Cruz
Anti-SUCGL2	SUCGL2	IF	1:200	Santa Cruz

IBV specific antibodies (blue), epitope tag antibodies (red), interferon-related antibodies (green), translation-related antibodies (purple), miscellaneous (grey). Clone number for monoclonal antibodies are noted in parentheses.

2.4 Cloning

2.4.1 Primers and DNA fragments

Primers (Sigma) were designed to amplify specific IBV cDNA sequences (**Table 2.6**). DNA fragments were designed and ordered from GeneArt (Invitrogen).

Table 2.6 Primers and DNA fragments for accessory protein expression plasmids.

Primers/DNA fragments	Direction	Sequence (5′ – 3′)	Restriction Site (Bold)
GFP-3aB	FWD	CATG**AAGCTT**GATGATCCAAAGTCCCACGTCC	HindIII
	REV	GTAC**CCGCGG**TTAGTCTAGACTGTGCCAAAGGG	SacII
GFP-3aM	FWD	CATG**AAGCTT**GATGATTCAAAGTCCCACGTCC	HindIII
	REV	GTAC**CCGCGG**TTAGTCTAGACTGTGACAAAGGGTCAG	SacII
GFP-3bB	FWD	CATG**AAGCTT**GATGTTAAACTTAGAAGTAATTATTGAAACTGG	HindIII
	REV	GTAC**CCGCGG**TTATTCAATAAATTCATCATCACCTG	SacII
GFP-3bM	FWD	CATG**AAGCTT**GATGTTAAACTTAGAAGCAATTATTGAAACTGG	HindIII
	REV	GTAC**CCGCGG**TTATTCAATAAATTCATCATCACCTG	SacII
GFP-4bM	FWD	CATG**AAGCTT**GATGTGTGTGTGTAGAGAGTATTTAAAATTATTC	HindIII
	REV	GTAC**CCGCGG**TTAATCTTTTTTATAACTCAACCACAACC	SacII

Primers/DNA fragments	Direction	Sequence (5′ – 3′)	Restriction Site (Bold)
4bB-C2	Fragment	CATG**AAGCTT**ATGTGTGTGTGTAGAGA GTATTTAAAATTATTCTTTAATAGCGC CTCTGTTTTAAGAGCGCATAAGAGTAT TTATTTTGAGGATACTAATATAAATCC TCTTTGTTTTATACTCTCCTTTCAAGA GCTATTAACGGTGTTACCTTTCAAGTA A**GGATCC**CATG	HindIII / BamHI
3aB-GFP	FWD	CATG**AAGCTT**ACCATGATCCAAAGTCC CACGTCC	HindIII
	REV	GTAC**CCGCGG**GTCTAGACTGTGCCAAA GGG	SacII
3aM-GFP	FWD	CATG**AAGCTT**ACCATGATTCAAAGTCC CACGTCC	HindIII
	REV	GTAC**CCGCGG**GTCTAGACTGTGACAAA GGGTCAG	SacII
3bB-GFP	FWD	CATG**AAGCTT**ACCATGTTAAACTTAGA AGTAATTATTGAAACTGG	HindIII
	REV	GTAC**CCGCGG**TTCAATAAATTCATCAT CACCTG	SacII
3bM-GFP	FWD	CATG**AAGCTT**ACCATGTTAAACTTAGA AGCAATTATTGAAACTGG	HindIII
	REV	GTAC**CCGCGG**TTCAATAAATTCATCAT CACCTG	SacII
4bM-GFP	FWD	CATG**AAGCTT**ACCATGTGTGTGTGTAG AGAGTATTTAAAATTATTC	HindIII
	REV	GTAC**CCGCGG**ATCTTTTTTATAACTCA ACCACAACC	SacII

Start codon (green), Stop codon (red), Kozak sequence (purple).

2.4.2 Reverse transcription

Cellular and viral RNA was isolated from the supernatant of infected cells using RNA clean-up protocol from the RNeasy Mini Kit (Qiagen). RNA was first incubated with random primer for 5 minutes at 65 °C (**Table** 2.7). Superscript III reverse transcriptase (Life Technologies) was then added to the reaction mix (**Table** 2.8) to reverse transcribe total RNA into cDNA as per the manufacturer's instructions (**Table** 2.9).

Table 2.7 Reagent mix for first strand cDNA synthesis (I)

Reagent	Volume (µl)
Random Primer (10 µm)	1
dNTPs (10 µm)	1
RNA	5
Water	6

Table 2.8 Reagent mix for first strand cDNA synthesis (II)

Reagent	Volume (µl)
First Strand Buffer (Invitrogen)	4
Dithiothreitol (DTT) (0.1 M)	1
RNase Out (Life Technologies)	1
Superscript III reverse transcriptase (Life Technologies)	1
Water	10

Table 2.9 Reverse transcription thermal cycle

Temperature	Time
25 °C	10 minutes
50 °C	1 hour
70 °C	15 minutes

2.4.3 Polymerase chain reaction

Polymerase chain reaction (PCR) was used to amplify specific DNA sequences in IBV or vaccinia virus (VV) cDNA. PCR was performed using Q5 (NEB) high-fidelity DNA polymerase (**Table** 2.10), using a thermal cycler (Applied Biosciences 2720) and cycle program per the manufacturer's instructions (**Table** 2.11).

Table 2.10 Reagent concentrations for PCR

Reagent	Final concentration (50 µl Reaction volume)
Q5 Buffer (5x) (NEB)	1x
dNTPs (10 mM)	200 µM
Primers (Forward and back)	25 µM
Q5 Taq (NEB)	0.02 U/µl
cDNA	5 µl

Table 2.11 PCR thermal cycle

Cycles	Temperature	Time
1	95 °C	2 minutes
25	95 °C	30 seconds
	Highest primer Tm -5 °C	30 seconds
	72 °C	1 minute/kb of template length
1	72 °C	10 minutes

2.4.4 Site-directed mutagenesis

Site-directed mutagenesis (SDM) was performed using the QuikChange II Site-Directed Mutagenesis Kit (Agilent) as per the manufacturer's instructions. Primers for SDM were 25-40 nucleotides in length and designed to have a high GC content (>40%) and melting temperature (Tm) (>78 °C).

Table 2.12 Reagent concentrations for SDM

Reagent	Final Concentration (Reaction volume 50 µl)
SDM reaction buffer (Aligent)	1x
dNTPs (Aligent)	10 mM
Primers (Forward and Reverse)	25 µM
Pfu Turbo (Agilent)	2.5 units
Vector	10 ng

Table 2.13 SDM thermal cycle

Cycles	Temperature	Time
1	95 °C	1 minute
16	95 °C	50 seconds
	60 °C	50 seconds
	68 °C	1 minute/kb of template length
1	68 °C	7 minutes

The sizes of the PCR products were confirmed by gel electrophoresis (0.6% agarose gel). Once confirmed the PCR products were digested with 2 µl of *Dpn*I (10 U) to digest methyl groups that will only be present on parent plasmid.

2.4.5 Agarose gel electrophoresis

DNA was separated and visualised using gel electrophoresis. Each gel contained 0.8-1% agarose dissolved in 1x Tris-borate EDTA (TBE) buffer (Invitrogen) or 1x Tris-acetic acid EDTA (TAE) buffer (Invitrogen) with 1x SYBR Safe (ThermoFisher). DNA loading buffer (**Table** 2.14) was added to each sample and loaded into a well. A 1 kb+ DNA ladder (Invitrogen) was added to a separate well to determine DNA size. The gel was submerged in TBE or TAE buffer, respectively, and a 150V current applied for 1 hour or until effective separation was seen. DNA was visualised by exposing the gel to 260 nm UV light.

Table 2.14 Recipe for DNA loading buffer

Reagent	Final concentration
Glycerol	60% v/v
Ficoll 400	25 µM
Bromophenol blue	15 mM

2.4.6 Restriction digest

Restriction digests were performed at 37 °C for 1 hour in the appropriate digestion buffer as per NEB instructions (NEB Double Digest Finder). For incompatible restriction enzymes, reactions were purified using the Nucleotide Removal Kit (Qiagen) and protocol in-between digests. Enzymes were deactivated by heating to 50 °C for 10 minutes before ligation and transformation.

2.4.7 Gel extraction/ PCR purification

PCR products and digested DNA fragments were purified and cleaned using the QIAquick PCR Purification Kit (Qiagen). PCR products were diluted in 30 µl of water and quantity calculated using the Nanodrop 1000. For purification of DNA fragments from digested plasmids, DNA was first separated by gel electrophoresis in a 0.8% TAE gel with 4 µl of SYBR Safe (ThermoFisher). DNA was extracted from exercised gel segments using the QIAquick Gel Extraction Kit (Qiagen) and protocol. DNA was reconstituted in 20 µl of RNase-free water and quantified using the Nanodrop 1000.

2.4.8 PCR purification

Plasmid DNA was purified using the PCR purification kit and protocol (QIAGEN) as per the manufacturer's instructions and eluted in 30 µl of RNase-free water.

2.4.9 DNA dephosphorylation

Digested plasmid was dephosphorylated before ligation to prevent self-ligation using shrimp alkaline phosphatase (Promega), per the manufacturer's instructions.

2.4.10 Ligation

T4 ligase (NEB) was used for ligation per the manufacturer's instructions (**Table** 2.15). An insert: vector molar ratio of 3:1 was used, and the reaction was performed at either room temperature for 3 hours or overnight at 4 °C.

Table 2.15 Reagent mix for ligation

Reagent	Volume
T4 DNA ligase (NEB)	1 µl
10x DNA ligase buffer (NEB)	2 µl
Vector DNA	50 ng
Insert DNA	3:1 Vector: insert ratio
Nuclease-free water	To final 20 µl volume

2.4.11 Transformation

Plasmids were transformed into DH5α-T1R library competent *E. coli* (NEB). After ligation, 5 µl of the sample was added to 50 µl of competent cells and incubated on ice for 30 minutes. The cells were then heat-shocked at 42 °C for 30 seconds before incubating on ice for 2 minutes. SOC media (Invitrogen) (350 µl) was added to the competent cells and incubated at 37 °C for 1 hour in a shaking incubator. After 1 hour, 350 µl of the transformation mix was plated onto Lysogeny broth-agar (LB-agar) plates containing ampicillin (100 µg/ml) or kanamycin (50 µg/ml). The plates were incubated for 16 hours at 37 °C.

Table 2.16 Reagent concentrations for Lysogeny broth

Component	Final concentration
Bacto tryptone	1% w/v
Yeast extract	0.5% w/v
NaCl	170 mM

2.4.12 DNA miniprep

Colonies were picked from LB-agar plates and placed in 5 ml of LB containing either ampicillin (100 µg/ml) or kanamycin (50 µg/ml). Cultures were incubated at 37 °C on a shaker overnight. Bacterial cultures were placed in a 15 ml falcon and centrifuged at 1,000 × g for 5 minutes to pellet the bacteria. Plasmids were then purified using the Plasmid Miniprep Kit (Qiagen) and protocol. Plasmids were

eluted in 50 µl of sterile RNase-free water. Plasmids were then sequenced by Sanger sequencing.

2.4.13 DNA maxiprep

Colonies were picked and grown in 2 ml of LB containing ampicillin (100 µg/ml) or kanamycin (50 µg/ml) for 8 hours. After which, 1 ml was then transferred to 100 ml of LB containing either ampicillin (100 µg/ml) or kanamycin (50 µg/ml) and incubated overnight on a shaker at 37 °C. Plasmids were then extracted and purified using the Plasmid DNA Maxiprep Kit (Qiagen) and protocol. Plasmids were reconstituted in 50 µl of RNase-free water. DNA concentration was determined using the NanoDrop 1000.

2.4.14 Sequencing

Plasmids were sent to Source Bioscience for sequencing by Sanger sequencing. Primers for sequencing of plasmids were provided by Source Bioscience. For sequencing of IBV specific sequences, primers were designed and ordered from Sigma. The sequences of primers are below (**Table** 2.17).

Table 2.17 Primers used for sequencing of expression vectors and IBV cDNA

Primer	Sequence (5'- 3')	Sequencing Region	Direction
EGFP_C_FWD	CATGGTCCTGCTGGAGTTCGTG	pEGFPC2 MCS	FWD
EGFP_C_REV	GTTCAGGGGGAGGTGTG	pEGFPC2 MCS	REV
EGFP_N_REV	CGTCGCCGTCCAGCTCGACCAG	pEGFPN1 MCS	REV
pEF1a_FWD	ATTTGCCCTTTTTGAGTTTGG	pEF1a MCS	FWD
CMVF_pCDNA3	CAACGGGACTTTCCAAAATG	pcDNA6.1 MCS	FWD
M42	CACCAACAACAACACCTAG	M41 ORF3ab	FWD
M43	CTTCCATTTTCCTCTAGCG	M41 ORF3ab	REV
M46	GCATCCAAGTTATGAGGATTG	M41 ORF4b	FWD
M47	GTTAGCGGGCTGGTCCTGTTCC	M41 ORF4b	REV
BG-69	CGAAAACGGTGATAATAGAAG	Beau-R ORF3ab	FWD
BG-142	AGGGATCAAATACTTCTGTG	Beau-R ORF3ab	REV
BG-56	GTTGTCGGCGGGTTTCTTC	IBV 3′-end FWD	FWD
93/100	GCTCTAACTCTATACTAGCCT	IBV 3′-end FWD	REV

FWD – Forward primer, REV – Reverse primer, MCS – multiple cloning site, Source Bioscience primers (blue), in-house designed primers (red)

2.5 Transfection

DF-1 or Vero cells were seeded on coverslips in a 24-well plate, 12-well plate or 6- well plate (70-80% confluence). Cells were washed once with PBSa and fresh growth media added to each well. Cells were transfected with expression vectors (**Table** 2.4), using Lipofectamine 2000 (Invitrogen) at a ratio of 1:3 DNA (μg) to lipofectamine (μl) and per the manufacturer's instructions. After 16-24 hours at 37 °C, the cells were washed twice with cold PBSa before processing.

2.6 Western blotting

2.6.1 Proteasome inhibitor

To inhibit the cellular proteasome during infection, 5 – 20 μm of MG132 (Sigma) dissolved in DMSO was added to cell media, 6 – 12 hours before harvesting. DMSO alone was added in equal volumes as a control. To inhibit the proteasome during transfection, media was removed and fresh media containing 5 – 20 μm MG132 was added to each well 4 – 8 hours before lysing cells. Mock transfected cells were replenished with fresh media containing DMSO.

2.6.2 Cell lysis

Cells were washed once with cold PBSa before being lysed with cold RIPA lysis buffer (**Table** 2.18) with 1x protease inhibitor cocktail (PIC) (ThermoFisher) added immediately before use. Lysis buffer containing phosphatase inhibitor cocktail (Sigma) was added for analysis of anti-eIF2α(P) levels. Cells were either harvested by adding 100 μl lysis buffer directly to the well or cell were scraped into cold PBSa and pelleted at 10,000 x g for 2 minutes before lysis. Cells were incubated in lysis buffer on ice for 20 minutes with regular agitation, centrifuged at 14,000 x g to pellet debris and lysates stored at -20 °C.

Table 2.18 Reagent composition of RIPA lysis buffer

Reagent	Final concentration
Sodium chloride (NaCl)	5 M
Trisaminomethane hydrochloric acid (Tris-HCl) buffer (pH 7.4)	1 M
Igepal	5% v/v
Sodium deoxycholate ($C_{24}H_{39}NaO_4$)	5% w/v
Sodium orthovanadate (Na_3VO_4)	1 M
Sodium fluoride (NaF)	1 M
PIC (added immediately before use)	1x

2.6.3 SDS-PAGE

Cell lysates were denatured using 1x Laemmli Sample Buffer (BIO-RAD) containing 5% Beta-mercaptoethanol and heating at 80 °C for 10 minutes. Samples were then loaded onto a Mini-PROTEAN TGX 4% - 20% gradient Precast gel (BIO-RAD) with Tris/Glycine SDS running buffer (**Table** 2.19). The gel was electrophoresed at 150V for 50 minutes.

Table 2.19 SDS Running Buffer

Reagent	Final Concentration
Glycine	1.92 M
Tris-HCl buffer (pH 7.4)	247 mM
SDS	34 mM

2.6.4 Western Blotting

Protein samples were transferred onto a 0.2 µm nitrocellulose membrane (BIO-RAD) using the Trans-Blot Turbo System (BIO-RAD) and 1x Trans-Blot turbo transfer buffer (BIO-RAD). Membranes were blocked for 1 hour at room temperature or overnight at 4 °C in either 5% milk powder (w/v) (Marvel) or 2% fish gelatine (w/v) (Sigma), both diluted in 0.1% Tween in PBSa (PBS-T). Membranes were labelled with primary antibodies (**Table** 2.5) diluted in either 5% milk powder or 2% fish gelatine blocking solution for 1 hour and then washed three times for 15 minutes in PBS-T. Secondary fluorescent IRDye antibodies (LI-COR) were added at a concentration of 1:10,000, diluted in PBS-T for 1 hour in the dark. Membranes were washed three times with PBS-T for 15 minutes and then washed once with sterile water. Membranes were visualised and quantified using the Odyssey Clx Imaging System and Image Studio software (LI-COR). The fluorescence of the protein of interest was normalised against actin or a viral protein, giving semi-quantification of protein levels.

2.7 Indirect Immunofluorescence

2.7.1 Fixation

DF-1 or Vero cells were seeded on glass coverslips in a 24-well plate (70-80% confluency). Cells were inoculated with 125 μl of IBV or transfected with 0.5 - 2 μg of an expression vector. Cells were washed once with PBSa and then fixed for 20 minutes with 0.5 ml of 4% paraformaldehyde (PFA) in PBSa. For staining mitochondria, cells were incubated with MitoTracker Red CMXRos (ThermoFisher) at a final concentration of 400 nM in media for 30 minutes before fixing.

2.7.2 Labelling

For intracellular labelling, cells were permeabilised with 0.1% Triton X-100 (Sigma) in PBSa for 10 minutes. After permeabilisation, cells were washed twice with PBSa and blocked for 1 hour using 0.5% BSA in PBSa on a shaker at 4 °C. Subsequently, cells were incubated with primary antibody (**Table** 2.5) for 1 hour, diluted to a working concentration in 0.5% BSA in PBSa. For labelling of IBV 4b, cells were incubated with anti-4b overnight at 4 °C. Cells were then washed three times for 5 minutes with PBSa. Alexa Fluor secondary antibodies (Invitrogen) were diluted in 0.5% BSA in PBSa to 1:500 and cells incubated in the dark for 1 hour on a shaker. Cells were washed three times for 5 minutes with PBSa. The nuclei of the cells were labelled with DAPI (4',6-diamidino-2-phenylindole) (1:20,000) or TO-PRO-3 iodide (1:10,000) (ThermoFisher) diluted in sterile water or PBSa respectively. Cells were washed once with sterile water for 5 minutes

then mounted upside down onto glass microscope slides with Vectashield Antifade Mounting Media (Vector Laboratories) and sealed with nail varnish. Cells were visualised and imaged using a Leica SP5 confocal microscope.

2.7.3 Image Analysis

Fluorescence signal was measured using the ImageJ software and Coloc2 plug-in. A region of interest was selected and levels of each fluorescence signal quantified. Colocalisation of the signal was also calculated using the Coloc2 plug-in. A region of interest was selected and percentage of the fluorescent signal that colocalises with a secondary signal calculated. In total, colocalisation was measured in 20 randomly selected cells, and average percentage determined.

2.8 Immunoprecipitation

2.8.1 Cell lysis

Cells were infected or transfected as described in 2.5 above. Cells were washed once with cold PBSa and then harvested in 1 ml of cold PBSa and centrifuged at 2,500 x g for 2 minutes. Pierce lysis buffer (25 µl/cm^2) (**Table** 2.20) with 1x Protease Inhibitor Cocktail (PIC) was added directly to the cells and placed on ice on a shaker for 20 minutes with extensive pipetting every 5 minutes. For lysis of cells for dsRNA immunoprecipitation, RIP RNA lysis buffer (25 µl /cm^3) (**Table** 2.21) was used with fresh 1x PIC and RNase (Invitrogen) added.

Table 2.20 Reagent composition of Pierce lysis buffer

Reagent	Final concentration
Tris-HCL buffer (pH 7.4)	25 mM
NaCl	150 mM
EDTA	1 mM
Igepal	1% v/v
Glycerol	5% v/v
PIC (added immediately prior to use)	1x

Table 2.21 Reagent composition of RNA RIPA buffer

Reagent	Final concentration
NaCl	100 mM
Tris-HCl (pH 7.4)	10 mM
EDTA	1 mM
Igepal	0.5% v/v
PIC (added immediately prior to use)	1x
RNaseI (added immediately prior to use)	100 units/ml

2.8.2 Immunoprecipitation (IBV 4b)

Cell lysates were incubated with 10 μl of anti-4b overnight at 4 °C with regular agitation. Samples were incubated for 4 hours with 50 μl of Protein G Dynabeads (ThermoFisher). Dynabeads were separated using a magnetic separator and supernatant discarded. Beads were washed three times with IP wash buffer (**Table** 2.22). Protein-antibody complexes were eluted using 50 μl of 200 mM glycine (pH 2.5).

Table 2.22 Reagent composition of IP wash buffer

Reagent	Final Concentration
Tris-HCl (pH 7.4)	10 mM
NaCl	150 mM
EDTA	0.5 mM

2.9 Reverse genetics system

2.9.1 pGPT vectors

Plasmids (pGPT) containing the desired IBV mutation with a xanthine-guanine phosphoribosyltransferase (gpt) gene from E. coli were constructed. The pGPT vector is used to insert the mutation into a recombinant vaccinia virus (rVV) containing the full-length IBV cDNA genome. The pGPT-FullTRS4b was constructed by ligating a DNA fragment containing a full TRS (CTGAACAA) sequence (GeneArt, Invitrogen) into a SalI digested pGPT vector. For the synthesis of pGPT-Sc3aM, primers were designed to amplify a 678bp fragment from M41 cDNA. The 3a start codon was situated in the middle of the DNA fragment. This fragment was then cloned into a pGPT vector using SalI restriction sites. Site-directed mutagenesis was then used to mutate the 3a start codon from ATG to AAC in the pGPT vector (**Table** 2.23).

Table 2.23 DNA fragments and primers for the synthesis of pGPT expression vectors.

Primer/ DNA fragments	Sequence (5′ – 3′)	Mutation
M41 3a Primers	GTAC**GTCGAC**CCCAAAAATTACCTCCTCTG CATG**GTCGAC**GCTACCAGACTTTGACAAATTC	
Sc3aAUG SDM Primers	CAGACCTAAAAAGTCTGTTTAAACATTCAAAGTCC CACGTCC GTCTGGATTTTTCAGACAAATTTGTAAGTTTCAGG GTGCAGG	ATG > AAC

SalI restriction sites (purple), mutated sequences (red), non-canonical TRS (green).

2.9.2 Transfection and infection

Recombinant vaccinia virus (VV) containing the M41 cDNA was sonicated for 2 minutes and diluted in 500 µl of EMEM to an MOI of 0.2. Vero cells seeded in a 6-well plate (70% confluence) were infected with rVV-M41-K in duplicate and left for 2 hours at 37 °C and 5% CO_2. Vero cells were washed twice with OPTI-MEM (Invitrogen) and transfected with 10 µg of pGPT vector using Lipofectin (Life Technologies) at a ratio of 1:2.4 DNA (µg): lipofectamine (µl) per the manufacturer's instructions (**Figure 2.1A**). Vaccinia replicates in the cytoplasm of the cell. The cells were incubated at 37 °C for 90 minutes then washed with and 5 ml of fresh 1x EMEM added. After overnight incubation at 37 °C, MXH selection reagents (75 µM mycophenolic acid (MPA), 165 µM Xanthine, 184 µM Hypoxanthine) were added to each well and incubated for a further two days at 37 °C to allow the first homologous recombination event to occur (**Figure 2.1B**). After incubation, the cells were carefully scraped off the wells and pipetted into a screw cap vial. Samples were stored at -20 °C.

2.9.3 Transient dominant selection

Vero cells were inoculated with serial dilutions of the recombinant VV generated above (10^{-1}, 10^{-2}, 10^{-3}) in 500 µl of 1x EMEM. The inoculum was removed after 2 hours at 37 °C. Cells were then overlaid with 1% agar, 1x EMEM and MXH selection media (**Table** 2.24) and incubated for three days. Cells were stained with 0.01% neutral red in 1x EMEM and 1% agar and placed back in the incubator for 24 hours. Single isolated plaques were picked using a cut 1 ml pipette tip and

stored in 400 µl of 1x EMEM at -20 °C. Further two rounds of plaque purification in the presence of MXH was performed using isolated plaques from the previous round (**Figure 2.1C**). The plaques were then grown in the absence of selection reagents, to induce the second homologous recombination event, this is performed three times using plaques from the previous round (**Figure 2.1D**).

Table 2.24 MXH selection media for TDS

Reagent	Final Concentration
2x E-MEM	1x
2% Agar	1% w/v
MPA (Mycophenolic Acid)	75 µM
Xanthine	165 µM
Hypoxanthine	184 µM

2.9.4 BHK stocks

Two recombinant VV isolates with the desired mutation in the IBV cDNA were selected for further processing. BHKs were seeded into 11x T150s flasks (70-80% confluency). Each flask was inoculated with 2 ml of rVV at an MOI of 0.1 diluted in 1x GMEM. The cells were incubated at 37 °C with the inoculum for 2 hours with regular rocking. After incubation, 25 ml of GMEM was added, and flasks were incubated until extensive CPE was visible. BHK cells were agitated to release any attached cells. The supernatant was pooled and transferred to 50 ml falcons. Cells were pelleted by centrifugation at 500 x g for 20 minutes at 4 °C. The supernatant

was removed and the cell pellet resuspended in 11 ml of TE buffer (pH 9.0) (**Table** 2.25). A stock of 1ml of rVV was stored at -80 °C.

2.9.5 Ministocks

After plaque purification, ministocks of the recombinant VV were grown for GPT screening and mutation sequencing. Recombinant VV with the most diverse lineage possible were screened to increase the chance of a identifying a successful recombination event. Vero cells were infected with 150 µl of rVV in 500 µl 1x BES for 2 hours at 37 °C. Afterwards, 1x BES was added and cells incubated for four days or until cytopathic effect (CPE) was visible. The cells were then carefully scraped off the well into the media and placed in a screw-capped vial. Viral stocks were deactivated and DNA extracted using the QIAmp DNA mini kit (Qiagen) and protocol. Extracted DNA was then screened by PCR for the absence or presence of the GPT gene and the presence of the IBV region containing the desired mutation (**Figure 2.1E**). Any samples lacking GPT and containing the region of interest were sequenced to confirm the mutation in the recombinant VV.

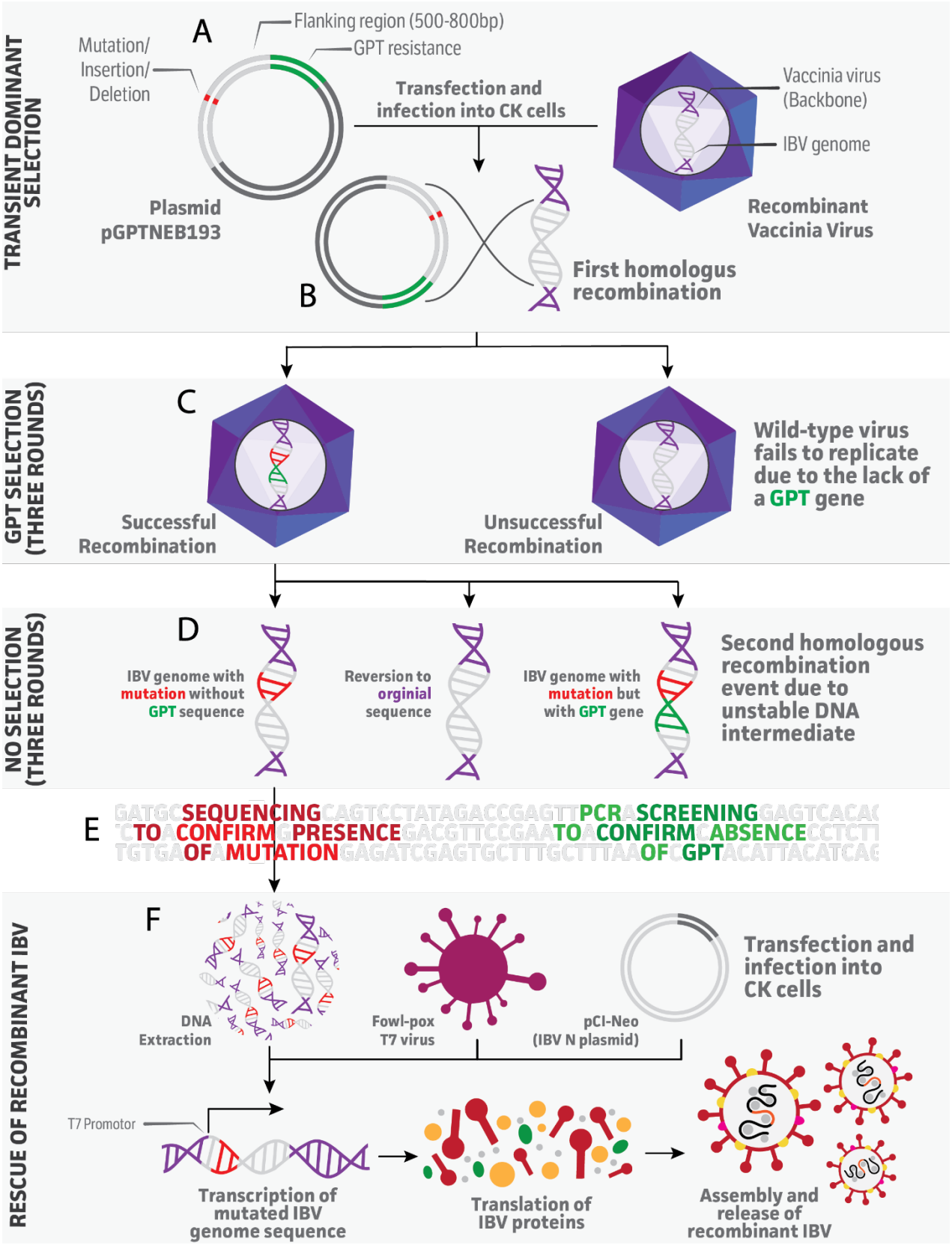
TRANSIENT DOMINANT SELECTION
A
Flanking region (500-800bp)
GPT resistance
Mutation/
Insertion/
Deletion
Transfection and
infection into CK cells
Vaccinia virus
(Backbone)
IBV genome
Plasmid
pGPTNEB193
Recombinant
Vaccinia Virus
B
First homologus
recombination
GPT SELECTION (THREE ROUNDS)
C
Successful
Recombination
Unsuccessful
Recombination
Wild-type virus
fails to replicate
due to the lack of
a GPT gene
NO SELECTION (THREE ROUNDS)
D
IBV genome with
mutation without
GPT sequence
Reversion to
orginial
sequence
IBV genome with
mutation but
with GPT gene
Second homologous
recombination
event due to
unstable DNA
intermediate
E
SEQUENCING
TO CONFIRM PRESENCE
OF MUTATION
PCR SCREENING
TO CONFIRM ABSENCE
OF GPT
RESCUE OF RECOMBINANT IBV
F
DNA
Extraction
Fowl-pox
T7 virus
pCI-Neo
(IBV N plasmid)
Transfection and
infection into
CK cells
T7 Promotor
Transcription of
mutated IBV
genome sequence
Translation of
IBV proteins
Assembly and
release of
recombinant IBV

Figure 2.1 Schematic diagram of the M41-K reverse genetics system.
(A) A vector containing the GPT gene along with the desired mutation was transfected into Vero cells along with recombinant VV containing the IBV M41-K cDNA genome. (B) The first homologous recombination event occurs between the pGPT vector and IBV cDNA due to identical flanking regions. (C) Successful recombination is selected for by treating cells with MXH selection media. (D) After three rounds of plaque purification, the cells are treated in media in the absence of MXH, and the highly unstable intermediate undergoes a second recombination event. (E) Recombinant VV are sequenced for the presence of the desired mutation and screened for the absence of the GPT gene. (F) CK cells are transfected and infected with extracted DNA from successful rVV, Fowl-pox virus and pCI-Neo to induce expression of IBV cDNA under the control of a T7 promoter. Rescued recombinant IBV are passaged and then sequenced.

2.9.6 Purification and DNA extraction

Cells were freeze-thawed three times and sonicated for 2 minutes to extensively lyse the cells. Lysates were centrifuged at 1,200 × g at 4 °C for 10 minutes to remove the cell nuclei. The supernatant was removed, and 13 ml of TE (pH 9.0) buffer added. The rVV was then partially purified through a sucrose gradient. The supernatant was layered onto 16 ml of 30% sucrose diluted in TE (pH 9.0) buffer (**Table** 2.25) and ultracentrifuged at 36,000 x g for 1 hour at 4 °C. The pellet was resuspended in 10 ml TE (pH 9.0) buffer. Proteinase K buffer (**Table** 2.26) containing 0.2 mg/ml of Proteinase K was added in equal volume to the partially purified rVV in TE buffer and was incubated at 50 °C for 2.5 hours. After digestion, rVV DNA was extracted from the samples using phenol/chloroform (ThermoFisher). The samples were divided into two 10 ml aliquots, and 10 ml of phenol-chloroform containing 8-hydroxyquinoline was added. The samples were

extensively mixed and then centrifuged at 1,200 × g for 15 minutes at 4 °C. The upper aqueous phase was removed, being careful not to remove the interphase, into a new 50 ml falcon. The phenol-chloroform extraction was repeated to purify the DNA. After the second extraction, a chloroform extraction was used to purify the DNA further and remove salts and sugars. The DNA was then precipitated by adding 0.1 volume of 3 M sodium acetate and 2.5 volumes of 100% ethanol (-20 °C). Samples were centrifuged for 30 minutes at 2,300 × g at 4 °C. The supernatant was discarded, and the pellet washed for 5 minutes with 10 ml of 70% ethanol (v/v) at 4 °C. Samples were centrifuged for 30 minutes at 2,300 × g. The ethanol supernatant was discarded, and any remaining ethanol carefully removed using blue roll. The pellet was air dried for 30 minutes before re-suspending in 100 µl sterile water. The pellet was left overnight at 4 °C to dissolve the DNA completely. DNA was quantified using the NanoDrop 1000.

Table 2.25 Recipe for TE buffer

Reagent	Final Concentration
Tris-HCl (pH 9.0)	10 mM
EDTA	1 mM

Table 2.26 Recipe for proteinase K buffer (2x)

Reagent	Final Concentration
NaCl	400 mM
Tris-HCl (pH 7.4)	200 mM
EDTA	10 mM
SDS	0.4 mM

2.9.7 Recombinant IBV rescue

CK cells were plated in a 6-well plate (50-60% confluence). Cells were infected with 1 ml of recombinant Fowlpox virus that expresses the bacteriophage T7 RNA polymerase (rFPV-T7) (Britton et al. 1996) at an MOI of 10. Cells were incubated for one hour at 37 °C and then washed once with OPTIMEM (Invitrogen). Cells were transfected with 10 µg of rVV DNA and 5 µg of a plasmid expressing the IBV N protein (pCi-Nuc). Protein N is expressed in complement as it required for the synthesis and egress of new virions (Siu et al. 2008). Plasmids were diluted in 1.5 ml of OPTI-MEM (Invitrogen) and then added dropwise to 50 µl of Lipofectin in 1.5 ml of OPTI-MEM. The transfection solution was added to the cells and then incubated overnight at 37 °C (**Figure 2.1F**). Transfection media was removed,

and 3 ml of 1x BES added. The cells were then incubated at 37 °C until extensive rFPV CPE was visible. The supernatant was harvested and rFPV removed by filtering through a 0.22 µm filter. The resulting solution was stored at -80 °C. To determine whether rIBV was successfully rescued, samples were serially passaged three times to increase viral titre. CK cells (6-well plate, 70-80 confluence) were inoculated with 1 ml of supernatant and incubated for 1 hour at 37 °C followed by addition of 2 ml of 1x BES. Cells were incubated for 2-3 days at 37 °C until CPE was visible. The supernatant was removed and passaged a further two times. After the third passage, RNA was extracted from the viral samples and screened to confirm rescue of rIBV and to identify the presence of the desired mutation.

2.10 Liquid Chromatography-Mass Spectrometry/Mass Spectrometry

2.10.1 Transfection

HEK293T cells were grown to 40 - 50% confluency in 10 cm^2 culture plates. Cells were transfected with plasmids expressing either GFP or GFP-tagged accessory proteins. Plasmids were chemically transfected using calcium phosphate. Plasmids were diluted in 2 M $CaCl_2$ (w/v) and then added dropwise to 2x Hank's Balanced Salt Solution (HBBS) recipe. The transfection solution was incubated at room temperature for 25 minutes and then added dropwise to the cells. Cells were incubated for 16 hours and were then washed once with cold PBSa and lysed with co-IP lysis buffer (**Table** 2.27).

Table 2.27 Co-IP lysis buffer

Reagent	Final Concentration
Tris-HCl buffer (pH 7.4)	10 mM
NaCl	150 mM
EDTA	0.5 mM
Igepal	0.5% v/v

2.10.2 GFP capture

GFP was immunoprecipitated using the GFP-Trap (ChromoTek) Kit and protocol. Each sample was incubated overnight at 4 °C with GFP beads. Beads were

centrifuged at 500 x g for 5 minutes and then washed three times with 1x Dilution Buffer (**Table** 2.28). Proteins were eluted from the beads in 50 µl glycine (50 mM, pH 2.7) for 5 minutes with 1 minute of vortexing. To concentrate the samples, the elution step was repeated in an additional 50 µl of glycine. Samples were stored at -20 °C until processing at the University of Liverpool.

Table 2.28 1x Dilution buffer

Reagent	Final Concentration
Tris-HCl (pH 7.5)	10 mM
NaCl	150 mM
EDTA	0.5 Mm
Sodium Azide	0.018% w/v

2.10.3 LC-MS/MS

Eluted samples were processed for liquid chromatography-mass spectrometry/mass spectrometry by Dr Stuart Armstrong or Dr Weining Wu. Samples were diluted 1:1 volume with 25 mM ammonium bicarbonate (NH_4HCO_3). Rapigest SF surfactant (Waters) was added to increase protein digestion at a final concentration of 0.05% (w/v) and boiled for 10 minutes at 80 °C. Proteins were reduced with 3 mM dithiothreitol (Sigma) and heated at 60 °C for 10 minutes. The samples were returned to room temperature, and 9mM iodoacetamide (Sigma) added for 30 minutes in the dark to alkylate the proteins. Proteins were trypsinised with 0.2 µg of proteomic grade trypsin (Sigma) and left to incubate at 37 °C

overnight. The resulting peptide samples were then treated with 1% (v/v) Trifluoroacetic acid (TFA) and heated to 37 °C for 2 hours to precipitate the Rapigest. Samples were centrifuged at 12,000 x g for 60 minutes at 4 °C to remove the Rapigest precipitate. Peptides were concentrated and desalted using C18 Stage tips (ThermoFisher Scientific) and then samples dried using a centrifugal vacuum concentrator (Jouan). Resulting precipitates were resuspended in solution containing 0.1% (v/v) trifluoroacetic acid and 3% (v/v) acetonitrile. For high-performance liquid chromatography (HPLC), the on-line nanoACQUITY-nLC system (Waters) was used. The Nano ACQUITY UPLCTM BEH130 (C18, 15 cm x 75 µm, 1.7 µm) (Waters) analytical column was used at a flow rate of 300 nl/minute to separate 2 µl of the peptide sample against a 3−40% acetonitrile in 0.1% formic acid gradient for 50 minutes ramping up to a gradient of 40−85% acetonitrile in 0.1% formic acid for 3 minutes. The mass spectrometer, LTQ-Orbitrap Velos (ThermoFisher Scientific) was used to acquire the full-scan MS spectra (MS1) at a resolution of 30,000. The 20 most intense ions were selected for a tandem in space mass analysis and were fragmented by collision-induced dissociation (CID) before spectra detection by the LTQ ion trap.

2.10.4 Analysis

MS spectra data was analysed by label-free quantification using the MaxQuant software (MQ) and searched against a human protein database (Uniprot release-2013_03) using the Andromeda search engine. The false discovery rate (FDR) was set to 0.01, and a decoy database was included in the search to remove

false-positives. LFQ results were further processed by the Perseus software (MQ) to determine significance between GFP alone compared to GFP tagged accessory proteins. Statistical T-test analysis was used to analyse intensity values. Proteins with a p-value <0.05 and a fold change >2 (Log2) were considered statistically significant. Identification and statistical analysis of the mass spectrometry data were performed by either Stuart Armstrong or Weining Wu.

Downstream analysis of mass spectrometry data was performed by me. Proteins were analysed using both String DB (v10.0) to identify interacting proteins and Panther DB to group similar proteins based on GO (v1.2) and PANTHER (v11.1) annotations.

2.11 Interferon methods

2.11.1 Interferon luciferase reporter assay

DF-1 cells seeded in a 24-well format (80-90% confluence) were washed once with PBSa, and 500 µl of 1x DMEM (10% FCS) added to each well. OPTI-MEM I reduced serum media (Invitrogen) was added to 500 ng of pFLAG-CMV2-3aB, pEGFPC2-3aB, pEGFPC2-3aM, pCAGGS-NS1-IAVPR8 or pEGFPC2, 80 ng of chIFNβ-luciferase reporter and 40 ng of Renilla luciferase plasmid pRL-CMV. The reporter construct consists of a chicken IFN-β promoter sequence upstream of a chemiluminescent Firefly luciferase gene. In a separate tube, 50 µl of OPTI-MEM was added to 7.5 µl of lipofectamine 2000 (Invitrogen). The samples were incubated at room temperature for 5 minutes, after which the DNA mixture was added to the lipofectamine in a drop-wise manner and incubated for a further 25 minutes. During incubation, the cell media was replaced with 400 µl of fresh 1x DMEM (10% FCS). The transfection mixture was added to the well, drop-wise and incubated for 16 hours at 37 °C. Poly(I:C) (dsRNA analogue) at a final concentration of 5 µg/ ml was transfected into each well 8 hours before lysis. In one tube 100 µl of OPTI-MEM was added to the poly(I:C) (Invivogen), and in a separate tube, 100 µl of OPTI-MEM added to 7.5 µl of lipofectamine 2000. The DNA and lipofectamine mixtures were incubated at room temperature for 5 minutes, the lipofectamine mixture was added dropwise to the poly(I:C) and incubated for a further 25 minutes. The transfection mixture was added directly to the well in a drop-wise manner and incubated at 37 °C for 2 hours to induce the interferon response. Afterwards, the media was removed and replaced with fresh

1x DMEM (10% FCS) and incubated at 37 °C for a further 16 hours. After 16 hours, the media was removed, and the cells washed once with PBSa. The Dual-Glo Luciferase Reporter Assay System (Promega) was used for lysis and to measure luminescence activity. Passive lysis buffer (100 µl) was added to each well. The plates were subsequently frozen for 30 minutes at -80 °C. The plates were thawed at room temperature on a shaker. Afterwards, 10 µl of lysate was added to a well of an opaque white 96-well plate. Firefly and Renilla luciferase were activated with the Dual-luciferase kit by adding 50 µl of LAR II and then Stop-and-Glo buffer sequentially. Luminescence was measured using the Glo-Max plate reader. Luminescence data was normalised using Renilla luminescence levels. Lysates (26 µl) were separated by SDS-PAGE and immunoblotted with anti-3a, as described in 2.6, to confirm successful expression of pEGFPC2-3aB and pFLAG-CMV2-3a.

2.11.2 Chicken interferon MxA reporter assay

Chicken type I interferon (chIFNβ) levels were quantified using a quail reporter cell line, CEC-32, expressing luciferase under the control of the MxA promoter (Peter Staeheli) (Schwarz et al. 2004). CK cells were seeded in a 24-well plate (70-80% confluent). Cells were washed twice with PBSa and infected with IBV at an MOI of 0.1 for 1 hour. The inoculum was removed and replaced with 1x BES media. Cells were incubated and supernatant harvested at the specified time. Samples were heat treated for 30 minutes hour at 56 °C to inactivate IBV before sampling. Samples were serially diluted and incubated with CEC-32 cells (96-well plate, 70-80% confluence) for 6 hours. Luciferase activity was then measured

using the Stop-and-Glo Luciferase Kit and protocol (Promega). Interferon levels were measured against a standard curve using two-fold dilutions of recombinant chIFNβ starting at 25 U/ml (Abbexa).

2.12 Apoptosis methods

2.12.1 Caspase 3/7 activity assay

DF-1 cells seeded in a 24-well plate (70-80% confluence) were transfected or infected. Cells were either mock infected or infected with IBV at an MOI of 4 for 1 hour. The inoculum was replaced with 1x DMEM (10% FCS). Transfected cells were either transfected with an empty plasmid or a plasmid expressing a tagged accessory protein as described in 2.5. As a positive control, staurosporine was added at a concentration of 10 µM in DMEM for 6 hours. Caspase 3/7 activity was measured using the Caspase-Glo 3/7 assay (Promega) and protocol. At the allocated time post infection/transfection, 900 µl of media was removed, and an equal volume of caspase substrate added directly to the cells. Cells were shaken for 1 minute and then incubated for 30 minutes in the dark. Cleavage of caspase-Glo substrate by caspase 3/7 results in aminoluciferin release and subsequent luciferase activity. Samples were added to an opaque 96-well plate, and caspase luminescence measured using the GloMAX luminometer (Promega).

2.12.2 Annexin-V-FITC FACS assay

DF-1 cells seeded in a 12-well plate (70-80% confluence) were transfected or infected. Cells were either mock infected or infected with IBV. As a positive control, staurosporine was added at a concentration of 10 µM in DMEM for 6 hours. After infection, cell media was harvested and cells detached using Accutase Cell Detachment solution (BD Bioscience) in PBS. The cell media and detached cells were pooled and centrifuged at 1,200 × g and then washed once with cold PBSa

and re-centrifuged at the same speed for 5 minutes to pellet the cells. Apoptosis was measured using the Annexin V Apoptosis Detection kit II (BD Bioscience) and protocol. The cell pellet was resuspended in 1ml 1x binding buffer and 100 µl of the sample transferred to a FACS tube. Five µl of Annexin V antibody was added to the sample and vortexed. Samples were incubated for 25 minutes at 4 °C on a rotator in the dark. Afterwards, 5 µl of Propidium iodide was added and samples incubated for 5 minutes. An additional 400 µl of 1x Binding Buffer was added to each sample. Cells were sorted, and fluorescence was measured and analysed using the MACS QUANT flow cytometry. Data analysis was completed using FCS Express (v5.0).

2.13 Stress granule methods

2.13.1 SG induction

Vero cells were seeded in a 24-well plate (70-80% confluence) and then transfected or infected. During infection experiments, cells were either mock infected or infected with IBV. Transfected cells were transfected with either an empty control plasmid or a plasmid expressing a tagged accessory protein. As an SG positive control, sodium arsenite was added 45 minutes before fixation at a final concentration of 0.5 mM. Stress granules were labelled with anti-G3BP1, a stress granule marker, and visualised by confocal microscopy. For each sample, 20 GFP positive cells were randomly selected and the number of stress granule positive cells counted. Any cells containing a single SG were considered SG positive.

2.13.2 Gene expression and translation efficiency

DF-1 or Vero cells seeded in a 24-well plate (70-80% confluence) were transfected with pRL-CMV, a Renilla luciferase expressing plasmid under control of a CMV promoter, along with either pEGFP-C2 or pEGFPC2-4b. After 16 hours, cells were washed once with PBSa, cells lysed and Renilla activated using the Stop and Glo (Promega) kit and protocol. Luminescence was measured using the GloMax 96-microplate luminometer (Promega). Background luminesce was determined by adding Renilla to media alone and subtracted from all samples.

2.14 Bioinformatics analysis

2.14.1 Sequence Alignment

Complete IBV sequences were downloaded from the VIPR Coronavirus database (http://www.viprbrc.org) (Jan 2017) and aligned using the BioEdit (Staden) program. Sequences were analysed using the unsorted six-frame translation tool to locate ORF4b. ORF4b sequences were then compiled into a new database for each IBV strain. ORF4b sequence identity and similarity were calculated by comparing all sequences against each other using the SIAS tool (imed.med.ucm.es/).

2.14.2 Eukaryotic Linear Motif Search

The complete M41 4b peptide sequence was entered into an ELM search, and results organised by the probability of the motif sequence occurring randomly (elm.eu.org/search/).

3. The role of accessory protein 3a

3.1. Introduction

IBV 3a is a 6 kDa accessory protein expressed from the first ORF in mRNA 3 (Liu et al. 1991). Previous work has shown that 3a is not required for replication *in vitro*, *in ovo* and *ex vivo* organ culture (Hodgson et al. 2006). Due to the high peptide sequence conservation between IBV strains, 3a is believed to be important and may be involved in pathogenicity (Jia et al. 1997). *In vitro* studies in Vero cells have shown that during infection, 3a localises to two main cellular compartments, the cytoplasm where it is diffuse and the smooth ER where it is membrane-bound, due to a transmembrane domain at the N-terminus (Pendleton et al. 2005). IBV 3a has also been shown to closely localise with the small GTPase, MxA (Pendleton et al. 2005). Kint *et al.* showed that 3a plays a role in both inhibiting and stimulating interferon-beta (IFNβ) expression in a time-dependent manner, with recombinant IBV lacking ORF3a expressing higher levels of IFNβ transcript 24 h.p.i, while at 36 h.p.i IFNβ translation was inhibited (Kint et al. 2015). The mechanism of action of how IBV 3a modulates IFNβ expression is not known. In this chapter, the mechanism of action of 3a on IFNβ expression is investigated. Utilising a chicken(ch)IFNβ luciferase assay, IBV 3a is shown to have a dose-dependent effect on IFNβ expression, and can both stimulate and inhibit expression by targeting two IFN signalling proteins, MAVS and IRF7. IBV 3a can both increase levels of MAVS while simultaneously decreasing levels of IRF7 in a dose-dependent proteasome-dependent manner. Furthermore, mass spectrometry has identified two interacting cellular partners for 3a which play a

role in regulating MAVS and IRF7 turnover, RNF5, and CAND1, respectively. RNF5 targets MAVS for proteasomal degradation while CAND1 is an E3-SCF ligase regulatory protein, a ligase complex that targets IRF3/7 for degradation (Zheng et al. 2002, Prakash et al. 2006, Zhong et al. 2010).

Results

3.2. Generation of GFP-tagged 3a expression vectors

Vectors for expression of GFP-tagged 3a from Beau-R (3aB) and M41-CK (3aM) were generated for *in vitro* IFN assays, immunofluorescence visualisation and for mass spectrometry protein purification. The expression vector, pFLAG-3aB was previously generated by Mark Davies (Davies 2009). Expression vectors with GFP-tagged at either the N- or C- terminus of 3a for both Beau-R and M41-CK were generated. For the generation of these vectors, RNA from Beau-R and M41-CK was isolated and reverse transcribed into cDNA using random primers. Complementary primers with flanking restriction sites were designed to amplify ORF3a by PCR. Resulting PCR products were purified and digested with the relevant restriction enzymes. Expression plasmids, pEGFPC2 (Clontech) and pEGFPN1 (Clontech), were digested with the same enzymes and purified by gel extraction. Digested expression plasmids and PCR products were ligated and transformed into competent cells. Vectors were purified and sequenced using Sanger sequencing. Four expression vectors, pEGFPC2-3aB, pEGFPC2-3aM, pEGFPN1-3aB, and pEGFPN1-3aM were generated (**Figure 3.1**). To confirm the generation of GFP-tagged 3a expression vectors, the molecular weight of GFP-

3aM, 3aM-GFP, GFP-3aB, and 3aB-were compared to GFP. Vero cells were transfected with each vector, and after 16 hours, cells were lysed, separated by SDS-PAGE, transferred to a membrane and labelled with anti-GFP. The molecular weight of GFP-tagged 3aB and 3aM were identified as expected (34 kDa) (**Figure 3.1E**).

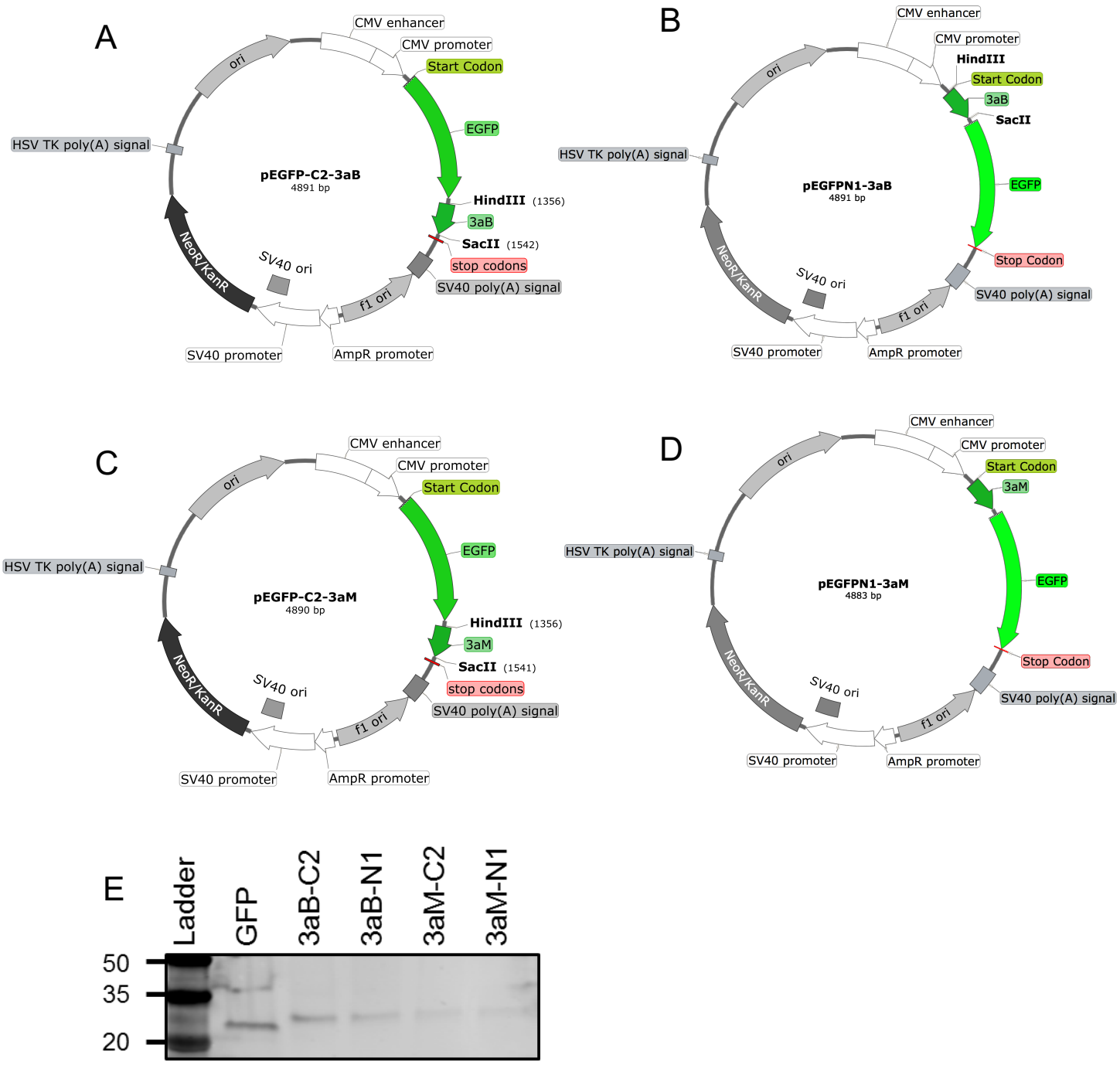

Figure 3.1 Plasmid map and confirmation of expression of the GFP-tagged 3a expression vectors.

(A) pEGFPC2-3aB (B) pEGFPN1-3aB (C) pEGFPC2-3aM (D) pEGFPN1-3aM (E) Vero cells were transfected with pEGFPC2, pEGFPC2-3aB/3aM, pEGFPN1-3aB/3aM expression vectors. After 16 hours, cells were lysed, proteins separated by SDS-PAGE and transferred to a membrane. Membranes were incubated with anti-GFP.

3.3. Testing anti-3a (JH3480)

Anti-3a (JH3480) was a gift from Carolyn Machamer. The antibody was tested against 3a expression to confirm this antibody can label both M41 and Beaudette isoforms of 3a. DF-1 cells were transfected with 3aB-FLAG or GFP-3aM expression vectors. After 16 hours, cells were lysed, proteins separated by SDS-PAGE, transferred to a membrane and labelled with anti-3a, anti-FLAG or anti-GFP. Blots were labelled with anti-GFP or anti-FLAG to confirm expression of GFP-3aM or 3aB-FLAG, with a band appearing at approximately ~35 kDa and 8 kDa, respectively. Anti-3a was also able to label both GFP-3aM and 3aB-FLAG, confirming that anti-3a can label both 3aB and 3aM by western blot (**Figure 3.2A,B**). Anti-3a failed to label a band in the pFLAG control, suggesting anti-3a was labelling 3a expression only (**Figure 3.2C**). Anti-3a was then tested against 3aB-FLAG expression. DF-1 cells were transfected with the 3aB-FLAG expression vector, and after 16 hours, cells were fixed, permeabilised and labelled with anti-3a. The antibody could label 3a in DF-1 cells (**Figure 3.2D**), confirming that anti-3a can label both 3a by indirect immunofluorescence.

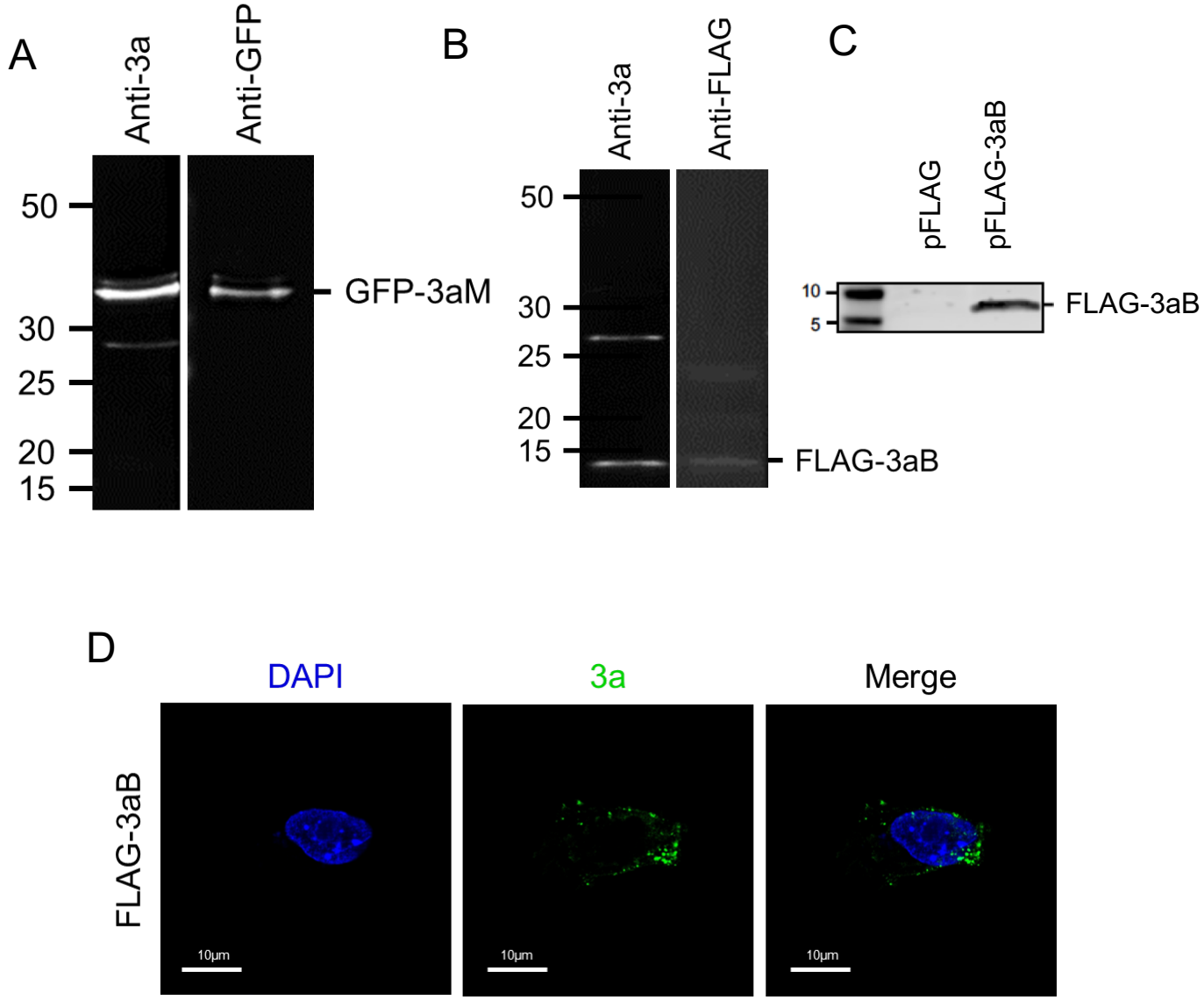

Figure 3.2 Anti-3a can label both 3aB and 3aM.

DF-1 cells were transfected with either (A) GFP-3aM, (B) 3aB-FLAG, (C) pFLAG or 3aB-FLAG expression vectors. After 16 hours, cells were lysed, proteins separated by SDS-PAGE, transferred to a membrane and labelled with anti-3a, anti-GFP or anti-FLAG. (C) DF-1 cells were transfected with 3aB-FLAG expression vectors. After 16 hours, cells were fixed, permeabilised and labelled with anti-3a. The nucleus was stained with DAPI.

3.4. Characterisation of IBV 3a effect on IFNβ expression

3.4.1. IBV 3a both inhibits and stimulates IFNβ expression

Previous work has shown that 3a can modulate IFNβ expression, with rIBV lacking 3a expression inducing less IFNβ expression 36 h.p.i compared to wild-type IBV (Kint et al. 2015). To further characterise this effect, a chicken(Ch)-IFNβ luciferase reporter assay was used, utilising a reporter plasmid expressing a luciferase gene under the control of a chicken IFNβ promoter (Liniger, 2012). This assay allows Firefly luciferase activity to be measured as a proxy for IFNβ promoter activity. The IFN signalling cascade can be simplistically split into five sections, detection of dsRNA by MDA-5, activation and aggregation of MAVS, phosphorylation of TBK1, phosphorylation of IRF7 and finally IFNβ transcription (Wu et al. 2014). To determine at which point in the IFN cascade IBV 3a affects IFNβ expression, cells were stimulated with either dsRNA, MDA-5, MAVS or IRF7. DF-1 cells were transfected with increasing levels of the pFLAG-3aB expression vector, made up to 1 μg with pFLAG. Increasing levels of pFLAG-3aB were transfected to determine if any effect observed was dose-dependent. The amount of transfected vector remained the same for each transfection. Cells were simultaneously transfected with a ch-IFNβ reporter plasmid and a Renilla luciferase plasmid as a transfection control. An influenza NS1 (IAV-PR8) expression vector was used as a positive control, as IAV NS1 is a potent IFNβ antagonist (Hatada et al. 1992, Gack et al. 2009, Rajsbaum et al. 2012). The IFN cascade was then stimulated by transfecting cells with either poly(I:C) or with plasmids expressing chicken MDA-5, MAVS or IRF7. After 16 hours, cells were

lysed, and luciferase activity measured. Firefly luciferase activity was normalised against Renilla luciferase expression. Firefly luciferase activity was shown as fold-change compared to the empty vector control. An aliquot of each sample was separated by SDS-PAGE, transferred to a membrane and labelled with anti-FLAG to confirm successful transfection for one replicate, and is shown as a representative of the three biological replicates performed subsequently. When cells were transfected with poly(I:C) and low levels of 3aB-FLAG (250 ng), Firefly luciferase activity was higher compared to the empty vector control meaning the IFNβ promoter is activated. Increasing levels of 3aB-FLAG did not increase this effect, with 1 µg of 3aB-FLAG inducing less luciferase activity compared to the empty vector control (**Figure 3.3A**). The positive control, IAV NS1, significantly inhibited poly(I:C) induced IFNβ expression. The same effect for poly(I:C) was observed when cells were transfected with the chMDA-5 vector. At low levels of 3aB-FLAG expression, Firefly luciferase activity was higher compared to the empty vector control (**Figure 3.3B**). Increasing levels of 3aB-FLAG had an overall inhibitory effect on luciferase activity. Conversely, when cells were transfected with chMAVS; 3aB-FLAG only had an inhibitory effect on luciferase activity (**Figure 3.3C**). The effect was not dose-dependent, with higher doses of 3aB-FLAG vector not significantly inhibiting Firefly luciferase activity compared to lower doses. When cells were overexpressing chIRF7, increasing levels of 3aB-FLAG also had an inhibitory effect on luciferase activity, but in comparison to MAVS overexpression, the effect was dose-dependent (**Figure 3.3D**). Expression of 3aB-FLAG alone without poly(I:C) treatment did not induce luciferase activity,

suggesting 3a alone does not induce IFN expression. As IRF7 is the last protein involved in IFN cascade, 3a most likely affects IRF7 activity in some manner. A different effect was observed upstream suggesting 3a also affects the cascade at either poly(I:C) detection, MDA-5 activity or possibly even MAVS activity. IBV 3a alone was unable to induce IFN expression when induced with poly(I:C), MDA-5, MAVS or IRF7. Overall this suggests that 3a has a dual mechanism of action on chIFNβ expression.

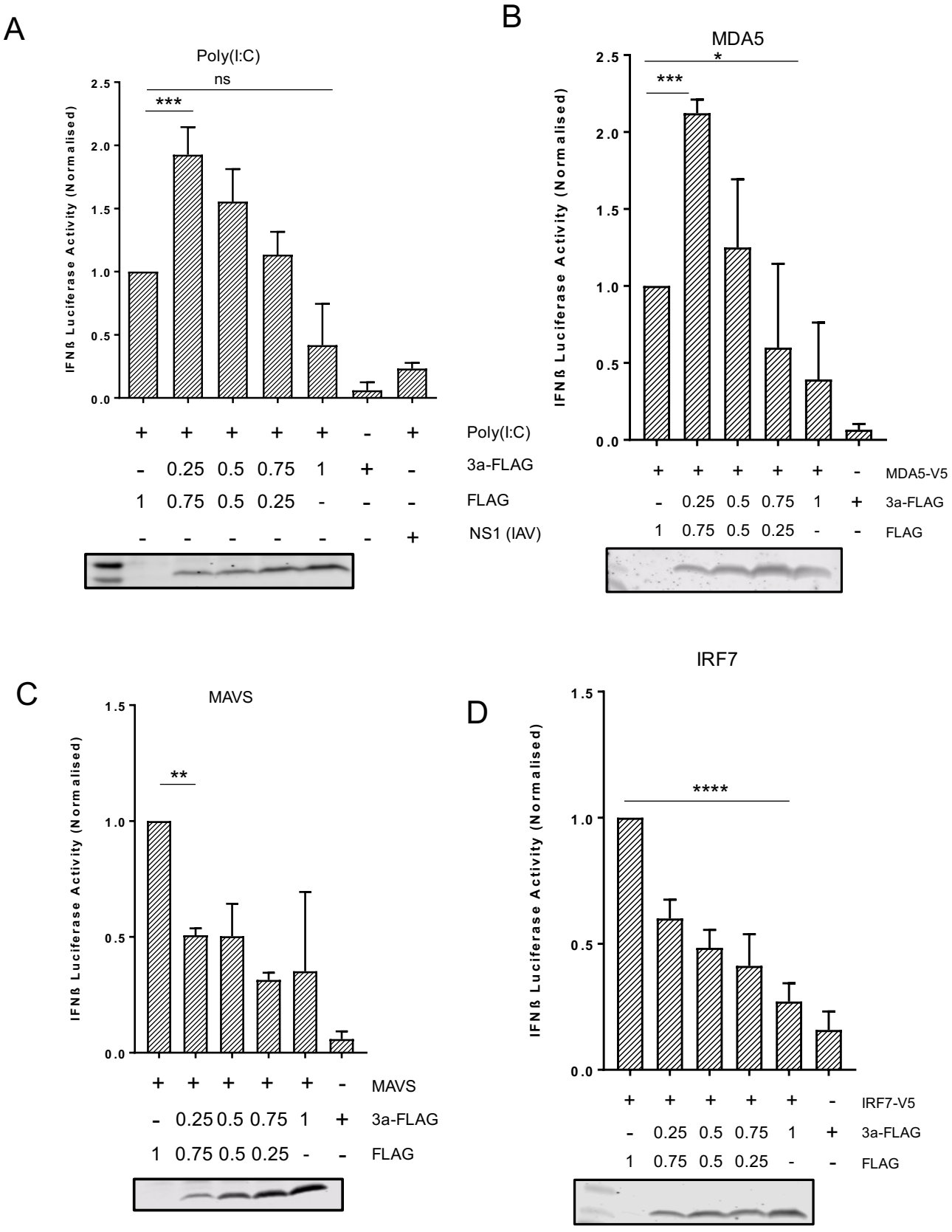
A
Poly(I:C)
ns
***
IFNß Luciferase Activity (Normalised)
2.5
2.0
1.5
1.0
0.5
0.0
+ + + + + - +
- 0.25 0.5 0.75 1 + -
1 0.75 0.5 0.25 - - -
- - - - - - +
Poly(I:C)
3a-FLAG
FLAG
NS1 (IAV)
B
MDA5
*
***
IFNß Luciferase Activity (Normalised)
2.5
2.0
1.5
1.0
0.5
0.0
+ + + + + - MDA5-V5
- 0.25 0.5 0.75 1 + 3a-FLAG
1 0.75 0.5 0.25 - - FLAG
C
MAVS
**
IFNß Luciferase Activity (Normalised)
1.5
1.0
0.5
0.0
+ + + + + - MAVS
- 0.25 0.5 0.75 1 + 3a-FLAG
1 0.75 0.5 0.25 - - FLAG
D
IRF7
****
IFNß Luciferase Activity (Normalised)
1.5
1.0
0.5
0.0
+ + + + + - IRF7-V5
- 0.25 0.5 0.75 1 + 3a-FLAG
1 0.75 0.5 0.25 - - FLAG

Figure 3.3 IBV 3a protein induces and inhibits IFNβ expression in a dose-dependent manner.

DF-1 cells were transfected with vectors expressing 3aB-FLAG/FLAG at varying ratios and with a chIFNβ Firefly luciferase reporter plasmid. Cells were also transfected with (A) poly(I:C) for 12 hours or with plasmids expressing (B) chMDA5-V5, (C) chMAVS-V5, (D) IRF7-FLAG. After 16 hours, cells were lysed, and luciferase activity measured. Results were normalised using a Renilla luciferase transfection control. Firefly luciferase activity is measured as fold-change in luminescence over the empty vector control. Successful transfection and expression of 3aB-FLAG vectors was confirmed by western blot and includes data from three biological replicates. Unpaired *t*-test * significant at $p < 0.05$, **significant at $p < 0.01$, *** significant $p < 0.005$, **** significant $p < 0.0005$, non-significant (ns) $p > 0.05$. Error bars represent one standard derivation from the mean.

3.4.2. IBV 3a from Beau-R and M41 have the same effect on IFNβ expression

IBV 3a is a highly conserved accessory protein and is expressed by both the apathogenic lab strain, Beau-R, and the pathogenic lab strain, M41-CK. Beau-R and M41-CK 3a have a high sequence identity of 96.48% with only two amino acids different at the C-terminal end (**Figure 3.4A**). To determine if this difference in peptide sequence affects the observed function of 3a on IFN expression, 3a from M41 and BeauR were compared. DF-1 cells were transfected with a chIFNβ luciferase reporter plasmid along with either GFP-3aB, GFP-3aM or GFP expression vectors. A Renilla luciferase plasmid was co-transfected as a transfection control. Cells were then transfected with either poly(I:C) or with vectors expressing chMDA-5, chMAVS or chIRF7. After 16 hours, cells were lysed, and luciferase activity measured. Results were normalised to Renilla luciferase expression and are represented as fold-change compared to the empty vector control. As seen previously, GFP-3aB had a stimulatory effect on IFNβ promoter

activity when induced with poly(I:C) or MDA-5, the same effect is seen with GFP-3aM (**Figure 3.4B**). Furthermore, GFP-3aM expression also inhibited IFNβ promoter activity when induced with MAVS or IRF7 to similar levels as GFP-3aB. Expression of 3aB or 3aM alone did not increase IFNβ Firefly luciferase activity compared to the GFP control, suggesting that 3a only has a stimulatory effect on IFN expression when induced with either poly(I:C) or MDA-5. Overall, this suggests that 3a from M41 and BeauR have a similar effect on IFNβ expression.

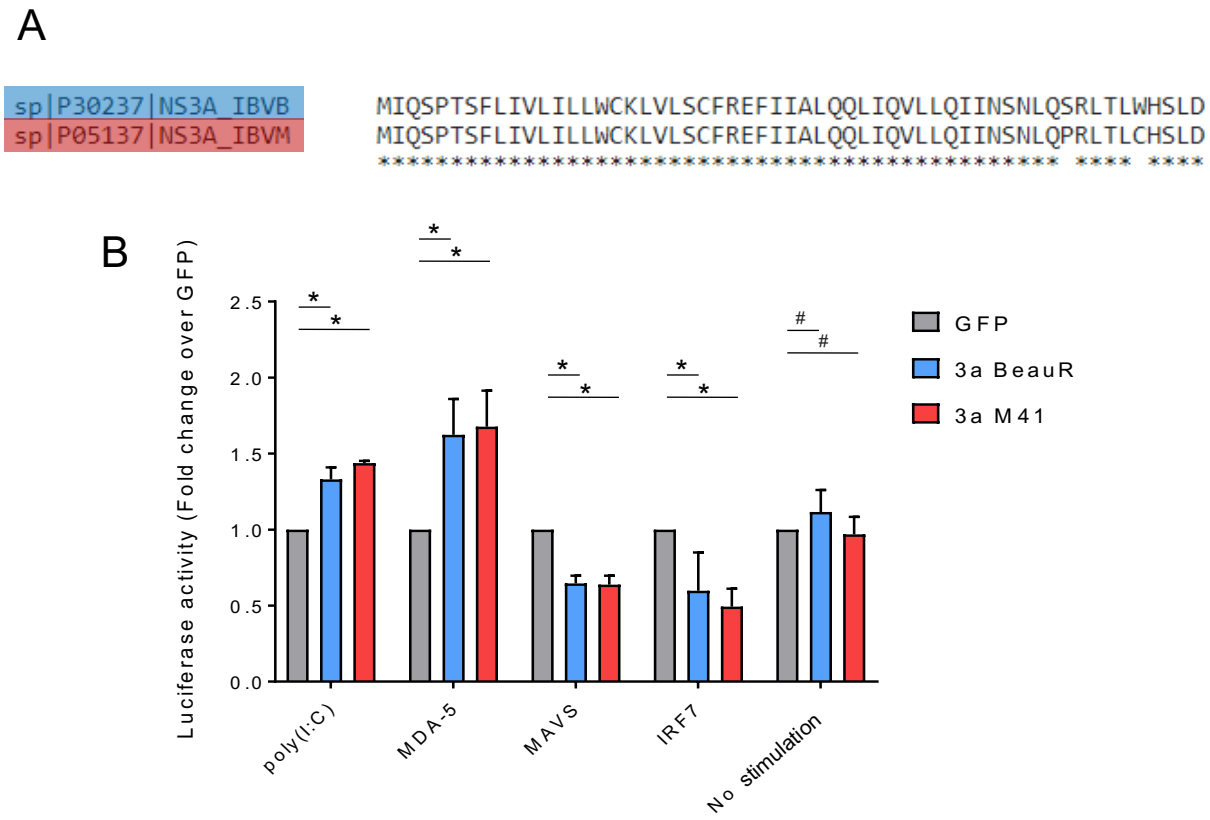

Figure 3.4 IBV 3a from M41-CK and Beau-R have the same effect on IFNβ signalling. (A) Protein sequence alignment of Beau-R 3a (blue) and M41-CK 3a (red). (B) DF-1 cells were transfected with GFP, GFP-3aB or GFP-3aM expression vectors and a chIFNβ-luciferase reporter plasmid. Cells were then either transfected with poly(I:C) for 12 hours or transfected with plasmids expressing chMDA-5, chMAVS, chIRF7 or mock transfected. A renilla luciferase plasmid was used as a transfection control. Firefly luciferase activity is shown as fold-change compared to the GFP control. Results are representative of three biological replicates. * significant $p < 0.05$, # non-significant $p > 0.05$.

3.5. Mass spectrometry analysis of GFP-3aM IPs

Mass spectrometry was utilised to identify any interacting partners for 3aM, that may help to determine IBV 3a mechanism of action on IFNβ expression and any additional functions. HEK-293T cells were transfected with pEGFPC2-3aM or pEGFPC2 expression vectors. After 16 hours, cells were lysed and GFP-3aM or GFP immunoprecipitated using GFP 'capture' beads (Chromotek). This assay was completed in triplicate for each plasmid, performed on different days. Input and eluate samples were analysed by western blot to confirm successful transfection of pEGFPC2-3aM and immunoprecipitation of GFP-3aM (**Figure 3.5**). GFP immunoprecipitation could be confirmed by directly visualising the GFP

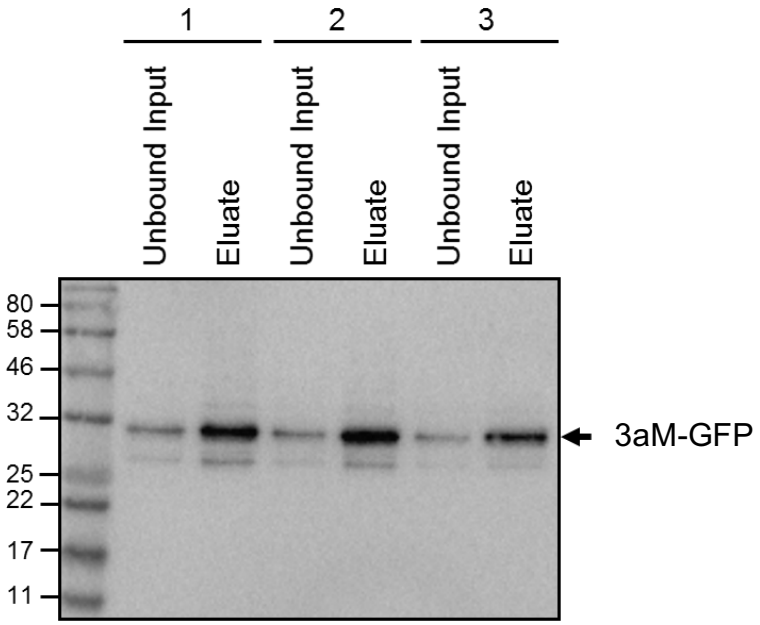

Figure 3.5 Confirmation of GFP-3aM transfection and IP.
HEK-293T cells were transfected with pEGFPC2-3aM or pEGFPC2. After 16 hours, cells were lysed, and GFP-3aM immunoprecipitated using GFP 'capture' beads. Input and eluate samples were separated by SDS-PAGE, transferred to a membrane and labelled with anti-GFP.

fluorescence when attached to the GFP capture beads. After confirmation, samples were analysed by LC-MS/MS (for method see **2.10.3**) by Weining Wu.

In total 554 proteins were identified in higher levels in the GFP-3aM eluate compared to the GFP control (**Appendix, Table 7.1**). Proteins were identified by comparing unique peptides to a database of human proteins. Proteins where only a single unique peptide was identified, were removed to reduce the chance of identifying the wrong protein. For each protein identified, the fold-change (Log2) in relative abundance was calculated by comparing GFP-3aM to the GFP control. From the three replicates the *p*-value, as determined by two-way ANOVA, was calculated. A *p*-value above one (-Log10) along with a fold-change (Log2) above two were considered significant interactions and had the highest chance of interacting with 3aM. For each protein, the confidence score (-Log2) was calculated, which is the cumulative value of *p*; the probability of the identified peptide sequence occurring randomly, for each unique peptide identified. In total 135 proteins were identified as significant (**Table** 3.1, **Figure 3.6**).

Table 3.1 Cellular proteins identified my LC-MS/MS that significantly interact with GFP-3aM.

Name	Unique Peptides	Confidence	Relative Protein Abundance						*p* Value (-Log10)	Fold-change GFP-3aM/GFP (Log2)
			pEGFPC2-3aM			pEGFPC2				
			1	2	3	1	2	3		
SUCB2	2	51.8	34391.31213	56821.77764	41196.20091	0	0	0	6.777403376	15.42968233
FND3A	2	34.79	74980.93704	24630.06568	33157.9421	0	0	0	5.344140575	15.43359571
GCP2	2	197.65	235809.9946	105676.1593	110856.7974	0	345.0779654	89.30009403	1.897724605	10.02425004
PLCD	2	67.93	84058.48747	29179.2505	55446.0788	337.888514	0	0	1.888070933	8.963558546
RNF5	3	65.41	40010.10628	41698.36451	40304.88571	23.67064605	0.851848723	533.6542995	1.847905735	7.772101223
SYIM	2	166.85	5264.343093	38673.28811	35924.49767	272.9815635	348.4995779	0	1.313803241	7.005657106
DAAF5	6	260.95	185725.9629	107943.9298	164079.893	1605.611852	2255.546652	1306.758243	4.399280401	6.468832572
CAND1	3	99.7	26745.14688	119865.8145	61450.09147	1327.312472	803.21403	283.1585313	2.681942232	6.429625692
DRS7B	2	69.99	73008.75546	24830.37773	40296.64166	0	2227.736805	0	1.410611949	5.954364395
ODR4	2	83.56	94227.5916	30091.39846	43740.62521	0	3355.46799	20.37944099	1.332618828	5.637579572
SAAL1	2	59.11	224746.8404	137702.9975	147900.2826	3261.366937	7876.208585	2769.976351	3.298068207	5.197546941
STX18	2	108.09	107680.8457	55375.96374	76556.75843	763.3016918	4024.461995	2021.70543	2.704016395	5.137023465
REEP5	5	390.12	749915.828	305879.2859	410196.8144	18877.25139	19977.9151	8195.371688	3.037728514	4.961522125
AL9A1	2	67.04	4154.176253	40434.74772	21783.00598	708.3351856	1021.334608	754.4832324	1.885859908	4.739747273
F134C	4	272.76	1141784.237	364034.8883	527764.8573	11166.44445	44095.2193	28322.67335	2.442071003	4.604648142
CLCC1	5	219	168918.3877	94932.29125	125618.1712	4675.755832	7539.017183	4068.684829	3.658382062	4.580028948
WLS	3	121.35	299226.2514	122157.0627	191376.7091	3018.354566	14975.83988	9071.20919	2.417495595	4.500800369
TRABD	3	258.46	356891.6626	151716.4333	245364.0152	13656.55863	13034.83679	9349.082979	3.395254749	4.386821094
MA1A2	2	66.59	215645.5795	96319.35766	62781.13751	1646.540633	14837.10708	1696.101165	1.879797504	4.36550919
COQ9	2	60.35	110354.4636	76056.90201	122233.2208	7079.981262	2429.067748	5573.197655	3.020661266	4.355023232
ERGI1	3	88.57	184876.8847	77101.71274	100338.6505	8938.181852	4635.605864	4641.070818	3.029781331	4.314065791
IPO8	2	119.01	127020.6783	69452.4371	88508.53162	3149.79612	8148.584352	3345.938955	2.995663854	4.282455959
CHCH9	2	160.86	67572.62096	360826.731	302878.3555	15159.59511	20122.69634	5962.35567	1.893115032	4.148140585
ABHGA	4	127.54	189095.1787	78592.56183	128659.5804	9674.639923	9766.763034	4021.874744	2.729636927	4.078288755
ALG1	4	151.32	170129.9637	82346.94547	107946.4187	8060.06312	15773.06095	58.78622242	1.07826702	3.915098275
EMD	6	265.85	354469.7995	237282.4663	259536.9101	42448.24268	5526.157523	9727.697304	2.103879379	3.882953619

PSMD9	2	85.09	97466.21523	109471.8329	93926.33154	8888.832258	4863.059305	6760.611141	3.944032605	3.874537882
TOIP2	3	84.63	77623.31948	39297.2789	53983.44755	4152.550815	3693.52834	3819.042182	3.727616163	3.872913332
NU205	3	209.73	165607.2579	73567.56396	88393.00183	12717.15794	3246.093207	7151.734314	2.375776447	3.824893291
UBQL2	2	205.45	156916.6578	90090.28071	134626.7302	2436.664802	12446.06126	12506.86639	2.122942277	3.800488751
HSBP1	3	258.09	1069888.163	432952.447	680367.7133	55457.68021	64433.27794	39498.43168	2.999605956	3.775822299
ETFB	4	185.54	41798.71172	207835.8111	108182.2776	7522.672393	17400.36104	2073.603152	1.607173674	3.728369544
COG6	2	71.11	180632.3455	78810.92161	115020.1304	16867.94446	9927.445399	2235.819871	1.89616613	3.689148112
RAB18	2	117.45	243256.9894	169447.9014	189251.4121	21479.72484	6982.005359	18221.40531	2.713937351	3.688685394
ADCK4	2	85.8	94351.38794	124276.4933	169895.0733	9743.372986	5945.63161	14697.11473	2.93702803	3.676515496
NU188	2	84.14	95331.89597	53360.69943	64829.48226	13794.7404	3787.279944	72.7493266	1.123306796	3.596255344
ERGI3	2	53.68	219301.3449	102332.5309	127577.4655	6756.005925	21309.44446	9099.654538	2.468726847	3.595373766
BAG6	15	916.5	1063956.239	530962.658	711738.9269	42002.06133	91895.37871	63409.09066	2.908753429	3.547293393
TMX3	3	184.24	177673.0447	90569.12216	113261.9522	17618.31514	12170.97451	3153.771662	2.034140564	3.533652102
UB2V1	2	100.47	27592.55046	130924.2247	72665.3887	12104.53234	6519.486272	1478.853929	1.538065097	3.523556524
MPU1	2	108.56	206718.9505	115636.736	154836.9192	11968.55877	16688.87392	13403.17914	3.617445411	3.504029947
UCHL5	2	38.07	92429.56	63525.80973	72599.37128	7537.009138	7284.613162	5715.556648	4.170116506	3.476229818
TNPO3	2	71.37	144621.9199	89592.6772	120392.315	338.2526679	21920.99861	10189.34018	1.206894959	3.449992898
HSDL1	3	128.07	238412.8931	138049.5039	165886.3749	9517.300629	9194.526284	34139.25141	2.255200215	3.359216101
DHC24	7	401.81	1051291.496	339981.1588	610383.6646	68147.61699	62371.05979	66381.60123	2.60705999	3.345657234
ASNS	4	218.18	27236.7698	171430.9769	107043.9983	14413.26977	13620.8357	3076.178357	1.39532784	3.296708518
CY1	2	175.68	390624.129	223018.99	286975.9681	28300.7047	61543.82476	3119.625862	1.4398207	3.276170592
FACD2	10	514.36	595535.0484	319918.416	363208.044	28414.5887	51827.93688	54517.52588	2.873840686	3.24616961
OLA1	3	84.02	6739.60173	96279.51464	45580.26839	1905.775694	11890.49948	2289.52478	1.010022552	3.207568554
AFG32	2	87.66	266218.8291	69763.81298	129982.134	29522.17136	10236.30475	12436.5197	1.884998623	3.1582375
NCLN	3	110.84	151810.5306	118798.335	51161.51211	4026.983579	5593.222541	27600.09858	1.635810305	3.111869746
TM109	3	193.95	2128557.196	741617.905	1571766.115	116270.3236	309108.138	91861.27652	1.979519337	3.102285278
ABCE1	2	100.28	180280.4528	228714.1151	176016.8733	5853.351265	15469.80009	47476.7658	1.812994348	3.087986108
APT	2	69.2	81678.52251	294963.2647	132224.1422	10003.55635	31941.67625	18455.73939	1.85368189	3.074641929
TMX2	2	106.81	371290.2604	164004.6936	155805.9568	30719.98496	41544.65033	9831.420076	1.87689274	3.073511572
PIGS	2	107.23	138516.2391	42629.73737	87801.7788	4391.904365	26815.13072	1538.305236	1.372564613	3.037964418

OPA1	4	134.56	130650.4255	74911.63272	80284.10455	3403.949867	28348.88231	3080.573341	1.614628993	3.036695492
VAPB	4	268.94	416506.9089	248489.2161	232945.3183	7744.79615	68440.53099	34218.44871	1.637538183	3.023831853
RN126	3	251.08	525994.1889	280502.4686	334225.2035	67045.77592	49805.14736	23678.40168	2.392041083	3.021003945
RAC2	2	102.54	80460.41231	167604.9329	103378.7411	12685.50953	15828.63451	14877.31877	3.091374769	3.017812051
THEM6	3	179.98	302460.6286	180902.6637	221584.6424	21322.33488	46595.37978	20573.93694	2.650100687	2.993903447
DCAKD	3	114	153464.2264	83490.88646	117275.0733	15636.9141	17987.39211	11058.22892	3.081243797	2.986904211
SRPRB	13	1168.22	2356606.499	1252445.881	1772697.713	158027.6169	300604.9945	235622.8531	2.842057521	2.954536867
MPRD	2	63.4	403758.5618	189455.7616	276185.7067	69385.26371	22423.46862	22296.68755	2.094753638	2.929652826
VDAC2	2	165.53	185298.4981	63587.4718	71200.78036	12150.61983	26309.77203	3554.436452	1.509309944	2.929492465
XPOT	5	315.05	192152.0222	87834.0223	111134.1342	18165.44461	22238.0125	11344.55236	2.552757573	2.918036695
CB047	2	115.34	284719.5493	130033.8812	190940.3121	8955.553702	55631.74442	15759.10915	1.746291063	2.914283087
LAT1	3	283.6	534554.2065	250774.0012	333575.6027	27904.31074	80223.30157	42965.13305	2.250548912	2.88857972
EI24	3	79.84	198309.5484	94782.3236	94516.17662	7846.197007	26812.32063	19324.82657	1.992223219	2.84401227
UCK2	4	351.21	631346.4811	332289.1155	395077.2849	65389.18535	73917.666	50587.2553	3.02699373	2.838973586
VATH	2	90.98	456719.8086	188749.7682	292946.563	46618.49369	49388.45914	38127.75768	2.675757196	2.80654521
AAAS	5	212.77	362041.0814	157400.2565	256438.8803	25003.63463	43440.29387	42638.97024	2.502024053	2.804197213
FUND2	3	170.07	155872.4144	66284.67575	81778.76974	789.0479602	2925.884841	40106.34656	1.207379135	2.794063392
SC61B	3	258.61	869805.8076	438596.665	524439.0833	17462.80943	148948.4918	98268.19402	1.495266895	2.791763736
PSD13	5	257.79	277050.6305	256645.2022	295326.395	32953.82472	64093.08353	22728.28042	2.569841114	2.791081698
RDH11	7	463.66	850810.1228	437694.0325	614862.5361	85815.05262	120185.5841	69154.65644	2.811724745	2.790235542
PSD11	5	162	444330.9905	280377.2573	290097.3742	31561.4464	94631.09858	21669.9923	1.972596832	2.778874937
AMFR	7	463.85	533332.3635	261206.8513	292356.2496	23102.56658	85447.40766	50282.16974	1.985911313	2.774638376
DDRGK	3	267.52	191321.119	126482.1814	121025.2369	24844.11805	34792.27865	5121.311773	1.626837608	2.760533508
NTPCR	4	209.44	224270.7179	168624.377	238995.4131	14326.87493	46072.97841	33918.06515	2.264501734	2.74407081
DJB12	2	137.64	357081.3372	141342.3714	266288.1612	77299.67567	20968.1364	18545.99923	1.726837144	2.710705409
CERS2	4	176.44	588705.7071	301052.9363	440293.7639	51635.83294	96843.20871	54830.06952	2.600350873	2.709736317
HM13	2	130.39	383225.6361	102529.1486	156671.5571	23272.99079	59221.12809	19069.04482	1.59629211	2.661153809
SAE1	2	72.69	3890.241389	36693.09155	21523.55023	2610.669668	4297.940906	3084.428027	1.013332855	2.635757835
CND1	6	200.77	257381.7777	128069.9417	154547.4966	20634.99669	47027.58195	19621.23527	2.214347347	2.629171265
PTN1	4	183.41	264518.1559	108556.2263	131336.4813	11256.64812	52480.40639	18327.22862	1.677121747	2.619772988

PLCA	2	193.64	441886.5586	180590.0349	272120.6475	54541.70239	41216.35918	50904.62574	2.521353275	2.60873643
DHRS7	4	237.89	401883.9402	226211.3298	335157.6891	49773.69627	69167.30762	39677.61297	2.815173693	2.602352605
AT2B4	3	154.72	257229.1241	140766.591	216913.1939	27902.04311	46870.77667	26887.84526	2.683630362	2.596611135
DPM3	2	151.82	578373.8828	313474.5882	356597.4686	35643.24243	63884.25145	107629.4208	2.133913771	2.591337469
FANCI	7	434.1	395294.5467	231748.3048	266809.9435	23677.31952	100412.6155	24300.87146	1.794114836	2.590635546
RTN4	6	613.34	2121249.96	1560747.279	2014244.737	159811.5296	493862.9157	303631.4221	2.277626803	2.572958576
RBM4B	2	98.18	61416.63114	33119.93986	38152.43033	4916.94302	8950.836281	8663.772401	2.556655045	2.558030212
PSMD3	2	245.18	114804.9216	146011.2766	98208.84142	10785.86589	37228.27732	13231.40081	2.055153907	2.551407678
PEX19	3	111.31	256611.5387	124402.0876	204015.0439	36221.04114	34849.66186	29990.88899	2.826869318	2.533272516
PIGT	2	48.14	39631.64016	16687.27352	21902.80234	3557.777583	6985.109388	2970.958715	2.071575356	2.5331309
MTX1	2	107.82	199779.0345	56382.52488	205912.0841	29400.98041	29975.51966	21267.56121	1.658718923	2.5184826
ARF4	2	414.66	83496.06429	106467.4647	86529.65113	5987.003745	24529.6364	17948.45289	1.917368162	2.51222597
ETFD	2	146.39	254740.0909	81643.01257	124750.6509	20051.33662	39664.18429	22563.43741	1.869501809	2.486589839
STX12	4	147.51	307407.5334	145356.9347	210470.3903	61214.81117	28791.95736	31703.75157	2.223126199	2.446065961
RAB21	4	383.93	430263.783	217757.6447	316930.8193	83941.37533	71040.20029	23516.33662	1.795960819	2.434550349
STX7	3	183.19	149866.5358	72172.90691	81657.27117	11483.51137	31535.27042	13658.48211	1.961911663	2.421789279
LCLT1	3	168.03	200207.5912	111411.7384	119419.2734	5447.028811	55163.06776	21584.71025	1.34525365	2.39069793
UBAC2	5	251.41	668492.4328	174492.2968	234308.6343	93470.15552	68910.54127	44404.09217	1.521798462	2.381209202
PCH2	7	370.58	274138.1814	148990.0612	178754.7844	87842.22272	8037.414571	27574.76832	1.297333141	2.285504812
SURF4	3	450.51	2326733.372	836510.7474	1029086.667	144164.5799	454369.4798	265216.8944	1.593777903	2.279065249
COPB	4	332.27	296998.3826	236737.9807	266841.8865	35332.90626	98141.41381	31800.93454	2.02700218	2.276171684
FACR1	9	593.27	1131804.623	441702.1667	696066.4254	213096.4901	103756.5821	154503.4005	1.966736971	2.267530585
STX5	2	93.65	326547.1604	161188.8443	221641.6748	44161.93164	35794.55173	67578.96681	2.316270349	2.265492286
RAB14	3	338.45	524554.0248	288185.7662	361188.4104	50150.38516	130743.0036	65390.84296	2.071224371	2.252948007
MET7A	2	139.31	229386.7968	112371.5828	151099.6361	13528.88939	27408.65651	62597.17065	1.601637099	2.251057486
SMN	4	207.52	262084.9768	233184.8888	193074.1244	48302.97518	76662.02219	24690.24407	2.048564816	2.201486903
RFT1	2	140.05	324282.9051	121907.1591	149878.7574	45844.43004	46461.21891	37649.44843	2.029915184	2.197465689
CHIP	2	65.87	28242.34548	61483.79093	58918.28396	6133.876898	12710.07019	13884.49323	1.860971788	2.183248553
F10A1	10	779.1	3605670.176	2452277.739	3487307.46	679652.1486	888615.1282	546578.9523	2.896366525	2.174231028
ABCD3	2	88.1	222127.9399	164279.1518	123607.2643	5461.72324	48391.36376	59235.48518	1.135779148	2.173084707

RDH10	3	163.73	658740.3396	289840.3984	429233.7152	90977.6557	181422.7298	33755.62092	1.426778706	2.170042724
DIC	3	191.4	355047.2263	153114.2225	218580.3995	62962.51284	45317.41289	55214.31943	2.274592668	2.152203129
PO210	7	264.46	224424.012	183069.182	169095.6943	34828.00755	54028.21941	44162.32255	3.19640142	2.11591559
P5CR2	2	362.2	165490.5299	197684.6675	178764.2287	25452.9813	54442.29878	46460.18873	2.497937846	2.1006435
PRRC1	2	121.83	191405.489	114688.5823	129522.4701	15714.16825	35294.36761	51502.05182	1.794921878	2.087285813
S23IP	4	265.91	333884.4498	232062.4698	223640.2458	29033.73614	102326.7892	54677.72385	1.806077084	2.085499271
T161A	2	63.17	108825.4657	61651.22554	68263.3478	15846.4006	18637.01003	22077.70179	2.683946144	2.077558141
TMED9	5	363.38	1253653.149	578157.0519	672913.3144	183378.6419	264903.5635	149474.1244	2.074456562	2.067021953
AR6P1	3	131.23	489285.9693	288949.3972	338721.8629	92220.09666	40426.1019	138925.167	1.726018494	2.040170668
RAB5B	2	287.25	209507.8602	128353.7983	178747.3835	41129.10539	41887.6554	43006.70038	3.181315249	2.035380556
ATD3A	6	832.07	2174020.325	732954.0369	1057578.753	370243.8775	219969.4182	378111.5939	1.663259947	2.033595172
SUCB1	2	224.49	125568.8631	179226.2471	151200.0127	25714.07654	69586.44793	16196.27991	1.639898078	2.032016032
TMM33	7	354.95	1913965.496	630100.331	842094.0235	229505.3295	316503.1442	283805.0703	1.702447933	2.02879097
RCN1	4	328.55	114844.7278	393001.1036	246926.7618	47442.28536	74828.6619	63206.94519	1.565444115	2.024794799
MPCP	11	551.93	1519012.27	599678.7053	776219.856	211155.7967	436821.1525	65996.64336	1.208816589	2.019576291
SCO1	3	135.25	267182.7672	158740.3064	192179.9676	39971.35238	73570.49852	38950.57203	2.279390498	2.019109804
HAT1	2	70.98	176300.8231	231910.0048	138430.4227	15584.79959	56372.4518	63386.10531	1.504908034	2.013970258
MARC1	3	233.52	285533.5531	147277.7749	223659.877	82800.02608	21974.86641	58031.0013	1.561397873	2.011578803
SRP68	3	193.7	247354.2736	223401.8082	249725.8688	58556.49659	51674.64419	69666.83771	3.925192934	2.001783313

Shown are cellular proteins identified by label-free mass spectrometry/mass spectrometry that interact with GFP-3aM. Protein identifier (ID) and the number of unique peptides used to identify proteins are indicated. Relative abundance score for each protein is shown. Confidence score (-Log2) is the score of the probability of the peptide sequence occurring randomly, added together for each unique peptide. The higher the confidence score, the higher the confidence in protein identification. The p-value (-Log10) is a comparison of the cellular protein abundance between GFP-3aM and GFP. The higher the p-value, the higher the probability the protein interacts with 3aM. The fold-change (Log2) is the change in the relative abundance of the cellular protein detected between GFP-3aM and GFP.

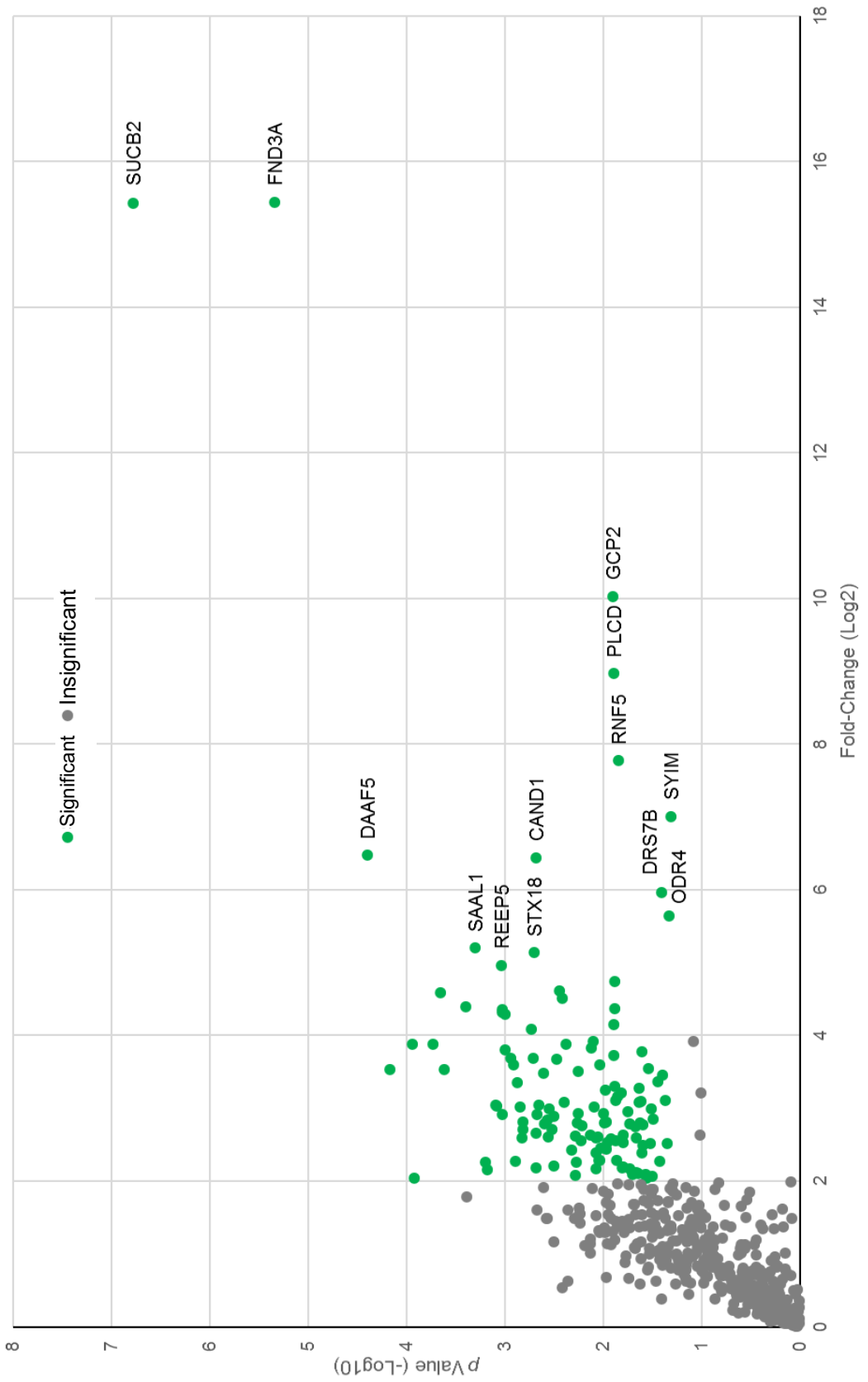
Significant
Insignificant
SUCB2
FND3A
DAAF5
SAAL1
REEP5
STX18
CAND1
RNF5
PLCD
GCP2
DRS7B
ODR4
SYIM
p Value (-Log10)
Fold-Change (Log2)
0
1
2
3
4
5
6
7
8
0
2
4
6
8
10
12
14
16
18

Figure 3.6 Scatter plot representing results from the GFP-3aM co-IP.

Proteins were identified in the GFP-3aM eluate by LC-MS/MS. Proteins were plotted by fold-change in abundance (Log2) compared to the GFP control and *p*-value (-Log10) of the *t*-test. Proteins with a *p*-value (-Log10) above one and a fold change (Log2) above two have the highest chance of interacting with 3aM and are considered significant (green). Proteins with a fold-change (Log2) in relative abundance above 5 over the GFP control are labelled. Results are from three biological replicates.

A panther over-representation test (pantherdb.org) was performed to categorise the cellular localisation of the significant proteins identified in the GFP-3aM eluate by LC-MS/MS. This test grouped cellular proteins by their Gene Ontology (GO) cellular compartment annotation and helped to determine if these cellular compartments are over-represented in the dataset. The test compared the number of proteins you would expect to find in the data set for each GO cellular compartment, to the actual number of proteins identified. A higher actual number of proteins would suggest that the interacting partners identified for 3aM localise to a specific cellular component (**Appendix, Table 7.2**). Cellular compartments with a *p*-value below 0.05 were considered significant. The number of proteins that localise to these significant GO cellular components were represented as a Venn diagram (**Figure 3.7**). Of the 135 proteins identified, 78 of the proteins can localise to membrane structures of the cell with a significant proportion of proteins localising to the nuclear envelope, ER, ER-GIC, mitochondria and Golgi membrane. Other cellular components that these interacting partners localise to also include the proteasome and peroxisome. The remaining 58 proteins, did not localise to a GO cellular component that was over-represented in the data set.

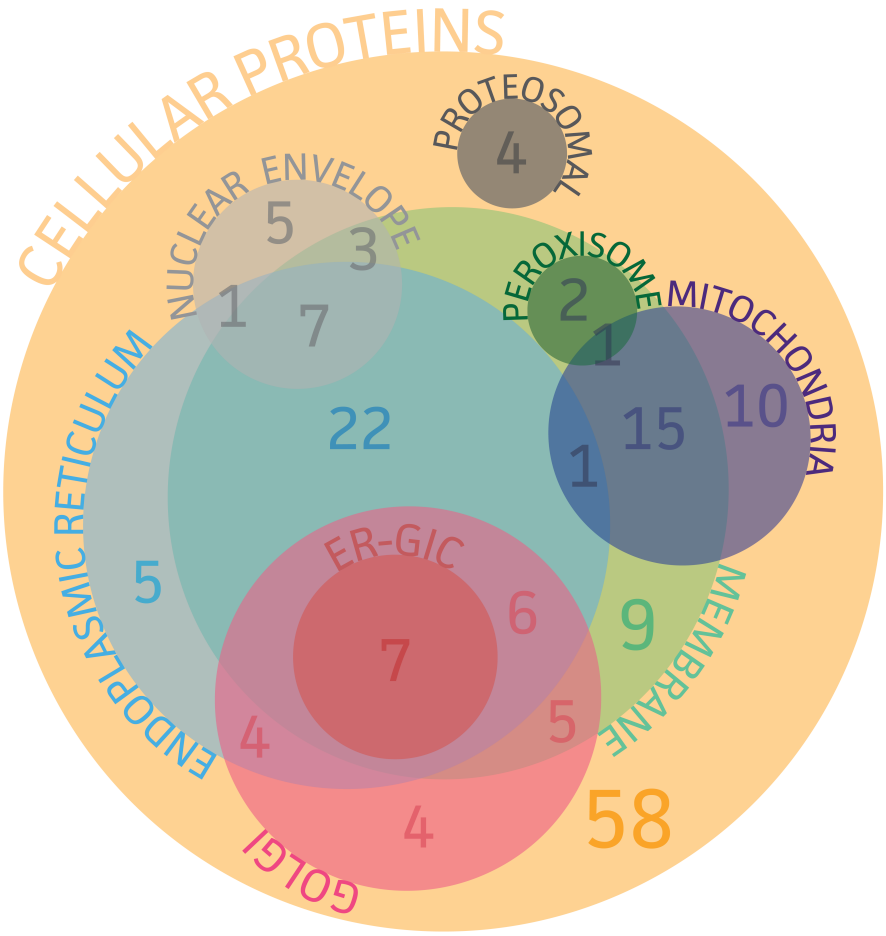

Figure 3.7 GO cellular component annotations of cellular proteins that interact with GFP-3aM.

Significant proteins identified by LC-MS/MS were analysed by a panther over-representation test (pantherDB.org). Proteins which localise to cellular components that are over-represented ($p < 0.05$) were collated and represented as a Venn diagram.

3.6. IBV 3a interaction with RNF5 and CAND1

Due to the role of 3a in IFNβ expression, proteins identified by LC-MS/MS that play a role in the IFN cascade were investigated. Three proteins were identified that play a regulatory role in IFN expression, RING Finger 5 (RNF5), Cullin-Associated NEDD8-Dissociated protein 1 (CAND1) and Autocrine Motility Factor Receptor (AMFR). RNF5 and AMFR both target MAVS for degradation by the addition of ubiquitin, while CAND1 is a regulatory protein of the E3-Skp1-Cul1-Fbox (SCF) ligase complex, which plays a role in IRF3/IRF7 degradation (Zheng et al. 2002, Zhong et al. 2010, Jacobs et al. 2014). RNF5 and CAND1 were the fifth and eighth highest confidence interacting partners for 3aM (**Table** 3.1). The interaction was first verified by looking at GFP-3aM and RNF5/CAND1 colocalisation. Vero cells were transfected with GFP-3aM or GFP expression vectors. After 16 hours, cells were fixed, permeabilised and labelled with anti-GFP and anti-CAND1 or anti-RNF5. To determine what percentage of 3a signal colocalised with RNF5 and CAND1, twenty cells expressing 3aB-FLAG were analysed using ImageJ. For each region of interest, the amount of anti-GFP signal that colocalised with anti-RNF5 or anti-CAND1 signal was calculated and averaged. This demonstrated that 9.63% and 27.4% of 3a-GFP signal colocalised with RNF5 and CAND1, respectively. Overexpressed GFP-3aM therefore partially colocalises with both CAND1 and RNF5 (**Figure 3.8A,B**), while 3a also partially colocalised with RNF5 during infection (**Figure 3.8C**). The result suggests that 3a does interact with RNF5 and CAND1 as the mass spectrometry data suggested.

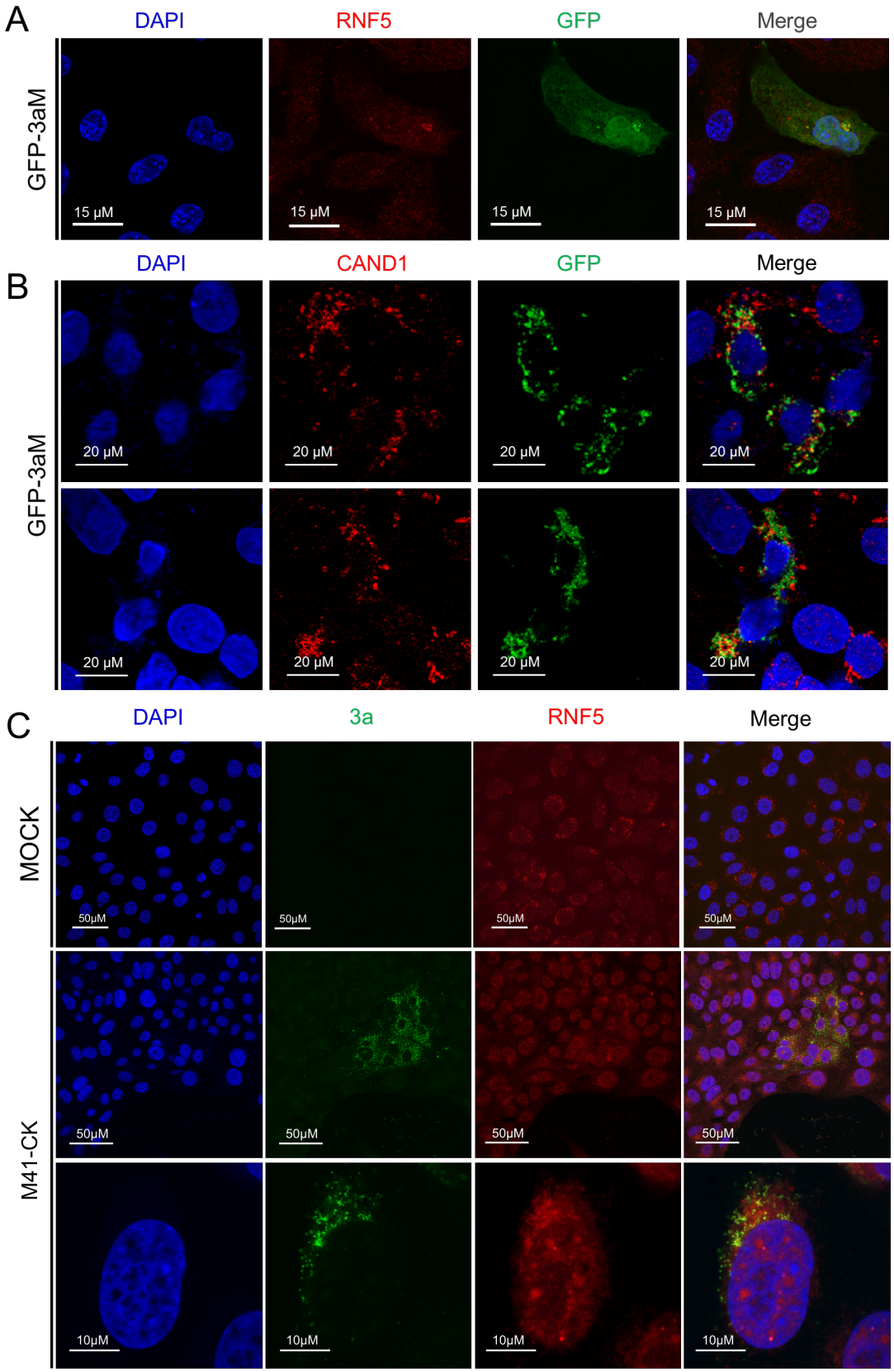

Figure 3.8 IBV 3a partially colocalises with RNF5 and CAND1.

Vero cells were transfected with GFP-3aM expression vectors. After 16 hours, cells were fixed, permeabilised, and labelled with (A) anti-RNF5 or (B) anti-CAND1. (C) Vero cells were mock infected or infected with M41-CK at an MOI above 4 for 24 hours. Cells were fixed and labelled with anti-RNF5. The nucleus was stained with DAPI.

3.7. Characterisation of IBV 3a interaction with MAVS

Mass spectrometry data identified two E3 ligases which regulate IFN expression through interaction with MAVS, RNF5 and AMFR (Zheng et al. 2002, Prakash et al. 2006, Zhong et al. 2010, Jacobs et al. 2014). RNF5 and AMFR poly-ubiquitinate MAVS, targeting MAVS for proteasomal degradation. The levels of MAVS was measured in the presence of 3aM, to determine the effect of these interactions.

3.7.1. IBV 3a increases levels of MAVS

The effect of 3a on MAVS was first investigated by quantifying levels of MAVS by western blot. Vero cells were transfected with pFLAG-3aB or pFLAG expression vector. Cells were then transfected with poly(I:C) to stimulate the IFN signalling cascade. After 12 hours, cells were lysed, samples separated by SDS-PAGE, transferred to a membrane and labelled with anti-MAVS (human), anti-3a and anti-actin. MAVS can be expressed as multiple isoforms, full-length MAVS (flMAVS) at around ~75 kDa and short MAVS (sMAVS) which is between 30 – 50 kDa. These MAVS isoforms play different roles in IFN signalling, with the flMAVS the primary signalling protein for the IFN cascade (Seth et al. 2005, Jacobs et al. 2013). Anti-MAVS can label both isoforms. Signal fluorescence was measured for flMAVS and sMAVS and then normalised against actin signal. Levels of flMAVS was visibly higher when expressed with 3aB-FLAG compared to the empty vector control (**Figure 3.9A**), while levels of sMAVS was unaffected (**Figure 3.9B**). This result suggests that 3a can stabilise or increase MAVS expression.

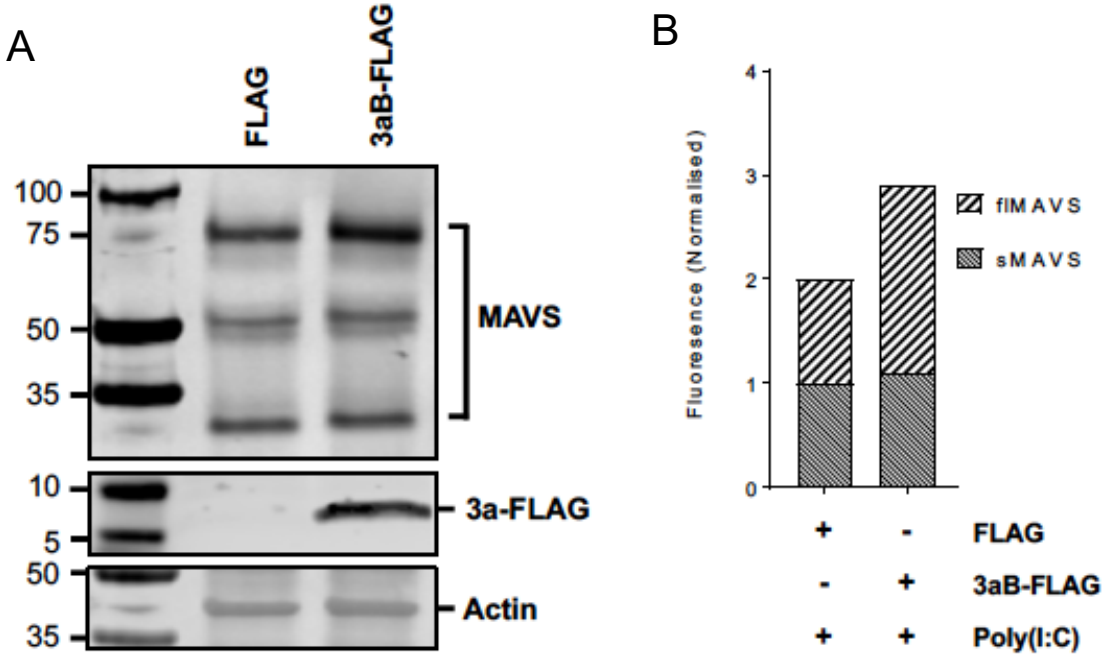

Figure 3.9 IBV 3a increases levels of MAVS.

(A) Vero cells were transfected with vectors expressing FLAG or 3aB-FLAG. After 16 hours cells were lysed, proteins separated by SDS-PAGE, transferred to a membrane and incubated with anti-3a, anti-MAVS and anti-actin. (B) Levels of full-length MAVS (75 kDa) and small MAVS (30-50 kDa) were semi-quantified by normalising fluorescence signal against actin using the Image Studio software (Li-Cor).

3.7.2. IBV 3a localises with MAVS

To further characterise the effect of 3a on MAVS, immunofluorescence was used to establish if MAVS and 3a colocalise. DF-1 cells were transfected with plasmids expressing 3aB-FLAG and chMAVS-V5. After 16 hours, cells were fixed, permeabilised and labelled with anti-V5, anti-FLAG and the nucleus stained with DAPI. Colocalisation of chMAVS and 3aB-FLAG was observed, as indicated by the yellow signal, although there was not perfect colocalisation

(**Figure 3.10A**). To determine what percentage of 3a signal colocalises with MAVS, twenty cells expressing 3aB-FLAG were analysed using ImageJ. For each region of interest, the amount of anti-FLAG signal that colocalises with anti-MAVS signal was calculated and averaged. Only 4.6% of 3aB-FLAG signal colocalised with MAVS. Nonetheless, 3aB-FLAG signal does visually localise closely with MAVS suggesting they localise to a similar domain (**Figure 3.10A**).

Vero cells were then infected with Beau-R, to determine if 3a also localises with MAVS during infection. At 24 or 48 h.p.i cells were fixed, permeabilised and labelled with anti-3a or anti-MAVS. During infection, 3a localised with MAVS signal at 24 hours. At 48 h.p.i 3a and MAVS signal did localise again, and colocalisation was visible. Anti-MAVS signal was visibly lower compared to non-infected cells at 48 h.p.i (**Figure 3.10B**). This result further suggests that 3a localises with MAVS although they may not interact directly. Furthermore, it appears MAVS levels decline at least 48 h.p.i.

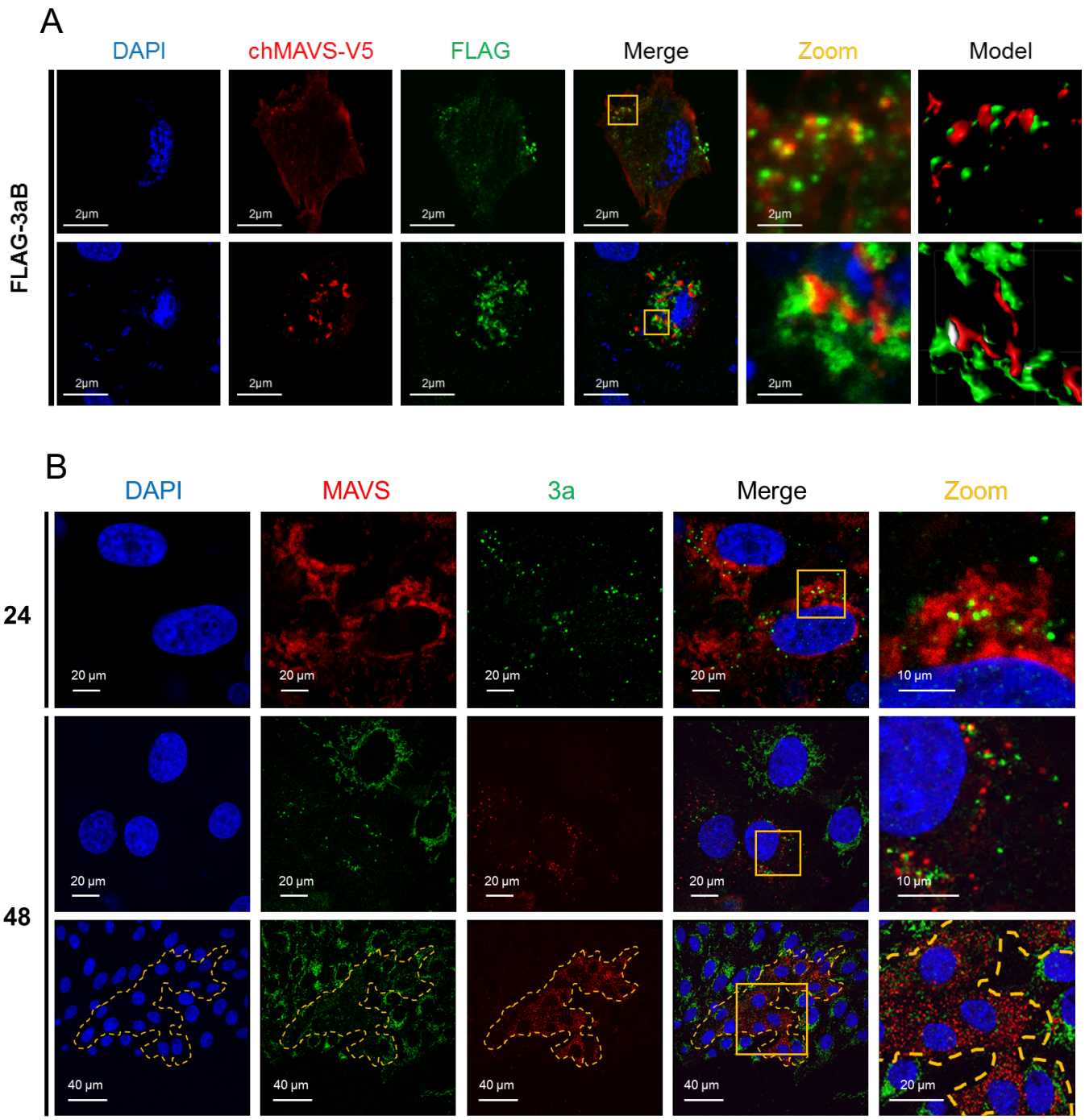

Figure 3.10 IBV 3a localises with MAVS.

(A) DF-1 cells were transfected with pFLAG-3aB and chMAVS-V5. After 16 hours, cells were fixed, permeabilised and labelled with anti-FLAG and anti-V5. The yellow box indicates the enlarged area. The model was generated using the Imaris software (Bitplane) 3D tool. (B) Vero cells were infected with Beau-R at a MOI above 4. After 24 or 48 h.p.i cells were fixed, permeabilised and labelled with anti-MAVS or anti-3a. The yellow outline indicates infected cells.

3.7.3. IBV 3a agonises IFNβ expression by interfering with MAVS

IBV 3a had a stimulatory effect on IFN expression when induced with poly(I:C) or chMDA-5 (**Figure 3.3A,B**). Conversely, it was shown that 3a had an inhibitory effect on IFN expression when induced with MAVS overexpression. The effect was not dose-dependent suggesting that the inhibitory effect is most likely because of the effect of 3a on IRF7 downstream (**Figure 3.3C,D**). For this reason, the chIFNβ-luciferase assay was repeated, and the effect of poly(I:C) stimulation along with MAVS overexpression on IFNβ expression was evaluated. DF-1 cells were transfected with increasing levels of 3aB-FLAG vector, made up to 1 μg with pFLAG. Cells were simultaneously transfected with the chMAVS-V5 vector. A Renilla luciferase expression vector was used as a transfection control. After 8 hours, cells were either mock transfected or transfected with poly(I:C). After 12 hours, cells were lysed, and luciferase activity measured. As seen before, 3aB-FLAG had an inhibitory effect on Firefly luciferase activity when induced with MAVS overexpression. When the cells were treated with poly(I:C) as well as 3aB-FLAG, there was a dose-dependent increase in Firefly luciferase activity (**Figure 3.11A**). This result could suggest that while 3aB-FLAG increases MAVS levels, this does not induce IFNβ expression unless stimulated upstream with poly(I:C) or even MDA-5. To further confirm this effect, the chIFNβ luciferase assay was repeated using four conditions. DF-1 cells were transfected with a combination of poly(I:C), MAVS and/or 3aB-FLAG expression vector as indicated and luciferase activity measured after 16 hours. As expected, transfection of MAVS and poly(I:C) induced significantly higher levels of Firefly luciferase activity compared to the poly(I:C) control. Low levels of 3a (250 ng), with poly(I:C)

treatment, induced higher levels of luciferase activity compared to poly(I:C) alone, as seen previously. Expression of MAVS, 3a, and treatment with poly(I:C) induced the highest level of Firefly luciferase activity (**Figure 3.11B**), suggesting that IBV 3a agonises IFNβ expression at the point of MAVS only after stimulation with poly(I:C). When the IFN cascade is not stimulated, 3a still increases MAVS levels, but no increase in IFNβ expression is observed. This effect could be due to the inhibitory effect of 3a on IRF7 activity downstream. When stimulated with poly(I:C) or MDA-5 upstream, signalling is exacerbated by increased MAVS levels; this is enough to overcome the inhibitory effect of 3a on IRF7 activity and thus an increase in IFN expression is observed.

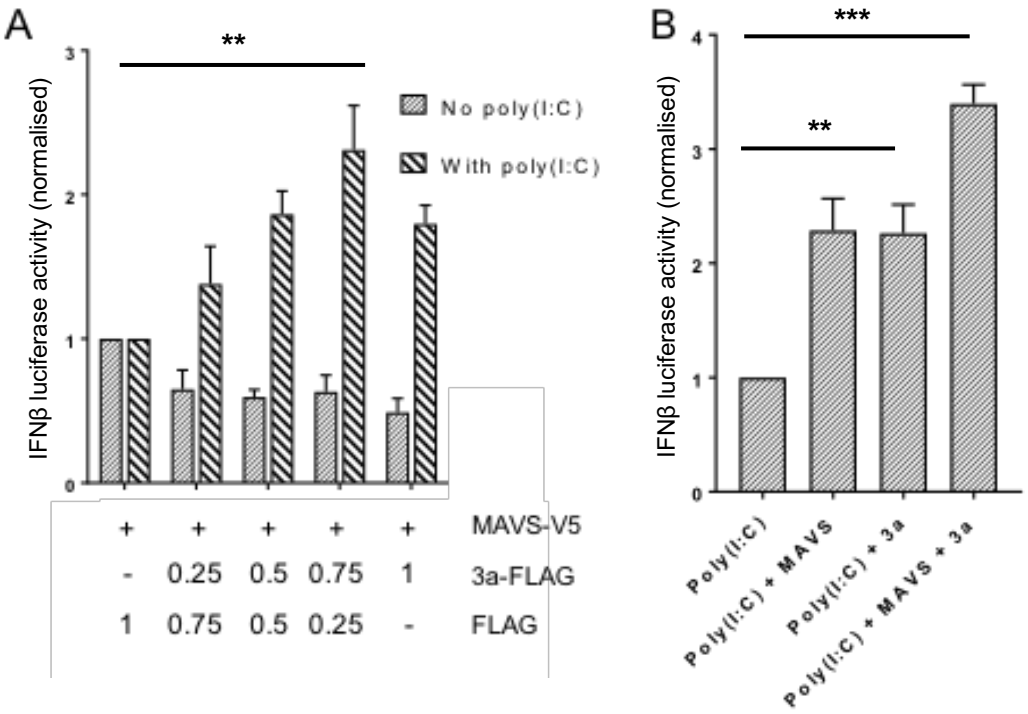

Figure 3.11 IBV 3a agonises IFNβ expression by interfering with MAVS, only after stimulation with poly(I:C).

(A) DF-1 cells were transfected with FLAG/ 3aB-FLAG and chMAVS-V5 expression vector along with a chIFNβ-luciferase reporter plasmid. After 8 hours, cells were either mock transfected or transfected with poly(I:C). After 12 hours cells were lysed and luciferase activity measured. A renilla luciferase plasmid was used as a transfection control. (B) DF-1 cells were transfected with plasmids expressing chMAVS-V5, 3aB-FLAG or/and transfected with poly(I:C) as indicated along with a chIFNβ-luciferase reporter plasmid. Empty V5/FLAG expression vectors were transfected to maintain levels of total plasmid transfected. Cells were lysed after 16 hours and luciferase activity measured. A renilla luciferase plasmid was used as a transfection control. Results are representative of three biological replicates. * significance $p < 0.05$, ** significance $p < 0.01$, *** significance $p < 0.001$.

3.8. Characterisation of IBV 3a interaction with IRF3/IRF7

3.8.1. IBV 3a degrades IRF3/7

Mass spectrometry data and immunofluorescence suggested that IBV 3a interacts with the IRF3/7 regulatory protein CAND1. CAND1 binds to Cullin-1 (CUL1) to inhibit the formation of the E3-SCF ligase complex, a complex that mediates the degradation of IRF3/7 (Zheng et al. 2002). To determine whether this interaction leads to a decrease in IRF3/7 levels, levels of IRF3 were measured in the presence of 3aB-FLAG. Endogenous levels of human IRF3 (huIRF3) were first measured in Vero cells as there is no antibody against chicken IRF7. Vero cells were transfected with pFLAG-3aB or pFLAG expression vectors. After 16 hours, cells were lysed, separated by SDS-PAGE and transferred to a membrane. The membrane was labelled with anti-huIRF3 and anti-3a. Compared to cells transfected with pFLAG, cells expressing 3a expressed lower levels of IRF3 (**Figure 3.12A**).

There is no antibody against chicken IRF7, so to determine if 3a has the same effect on the chicken isoform a V5-tagged chicken IRF7 expression vector was used. DF-1 cells were transfected with increasing levels of pFLAG-3aB and made up to 1 µg with pFLAG, along with 500 ng of pEF1a-chIRF7-V5. After 16 hours, cells were lysed, separated by SDS-PAGE and transferred to a membrane. Membranes were incubated with anti-V5, anti-FLAG, and anti-actin. Levels of chIRF7 decreased as levels of 3aB-FLAG increased (**Figure 3.12B**). This result

suggests that 3aB-FLAG can decrease levels of chIRF7 in a dose-dependent manner.

To determine if this effect is due to proteasomal degradation, a proteasomal inhibitor, MG132, was used. DF-1 cells were transfected with GFP-3aM expression vector along with chIRF7-V5 for 12 hours. Cells were then treated with either MG132 or DMSO for 8 hours. Cells were lysed, proteins separated by SDS-PAGE, transferred to a membrane and incubated with anti-V5 and anti-GFP. Compared to DMSO treatment, cells transfected with GFP-3aM treated with MG132 expressed higher levels of IRF7-FLAG (**Figure 3.12C**). This result suggests that 3a initiates IRF7 degradation in a dose-dependent manner, proteasome-dependent manner.

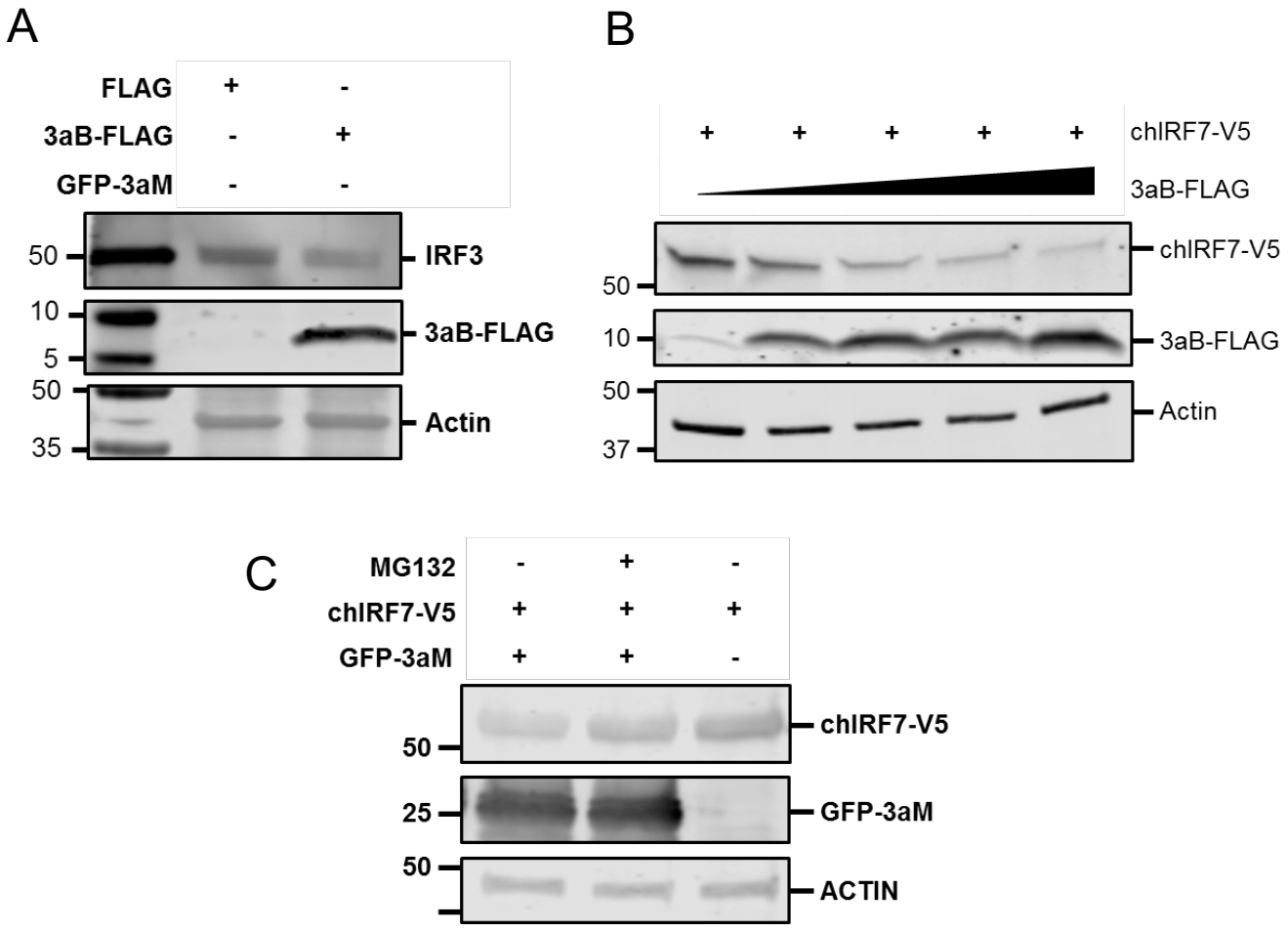

Figure 3.12 IBV 3a induces degradation of IRF7 in a dose-dependent, proteasome-dependent manner.

(A) Vero cells were transfected with either 3aB-FLAG or FLAG expression vectors. After 16 hours, cells were lysed, separated by SDS-PAGE and transferred to a membrane. The membrane was labelled with anti-huIRF3 and anti-3a. (B) DF-1 cells were transfected with increasing levels of 3aB-FLAG expression vector made up to 1μg with pFLAG along with an IRF7-V5 expression vector. After 16 hours, cells were lysed, proteins separated by SDS-PAGE and transferred to a membrane. Membranes were labelled with anti-V5 and anti-FLAG. (C) DF-1 cells were transfected with either GFP or GFP-3aM expression vectors along with the chIRF7-V5 vector. After 12 hours, cells were treated with either DMSO or MG132 for 8 hours. Cells were then lysed, separated by SDS-PAGE, transferred to a membrane and labelled with anti-GFP and anti-FLAG.

3.8.2. IBV 3a colocalises with IRF7

IBV 3a affects the activity of IRF7, to further characterise this effect, colocalisation of 3aM and IRF7 was investigated. DF-1 cells were transfected with plasmids expressing chIRF7-V5 and GFP-3aM or GFP. Cells were fixed, permeabilised and labelled with anti-V5. Cells were visualised, and images taken using a Leica SP5 confocal microscope. GFP-3aM signal colocalised with the IRF7-V5 signal (yellow), while GFP signal alone did not (**Figure 3.13**). This result shows that GFP-3aM colocalises with IRF7 and they may interact.

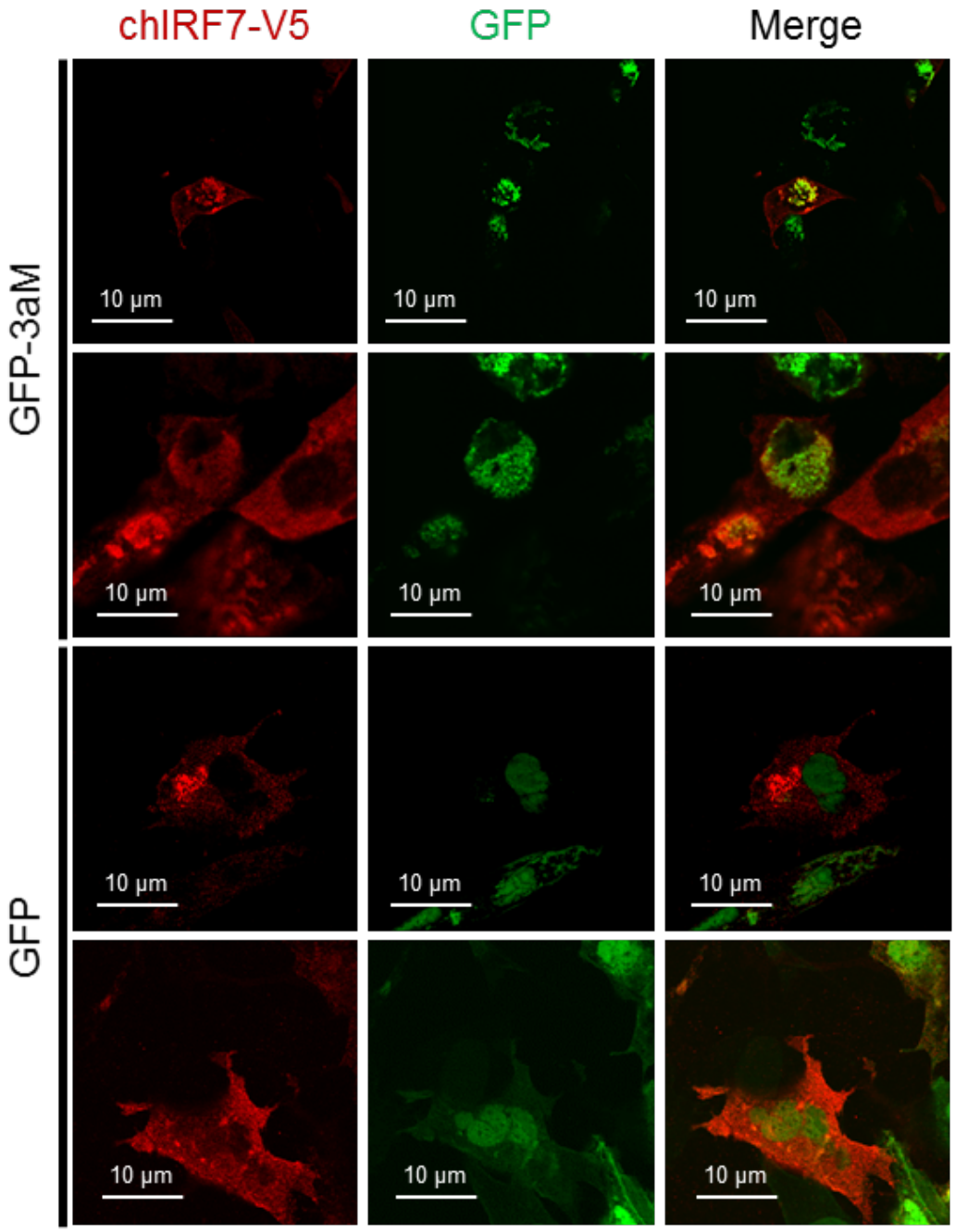

Figure 3.13 IBV 3a colocalises with IRF7.

DF-1 cells were co-transfected with vectors expressing chIRF7-V5 or GFP-3aM /GFP. After 16 hours, cells were fixed, permeabilised and labelled with anti-V5.

3.9. Effect of 3a levels on IFNβ during infection

The effect of IBV 3a on poly(I:C)-induced IFNβ expression was dose-dependent with low levels of 3a having a stimulatory effect on IFNβ expression and higher levels of 3a having an overall inhibitory effect on IFNβ expression (**Figure 3.3**). Levels of 3a were semi-quantified with IFNβ expression to determine the effect of changes in expression on the action of 3a. CK cells were infected with Beau-R or BeauR-Sc3aAUG at an MOI of 0.1. The supernatant was harvested at 24, 36, 48 and 60 h.p.i. The supernatant was heat inactivated for 1 hour at 65 °C to inactivate IBV. Levels of IFNβ was then quantified using a quail reporter cell line (CEC-32) with a MxA promoter upstream of a Firefly luciferase reporter gene (Schwarz et al. 2004). A standard curve was generated to calculate IFNβ levels relative to Firefly luciferase activity using serial dilutions of recombinant chIFNβ. As seen in previous studies, there was no difference in IFNβ levels 24 h.p.i between Beau-R and BeauR-Sc3aAUG (**Figure 3.14A**). While at and after 36 h.p.i, BeauR-Sc3AUG induced less IFNβ expression compared to wild-type Beau-R, suggesting 3a induces IFNβ expression late in infection.

Levels of 3a can affect the role of this protein in inducing or inhibiting IFN expression. To determine if induction of IFNβ by 3a during infection is coupled with lower levels of 3a, a time course was performed. CK cells were infected with Beau-R at an MOI of 0.1 for 4, 8, 12, 16, 24, 36 and 48 hours. Cells were then lysed, proteins separated by SDS-PAGE, transferred to a membrane and labelled with anti-3a and anti-actin. Peak levels of 3a occurred at 24 h.p.i and declined at

36 h.p.i (**Figure 3.14C**). The decline in 3a levels coincided with increased IFNβ levels, possibly suggesting low levels of 3a are, in part, responsible for the induction of IFNβ expression seen during infection, although the role of other IBV viral proteins has not been discounted.

An MG132 proteasome inhibitor was then used to determine if this decrease in 3a levels is due to proteasomal degradation. DF-1 cells were infected with Beau-R and after 28 hours, cells were either treated with DMSO or 5/10 μM of MG132. After 8 hours, cells were lysed, proteins separated by SDS-PAGE, transferred to a membrane. Membranes were labelled with anti-3a. Higher levels of 3a were detected for infected cells treated with 10 μM of MG132 (**Figure 3.14C**). This result suggests that proteasome degradation of 3a is, in part, responsible for the decrease in 3a levels 36 h.p.i.

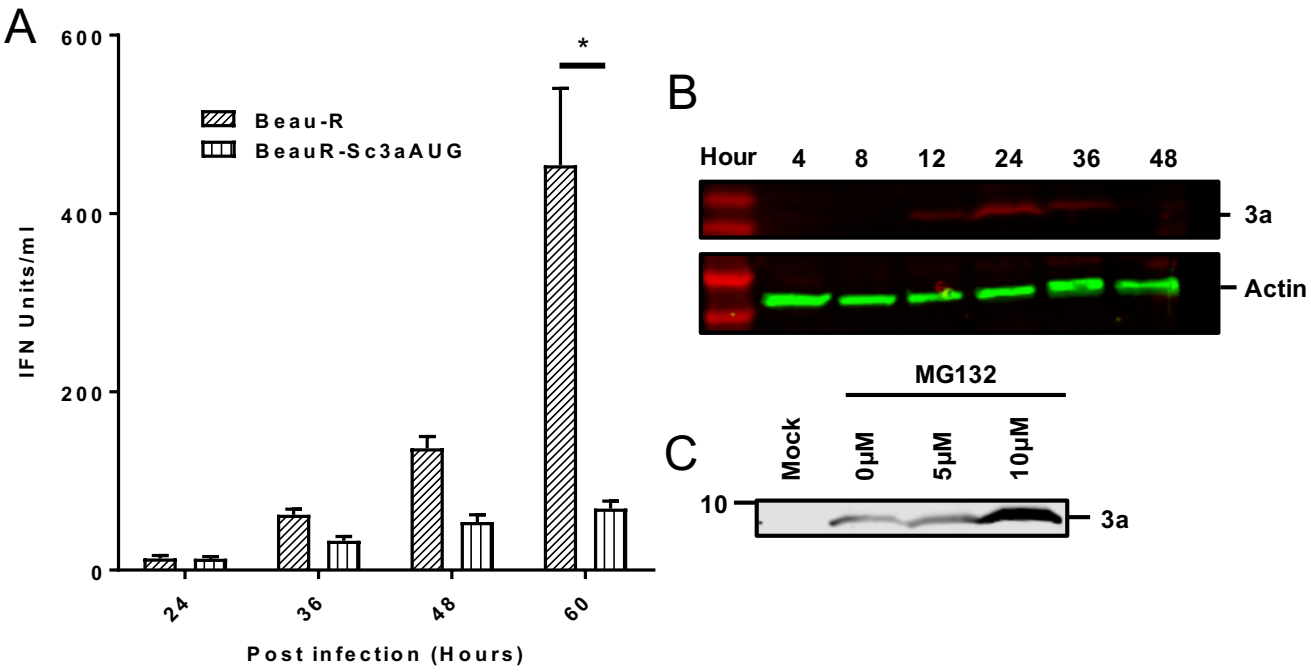

Figure 3.14 IBV 3a induces IFNβ expression during infection, coinciding with a decrease in 3a levels.

(A) CK cells were infected with Beau-R or BeauR-Sc3aAUG at an MOI of 0.1. At each indicated time-point the supernatant was removed and IFNβ levels quantified using a MxA-luciferase reporter cell line. Recombinant chIFNβ was used to generate a standard curve. Results are from three biological replicates. (B) CK cells were infected with Beau-R at an MOI of 0.1. At 4, 8, 12, 24, 36 and 48 h.p.i, cells were lysed, proteins separated by SDS-PAGE and transferred to a membrane. Membranes were incubated with anti-3a and anti-actin. (C) CK cells were infected with Beau-R at an MOI of 0.1. Cells were treated with DMSO or 5/10 μM of MG132. After 8 hours, cells were lysed, proteins separated by SDS-PAGE, transferred to a blot and labelled with anti-3a. Results are representative of three biological replicates. * significance $p < 0.05$.

3.10. Discussion

Previous work has shown that IBV 3a localises to two compartments during infection and transfection in Vero cells, the cytoplasm; where it is diffuse, and the smooth ER, where it is membrane-bound (Pendleton et al. 2005). Analysis of the GFP-3aM mass spectrometry data predominantly identified membrane-bound ER proteins but did also identify proteins that localise to the Golgi, mitochondria, and ER-GIC membrane as well as the nuclear envelope and proteasome regulatory units (**Figure 3.7**). Previous work has shown that adding a GFP-tag to 3a increased ER membrane localisation while decreasing cytoplasmic localisation (Pendleton et al. 2005). It was suggested that extension of the 3a peptide sequence increased the efficiency of the signal peptide sequence in 3a, increasing ER translocation by signal recognition particles. (Pendleton et al. 2005). This observation could explain why a significant proportion of proteins detected in the GFP-3aM co-IP eluate were ER membrane proteins (**Figure 3.7**). A GFP-tag was used in the co-IP as GFP 'capture' beads are highly efficient in pulling down GFP and are thus suited for LC-MS/MS. Nonetheless, as the GFP-tag may have skewed the localisation of 3a to the ER, a different, smaller tag should be used in any future repeats. A smaller epitope tag would better replicate the pattern of 3a localisation seen during infection and would give more representative mass spectrometry results, potentially allowing other 3a functions to be identified. The GFP co-IP was used with 3a from M41-CK as opposed to Beau-R. Beau-R and M41-CK 3a have a high sequence similarity (**Figure 3.4A**) and are unlikely to have different roles or functions when overexpressed alone. Furthermore, 3aB

and 3aM have a similar effect on IFNβ promoter activity suggesting they are functionally comparable (**Figure 3.4B**). The mass spectrometry data identified a range of proteins that interact with GFP-3aM, and while many were membrane-bound, there was no consensus regarding their cellular role (data not shown). The identification of membrane proteins in a range of cellular components suggests that 3a can localise to a range of cellular structures when expressed alone (**Figure 3.7**). These cellular membrane proteins can often localise to multiple cellular organelles and highlight the dynamic nature that exists between the ER, ER-GIC and Golgi, and the ER, mitochondria, and peroxisomes, through membrane-associated membrane (MAM) structures (Prinz 2014). The mass spectrometry was not repeated with a vector expressing 3aM-GFP, which may have identified proteins that interact with the N-terminus or additional proteins. Instead, the decision was made to save time and cost by focusing on proteins identified in the LC-MS/MS that play a role in the IFN cascade (**Figure 3.3**). Future work should focus on the other proteins identified by mass spectrometry as they may allude to additional functions for 3a. Furthermore, expression vectors with 3a tagged at the N- and C- terminus should also be used to identify the full repertoire of 3a interacting partners.

Previous work has shown that 3a plays a role in regulating the IFNβ response during IBV infection (Kint et al. 2015). Recombinant viruses lacking 3a showed increased IFNβ transcription but only at 24 h.p.i. No effect on IFNβ protein expression was observed at this time. Conversely, deletion of 3a caused a

decrease in IFNβ protein expression at 48 h.p.i. The reason for this discrepancy is unknown but does show a possible complicated relationship between 3a and the IFN cascade (Kint et al. 2015). This result was confirmed here in CK cells (**Figure 3.14**). The reason for this seemingly contradictory effect is not fully understood, as is the mechanism of action of 3a on the IFN cascade (Kint 2015). To determine the mechanism of action, a chIFNβ-luciferase assay was used to measure IFNβ promoter activity in DF-1 cells. By stimulating the IFN cascade at different points, the effect of 3a activity on each section of the cascade could be investigated. When the cascade was induced with poly(I:C), low levels of 3a exacerbated IFNβ expression, while at higher levels IFNβ expression dropped until it was not significantly different to the poly(I:C) control (**Figure 3.3A**). This observation was also seen with MDA-5 overexpression (**Figure 3.3B**). This result correlates with previous work which has shown that IBV infected cells, once stimulated with poly(I:C), leads to higher levels of IFN expression compared to either poly(I:C) transfection or IBV infection alone and suggests 3a is responsible for this previously observed feature (Kint et al. 2015). Conversely, 3a only had an inhibitory effect on MAVS and IRF7 induced IFNβ expression, with the effect on IRF7 being dose-dependent (**Figure 3.3C,D**). Therefore, IBV 3a interacts with the IFN cascade in two ways, by i) exacerbating MDA-5 and poly(I:C) signalling and ii) inhibiting IRF7 activity. These two interactions affect the overall action of 3a on IFNβ expression. Higher levels of 3a favour the inhibitory role of 3a, while lower levels favour the stimulatory role on IFNβ expression. This result suggests that 3a is more efficient at stimulating IFNβ expression but is less responsive to

increases in 3a, most likely suggesting there is a cap on how much 3a can stimulate IFNβ expression. Conversely, the 3a inhibitory effect is not efficient enough at low levels to overcome the stimulatory effect upstream but is more responsive to increases in dose. This implies there is a tipping point between when the stimulatory effect and the inhibitory effect is observed, dependent on levels of 3a. A similar effect was seen during infection, where the decline in 3a levels coincided with increased levels of IFNβ expression (**Figure 3.14A**). During infection, 3a was detectable at 4 h.p.i and reached peak levels at 24 h.p.i (**Figure 3.14B**), after which levels started to decline due to both a reduction in viral expression and proteasome-dependent degradation (**Figure 3.14C**). These changes in 3a levels could have a significant effect on the role of this protein during infection. The decline in 3a levels at 36 h.p.i could mark the tipping point between the inhibitory effect and stimulatory effect of 3a. At 24 h.p.i the inhibitory effect of 3a counteracts the stimulatory effect, but after 36 h.p.i, the decline in 3a levels causes a shift, and the stimulatory effect is observed, resulting in an increase in IFNβ expression. As seen in previous studies there was no difference in IFNβ expression pre-24 h.p.i between the BeauR-Sc3aAUG and wild-type Beau-R (Kint et al. 2015). While this could imply that 3a does not have an inhibitory effect on IFNβ expression early on in infection, this most likely reflects the role of other viral proteins in inhibiting IFNβ expression. Indeed, IBV accessory protein 5b has been shown to inhibit cellular translation to prevent IFN expression (Kint et al. 2016). Future work should aim to qualify the role of 3a in the context of infection and relate it to the other IBV IFN antagonists.

The mechanism of action of 3a on IFN signalling can be explained by the interacting partners identified by mass spectrometry. Three proteins were identified that play a role in regulating the IFN cascade, RNF5, AMFR and CAND1 (**Table** 3.1, **Figure 3.6**). RNF5 and AMFR regulate the turnover of MAVS, while CAND1 is a protein that regulates the formation of the SCF-E3 ligase, a multi-protein complex that degrades IRF3/7 (Zheng et al. 2002, Prakash et al. 2006, Zhong et al. 2010). RNF5 and CAND1 were identified as significant 3aM interacting partners and colocalise with 3a during transfection and infection for RNF5 (**Figure 3.8**). RNF5 is an E3 ubiquitin ligase that controls IFN expression in a negative feedback loop (Zhong et al. 2010). During infection, IFN increases RNF5 expression and causes it to translocate from the ER to MAM structures where it interacts with MAVS (Zhong et al. 2010). These MAM structures are an important structure for IFN signalling cascade as a site for MAVS aggregation and activation (Jacobs et al. 2014). RNF5 polyubiquitinates MAVS to target it for proteasomal-degradation and thus inhibits IFN signalling. The IFN cascade is a highly controlled cellular pathway as over-expression of IFN can have a deleterious effect on the cell and the organism as a whole (Hu et al. 2016). Post-translational conjugation of ubiquitin and degradation of IFN signalling proteins is a major mechanism used to regulate the IFN signalling cascade, both positively and negatively (Lin et al. 2006, Castanier et al. 2012, Fuchs 2012, Hu et al. 2016). The interaction between RNF5 and 3a could explain the increase in MAVS levels observed during 3a expression (**Figure 3.9**). Expression of 3a increased or

stabilised levels of MAVS (**Figure 3.9**), this increase was responsible for the agnostic effect of 3a on IFN signalling (**Figure 3.11**), that is, 3a increased MAVS levels which exacerbated RLR signalling. This effect could be due to 3a inhibiting RNF5 activity and thus preventing turnover of MAVS (**Figure 3.15A**). Future work should aim to determine if these proteins interact during infection and determine if overexpression of RNF5 can abrogate the agonistic effect of 3a on IFNβ expression. While a small proportion of 3a did colocalise with MAVS during transfection in DF-1 cells, most of the signal was juxtaposed (**Figure 3.10A**). Immunoprecipitation of 3a failed to identify MAVS as a 3aM binding partner by co-transfection (data not shown) and was not identified in the GFP-3aM mass spectrometry data. This result implies that MAVS and 3a do not interact directly but may localise to similar cellular compartments, possibly even MAM structures.

The other IFN regulatory protein identified by mass spectrometry was CAND1. This protein inhibits the recruitment of CUL1 to the SCF-E3 ligase complex, a complex which is involved in the degradation of IRF3/IRF7 (Zheng et al. 2002, Prakash et al. 2006). Expression of 3a decreased levels of IRF7 in a dose-dependent, proteasome-dependent manner (**Figure 3.12**). This effect coincides with the dose-dependent effect of 3a on IRF7 induced IFNβ expression (**Figure 3.3D**). A proposed mechanism of action was that 3a interacts with CAND1, increasing CUL1 recruitment to the SCF-E3 ligase, thus increasing degradation of IRF7 (**Figure 3.15B**). Future work should aim to confirm this mechanism of action and determine if CAND1 overexpression can abrogate the decrease in

IRF7 levels by 3a. While CAND1 and 3aM do colocalise; as determined by immunofluorescence (**Figure 3.8**), future work should also aim to confirm this interaction during infection by IP.

Manipulating the cellular ubiquitin degradation pathway is an attractive option for viruses, as it allows viruses to modulate the host-cell environment by targeting cellular proteins for degradation. IAV NS1 targets RNF135, a protein essential for the ubiquitination and activation of RIG-I, while SARS-CoV N has been shown to interact with the RLR and MAVS regulatory protein TRIM25 (Rajsbaum et al. 2012, Hu et al. 2017). Hepatitis B virus (HBV) protein HBx directly interacts with MAVS and targets it for degradation through the addition of ubiquitin residues, while KSHV RTA protein has been shown to amplify the activity of RAUL, an E2 ligase involved in the ubiquitination of IRF3 and IRF7 (Wei et al. 2010, Yu et al. 2010). The main aim of these viral proteins is to inhibit IFN signalling by modulating levels of IFN signalling proteins. This appears to be how IBV 3a effects IFNβ expression, by interacting with RNF5 and CAND1, 3a can modulate levels of both MAVS and IRF7. This interaction appears to be dynamic, allowing 3a to both inhibit and stimulate IFN expression depending on dose and thus time. While it is more common for viral proteins to inhibit IFN expression, it is not unheard of for viral proteins to stimulate IFN expression too. Mopeia Virus L protein has been shown to induce IFN expression by activating the RLR/MAVS pathway (Zhang et al. 2016), while HCV RdRp has been shown to actively produce dsRNA based on cellular RNA that can induce IFN expression (Yu et al. 2012). This function may

seem counterproductive for the virus, but it can help to prevent excessive host damage or disease that can be detrimental for viral replication. For example, piglets infected with a recombinant TGEV that does not express accessory protein 7, showed increased pathogenicity, suggesting protein 7 plays a role in inhibiting excessive host damage (Cruz et al. 2011).

The interesting dynamic between 3a and the host could have serious implications for pathogenicity. While it may seem counterproductive to induce IFN expression, it may be beneficial in a disease which is associated with immunopathology (Zhong et al. 2012, Kameka et al. 2014). IBV pathogenesis has been linked to an exacerbated immune response with serve symptoms like nephrotoxicity associated with a high influx of effector cells and interleukins (Okino et al. 2014). The full link between host-interaction and pathogenicity has yet to fully elucidated but these interactions, shown here, could explain the unique and complex relationship between host immune system and IBV.

The IFN response is the primary battleground for the evolutionary arms race between virus and host (Randall et al. 2008). Coronaviruses have been shown to use a range of mechanisms to combat the IFN response with IBV being no exception (Fung et al. 2014). Here accessory protein 3a has been shown to have a dynamic relationship with two parts of the IFN cascade, MAVS and IRF7. While this has offered a glimpse into the relationship between IBV and host, much more

work is required to determine how IBV manipulates the IFN response and the impact this has on pathogenicity.

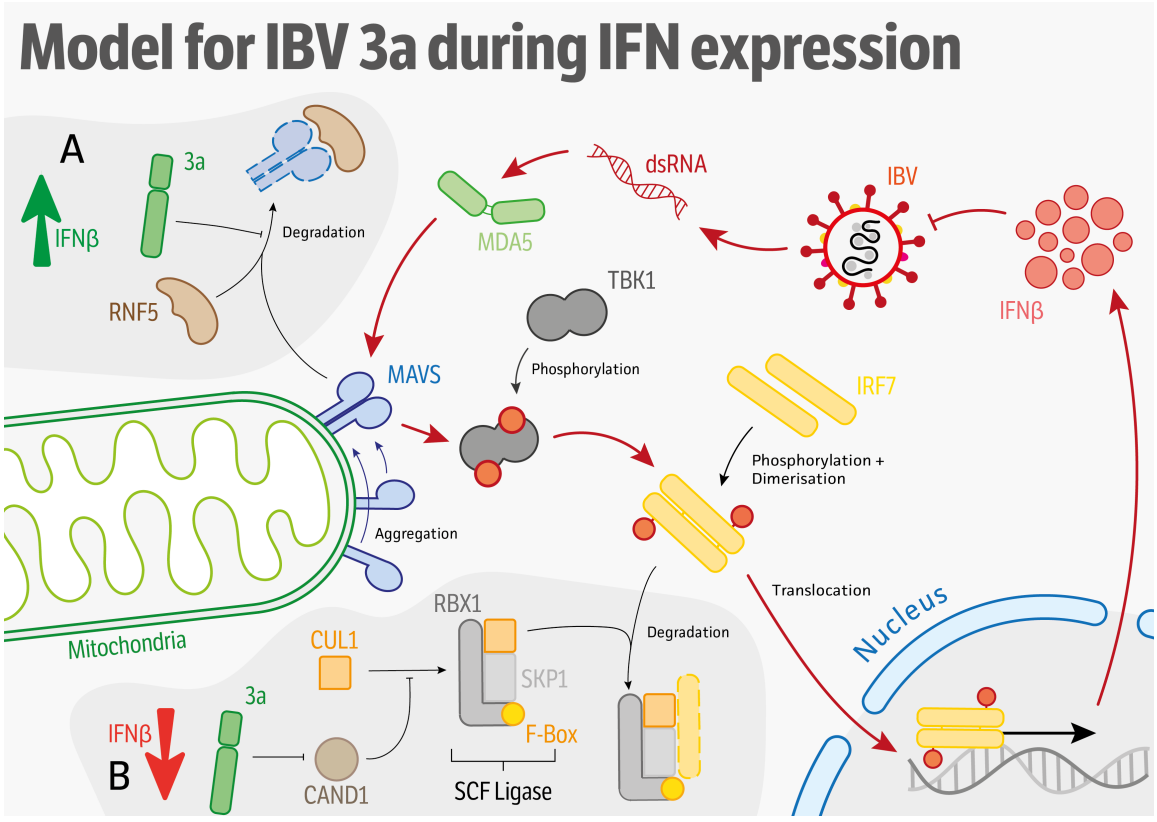

Figure 3.15 Proposed model for the mechanism of action of IBV 3a on IFNβ expression.

During infection, IBV produces dsRNA which is detected by MDA-5 which initiates the IFN signalling cascade. IBV 3a modulates the IFN cascade by two proposed mechanism, (A) IBV 3a interacts with and inhibits RNF5 degradation of MAVS, leading to increased RLR signalling and thus increased IFNβ expression. (B) IBV 3a interacts with and inhibits CAND1, increasing the recruitment of CUL1 to the E3 SCF-ligase complex. These complexes target IRF3/7 for degradation leading to a reduction in IFNβ expression.

4. The role of Accessory Protein 3b

4.1. Introduction

Accessory protein 3b is a 7.4 kDa protein encoded by the second ORF of sgRNA3, which is translated by leaky ribosomal scanning (Le et al. 1994). Protein 3b is highly conserved among strains of IBV and TCoV suggesting an important role for this protein (Cavanagh et al. 2002, Britton et al. 2006). Little is known about the function of 3b, although it is known that this protein does not play a role in *in vitro* replication as recombinant IBV lacking 3b expression grew to similar titres as wild-type IBV (Hodgson et al. 2006). Furthermore, recombinant viruses with a scrambled 3b start codon expressed higher levels of IFNβ at 24 h.p.i suggesting 3b can inhibit the IFN cascade in some, as yet unknown, manner (Kint et al. 2015). Protein 3b displays different localisation in mammalian and avian cells, with a nuclear localisation in Vero cells and a diffuse cytoplasmic pattern in DF-1 cells (Pendleton et al. 2006). A truncated variant of 3b has been detected in a serially passaged strain of Beau-R, resulting in higher viral titres *in vitro* suggesting an advantageous mutation (Shen et al. 2003). This truncation resulted in a different cellular localisation in mammalian COS-7 cells, from the nucleus to the cytoplasm, suggesting that the cytoplasmic localisation is important for the function of 3b. Protein 3b is degraded quickly by the proteasome in mammalian cells and is degraded independently of the proteasome in avian cells. This leads to a short half-life for 3b making it difficult to detect during transient expression and infection (Pendleton et al. 2006). In this chapter, interacting partners for 3b were identified which play a role in regulating IFN expression and apoptosis. Furthermore, a

recombinant virus lacking 3b expression was shown to induce less caspase-dependent apoptosis during infection, suggesting 3b has a role in inducing apoptosis.

Results

4.2. Bioinformatic analysis of 3b

IBV 3b is a highly conserved accessory protein present in IBV and TCoV strains with a sequence identity of 60.4% - 100% (Britton et al. 2006). To investigate the role of 3b, four isoforms of 3b were aligned, and a eukaryotic linear motif (ELM) search was performed to identify motifs which may suggest a function. Protein 3b is dispensable for *in vitro* replication and therefore has been suggested that 3b is a pathogenicity factor (Hodgson et al. 2006). For this reason, 3b from Beau-R (3bB), M41-CK (3bM), Qx (3bQ) and from a serially passaged strain of Beau-R which expresses a truncated form of 3b (3bT) were investigated. Beau-R and M41-CK are lab strains, which are apathogenic and pathogenic, respectively, while Qx is a highly pathogenic field strain. Protein 3bT is expressed from a serially passaged strain of Beau-R and has a C-terminal truncation resulting in a 34 amino acid long protein (Shen et al. 2003). This truncated variant localises to the cytoplasm in COS-7 cells as opposed 3bB which localises to the nucleus. Peptide sequences of 3bM, 3bQ, and 3bT were aligned against 3bB and sequence identity determined (**Figure 4.1**). Sequence alignment of 3bB and 3bM showed that 3b is highly conserved between these two strains, with a sequence identity of 98.43% and only one amino acid difference (V > A). Interestingly the

high pathogenic strain, Qx, was more diverse with a sequence identity of 67.2% compared to 3bB. The truncated variant 3bT had a lower sequence identity of 52.94%, although the N-terminus of 3bT was highly conserved with the N-terminus of 3bB.

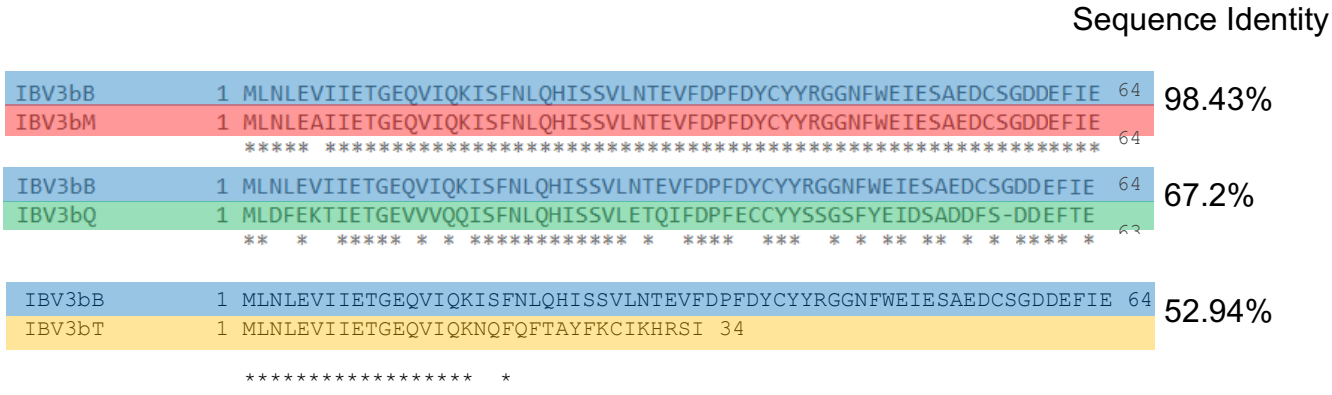

Figure 4.1 Sequence alignment and sequence identity of 3b isoforms.
Peptide sequences of 3b from M41-CK (red), Qx (green) and a truncated isoform identified in a serially passaged strain of Beau-R were aligned to 3b from Beau-R (yellow). The asterisk marks conserved amino acids.

The Eukaryotic Linear Motif (ELM) tool was used to identify any motifs that may help to determine function. This tool aims to identify motifs which have previously been shown to mediate protein-protein interactions. Due to the high incidence of false positives when using this tool, little can be inferred from these results alone. ELM analysis of 3bB and 3bM identified 11 motifs with LIG_DCNL_PONY_1 and DOC_AGCK_PIF_2 being the most significant and are described in **Table** 4.1. Interestingly the ELM search for 3bQ did not identify these two motifs. The third most significant interaction, AP2alpha_2, which did appear in Qx, is a motif which mediates binding to AP2, an adaptor protein of clathrin-coated vesicles (Edeling

et al. 2006). The 3bT variant, when expressed in mammalian cells, shows a diffuse cytoplasmic distribution compared to 3bB which localises to the nucleus. The ELM search only identified one nuclear retention domain, RVxF, which appears in 3bB/3bM but does not appear in 3bT (Lesage et al. 2004). Only one motif identified, DEG_Nend_Nbox_1, was conserved between all isoforms of 3b. This motif is a destabilising motif that is recognised by N-recognins and may in part be responsible for the short half-life of this protein (Varshavsky 2011).

Table 4.1 Eukaryotic linear motifs (ELM) identified in the 3b peptide sequence.

ELM ID	Matched Sequence in 3aB	Pattern	Position	Elm Description	Cell Compartment	Probability	3bB	3bM	3bQ	3bT
LIG_DCNL_PONY_1	MLNL	^M[MIL].[MIL]	1-4	DCNL PONY domain binding motif variant based on the UBE2M and UBE2F interactions.	ubiquitin ligase complex, nucleus	4.87E-07	X	X		X
DOC_AGCK_PIF_2	FDPFDY	F..[FWY][DE][FY]	34-39	In the DOC_AGCK_PIF_2 motif the phosphorylatable serine/threonine residue is replaced by an acidic aspartate or glutamate residue.	cytosol, internal side of plasma membrane	3.27E-06	X	X		
LIG_AP2alpha_2	DPF	DP[FW]	35-37	DPF/W motif binds alpha and beta subunits of AP2 adaptor complex.	clathrin-coated endocytic vesicle, cytosol	0.00012	X	X	X	
DEG_Nend_Nbox_1	MLN	^M{0,1}[FYLIW][^P]	1-3	N-terminal motif that initiates protein degradation by binding to N-recognins.	cytosol	0.00023	X	X	X	X
LIG_Pex14_2	FTAYF	F...[WF]	22-26	Fxxx[WF] motifs are present in Pex19 and S. cerevisiae Pex5 cytosolic receptors that bind to peroxisomal membrane docking member, Pex14	cytosol, peroxisome, glycosome	0.00046				X
DOC_PP1_RVXF_1	IQKISFN	..[RK].{0,1}[VIL][^P][FW].	15-21	Protein phosphatase 1 catalytic subunit (PP1c) interacting motif binds targeting proteins that dock to the substrate for dephosphorylation.	nucleus, protein phosphatase type 1 complex, cytosol	0.00083	X	X		
DOC_PP2A_B56_1	LEAIIE	([LMFYWIC]..I.E)|(L..[IVLWC].E).	4-9	Docking site required for the regulatory subunit B56 of PP2A for protein dephosphorylation.	nucleus, kinetochore, chromosome, centromeric region, cytosol	0.00146	X	X		X
LIG_TRAF6	FDPFECCYY	..P.E..[FYWHDE]	34-42	TRAF6 binding site. Members of the tumor necrosis factor receptor (TNFR) superfamily initiate intracellular signaling by recruiting the C-domain of the TNFR-associated factors (TRAFs) through their cytoplasmatic tails.	cytosol	0.001715				X
LIG_SH2_STAT5	YCYY	(Y)[VLTFIC]..	25-28	STAT5 Src Homology 2 (SH2) domain binding motif.	cytosol	0.00330				X
			39-42				X	X		

3bB – 3b Beau-R, 3bM – 3b M41-CK, 3bQ – 3b Qx, 3bT – 3b truncated (Beau-R). Results are ordered by p, the probability of the sequence occurring randomly

4.3. Generation of 3b-GFP expression vectors

To investigate the role of accessory protein 3b, vectors were generated for expression of 3b from Beau-R (3bB) and M41 (3bM) fused with a GFP tag at either the N- or C- terminus. These expression vectors were used for mass spectrometry protein purification. Previous work has shown that 3b fused with a FLAG tag was not detectable during transient expression, possibly due to the short half-life of this protein (Davies 2009). A GFP-tag was used to increase the stability of 3b during transient expression, due to its large size and biological stability (Chalfie 2001). For the generation of the 3bB and 3bM expression vectors, M41 and Beau-R viral RNA was isolated and reverse transcribed into cDNA using random primers. ORF3b was amplified by PCR using complementary primers with flanking restriction sites. The PCR product was purified and digested with the relevant restriction enzymes. Plasmids pEGFPC2 (Clontech) and pEGFPN1 (Clontech) were also digested with the same restriction enzymes. Digested plasmids and PCR products were ligated and transformed. Vectors were sequenced by Sanger sequencing. The vectors generated were pEGFPC2-3bB, pEGFPN1-3bB, pEGFPC2-3bM and pEGFPN1-3bM (**Figure 4.2A,B,C,D**). To confirm expression of GFP-tagged 3b from these vectors, DF-1 cells were transfected with GFP-3bB, GFP-3bM, 3bB-GFP, 3bM-GFP vectors. After 16 hours, cells were lysed, proteins separated by SDS-PAGE, transferred to a membrane and labelled with anti-GFP. Bands with the predicted molecular weight of GFP-tagged 3bB and 3bM were identified as expected, confirming the successful generation of these vectors (**Figure 4.2E**).

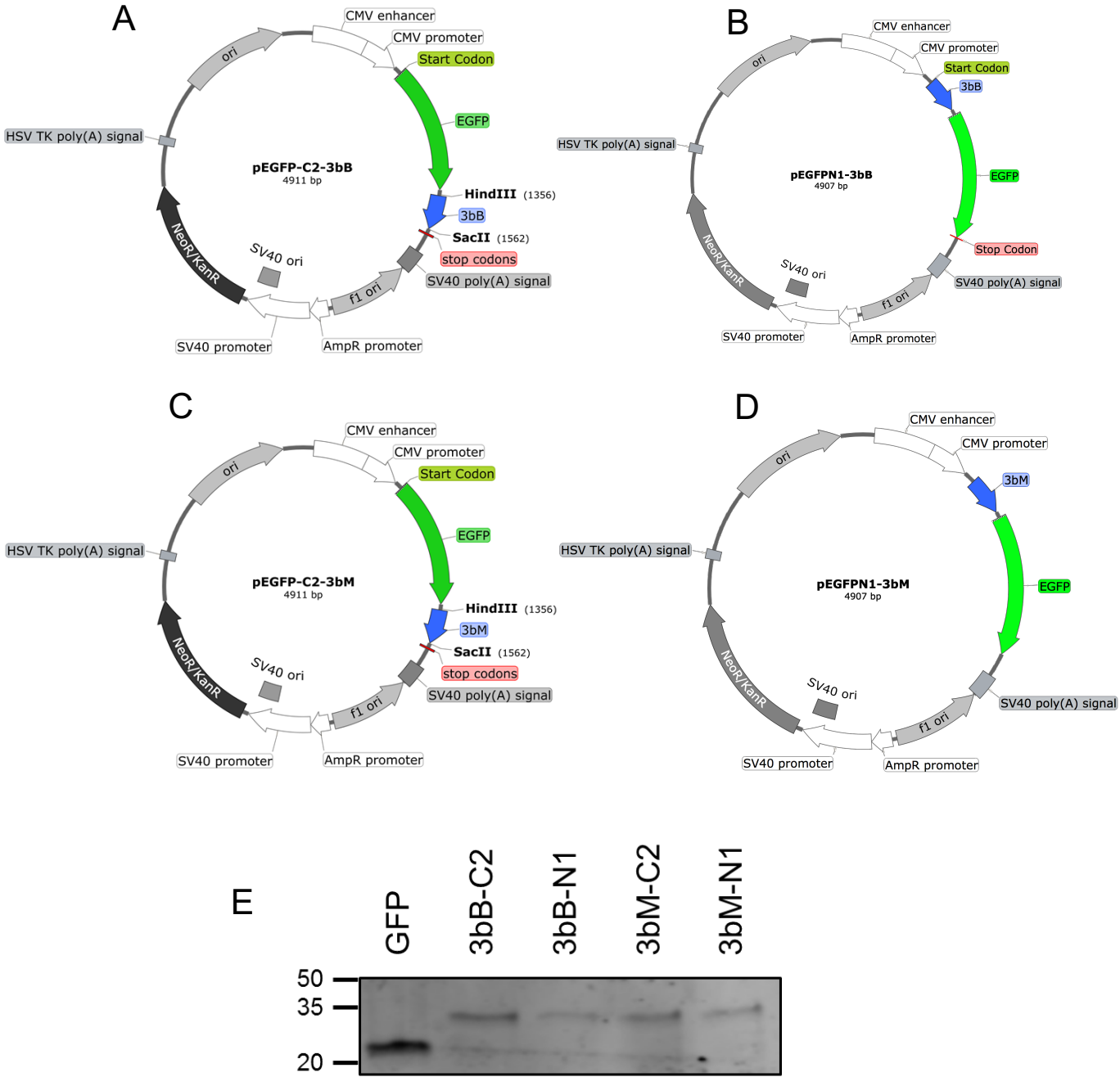

Figure 4.2 Expression maps and confirmation of expression of GFP-tagged 3b vectors.

(A) pEGFPC2-3bB (B) pEGFPN1-3bB (C) pEGFPC2-3bM (D) pEGFPN1-3bM. (E) DF-1 cells were transfected with pEGFPC2, pEGFPC2-3bB/3bM, pEGFPN1-3bB/3bM expression vectors. After 16 hours, cells were lysed, proteins separated by SDS-PAGE and transferred to a membrane. Membranes were labelled with anti-GFP.

4.4. Mass spectrometry analysis of 3b-GFP pull-downs

Mass spectrometry was utilised to identify any cellular interacting partners for GFP-3bM and 3bM-GFP that may allude to function. As 3bB and 3bM have a high sequence identity of 98.43% and are unlikely to function differently when expressed alone, the decision was made to save time and cost by investigating 3bM only. HEK-293T cells were transfected with pEGFPC2-3bM or pEGFPN1-3bM expression vectors or with a GFP control plasmid. After 16 hours, cells were lysed and GFP-3bM, 3bM-GFP or GFP immunoprecipitated using GFP 'capture' beads (Chromotek). Three biological replicates were performed for each plasmid. Before samples were processed, input and eluate samples were separated by SDS-PAGE and blots labelled with anti-GFP to confirm successful transfection and immunoprecipitation (**Figure 4.3**). GFP immunoprecipitation could be confirmed by directly visualising the GFP fluorescence when attached to the GFP capture beads. After confirmation, eluate samples were analysed by LC-MS/MS by Stuart Armstrong to identify cellular proteins in the eluates.

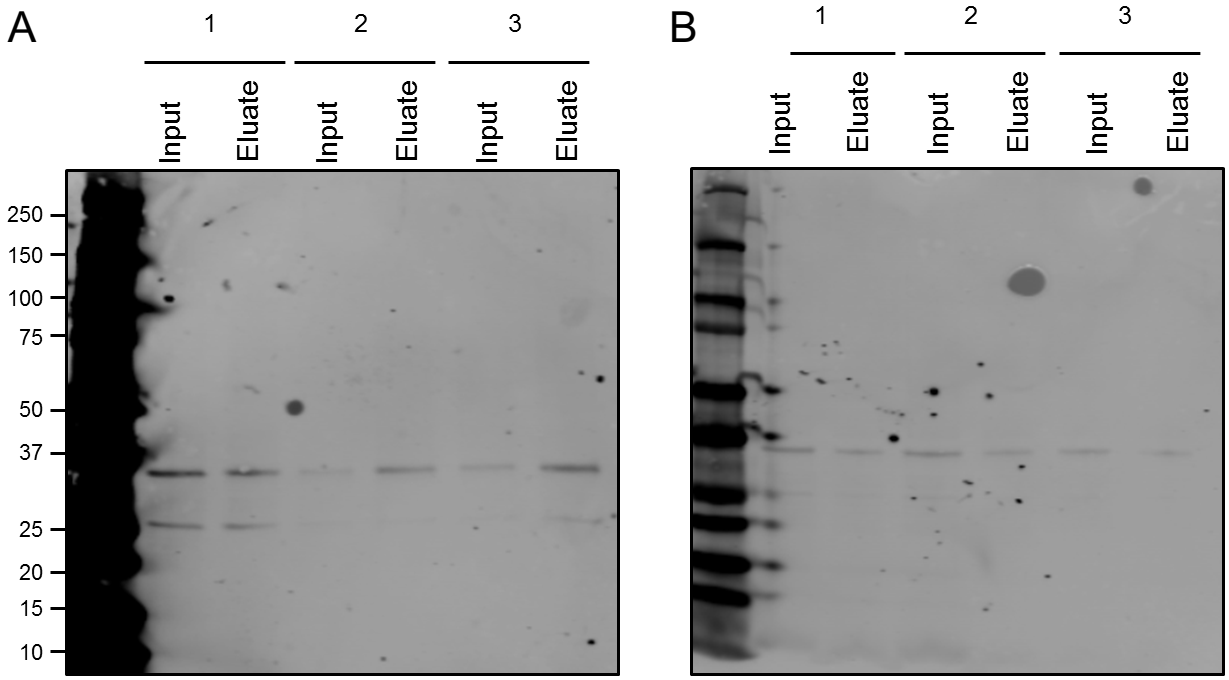

Figure 4.3 Western blot analysis of 3bM-GFP, GFP-3bM expression and immunoprecipitation.

HEK-293T cells were transfected with (A) pEGFPC2-3bM and (B) pEGFPN1-3bM expression vectors. After 16 hours, cells were lysed and GFP immunoprecipitated using GFP 'capture' beads (Chromotek). Samples were eluted in the elution buffer. Input and eluate samples were separated by SDS-PAGE, transferred to a membrane and labelled with anti-GFP.

In total 69 and 54 cellular proteins were detected in higher amounts in the GFP-3bM and 3bM-GFP eluates, respectively, compared to the GFP control. Of these, 47 appeared in both samples, with 22 unique to GFP-3bM and 7 for 3bM-GFP (**Appendix Table 7.3, 7.4**). Proteins were identified by comparing unique peptides to a database of human proteins. Proteins, where only a single unique peptide was identified, were removed to reduce the chance of identifying the wrong protein. Cellular proteins deemed significant interactions have a *p*-value (-Log10)

above one and a fold-change (Log2) above two. The *p*-value was determined by two-tailed unpaired ANOVA on the three replicates. The fold-change is the change in average relative protein abundance of each protein between GFP-tagged 3bM and the GFP control. For each identified protein, the confidence score (Log2) was calculated as the cumulative score of *p*, the chance of the unique peptide sequence occurring randomly. The higher the score, the higher the confidence in the correct protein identification. Of the 76 proteins identified, six were considered significant for GFP-3bM (**Figure 4.4**, **Table 4.2**). None of the proteins for 3bM-GFP were considered significant, although the proteins that appeared significantly in GFP-3bM also appeared in the 3bM-GFP data, as labelled on the scatter plot (**Figure 4.5**).

Table 4.2 Cellular proteins that significantly interact with GFP-3bM

Protein ID	Protein	Unique peptides	Confidence Score	Relative Protein Abundance						P-value (-log10)	Fold Change GFP-3bM/GFP (Log2)
				pEGFPC2-3bM			pEGFPC2				
				1	2	3	1	2	3		
BAG6*	Large proline-rich protein BAG6	7	43.529	16470945.06	28858040.37	24418986.71	9586813.925	6962480.736	3957176.544	2.906321357	2.487846495
VDAC2*	Voltage-dependent anion-selective channel protein 2	3	20.668	25898945.09	14765020.26	15152998.83	7499120.63	17683984.02	17660954.73	2.576106121	2.131061799
COX5B*	Cytochrome c oxidase subunit 5B, mitochondrial	4	23.644	30800063.72	19350935.8	16642052.05	29899955.47	5815533.034	17579004.05	2.136701975	2.009682233
HSPB1*	Heat shock protein beta-1	2	14.253	10848031.97	39054893.75	27991976.06	3245524.014	6800974.256	4806149.184	1.786641052	3.158306491
CLTB*	Clathrin light chain B	5	34.721	82785226.63	18960977.42	18320048.67	31371039.53	12264031.74	3230799.969	1.726453339	3.287103251
RPS24*	40S ribosomal protein S24	3	22.269	30267999.7	24865980.78	17672955.62	28521964.15	29375905.76	4223711.897	1.327963149	2.103594221

Shown are cellular proteins identified by label-free mass spectrometry/mass spectrometry that interact with GFP-3bM. Protein identifier (ID), protein name and number of unique peptides used to identify proteins are indicated. Relative abundance score for each protein is indicated. Confidence score (-Log2) is the score of the probability of the unique peptide sequence occurring randomly, added together for each unique peptide. The higher the confidence score, the higher the confidence in protein identification. The p-value (-Log10) is a comparison of the cellular protein abundance between 3bM and GFP. The higher the p-value, the higher the probability the protein interacts with 3b. The fold-change is the change in the abundance of the cellular protein between GFP-3bM and GFP. Cellular proteins which appear in both GFP-3bM and 3bM-GFP data are labelled with an asterisk (*).

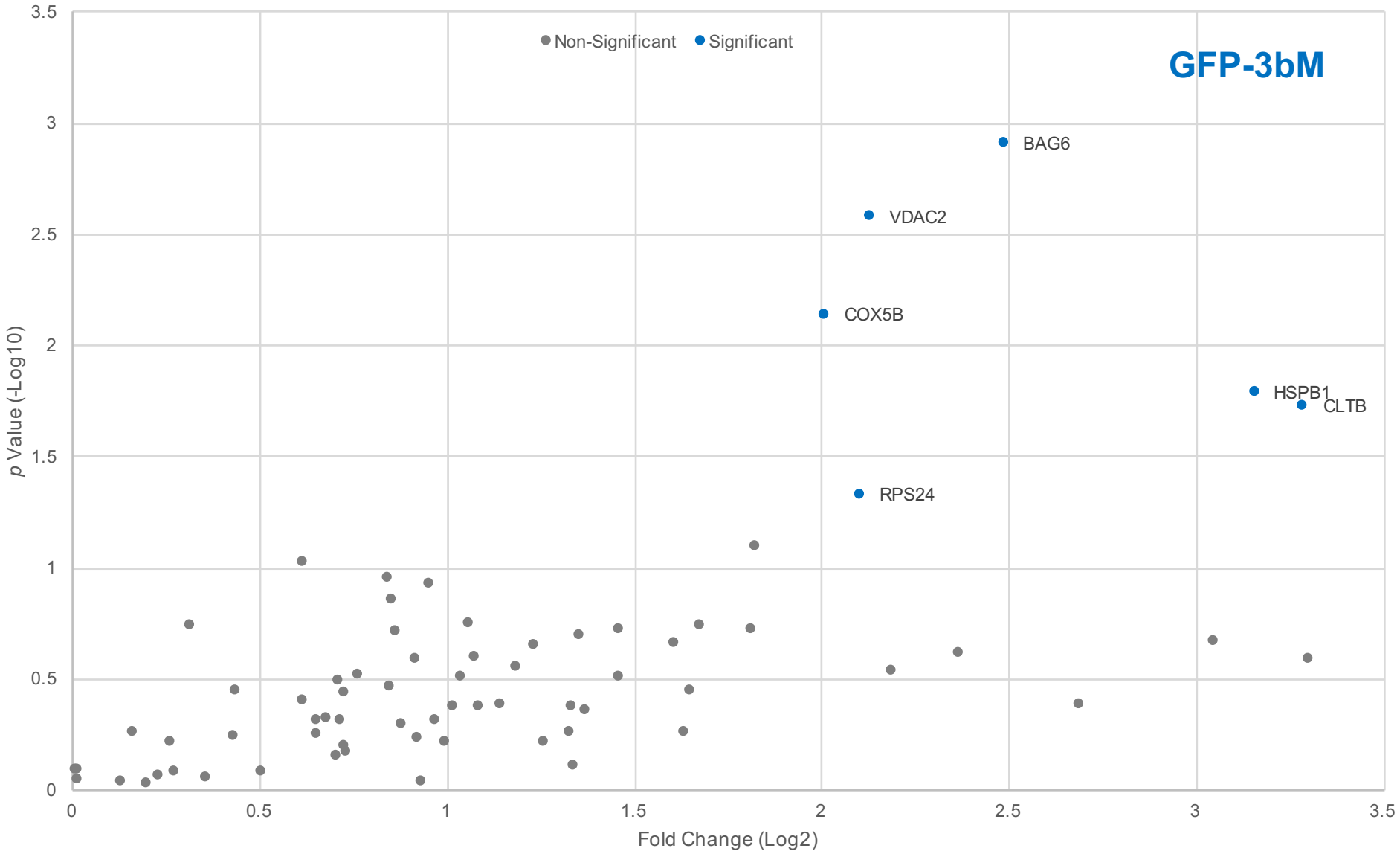
Non-Significant
Significant
GFP-3bM
BAG6
VDAC2
COX5B
HSPB1
CLTB
RPS24
p Value (-Log10)
Fold Change (Log2)
0
0.5
1
1.5
2
2.5
3
3.5

Figure 4.4 Scatter plot representing results from the GFP-3bM co-IP.

Proteins were identified in the GFP-3bM eluate by LC-MS/MS. Proteins are plotted by fold-change in relative abundance compared to the GFP control and *p*-value (Log10) of the *t*-test. Proteins with a *p*-value (-Log10) above 1 and a fold change above 2 have the highest chance of interacting with 3bM and are considered significant (blue). Results are from three biological replicates.

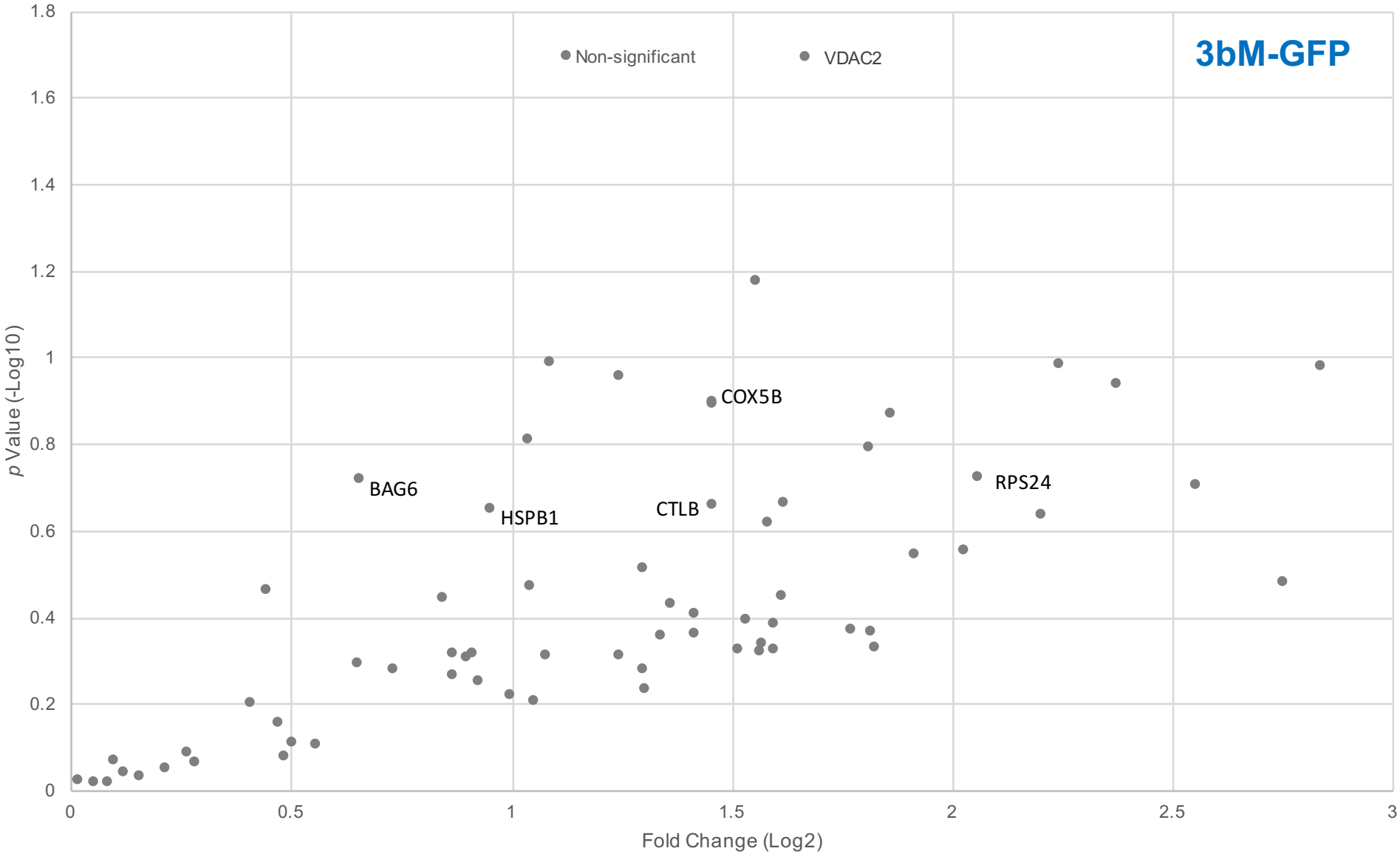
3bM-GFP
Non-significant
VDAC2
COX5B
BAG6
HSPB1
CTLB
RPS24
p Value (-Log10)
Fold Change (Log2)
0
0.2
0.4
0.6
0.8
1
1.2
1.4
1.6
1.8
0
0.5
1
1.5
2
2.5
3

Figure 4.5 Scatter plot representing results from the 3bM-GFP co-IP.

Proteins identified in the 3bM-GFP eluate by LC-MS/MS. Proteins are plotted by fold-change in abundance over the GFP alone and *p*-value (-log10) of the *t*-test. Proteins with a *p*-value (-log10) above 1 and a fold change above 2 have the highest chance of interacting with 3bM and are considered significant (blue). Results are from three biological replicates. Proteins labelled were identified as significant interactions for GFP-3bM.

LC-MS/MS identified six proteins that are significant interacting partners for 3bM (**Table** 4.3). Gene ontology (GO) analysis of the proteins failed to group the proteins based on function or location (data not shown). Nonetheless, three proteins were identified that play a role in regulating apoptosis. Voltage-dependent anion channel 2 (VDAC2) inhibits apoptosis by interacting with and inhibiting the pro-apoptotic Bcl-2 homologous antagonist killer (BAK) protein (Cheng et al. 2003). BCL2 associated athanogene 6 (BAG6) is a multi-functional protein that has been shown to stabilise Apoptosis-inducing factor (AIF), a pro-apoptotic protein as well as conferring resistance to ER-stress related apoptosis (Desmots et al. 2008). Cytochrome c oxidase subunit 5B (COX5B) is a protein mainly involved in the electron transport chain, but also interacts with and negatively regulates MAVS aggregation by repressing reactive oxygen species (ROS) production. COX5B is also a negative regulator of apoptosis as over-expression of MAVS, or ROS can lead to intrinsic apoptosis (Zhao et al. 2012). Furthermore, mass spectrometry data also identified a ribosomal protein, ribosomal small protein 24 (RPS24), clathrin light chain B (CTLB) and heat shock protein B1. RPS24 is part of the 40S ribosomal complex, while HSPB1 is a molecular chaperone that is multi-functional (Bryantsev et al. 2007, Choesmel et al. 2008). It has also been reported that HSPB1 inhibits apoptosis by binding to both cytochrome C and the pro-apoptotic Bcl-2-associated X protein (BAX) protein as well as inhibiting activation of both procaspase-3 and 9 (Bruey et al. 2000, Concannon et al. 2001, Havasi et al. 2008). CLTB is a structural protein that coats the cytoplasmic face of vesicles (Saffarian et al. 2009). Ribosomal

proteins and heat-shock proteins are common in mass spectrometry data and may represent 'sticky' proteins (Mellacheruvu et al. 2013).

Table 4.3 Function and localisation of proteins classified as significant interacting partners for GFP-3bM

Protein ID	Protein	Function	Go Cellular Component
BAG6*	BCL2 Associated Athanogene 6	Multi-functional protein, regulates AIF expression preventing ER-stress related apoptosis	Cytoplasm/ Nucleus
VDAC2*	Voltage-Dependent Anion Channel 2	Membrane channel, involved in intrinsic apoptosis	Mitochondrial outer membrane
COX5*	Cytochrome C Oxidase Subunit 5B	Role in electron transport and negative MAVS regulatory protein	Mitochondrial inner membrane
HSPB1*	Heat Shock Protein B-1	Molecular chaperon, multi-functional protein	Nucleus/ Cytoplasm/ Cytoskeleton
CLTB*	Clathrin Light Chain B	Clathrin regulatory protein essential for endocytosis	Plasma membrane/ Cytoplasm
RPS24*	Ribosomal Protein S24	Small ribosomal protein	Cytoplasm/ Nucleus

An asterisk (*) indicates proteins that also appeared in the 3bM-GFP eluate but were not statistically significant.

4.5. Effect of protein 3b on apoptosis

4.5.1. IBV induces apoptosis

Mass spectrometry data for GFP-3bM identified three proteins involved in apoptosis, VDAC2, BAG6 and COX5B (Cheng et al. 2004, Desmots et al. 2008, Zhao et al. 2012). Previous studies have shown that IBV infection can induce caspase-dependent apoptosis in Vero cells (Liu et al. 2001, Li et al. 2007). To determine if IBV can also induce apoptosis in DF-1 cells a fluorescence-activated cell sorting (FACS) assay was used to measure levels of phosphatidylserine (PS) expression on the cell surface. In viable cells, PS is expressed on the interior of the plasma membrane, while during apoptosis PS is expressed on the exterior of the plasma membrane. Annexin V is used to label apoptotic cells due to its ability to bind to PS. As it cannot transverse the cellular membrane, it can only label externally expressed PS. DF-1 cells were mock infected, infected with Beau-R or BeauR-Sc3bAUG at an MOI of 4. After 24 hours, cells were gently trypsinised and labelled with Annexin V to detect apoptotic cells. Dead apoptotic cells were labelled with propidium iodide (PI). PI is a chromatin stain that cannot pass through the membrane of viable cells and so can only label dead cells which have a permeabilised membrane (Steinkamp et al. 1999). Cells were treated with the caspase-dependent apoptosis inducer staurosporine for 6 hours at a concentration of 1 μM as a positive control (Belmokhtar et al. 2001). Cells were sorted, and fluorescence measured using the MACSQuant FACS machine and software (Miltenyibiotec). Cells were first sorted by the side scatter area (SSC-A) and the forward scatter area (FSC-A) to sort cells by their cellular granularity and

size, respectively. DF-1 cells were then selected for and gated (**Appendix 7.1**). Gated DF-1 cells were sorted by forward scatter height (FSC-H) and FSC-A, to select for single cell populations. FCS-H and FCS-A have the same value when a single cell is detected. Cells were then plotted by Annexin V (FITC) fluorescence and PI fluorescence and represented as a density plot. Cells were separated into three gates, representing cells that are viable (dark green), viable cells undergoing apoptosis (light green) and cells which are dead from apoptosis (red) (**Figure 4.6**). The percentage of viable cells, viable cells undergoing apoptosis, and dead cells were calculated for mock, Beau-R and BeauR-Sc3bAUG infected cells. The percentage of mock infected cells that were viable was 82.60%, with 26.80% of those cells undergoing apoptosis (**Figure 4.6A**). The remaining cells, 17.57%, were dead as they stained for propidium iodide as well as annexin. Beau-R infected cells saw 52.68% of cells viable, with 21.00% of those cells undergoing apoptosis. The remaining cells, 47.28%, were dead (**Figure 4.6B**). BeauR-Sc3bAUG infected cells had 79.09% viability with 16.56% of those cells undergoing apoptosis. The remaining, 30.53%, were dead (**Figure 4.6C**). The staurosporine positive control actively induced apoptosis with 47.77% of cells viable, of which 20.52% were undergoing apoptosis, the remaining cells, 52.39%, were dead (**Figure 4.6D**). Compared to mock infected cells, Beau-R infected cells saw higher levels of dead cells but saw lower levels of actively apoptotic cells. This result suggests that at 24 h.p.i Beau-R causes a ~30% increase in apoptotic cell death compared to mock. This confirms that IBV infection induces apoptosis in DF-1 cells as seen previously for Vero cells (Liu et al. 2001). A similar pattern

was observed for BeauR-Sc3bAUG with saw an increase of 13% in apoptotic cells compared to the mock. This increase was smaller compared to Beau-R infected cells and suggests that 3b expression causes an increase in the rate of apoptosis. Scrambling of the 3b AUG codon does not abrogate apoptosis completely and suggests 3b is not solely responsible for IBV-induced apoptosis.

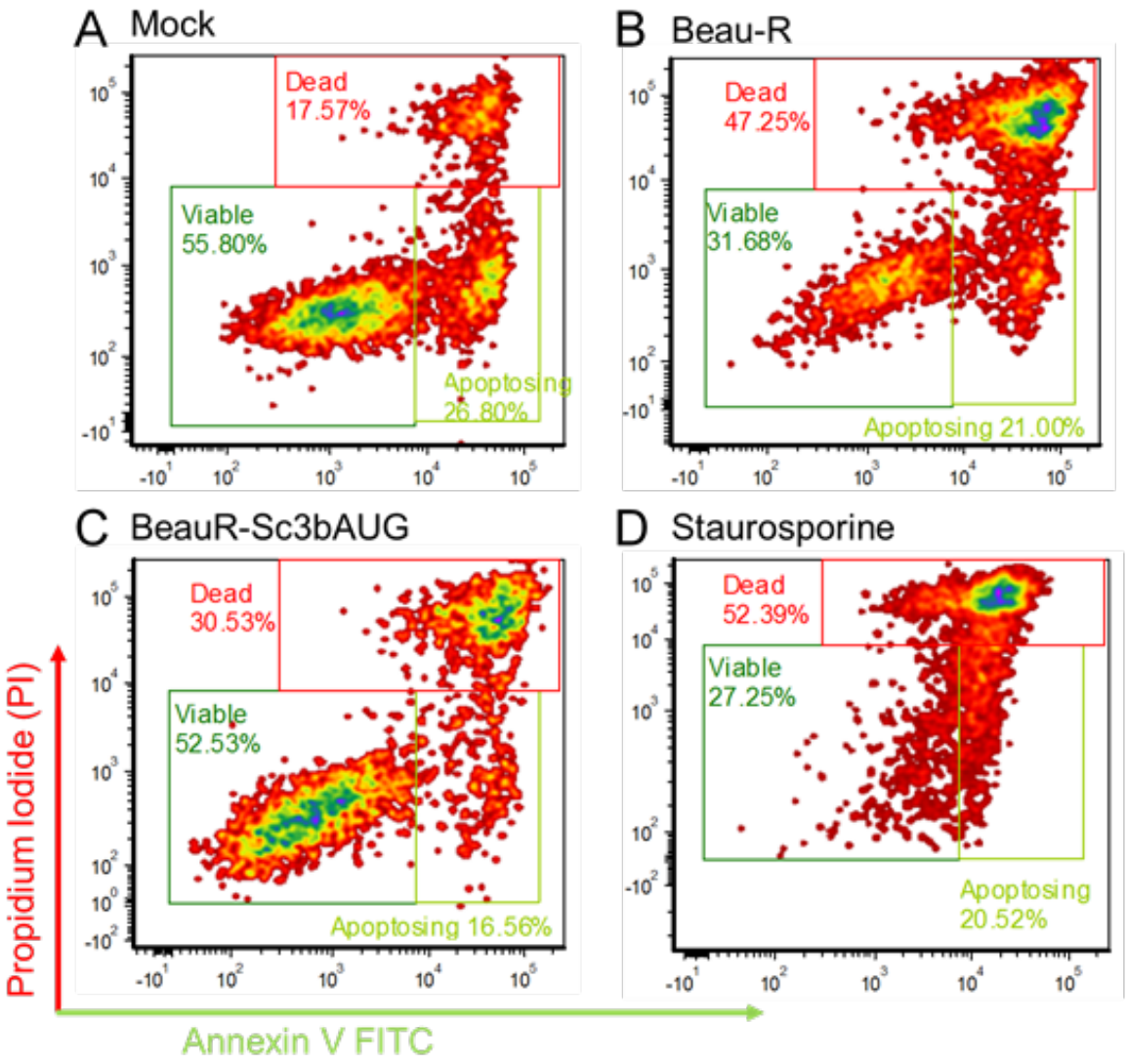

Figure 4.6 IBV 3b induces apoptosis.

DF-1 cells were (A) mock infected or infected with (B) Beau-R or (C) BeauR-Sc3bAUG at an MOI of 4 for 24 hours. As a positive control, cells were treated with (D) staurosporine for 6 hours. Cells were harvested, washed with PBS and labelled with anti-PS and propidium iodide. Cells were sorted by forward scatter area (FSC-A), and side scatter area (SSC-A) to gate DF-1 cells. DF-1 cells were then sorted by forward scatter area (FSC-A) and forward scatter height (FSC-H) to gate single cell populations. Single DF-1 cells were then sorted by annexin V (FITC) and propidium iodide (PI) fluorescence and shown as a density plot. Cells were separated into three gates, representing cells that are viable (dark green), viable cells undergoing apoptosis (light green) and cells which are dead from apoptosis (red).

4.5.2. IBV 3b induces caspase-dependent apoptosis

To further confirm that 3b can induce apoptosis during infection, a caspase assay was used. This assay also helped to determine whether 3b induces caspase-dependent or caspase-independent apoptosis. To measure caspase activity, a caspase-Glo 3/7 kit (Promega) was used. Caspase 3/7 are the primary cysteine proteases which initiate the apoptotic signalling cascade leading to irreversible apoptosis (Taylor et al. 2008). DF-1 cells were either mock infected or infected with Beau-R or BeauR-Sc3bAUG at an MOI of 4. Cells were harvested at 12, 24 and 36 h.p.i. Firefly luciferase activity was measured as a proxy for caspase 3/7 enzymatic activity using the Caspase-Glo 3/7 assay (Promega). Results are shown as fold-change compared to the mock control and are from three biological replicates. At 12 h.p.i there was no significant difference between mock and IBV. At 24 h.p.i and 36 h.p.i, there was significantly more Firefly luciferase activity from cells infected with Beau-R compared to mock infected cells. BeauR-Sc3bAUG also showed significantly more Firefly luciferase activity compared to the mock control, although this was significantly less than Beau-R at 24 h.p.i. This result correlates with the FACS data and suggests that IBV does induce apoptosis during infection in DF-1 cells as in Vero cells, and that protein 3b is responsible, in part, for IBV-induced apoptosis.

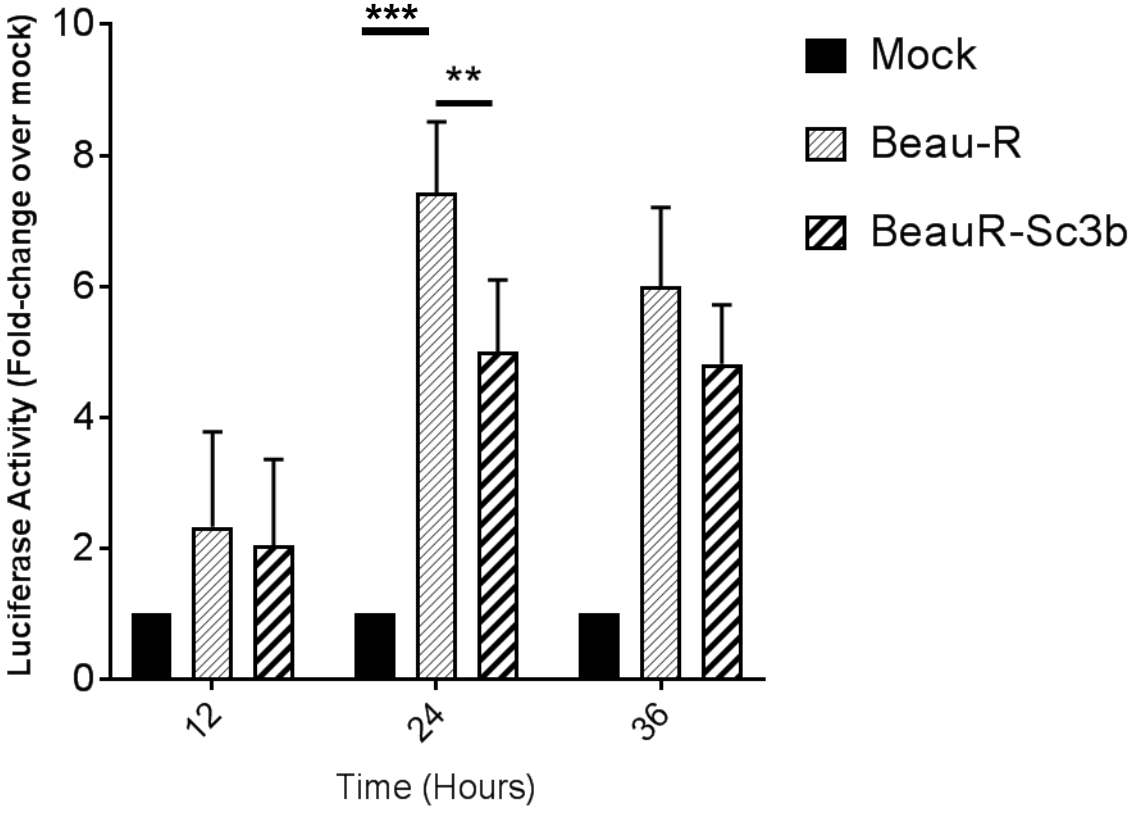

Figure 4.7 Protein 3b induces caspase-dependent apoptosis.

DF-1 cells were either mock infected or infected with Beau-R or BeauR-Sc3b at an MOI of 4. After 12, 24 or 36 hours, cells were lysed and caspase 3/7 activity measured. ** significance $p < 0.01$, *** significance $p < 0.001$

4.6. Discussion

IBV accessory protein 3b is a small accessory protein at 7.4 kDa, expressed from sgRNA3 along with 3a and E (Le et al. 1994). Protein 3b is highly conserved between Beau-R and M41-CK but is less conserved with the highly pathogenic Qx strain with a 67.2% sequence identity (**Figure 4.1**). Furthermore, a truncated variant of Beau-R 3b, 3bT, which shows different localisation patterns in Vero cells compared to 3bB, only has a sequence identity of 52.49%, although the N-terminal end was highly conserved. An ELM search only identified one motif (DEG_Nend_Nbox_1), a destabilising motif, that is conserved between all four isoforms of 3b (**Table** 4.1). IBV 3bT localises to the cytoplasm in COS-7 cells during transient expression while 3bB and 3bM both localise to the nucleus, this suggests that a nuclear localisation signal is present in the C-terminus of 3b (Shen et al. 2003). Only one nuclear retention motif was identified, RVxF, that is present in 3bB/3bM and not present in 3bT. This motif allows interaction with the catalytic domain of PP1c and is present and functionally important in IBV accessory protein 4b (**Chapter 5**) and TGEV accessory protein 7 (Cruz et al. 2011). PP1 is a phosphatase protein which plays a role in a range of cellular pathways (Szyszka et al. 1989, Hartshorne et al. 2004). This motif was not present in the Qx isoform of 3b. Knockout of RVxF may help to determine the role of this motif in 3B/3bM nuclear localisation in mammalian cells, although why this motif would act differently in avian cells is not known (Lesage et al. 2004). None of these motifs are obviously important for the interacting partners identified by LC-MS/MS for 3bM (**Appendix 7.3, 7.4**), which could suggest none of these motifs are important.

Mass spectrometry analysis of 3b identified six significant interacting partners for GFP-3bM and failed to identify any significant proteins for 3bM-GFP (**Table 4.2**). Compared to 3a and 4b, the number of interacting partners was lower for 3b. IBV 3b has a very short half-life of 7.5 minutes in Vero cells (Pendleton et al. 2006) and could explain the low expression levels of GFP-tagged 3bM in the eluate samples and thus the low number of cellular interacting partners identified (**Figure 4.3**). HEK-293T cells were used for the co-IP due to the high transfection rates and the ability to characterise mammalian proteins by mass spectrometry. Nonetheless, there are differences in 3b cellular localisation between mammalian and avian cells which could skew the accuracy of the mass spectrometry data. The M41 isoform of 3b was used for the co-IP; future work would be encouraged to repeat this assay with both 3bQ and 3bT to detect different interacting partners that could suggest reasons for the highly pathogenic nature of Qx or the different cellular compartmentalisation of 3bT.

Three proteins that have a role in regulating apoptosis were identified by mass spectrometry. The first was BAG6 a molecular chaperone which interacts with and stabilises the pro-apoptotic protein AIF (Desmots et al. 2008). The second, VDAC2, is a pore-forming protein that localises to the outer membrane of the mitochondria where it is involved in the mitochondrial apoptotic pathway (Cheng et al. 2003). The third protein identified, COX5b, also localises to the mitochondria where it plays a role in ATP production (Galati et al. 2009) and has been shown

to inhibit ROS levels and thus has a role in regulating intrinsic apoptosis (Zhao et al. 2012). Viruses have been shown to express proteins that both inhibit and induce apoptosis (Koyama et al. 1998). Accessory proteins PB1-F2 from IAV and VP5 from IBDV have been shown to induce apoptosis through the interaction with VDAC1 and VDAC2, respectively (Zamarin et al. 2005, Li et al. 2012), while HIV-1 Tat accessory protein has been shown to interact with COX5b to induce mitochondrial membrane permeabilisation, leading to apoptosis (Lecoeur et al. 2012). Cellular apoptosis is a common feature of coronavirus infection, with alpha- beta- and gammacoronaviruses all able to induce apoptosis in some manner (Fung et al. 2014). No anti-apoptotic proteins have been identified for coronaviruses with viral proteins primarily inducing apoptosis (Liu et al. 2014). For example, SARS-CoV accessory proteins 3a and 3b have been shown to induce caspase-dependent apoptosis when overexpressed in Vero cells (Law et al. 2005, Khan et al. 2006) (Tan et al. 2004), while SARS-CoV 7a has also been shown to induce apoptosis by interacting with the pro-survival protein, Bcl-X_L (Tan et al. 2007). Previous work has shown that caspase-dependent apoptosis is actively induced during IBV infection (Li et al. 2007, Liao et al. 2013). Furthermore, IBV-induced apoptosis has been shown to involve the Blc-2 family of proteins including Bak, a VDAC2 interacting protein (Zhong et al. 2012). The pro-apoptotic PERK and eIF2α pathways are also active during IBV infection, although it is not known if this is directed by the virus or is activated as a host response to infection (Liao et al. 2013). Inhibiting apoptosis during IBV infection does not affect viral titres, suggesting apoptosis is not required for IBV replication (Liu et al. 2001). Here,

IBV-induced apoptosis has been further confirmed in an avian cell line using FACS (**Figure 4.6B**) and has been shown to be caspase-dependent (**Figure 4.7**). Although BeauR-Sc3bAUG did also induce apoptosis and cell death in higher amounts compared to the mock control (**Figure 4.6C**), levels were significantly lower compared to wild-type Beau-R. The same effect was seen for the caspase 3/7 assay which showed higher caspase activity when cells were infected with Beau-R compared to BeauR-Sc3bAUG (**Figure 4.7**). This result suggests that 3b expression, during Beau-R infection, increases cellular apoptosis. Scrambling of 3b did not completely abrogate apoptosis as seen by FACS and caspase activity, suggesting that IBV either expresses additional pro-apoptotic protein/s or apoptosis is a cellular response to viral replication. Levels of caspase 3/7 at 36 h.p.i were not significantly different between wild-type and BeauR-Sc3bAUG, most likely representing host-induced apoptosis, as the cell responds to depleted resources after peak replication. Both the FACS and caspase assay should be repeated measuring apoptosis during transient expression of 3b. These assays could also be used to measure and compare the apoptotic activity of 3bB, 3bM, 3bQ, and 3bT and further include the use of Vero and DF-1 cells to determine the functionality of 3bB against 3bT in different cell lines.

The apoptotic and innate immune signalling pathways are linked, with many coronavirus accessory proteins including SARS 3a and 7 shown to modulate both pathways (Alcami et al. 2000, Liu et al. 2014). Indeed, previous work has shown that recombinant IBV that lacks 3b expresses more IFNβ, suggesting 3b inhibits

IFNβ expression in some unknown manner (Kint et al. 2015). A potential mechanism, as alluded to in the mass spectrometry data, could be an interaction between 3b and COX5b, a protein that negatively regulates IFN expression by controlling MAVS aggregation at the mitochondria (Zhao et al. 2012). Future work should aim to confirm this interaction and determine if 3b can inhibit IFNβ expression using the chIFNβ luciferase assay. This assay will help to determine whether the effect of 3b on IFNβ expression occurs at the point of MAVS signalling as seen for accessory protein 3a.

More work is required to determine the function of 3b during infection and has been hampered by the difficulties in transiently expressing 3b and detecting 3b during infection. Due to time constraints and a lack of an anti-3b antibody, none of the interacting partners for 3bM were confirmed by immunofluorescence or IP. Any future work should first focus on confirming these interactions during infection, either by raising an antibody against 3b or using the reverse genetic system to introduce an epitope tag onto 3b. Future work should also focus on comparing 3bB/3bM with 3bT and 3bQ to determine any functional changes in apoptosis using the assays established here, and interferon signalling, using the chIFNβ assay previously used for 3a. Accessory protein 3b is non-essential for *in vitro* replication and thus could play a role as a pathogenicity factor. Determining differences between the function of 3b between low and highly pathogenic strains may help to establish the importance of this small accessory protein.

5. The role of Accessory Protein 4b

5.1. Introduction

IBV expresses four known accessory proteins during infection, 3a and 3b from gene 3, and 5a and 5b from gene 5 (Casais et al. 2005, Britton et al. 2006, Hodgson et al. 2006). They were shown to be accessory proteins, as scrambling of the AUG start codon (ATG>ACC) had no effect on viral replication *in vitro*. Nonetheless, these proteins are highly conserved, and it is assumed they play a role in pathogenicity and/or viral-host interaction. IBV and the closely related TCoV contain an ORF known as ORF4b within the intergenic region (IR), a region in-between gene M and gene 5 (Bentley et al. 2013). This ORF from M41-CK has the potential to encode a 94 amino acid protein with a molecular weight of around 11 kDa, while Beau-R ORF4b is smaller and could encode a protein with a molecular weight of 6 kDa. Due to a lack of a canonical TRS (CUUAACAA) it was assumed that there was no corresponding mRNA for expression of ORF4b (Bentley et al. 2013). For this reason, ORF4b was, until recently, believed to be a pseudogene. Bentley et al (2013) showed that IBV expressed a sgRNA that is regulated by a non-canonical TRS (CAA) (Bentley et al. 2013). This non-canonical TRS regulates the transcription of sgRNA 4b at lower levels than is expected for its genome location. Previous work has shown that deleting the intergenic region containing ORF4b from Beau-R has no effect on viral replication and if expressed is most likely an accessory protein (Bentley et al. 2013). Northern blot analysis has shown that sgRNA 4b is expressed by IBV strains M41-CK and Beau-R, and some strains of TCoV. It is not known whether this sgRNA is translated into a

protein. In this chapter, expression of 4b during M41-CK infection has been confirmed. Furthermore, the role of 4b is investigated and has been shown to play a role in regulating cellular translation and stress granule formation.

Results

5.2. Bioinformatic analysis of IBV and TCoV 4b

Previous work has shown that M41-CK and Beau-R encode an ORF in the intergenic region known as ORF4b (Bentley et al. 2013). Beau-R ORF4b is predicted to encode a 50 amino acid protein while M41-CK is predicted to encode a 94 amino acid isoform. TCoV strains also contain an ORF in the intergenic region (Bentley et al. 2013). Frequency and sequence similarity of 3a, 3b, 5a, and 5b has previously been determined by analysing and comparing the ORFs encoded by different strains of IBV (Britton 2007). The full-genome sequences of IBV and TCoV strains were downloaded from the viper database (viprdb.org) to determine the frequency and sequence similarity of ORF4b. In all, 178 sequences (Jan 2017) were downloaded and contained a mix of lab, vaccine, and field strains. ORF4b and the non-canonical TRS were identified in each strain using the unsorted six-frame translation tool in BioEdit. In the 178 strains studied, 78% of strains had both ORF4b and the non-canonical TRS (**Table** 5.1). ORF4b varied in size between the strains, the smallest length was 40 amino acids and the largest was 100 amino acids. The most common form of ORF4b was 94 amino acids with 69% of strains encoding this length. Due to the frequency of this length, this was considered the full-length version of ORF4b. The other IBV accessory

proteins have a high level of percentage similarity (Britton et al. 2006). To determine sequence similarity/identity of 4b, the sequence alignment for 4b was entered into the sequence identity and similarity (SIAS) tool (imed.med.ucm.es). Each sequence was aligned to each other sequence, and percentage similarity or identity was calculated. The average percentage similarity or identity was then calculated. Sequence identity for 4b was 86% while similarity was 81%.

The M41-CK 4b peptide sequence was further characterised to determine any domains, motifs, or conserved regions. The Eukaryotic Linear Motif (ELM) tool was used to identify any motifs that may help to determine function. This tool aims to identify motifs which have previously been shown to mediate protein-protein interactions. In total 21 motifs were identified, ranked by the probability of the motif occurring randomly in a 94 amino acid protein (**Table 5.2**). Due to the high incidence of false positives when using this tool, little can be inferred from these results alone. Nonetheless, two motifs were of interest from the search, Phosphoprotein 1c (PP1c) SILK (.[GS]IL[KR][^DE]) and RVxF (..[RK].{0,1}[VIL][^P][FW].) Individually these motifs have a low probability of occurring randomly in a 94 amino acid protein. Furthermore, their presence together in the same peptide sequence is even more unlikely. Both motifs are involved in PP1c binding and cooperate to increase PP1c affinity. For this to occur these motifs should be near as they are in 4b (Hendrickx et al. 2009). PP1c_RVxF is at position 7-13 while PP1c_SILK is at position 15-20. PP1c is a multi-functional protein involved in the dephosphorylation of phosphorylated proteins (Szyszka et

al. 1989, Mochida et al. 2012). Due to the promiscuous nature of this protein, the exact cellular pathway being controlled cannot be determined. Sequence alignment of 4b isoforms showed that the N-terminal end of 4b is more conserved than the C-terminal end, due in part to the presence of C-terminal truncations in many 4b isoforms. RVxF and SILK motifs, as identified by the EML search, are present in 93.75% and 93% of 4b sequences, respectively (**Figure 5.1**).

Table 5.1 Bioinformatic analysis of the ORF4b predicted peptide sequence in IBV/TCoV strains

IBV/TCoV Strains	Strains with 4b + TRS	4b Isoforms	Count	IBV Strain	Sequence Similarity	Sequence Identity
183	144 (78%)	Elongated	3 (2%)		81%	86%
		Full-length94	100 (69%)	M41, QX		
		Truncated92	1 (0.7%)			
		Truncated80	31 (21.5%)			
		Truncated50	7 (4.8%)	Beau-R		
		Truncated40	2 (1.4%)			

Table 5.2 Eukaryotic linear motifs identified in 4b (M41) peptide sequence.

ELM ID	Matched sequence	Pattern	Position	Description	Cell Compartment	Probability
DEG_Nend_UBRbox_4	MCV	^M{0,1}(C).	1-3	N-terminal motif that initiates protein degradation by binding to the UBR-box of N-recognins. This N-degron variant comprises N-terminal Cys as destabilizing residue.	cytosol	1.77E-05
DOC_PP1_SILK_1	ASILRA	.[GS]IL[KR][^DE]	15-20	Protein phosphatase 1 catalytic subunit (PP1c) interacting motif that often cooperates with and is located N-terminal to the RVXF motif to dock proteins to PP1c.	cytosol, nucleus, protein phosphatase type 1 complex	3.78E-05
DOC_PP1_RVXF_1	YLKLFFN	..[RK].{0,1}[VIL][^P][FW].	7-13	Protein phosphatase 1 catalytic subunit (PP1c) interacting motif binds targeting proteins that dock to the substrate for dephosphorylation.	nucleus, protein phosphatase type 1 complex, cytosol	8.30E-04
DOC_MAPK_NFAT4_5	REYLKLFFN	[RK][^P][^P][LIM].L.[LIVMF].	5-13	An extended D site specifically recognized by the JNK kinases	cytosol, neuron projection nucleus, protein complex,	1.64E-04
LIG_Pex14_2	FILSF	F...[WF]	36-40	Fxxx[WF] motifs are present in Pex19 and S. cerevisiae Pex5 cytosolic receptors that bind to peroxisomal membrane docking member, Pex14	cytosol, peroxisome, glycosome	4.63E-04
	FKKQF		45-49			
	FFHSF		49-53			
LIG_SH3_4	KPIFQKGC	KP..[QK]...	77-84	This is the motif recognized by those SH3 domains with a non-canonical class II recognition specificity	focal adhesion, cytosol	6.78E-04
LIG_BRCT_BRCA1_1	NSIIF	.(S)..F	22-26	Phosphopeptide motif which directly interacts with the BRCT (carboxy-terminal) domain of the Breast Cancer Gene BRCA1 with low affinity	nucleus, BRCA1-BARD1 complex	1.91E-03
DOC_MAPK_MEF2A_6	REYLKLFF	[RK].{2,4}[LIVMP].[LIV].[LIVMF]	5-12	A kinase docking motif that mediates interaction towards the ERK1/2 and p38 subfamilies of MAP kinases.	cytosol, Transcription factor complex, nucleus	2.58E-03
TRG_ENDOCYTIC_2	YLKL	Y..[LMVIF]	7-10	Tyrosine-based sorting signal responsible for the interaction with mu subunit of AP (Adaptor Protein) complex	plasma membrane, clathrin-coated endocytic vesicle, cytosol	2.59E-03

LIG_SH2_STAT5	YLKL	(Y)[VLTFIC]..	7-10	STAT5 Src Homology 2 (SH2) domain binding motif.	cytosol	3.30E-03
LIG_TRAF2_1	SFQE	[PSAT].[QE]E	39-42	Major TRAF2-binding consensus motif. Members of the tumour necrosis factor receptor (TNFR) superfamily initiate intracellular signalling by recruiting the C-domain of the TNFR-associated factors (TRAFs) through their cytoplasmic tails.	cytosol	4.30E-03
LIG_14-3-3_CanoR_1	RLWLSYK	R[^DE]{0,2}[^DEPG]([ST])(([FWYLMV].)|([^PRIKGN]P)|([^PRIKGN].{2,4}[VILMFWYP]))	86-92	Canonical Arg-containing phospho-motif mediating a strong interaction with 14-3-3 proteins.	cytosol, internal side of plasma membrane, nucleus	4.48E-03

Results are ordered by the probability of the sequence occurring randomly (p).

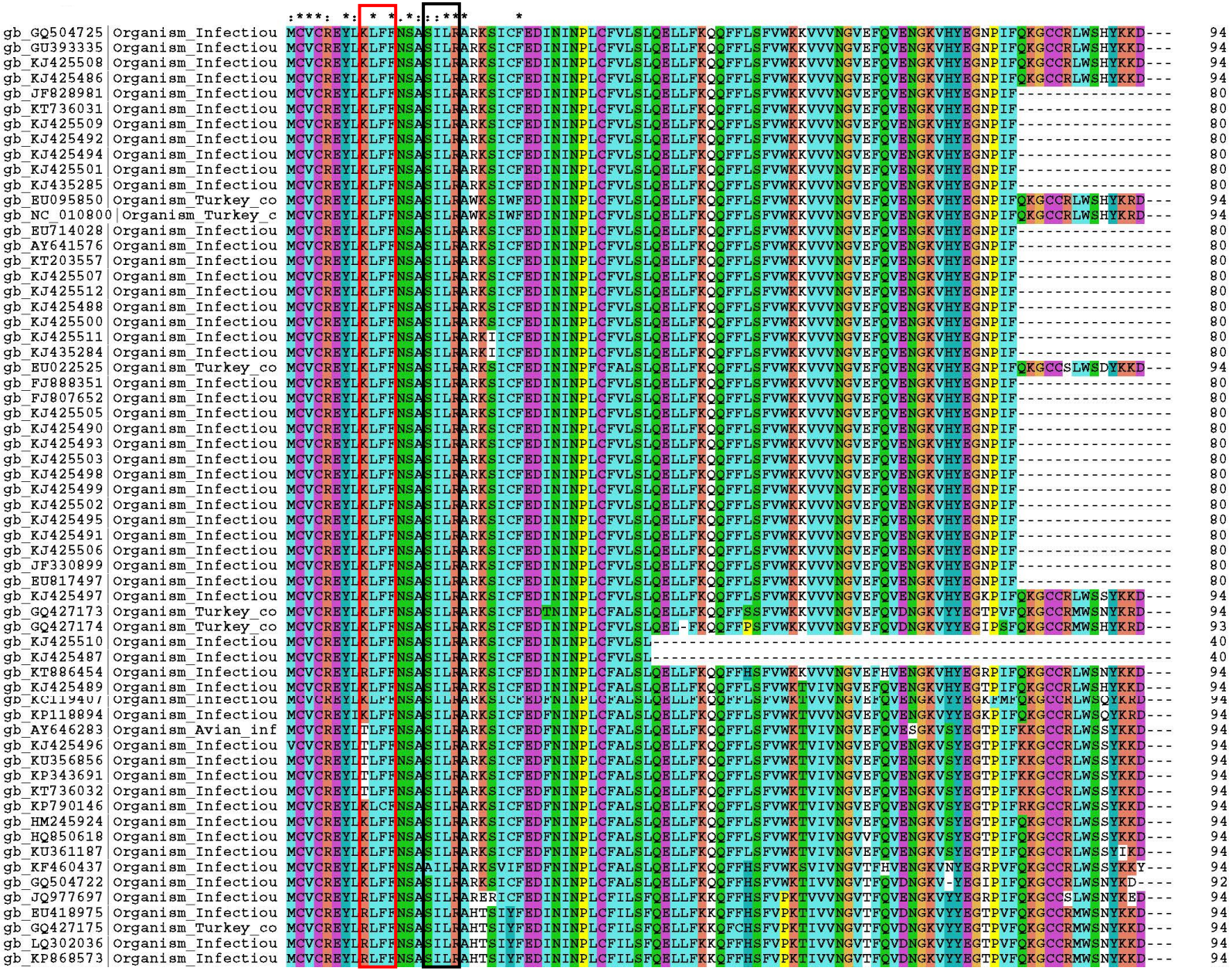

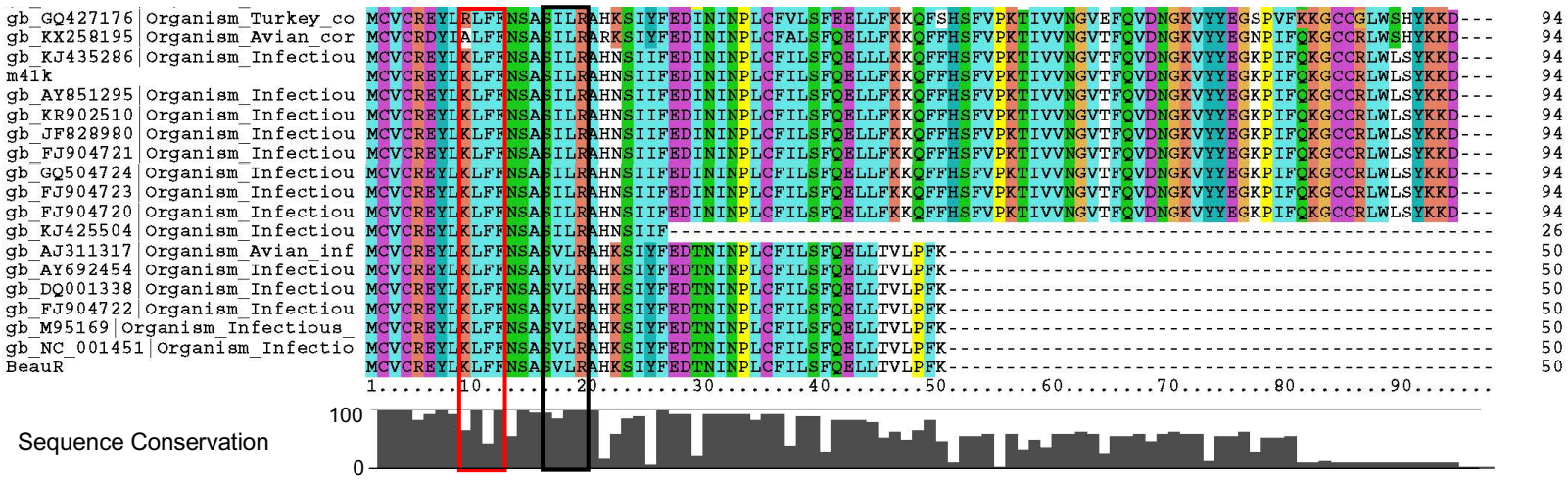

Figure 5.1 Peptide sequence alignment of 4b.

ORF4b was identified in IBV strains (viperdb.com) and aligned and translated using Clustalw. Amino acids with a (*) are conserved throughout, (:) indicates amino acids that are conserved within similar property groups. RVxF (red) and SILK (black) motifs identified by the ELM tool are labelled.

5.3. Generation of GFP-tagged 4b expression vectors

Vectors for expression of GFP-tagged 4b from M41-CK (4bM) were generated for mass spectrometry protein purification and for protein visualisation by immunofluorescence. GFP was fused to the N- or C- terminus of 4bM and both constructs were used in conjunction to reduce the effect of the GFP tag on co-IPs. The 4b from Beau-R (4bB) was tagged at the N-terminus and was used for comparison to GFP-4bM in *in vitro* assays. For the construction of the 4bM expression vectors, M41 viral RNA was isolated and reverse transcribed into cDNA. The 4b ORF was amplified from the cDNA using complementary primers with flanking restriction sites by PCR. The resulting PCR product was purified and; along with the pEGFPC2 (Clontech) and pEGFPN1 (Clontech) plasmids, were digested with the relevant restriction enzymes. Digested vectors were purified by gel extraction. Digested vectors and PCR products were then ligated together. Vector sequences were confirmed by Sanger sequencing. The 4bB cDNA was ordered as a genestring from Invitrogen and contained flanking restriction sites. The GeneArt String (ThermoFisher) was digested with relevant restriction enzymes and ligated into a digested pEGFPC2 vector. The final vectors generated were pEGFPC2-4bM, pEGFPN1-4bM and pEGFPC2-4bB (**Figure 5.2A,B,C,**). To confirm expression of GFP-tagged 4b from these vectors, DF-1 cells were transfected with GFP-4bM, 4bM-GFP, GFP-4bB, or GFP vectors. After 24 hours, cells were lysed, proteins separated by SDS-PAGE, transferred to a membrane and labelled with anti-GFP. Bands with the molecular weight of GFP-

4bM, 4bM-GFP and GFP-4bB were identified as expected (**Figure 5.2D,E,F**), confirming expression from these vectors was successful.

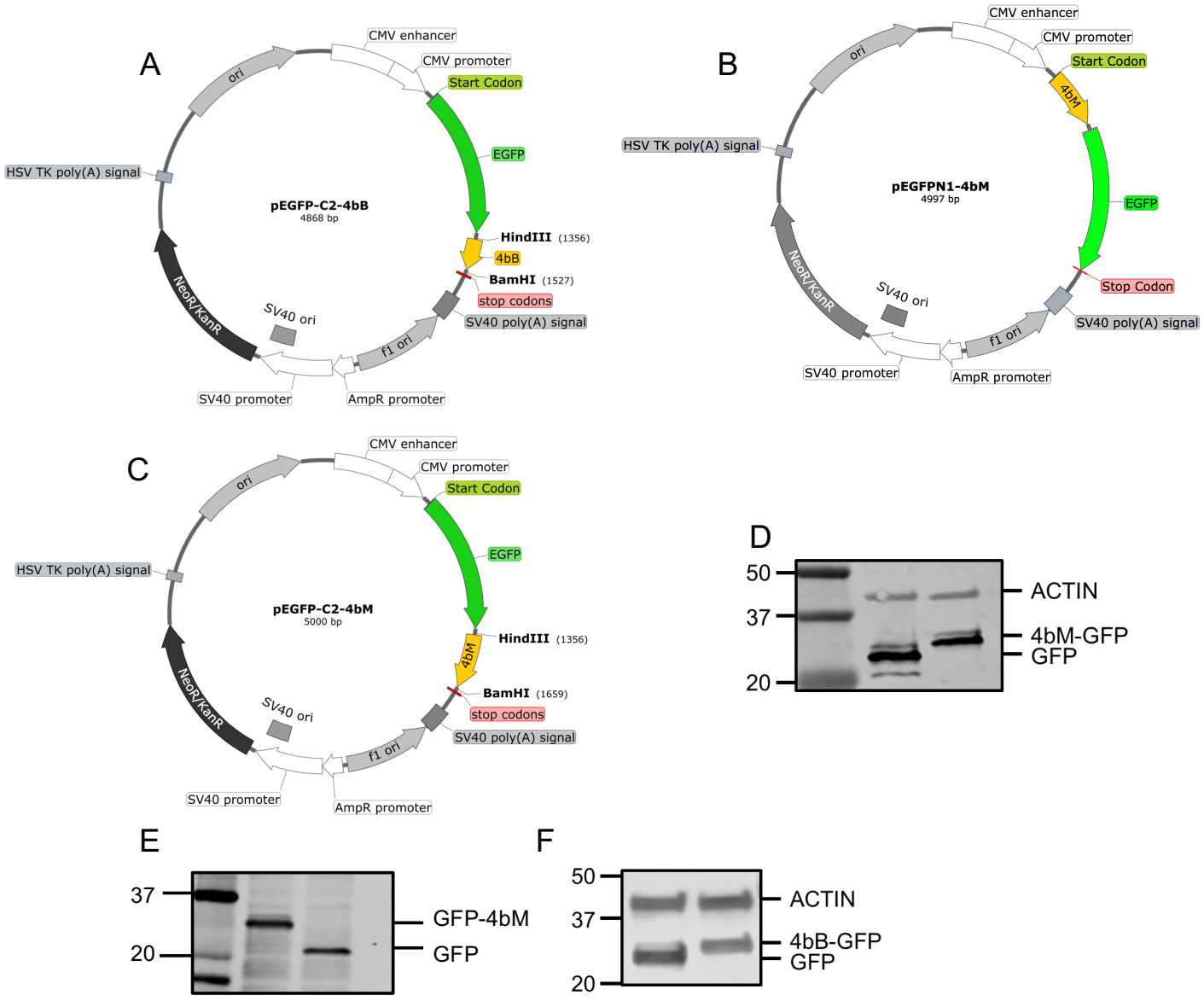

Figure 5.2 Plasmid map and confirmation of expression of the GFP-tagged 4b expression vector.

(A) pEGFPC2-4bB, (B) pEGFPN1-4bM, (C) pEGFPC2-4bM. DF-1 cells were transfected with GFP-4bM (D), 4bM-GFP (E) GFP-4bM (F) GFP-4bB and a GFP control. After 16 hours, cells were lysed, separated by SDS-PAGE, transferred to a membrane, and labelled with anti-GFP or anti-actin.

5.4. Detection of 4b during infection

5.4.1. Validation of anti-4b

Polyclonal anti-4b was raised against the DNGKVYYEGKSI peptide sequence present in the C-terminus of 4bM. Previous work with this antibody failed to detect 4b during M41-CK infection (Bentley et al. 2013). To confirm whether anti-4b can indeed detect 4b, the antibody was first used to detect expression of GFP-tagged 4b. DF-1 cells were transfected with GFP-4bM, 4bM-GFP or GFP expression vectors. After 16 hours, DF-1 cells were fixed, permeabilised and labelled with anti-4b at a concentration of 1:50 and visualised by confocal microscopy. GFP-4b signal colocalised with the anti-4b signal, while GFP signal did not (**Figure 5.3**). This result indicates that anti-4b specifically binds to the 4b peptide. In untransfected cells, a weak signal was detected predominantly in the nucleus, possibly suggesting anti-4b may also bind to a cellular nuclear protein.

To further confirm that anti-4b can label 4b, the antibody was used to detect GFP-4bM overexpression by western blot. DF-1 cells were transfected with the GFP-4bM expression vector at varying doses, and after 16 hours cells were lysed. Samples were separated by SDS-PAGE, transferred to a membrane and labelled with anti-4b at a range of concentrations. The antibody failed to detect 4b expression when transfected with 250 ng and 500 ng of pEGFPC2-4bM but was able to detect GFP-4bM when transfected with a higher dose at 1000 ng (**Figure 5.4**). The size of the band was around 35 kDa, the expected size of GFP-4bM.

This result demonstrates that anti-4b can detect GFP-tagged 4b by western blot and possibly by immunofluorescence.

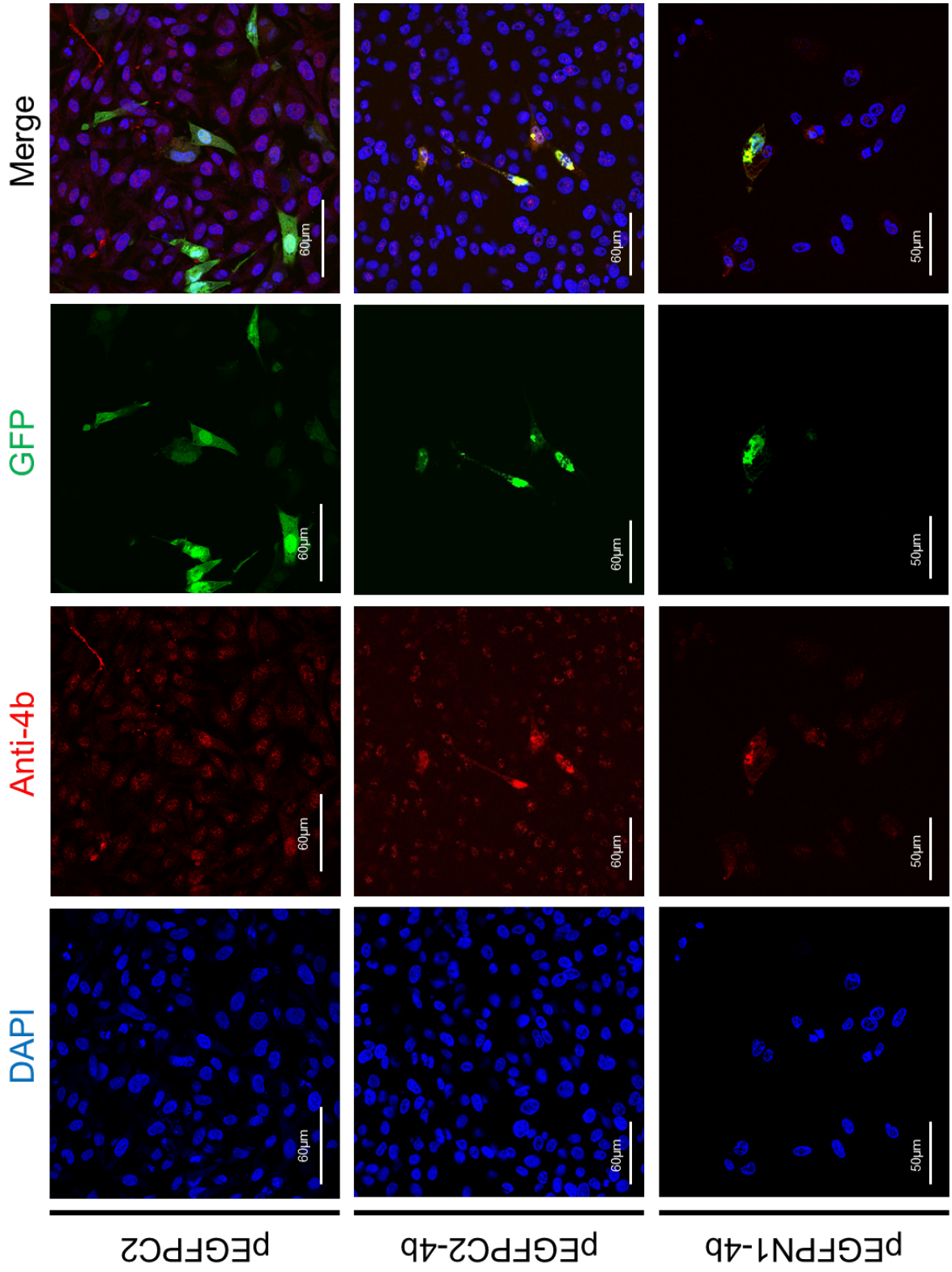

Figure 5.3 Anti-4b can detect the presence of GFP-tagged 4bM.

DF-1 cells were transfected with plasmids encoding N- and C-terminally GFP-tagged 4b protein. After 24 hours, cells were fixed and stained with anti-4b and DAPI.

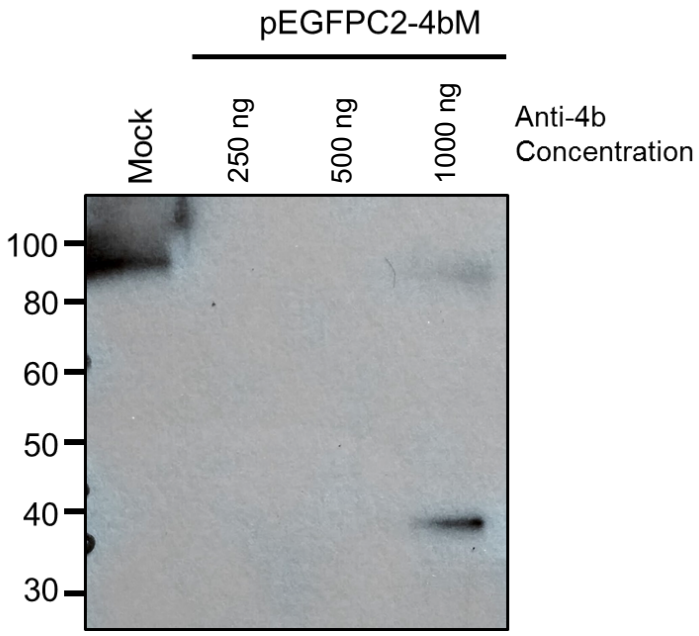

Figure 5.4 Anti-4b can label GFP-4bM.
DF-1 cells were transfected with the GFP-4bM expression vector. After 16 hours, cells were lysed and separated by SDS-PAGE. Blots were incubated with anti-4b.

5.4.2. Detection of 4b during M41 infection

After validating that anti-4b specifically binds to 4bM, the antibody was used to determine whether 4b is expressed during M41 infection. The antibody was raised against a C-terminal peptide sequence not present in ORF4b from Beau-R. Therefore, anti-4b can only be used to label the M41 4b isoform. The antibody was initially used to label 4b by western blot analysis. CK cells were mock infected or infected with M41 at an MOI above 4 and lysed 24 hours later. The samples were separated by SDS-PAGE and transferred to a nitrocellulose membrane. Membranes were labelled with anti-4b at a concentration of 1:50 and anti-actin

for 16 hours. An actin band was detected at 40 kDa in both the mock and infected lanes; a band was also detected in the M41-CK lane at approximately 10 kDa (**Figure 5.5A**). This result provided preliminary evidence that 4b was expressed during M41 replication.

To further confirm expression of 4b, a range of recombinant viruses were used as controls. These viruses, M41K-del4b and BeauR-IR(M41) were previously generated by Sarah Keep and Kirsten Bentley, respectively. M41K-del4b has a deletion of ORF4b in the M41-K backbone. BeauR-IR(M41) contains the intergenic region; the region between M and ORF5ab, from M41, inserted into Beau-R and therefore contains ORF4bM. Anti-4b was also tested against Beau-R. As the antibody was raised against a peptide sequence at the C-terminus of 4b, not present in Beau-R ORF4b, the antibody should be able to label Beau-R 4b. Furthermore, anti-4b should also fail to label M41K-del4b due to deletion of ORF4b. Conversely, anti-4b should be able to label BeauR-IR(M41) as this recombinant IBV will express the full-length 4b. CK cells were infected with M41K-del4b, BeauR-IR(M41), Beau-R and M41-CK for 24 hours. Cells were then lysed, proteins separated by SDS-PAGE, transferred to a membrane and labelled with anti-actin and anti-4b. Actin was present in all samples. Anti-4b was unable to detect a protein band in the M41K-del4b or Beau-R lane but did detect a protein band in the M41-CK and the BeauR-IR(M41) lane (**Figure 5.5A**, **B**). This confirms the 10 kDa band is indeed the predicted 4b protein.

After confirming 4b is expressed, IBV 4b levels were characterised during infection. CK cells were infected with M41-CK at an MOI of 4 or mock infected. Cells were harvested at 4, 8, 12, 16, 24 and 48 h.p.i. The samples were separated by SDS-PAGE, transferred to a membrane and labelled with anti-actin and anti-4b. Western blot analysis showed that anti-4b could detect 4b expression from 16 h.p.i and that peak 4b expression occurred at 24 hours (**Figure 5.5C**).

IBV 4b was further characterised by immunofluorescence to study cellular localisation of 4b. CK cells were infected with M41-CK, and after 24 hours, cells were fixed, permeabilised and labelled with anti-4b. As a control for infection, cells were labelled with anti-dsRNA. The anti-4b signal appeared stronger in cells positive for dsRNA (**Figure 5.6A**). The anti-4b signal is predominantly cytoplasmic with a granular-like pattern and appeared to aggregate in large structures during infection. However, there was a high level of the anti-4b signal in non-infected cells. Furthermore, labelling of 4b did not occur in all infected cells. To confirm that the use of a primary CK cell line, which can have a high proportion of cell debris and stressed cells was not responsible for this observation, the experiment was repeated in DF-1 cells. M41 cannot infect DF-1 cells; therefore, a recombinant M41 virus with the spike protein from Beau-R (M41R-BeauR(S)) was used. The Beaudette spike permits M41-K entry into DF-1 cells. DF-1 cells were infected with M41R-BeauR(S) for 24 hours, then fixed, permeabilised and labelled with anti-4b and anti-dsRNA. The background 4b signal was lower in DF-1 cells but, as seen previously, not all infected cells contained 4b signal (**Figure 5.6B**).

Altogether, the western blot and immunofluorescence data confirms that the M41-CK 4b transcript, previously identified by Bentley *et al,* is translated during infection and confirms 4b as the fifth IBV accessory protein.

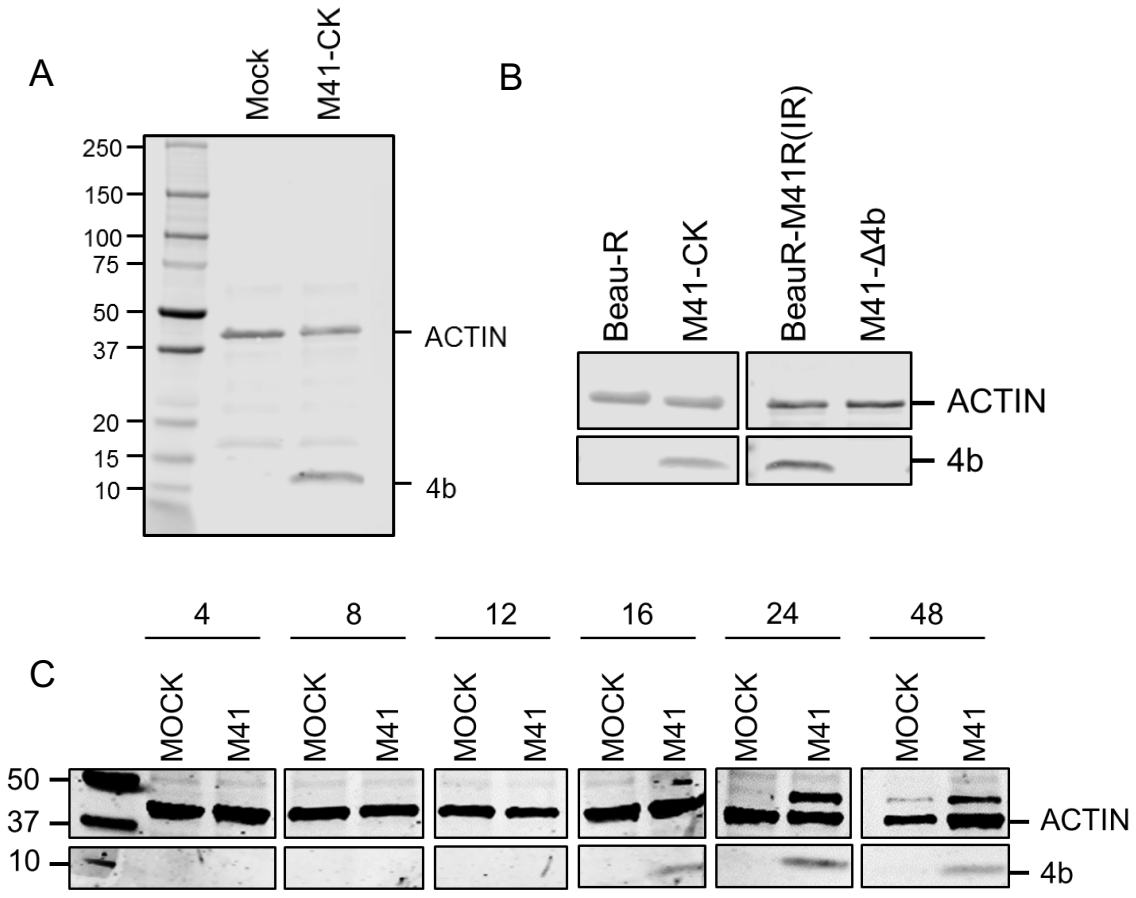

Figure 5.5 M41-K expresses an 11 kDa protein known as 4b during infection.
CK cells were (A) Mock infected or infected with M41-K, (B) infected with Beau-R, M41-CK, BeauR-M41R(IR) or M41K-del4b at an MOI of 4. At 24 h.p.i cells were lysed, proteins separated by SDS-PAGE and transferred to a membrane and labelled with anti-4b and anti-actin. (C) CK cells were mock infected or infected with M41 at an MOI of 4. Cells were lysed at indicated time-points, proteins separated by SDS-PAGE, transferred to a membrane and labelled with anti-actin and anti-4b.

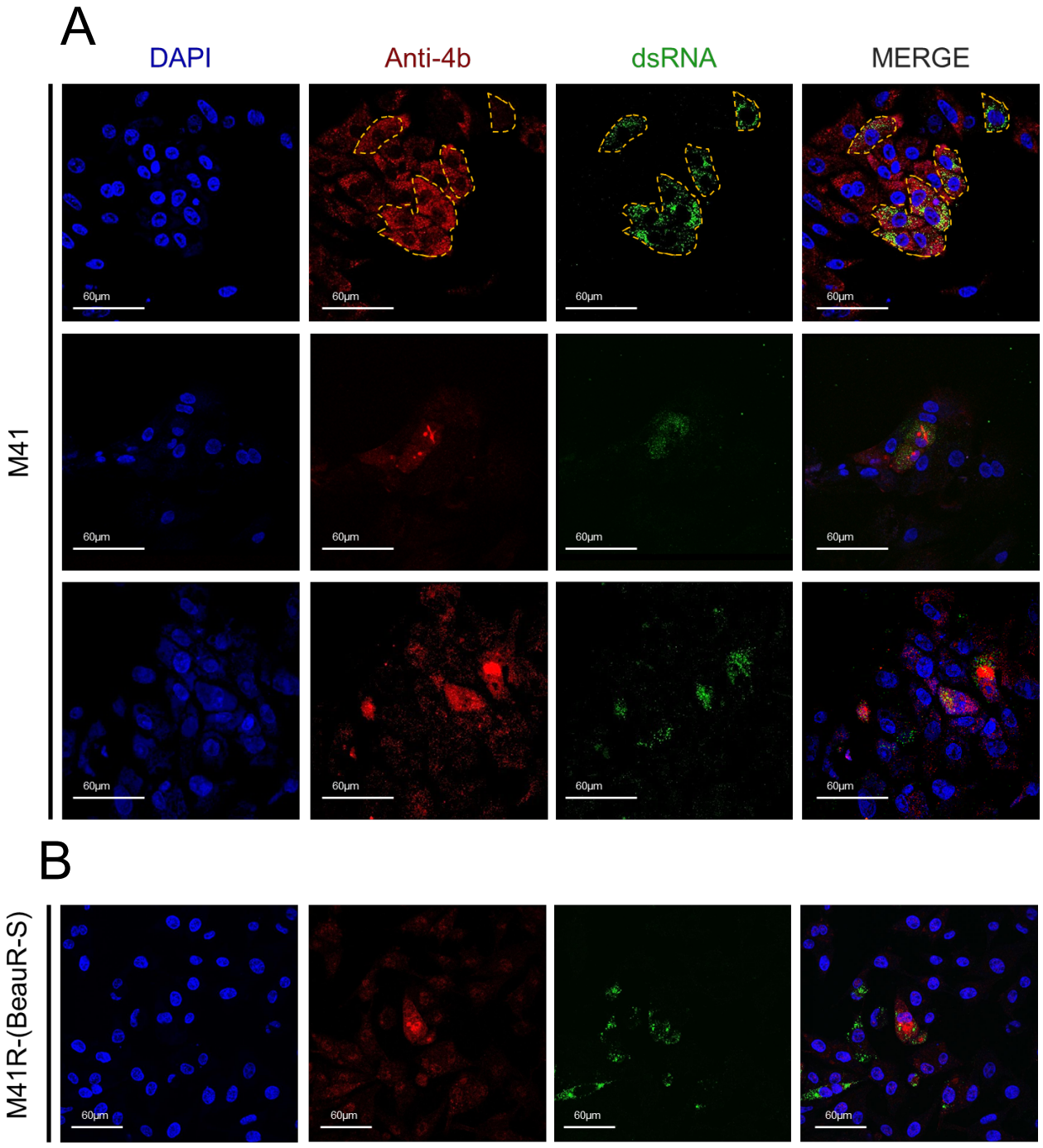

Figure 5.6 Anti-4b can detect 4b during infection.

CK cells were infected with either (A) M41-CK or (B) M41R-BeauR(S) at a MOI above 4. After 24 hours, cells were fixed and labelled with anti-dsRNA and anti-4b. The nuclei were stained with DAPI.

5.5. Effect of 4b on viral replication

It is assumed that 4b is an accessory protein as 22% of IBV/TCoV strains lack ORF4b (**Table** 5.1). To confirm this, recombinant IBVs were generated with ORF4b deletions. Two viral isolates, M41K-del4b-2 and 16 were designed and generated using the M41-K reverse genetics system (Keep *et al.* unpublished). The generation of these IBVs and subsequent growth curves were completed by Sarah Keep, as part of another project. CK cells were infected with M41-CK, M41-K, and M41K-del4b-2/16 at an MOI of 0.01. Two recombinant clones (clone 2 and

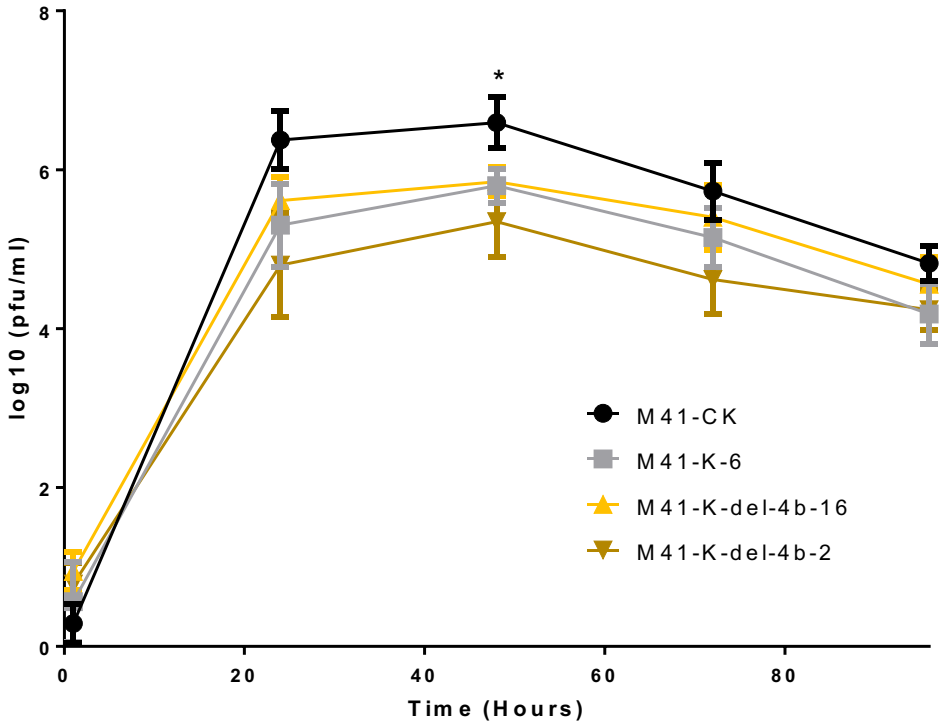

Figure 5.7 Protein 4b is not required for in vitro viral replication.
CK cells were infected with M41-CK, M41-K, or M41-K-del-4b at an MOI of 0.01. The supernatant was harvested at the indicated time-point and titration calculated using the CK plaque assay. Data was from three experimental repeats. Growth curve completed by Sarah Keep. Results are from three biological replicates. Unpaired *t*-test *significant at $p < 0.05$. Error bars represent one standard derivation from the mean.

clone 16) were generated to take into account IBV genome mutations that can arise during the reverse genetics system. The supernatant was removed at 0, 24, 48, 72 and 96 h.p.i and virus titre determined by CK cell plaque assay. Results are from three biological repeats. The full-length molecular clone, M41-K, grew to similar titres as M41K-del4b, with both peaking at 48 h.p.i at 2-5x10^5 pfu/ml (**Figure 5.7**). M41-CK grew to higher titres at hour 48 compared to the molecular clone, M41-K, while the reason for this discrepancy is unknown, it is possibly due to the mixed population of viruses within the M41-CK inoculum. Despite this discrepancy, this result indicates that 4b has no effect on viral *in vitro* replication and is therefore an accessory protein.

5.6. Mass spectrometry analysis of GFP-tagged 4b Co-IPs

To determine the role of accessory protein 4b, mass spectrometry was utilised to identify proteins that interact with GFP-4bM or 4bM-GFP. HEK-293T cells were transfected with the pEGFPC2-4bM or pEGFPN1-4bM expression vectors or a GFP control plasmid. After 16 hours, cells were lysed and GFP-4bM/4bM-GFP/GFP immunoprecipitated using GFP ‘capture’ beads (Chromotek). Three biological replicates were completed for each plasmid. Input and eluate GFP-4bM and 4bM-GFP samples were analysed by western blot to confirm successful transfection and immunoprecipitation (**Figure 5.8**). Samples were analysed by LC-MS/MS by Stuart Armstrong.

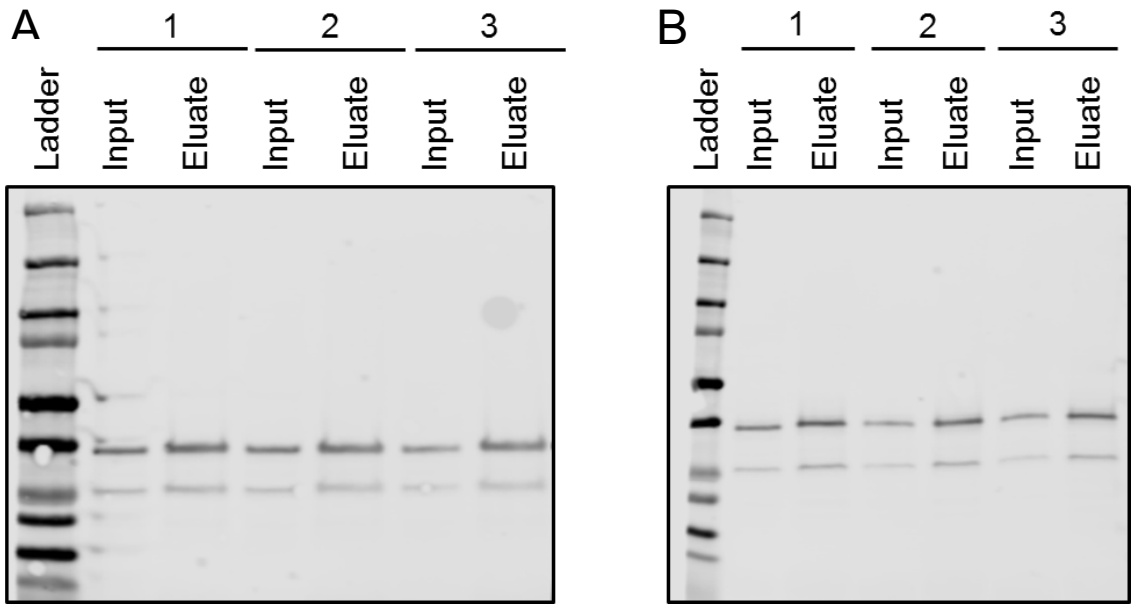

Figure 5.8 Confirmation of GFP-4bM/4bM-GFP transfection and IP.
HEK-293T cells were transfected with (A) GFP-4bM or 4bM-GFP expression vectors. After 16 hours, cells were lysed, and GFP-tagged 4bM immunoprecipitated using GFP 'capture' beads (Chromotek). Input and eluate samples were separated by SDS-PAGE, transferred to a membrane and labelled with anti-GFP.

In total 87 and 137 cellular proteins were detected in higher amounts in the GFP-4bM or 4bM-GFP samples, respectively, compared to the GFP control, of which 24 appeared in both (**Appendix Table 7.4, 7.5**). Due to an unknown reason, replicate three did not align with the previous two replicates for either plasmid and was removed from the analysis (**Appendix Table 7.4, 7.5**). Proteins where identified by comparing unique peptides to a database of human proteins. Proteins where only a single unique peptide was identified, were removed to reduce the chance of identifying the wrong protein. The significance (*p*-value) of the mass spectrometry data was determined by two-tailed unpaired ANOVA on two biological replicates, as well as the fold-change in relative protein abundance

over the GFP control. Interacting proteins were then ranked by significance (*p*-value). Proteins that had a *p*-value (-Log10) above one and a fold-change (Log2) above two were considered significant (**Figure 5.9, Figure 5.10**). For each protein, the confidence score was calculated, which is the cumulative value of *p*; the probability of the identified peptide sequence occurring randomly, for each unique peptide identified. The higher the confidence score, the higher the confidence in protein identification. Mass spectrometry data identified 15 cellular proteins for GFP-4bM that were significant, and 17 proteins for 4bM-GFP, eight proteins appeared in both datasets (**Table** 5.5).

A panther over-representation test (pantherdb.org) was performed to categorise the cellular localisation of the significant proteins identified in the GFP-tagged 4bM eluate. This test grouped cellular proteins by their Gene Ontology (GO) cellular compartment annotation and helped to determine if these cellular compartments are over-represented in the dataset. The test compared expected number of proteins to actual number of proteins. Cellular compartments with a *p*-value below 0.05 were considered significant. The number of proteins that localise to these significant GO cellular components were represented as a Venn diagram. Of the 21 unique proteins identified, 13 proteins localise to the ribosomal translational machinery, while three proteins localise to and regulate stress granule or p-body assembly (**Figure 5.11**).

Table 5.3 Cellular proteins identified by LC-MS/MS that significantly interact with GFP-4bM.

Protein ID	Protein	Unique peptides	Confidence	Relative Protein Abundance				*p* Value (-Log10)	Fold Change GFP-4bM/GFP (Log2)
				pEGFPC2-4bM		pEGFPN1			
				1	2	1	2		
RRBP1*	Ribosome-binding protein 1	4	255.74	1889.294019	3590.533721	100.8331958	80.90184734	1.99823936	4.914222002
EF1D	Elongation factor 1-delta	4	391.08	15495.05071	13726.6983	239.4231988	504.5743565	1.997433404	5.29560084
RT18A*	28S ribosomal protein S18a, mitochondrial	2	140.61	745.3216979	6387.487721	0	0	1.795023111	10
RL40*	Ubiquitin-60S ribosomal protein L40	4	1272.81	192391.0279	309618.5155	36265.8443	28315.76306	1.769525206	2.958519537
POP7*	Ribonuclease P protein subunit p20	2	134.3	2829.72501	359.3812335	0	0	1.747300551	10
RRS1*	Ribosome biogenesis regulatory protein homolog	2	77.67	1556.740123	20216.67469	0	0	1.735695533	10
RL14	60S ribosomal protein L14	8	582.74	41072.21332	106616.499	4213.913143	5345.27756	1.480392825	3.949527274
CHCH1	Coiled-coil-helix-coiled-coil-helix domain-containing protein 1	3	189.97	399.1320538	32.41494431	0	0	1.304962603	10
PRDX2*	Peroxiredoxin-2	3	263.01	5215.96236	16505.10114	1287.62327	855.4837881	1.152184348	3.341318915
LS14A*	Protein LSM14 homolog A	3	206.55	69195.71256	265077.3598	10689.58084	15915.39419	1.101850069	3.651259188
RM43*	39S ribosomal protein L43, mitochondrial	3	236.52	13414.7761	10110.47499	987.1212169	3179.171192	1.052064956	2.497374119
ATX2L*	Ataxin-2-like protein	6	366.47	56290.80765	23285.8282	10275.79864	5527.036502	0.997400796	2.332161498
LAP2B*	Lamina-associated polypeptide 2, isoforms beta/gamma	3	367.06	136685.3054	216452.7164	80902.72867	92397.04123	0.98850445	1.026962423
CHTOP*	Chromatin target of PRMT1 protein	11	1048.35	203225.8432	356271.6694	128674.1111	105193.5423	0.972053732	1.258439383

Shown are cellular proteins identified by label-free mass spectrometry/mass spectrometry that interact with GFP-4bM. Protein identifier (ID), protein name and number of unique peptides used to identify proteins are indicated. Relative abundance score for each protein is indicated. Confidence score (-Log2) is the score of the probability of the unique peptide sequence occurring randomly, added together for each unique peptide. The higher the confidence score, the higher the confidence in protein identification. The p-value (-Log10) is a comparison of the cellular protein abundance between 4b and GFP. The higher the p-value, the higher the probability the protein interacts with 4b. The fold-change (Log2) is the change in the relative abundance of the cellular protein between GFP-4bM and GFP. Cellular proteins which appear in both GFP-4bM and 4bM-GFP data are labelled with an asterisk (*). Proteins which appeared in the third replicate are labelled with (*).

Table 5.4 Cellular proteins detected by LC-MS/MS that significantly interact with 4bM-GFP.

Protein ID	Protein	Unique peptides	Confidence	Relative Protein Abundance				*p* Value (-Log2)	Fold Change (Log10) 4bM-GFP/GFP
				pEGFPN1-4bM		pEGFPN1			
				1	2	1	2		
POP7*	Ribonuclease P protein subunit p20	2	134.3	911.8707526	1588.670511	0	0	2.896713159	10
UBC1*	NEDD8-conjugating enzyme Ubc12	2	44.93	1367.008451	2926.933855	0	0	2.67783124	10
LAP2B*	Lamina-associated polypeptide 2, isoforms beta/gamma	3	367.06	308301.4581	308630.484	80902.72867	92397.04123	2.566031474	1.831841606
EF1D	Elongation factor 1-delta	4	391.08	22074.23517	26765.49226	239.4231988	504.5743565	2.09068515	6.036613458
CHCH1*	Coiled-coil-helix-coiled-coil-helix domain-containing protein 1	3	189.97	127168.0035	7353.350223	0	0	1.787452827	10
CALM	Calmodulin	7	841	159297.0479	235917.7982	36906.94512	42441.29678	1.775356602	2.316366979
SRP14	Signal recognition particle 14 kDa protein	11	1902.3	470648.7836	588968.9287	205603.9915	238126.7524	1.636728076	1.255787446
PDIP3	Polymerase delta-interacting protein 3	18	1732.04	111313.3434	167835.0644	46234.96748	37622.19365	1.450047289	1.735026432
PABP4*	Polyadenylate-binding protein 4	9	2074.35	51414.76432	57641.95842	16367.35231	9263.514578	1.442636493	2.089124527
RPS25*	40S ribosomal protein S25	8	820.46	737016.6507	450290.2693	96942.49295	143057.6572	1.43241781	2.306585708
ASHWN	Ashwin	6	690.7	93116.90466	51436.06016	9247.174195	14188.57335	1.409175412	2.62481548
RS3A	40S ribosomal protein S3a	14	1663.2	541864.1072	766618.8533	284098.6775	228316.5036	1.342278931	1.352510014
HTRA2	Serine protease HTRA2, mitochondrial	3	391.28	3378.013648	6081.843557	1168.164744	746.6740556	1.295892979	2.304595462
RRBP1*	Serine protease HTRA2, mitochondrial	4	255.74	13264.28431	1920.542701	100.8331958	80.90184734	1.269542034	6.384650028
RS30*	40S ribosomal protein S30	5	469.49	1550201.705	792446.3427	258417.5316	307780.9791	1.23218978	2.048760365
NUP50*	Nuclear pore complex protein Nup50	2	130.82	3210.501069	5226.965795	836.9350926	311.755658	1.198085759	2.876819482
ATX2L*	Ataxin-2-like protein	6	366.47	41675.76547	23737.19591	10275.79864	5527.036502	1.117991455	2.049393118
IF2G*	Eukaryotic translation initiation factor 2 subunit 3	10	1075.97	139134.0286	140818.5171	28920.04337	59192.69474	1.115893157	1.667759795
TCPH*	T-complex protein 1 subunit eta	2	214.33	3341.124075	8993.922182	921.0552625	1101.108238	1.107961795	2.60879157
RUSD3*	RNA pseudouridylate synthase domain-containing protein 3	3	326.92	4693.749633	18760.2069	812.4205472	1109.279448	1.075139497	3.609376283
KNOP1*	Lysine-rich nucleolar protein 1	3	344.24	7699.489829	10379.41236	1375.459289	3321.386324	1.038569946	1.944542998
TAF9B	Transcription initiation factor TFIID subunit 9B	3	208.71	21205.1945	22073.88677	1634.801506	5817.237841	1.036993965	2.537962677
IF2B1	Insulin-like growth factor 2 mRNA-binding protein 1	13	1681.43	240192.9464	148950.8683	86125.40777	94522.56675	1.030356349	1.107122347
RL26L*	60S ribosomal protein L26-like 1	2	1535.13	7910.635426	5054.666181	0	52.82109283	1.029975496	7.939325902
NHRF2*	Na(+)/H(+) exchange regulatory cofactor NHE-RF2	6	658.58	123937.8009	87441.99072	42755.90333	19697.35678	1.021638929	1.758988669
ATPO*	ATP synthase subunit O, mitochondrial	4	454.17	47430.7275	98114.17914	23943.06679	14640.81302	1.006701625	1.915394227
CHTOP	Chromatin target of PRMT1 protein	11	1048.35	494204.2965	229409.3663	128674.1111	105193.5423	0.93673901	1.629527314

Shown are cellular proteins identified by label-free mass spectrometry/mass spectrometry that interact with 4bM-GFP. Protein identifier (ID), protein name and number of unique peptides used to identify proteins are indicated. Relative abundance score for each protein is indicated. Confidence score (-Log2) is the score of the probability of the unique peptide sequence occurring randomly, added together for each unique peptide. The higher the confidence score, the higher the confidence in protein identification. The p-value (-Log10) is a comparison of the cellular protein abundance between 4b and GFP. The higher the p-value, the higher the probability the protein interacts with 4b. The fold-change (Log2) is the change in the relative abundance of the cellular protein between GFP-4bM and GFP. Cellular proteins which appear in both GFP-4bM and 4bM-GFP data are labelled with an asterisk (*). Proteins which appeared in the third replicate are labelled with (*).

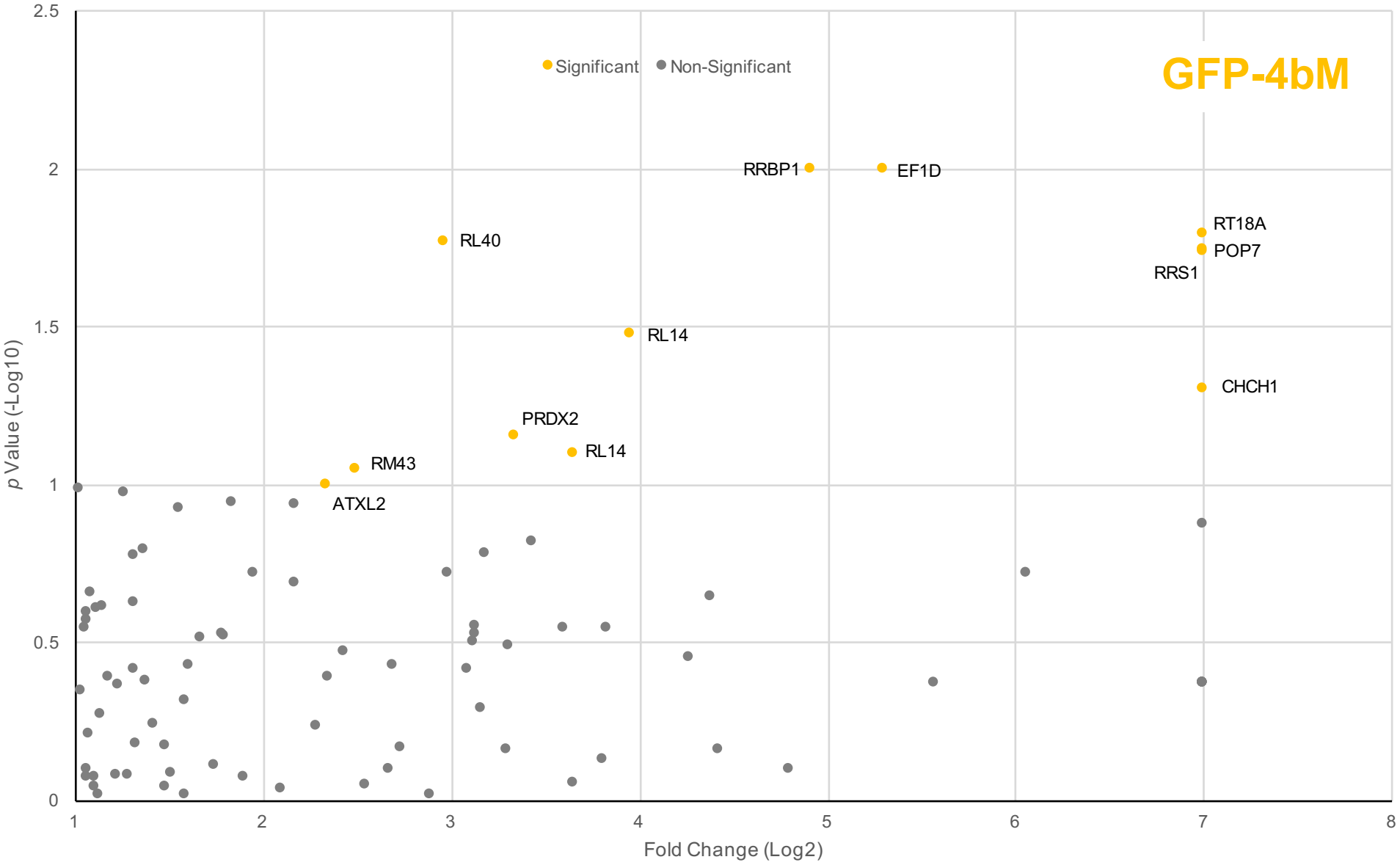
GFP-4bM
Significant
Non-Significant
RRBP1
EF1D
RT18A
POP7
RRS1
RL40
RL14
CHCH1
PRDX2
RL14
RM43
ATXL2
p Value (-Log10)
Fold Change (Log2)
2.5
2
1.5
1
0.5
0
1
2
3
4
5
6
7
8

Figure 5.9 Scatter plot representing results from the GFP-4bM co-IP.

Proteins were identified in the GFP-4bM IP eluate by LC-MS/MS. Proteins are plotted by fold-change in abundance (Log2) compared to GFP alone and *p*-value (-Log10) of the *t*-test. Proteins with a *p*-value (-Log10) > 1 and a fold change (Log2) > 2 have the highest chance of interacting with 4b and are considered significant and are labelled (yellow). Results are representative of two biological replicates.

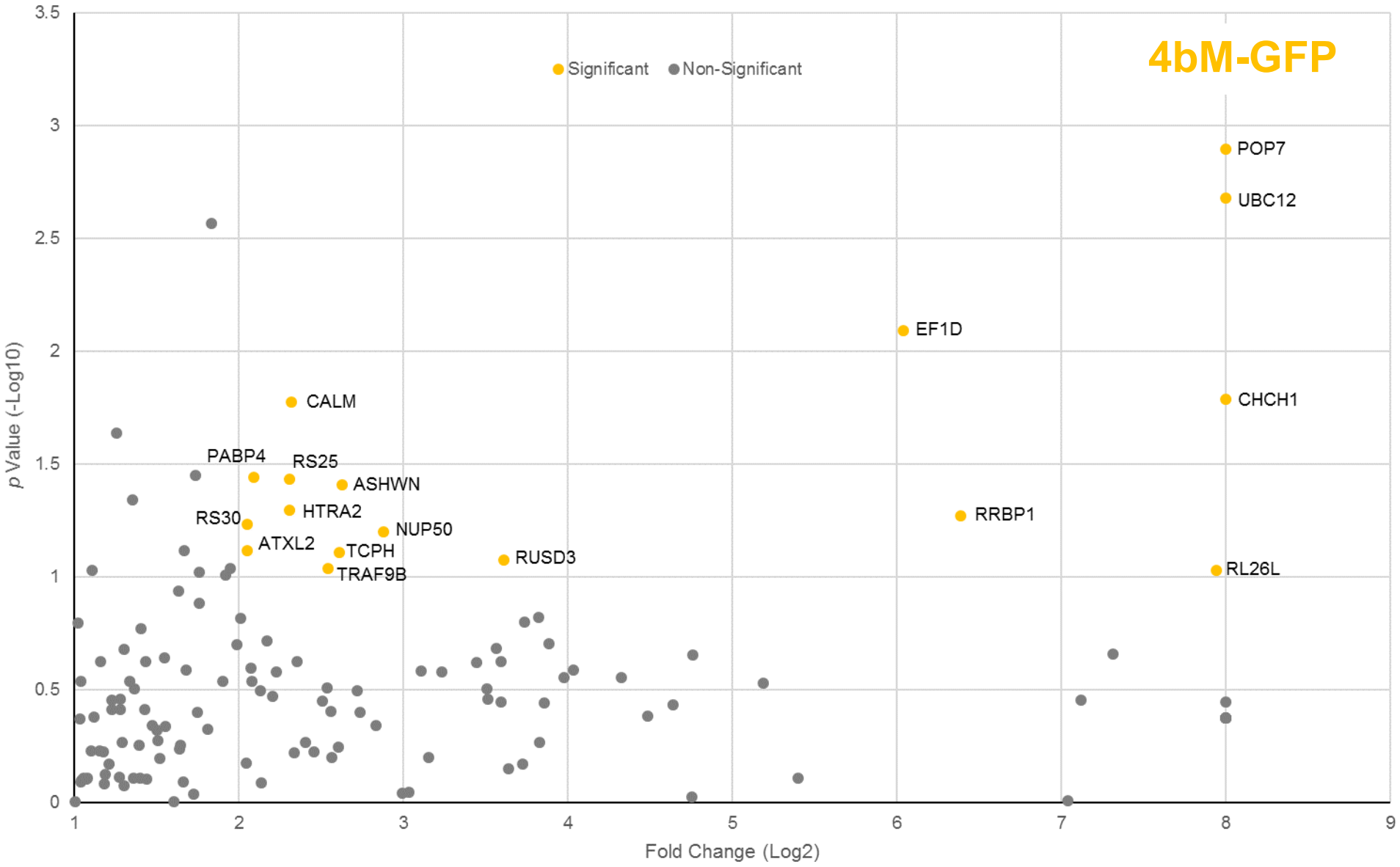
4bM-GFP
Significant
Non-Significant
p Value (-Log10)
Fold Change (Log2)
3.5
3
2.5
2
1.5
1
0.5
0
1
2
3
4
5
6
7
8
9
POP7
UBC12
EF1D
CHCH1
CALM
PABP4
RS25
ASHWN
HTRA2
RS30
NUP50
ATXL2
TCPH
TRAF9B
RUSD3
RRBP1
RL26L

Figure 5.10 Scatter plot representing results from the 4bM-GFP co-IP.

Proteins were identified in the 4bM-GFP IP eluate by LC-MS/MS. Proteins are plotted by fold-change in abundance (Log10) compared to GFP alone and *p*-value (-Log10) of the *t*-test. Proteins with a *p*-value (-Log10) > 1 and a fold change (Log2) > 2 have the highest chance of interacting with 4b and are considered significant and are labelled (yellow). Results are representative of two biological replicates.

Table 5.5 Function and localisation of proteins classified as significant that interact with GFP-4bM and/or 4bM-GFP.

Protein ID	Protein	GFP-4bM	4bM-GFP	Function	Location
RRBP1*	Ribosome-binding protein 1	X	X	Protein processing in endoplasmic reticulum	Ribosome, Nucleus, Cytosol
EF1D*	Elongation factor 1-delta	X	X	Responsible for the enzymatic delivery of aminoacyl tRNAs to the ribosome, interacts with HIV Tat	Ribosome, Nucleus, Cytosol
RT18A	28S ribosomal protein S18a	X		Part of the 40S ribosome	Ribosome, Cytosol, Nucleus
RL40	Ubiquitin-60S ribosomal protein L40	X		Part of the 60S ribosome	Ribosome, Cytosol, Nucleus
POP7*	Ribonuclease P protein subunit p20	X	X	Component of ribonuclease P, component of RNase MRP complex	Ribosome, Nucleus
RRS1	Ribosome biogenesis regulatory protein	X		Ribosome regulatory protein	Ribosome, Cytosol, Nucleus
RL14	60S ribosomal protein L14	X		Part of the 60S ribosome	Ribosome, Cytosol, Nucleus
RPS25	40S ribosomal protein S25		X	Structural constituent of 40S ribosome	Nucleus, Cytosol
CHCH1*	Coiled-coil-helix-coiled-coil-helix domain-containing protein	X	X	Mitochondrial translation	Mitochondria, cytoplasm
RS30	40S ribosomal protein S30	X	X	Structural part of the 60S ribosome	Ribosome, Cytosol, Nucleus
RL26L	60S ribosomal protein L26-like 1		X	Component of the 60S ribosome	Ribosome, Cytosol, Nucleus
RM43	39S ribosomal protein L43	X		Part of the 40S ribosome	Ribosome, Cytosol, Nucleus
ATX2L*	Ataxin-2-like protein	X	X	Involved in the regulation of stress granule and P-body formation	Nucleus, Cytosol
LS14A	Protein LSM14	X		Stress granule and P-Body regulation	Cytosol, Nucleus

PABP4	Polyadenylate-binding protein 4		X	Binds the poly(A) tail of mRNA. Involved in stress granule regulation and mRNA processing	Ribosome, Nucleus, Cytosol
CALM	Calmodulin		X	Mediates the control of a large number of enzymes, ion channels, aquapobrins and other proteins by Ca(2+)	Plasma membrane, Cytoskeleton, Nucleus, Cytosol
UBC12	NEDD8-conjugating enzyme Ubc1		X	Accepts the ubiquitin-like protein NEDD8 from the UBA3-NAE1 E1 complex	Cytosol
ASHWN	Ashwin		X	tRNA processing and Gene Expression	Nucleus, Cytosol
HTRA2	Serine protease HTRA2		X	Promotes or induces cell death	Mitochondria, Nucleus, Cytosol, ER
TCPH	T-complex protein 1 subunit eta	X	X	Molecular chaperone; assists the folding of proteins upon ATP hydrolysis	Cytosol. Cytoskeleton
RUSD3	RNA pseudouridylate synthase domain-containing protein 3		X	poly(A) RNA binding and pseudouridine synthase activity	Nucleus
TAF9B	Transcription initiation factor TFIID subunit 9B		X	Involved in transcriptional activation	Nucleus
NUP50	Nuclear pore complex protein Nup50	X	X	Component of the nuclear pore complex that has a direct role in nuclear protein import	Nucleus, Nuclear Envelope
PRDX2	Peroxiredoxin-2	X		Involved in redox regulation of the cell	Cytosol

The function and localisation of significant proteins (FC Log2 > 2, p-value Log10 > 1) that interact with GFP-4bM and/or 4bM-GFP.

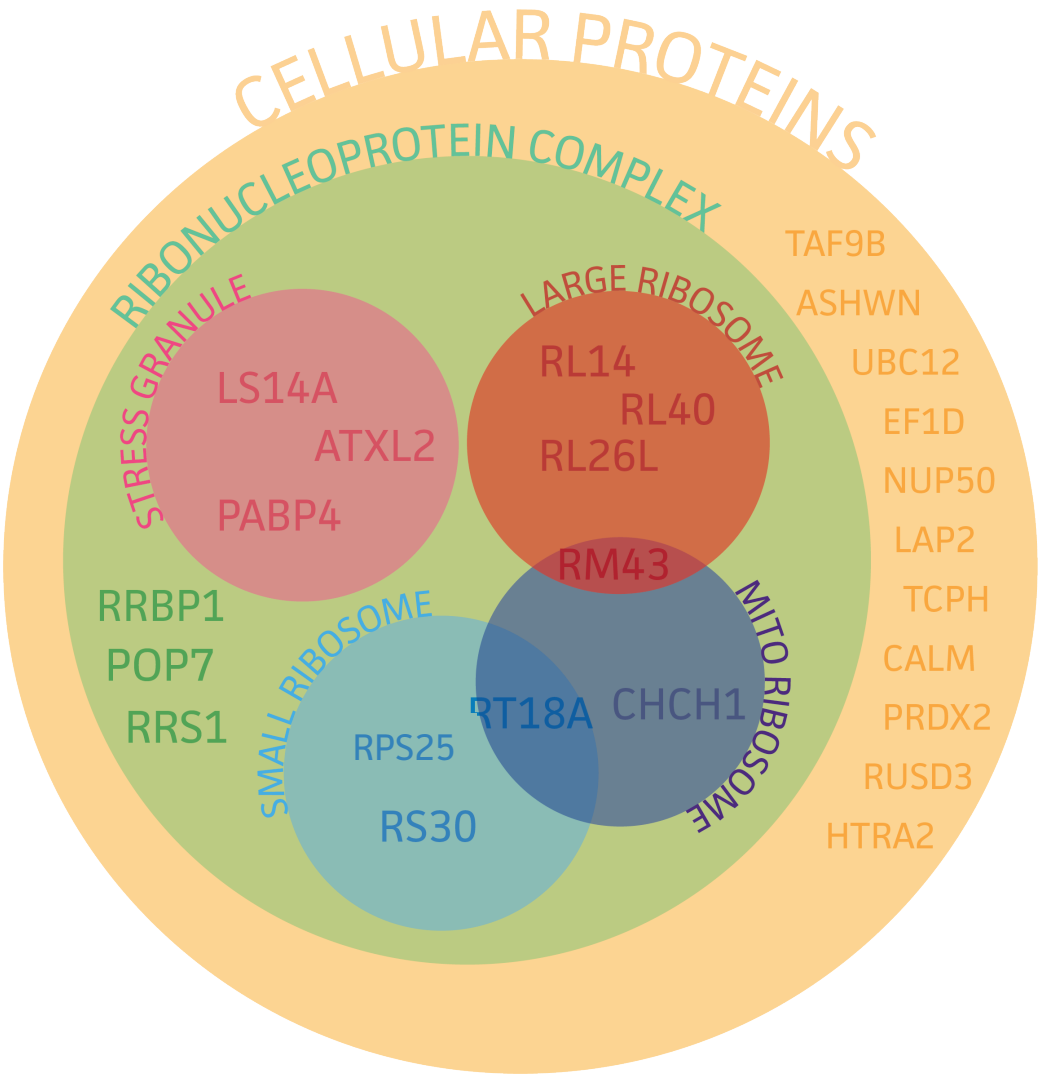

Figure 5.11 IBV 4b interacts with a higher proportion of ribonucleoproteins. Significant interacting partners identified for GFP-tagged 4bM by LC-MS/MS were analysed by a panther over-representation test (pantherdb.org). Proteins which localise to cellular components that are over-represented in the data set ($p < 0.05$) were collated and shown as a Venn diagram.

5.7. IBV 4b interaction with RPS25 and LAP2

Localisation of 4b and cellular proteins were visualised to validate the 4b mass spectrometry data. RPS25 was a significant interaction for 4bM-GFP and was chosen as the candidate ribosomal protein as it is highly conserved, increasing the chance of labelling RPS25 in avian cells. Lamina polypeptide 2 (LAP2) is a nuclear envelope protein and was chosen as the candidate nuclear protein from the mass spectrometry data. DF-1 cells were first transfected with 4bM-GFP and GFP expression vectors, and after 24 hours, cells were fixed, permeabilised and labelled with anti-RPS25 and anti-LAP2. Both LAP2 and RPS25 were shown to partially colocalise with 4bM-GFP (**Figure 5.12, Figure 5.13**). Colocalisation studies allude to an interaction between 4b and RPS25 and LAP2, to further validate this observation a co-IP was performed. CK cells were infected with M41-CK at an MOI above 4 or mock infected. After 24 hours cells were lysed. Cell lysates were incubated with anti-4b overnight and then incubated with magnetic protein G beads for 4 hours. Beads were separated and washed three times with co-IP wash buffer, and protein-antibody complexes eluted from the beads using acidic glycine. A mock antibody sample was used to confirm specific pull-down of 4b. The input and eluate samples were separated by SDS-PAGE, transferred to a membrane and labelled with anti-RPS25 and anti-4b. The analysis confirmed successful immunoprecipitation of 4b from M41-CK infected cells (**Figure 5.14A**). Furthermore, RPS25 was also detectable in the 4b eluate but not detectable in the mock infected cells (**Figure 5.14B**). This result confirms that 4b could interact with the small ribosomal protein S25 during M41 infection.

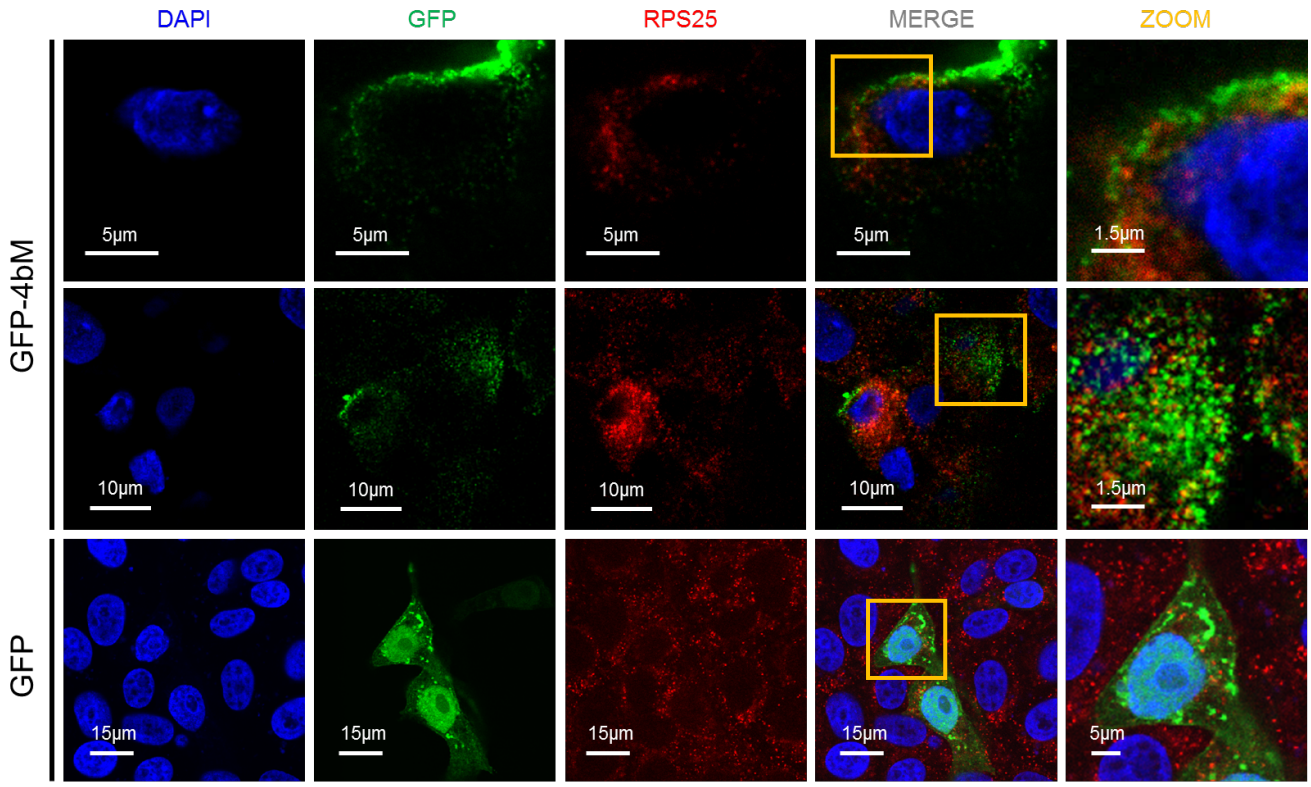

Figure 5.12 RPS25 partially colocalises with GFP-tagged 4b.

DF-1 cells were transfected with GFP-tagged 4b expression vectors for 16 hours. Cells were fixed, permeabilised and labelled with anti-RPS25. Yellow boxes indicate enlarged areas. Cells were visualised by confocal microscopy.

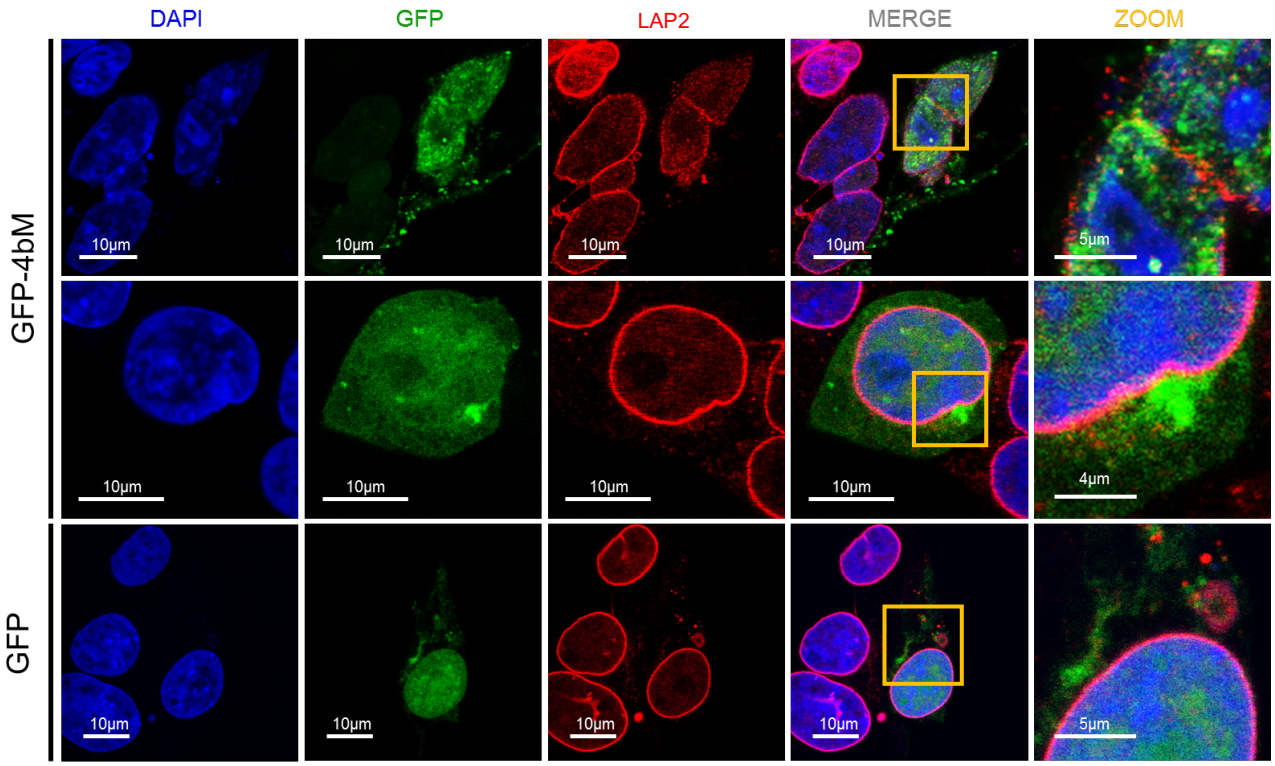

Figure 5.13 LAP2 partially colocalises with GFP-tagged 4b.

DF-1 cells were transfected with GFP-tagged 4b expression vectors for 16 hours. Cells were fixed, permeabilised, and labelled with anti-LAP2. Yellow boxes indicate enlarged areas. Cells were visualised by confocal microscopy.

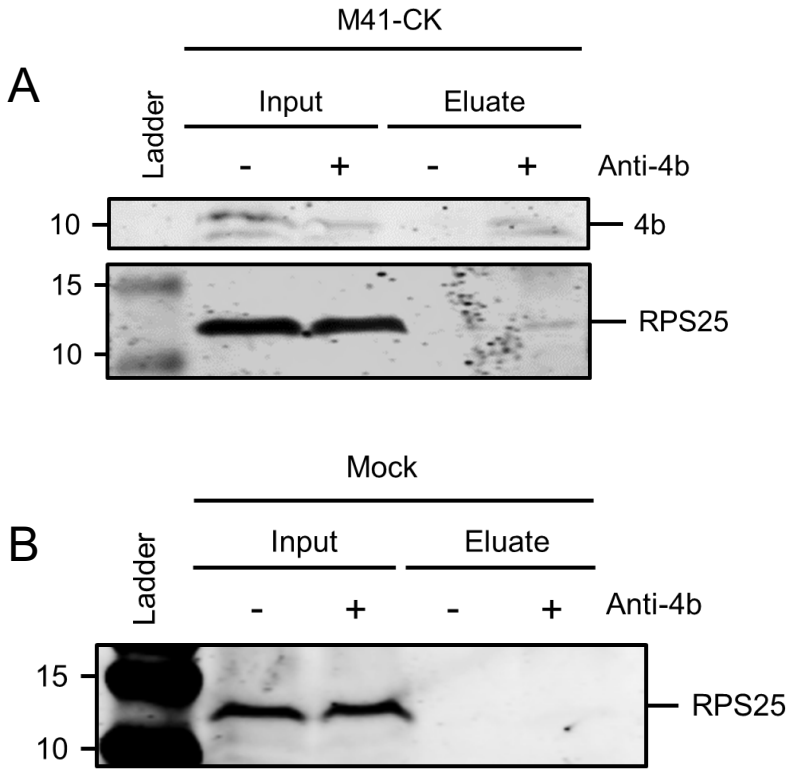

Figure 5.14 RPS25 interacts with 4b during M41-CK infection.

CK cells were (A) infected with M41-CK or (B) mock infected. After 24 hours, cells were lysed and incubated with anti-4b or mock incubated as indicated. Samples were then incubated with antibody capture beads. Beads were removed, washed and protein-antibody complexes eluted. Input and eluate samples were analysed by western blot and labelled with anti-4b or anti-RPS25.

5.8. Effect of 4b on stress granule assembly

Mass spectrometry data identified that GFP-tagged 4bM interacts with a high proportion of ribosomal and stress granule/p-body proteins (**Figure 5.11**). IBV has previously been shown to induce stress granule formation in a proportion of infected cells (Kint 2015). To confirm this, Vero cells were infected with Beau-R, M41K-BeauR(S) or mock infected. After 24 hours, cells were fixed, permeabilised and labelled with anti-G3BP1 and anti-dsRNA. Cells were labelled with anti-G3BP1, a stress granule regulatory protein that localises to stress granules during stress (Matsuki et al. 2013). Mock infected cells were not positive for stress granules as opposed to dsRNA positive cells, which contained noticeable more G3BP1 puncta (**Figure 5.15**). This result confirms that Beau-R induces stress granule assembly during infection and that M41-K in Vero cells can also induce stress granule assembly.

To determine if 4b can alone induce stress granule formation, Vero cells were transfected with either GFP-4bM or GFP expression vectors, and after 16 hours were fixed, permeabilised and labelled with anti-G3BP1. Sodium arsenite treatment induce oxidative stress and stress granule formation and was used as a positive control for induction and labelling stress granules. For each sample, 20 GFP positive cells were randomly selected and the number of stress granule positive cells counted. The results are representative of three biological repeats. Significantly more GFP-4bM expressing cells contained stress granules compared to GFP expressing cells (**Figure 5.16B,D**). This result suggests 4b

expression alone induces stress granule formation. Furthermore, GFP-4bM signal colocalised with G3BP1 signal (**Figure 5.16A,C**), suggesting 4b is targeted to these stress granules.

Beau-R 4b is truncated and lacks the C-terminal end present in 4bM. To determine if 4b from Beau-R can also induce stress granule formation, Vero cells were transfected with either GFP-4bB or GFP expression vectors for 16 hours. Cells were then fixed, permeabilised and labelled with anti-G3BP1. For each sample, 20 GFP positive cells were randomly selected and the number of stress granule positive cells counted. The results are representative of three biological replicates. Significantly more GFP-4bB expressing cells contained stress granules compared to GFP expressing cells (**Figure 5.16A,C**), indicating that both M41-CK and Beau-R 4b induce stress granule assembly.

Previous work has shown that IBV can inhibit sodium arsenite-induced stress granule assembly (Kint 2015). To determine if 4b is responsible for this effect, Vero cells were transfected with GFP-4bM or GFP expression vector, for 18 hours. Cells were treated with sodium arsenite for one hour before fixing. Cells were fixed, permeabilised and labelled with anti-G3BP1. Expression of GFP-4bM failed to inhibit sodium arsenite-induced stress granule assembly, indicating 4bM is not responsible for this previously observed effect (**Figure 5.17**). Interestingly, GFP-4bM did not localise with sodium arsenite-induced stress granules, as seen with GFP-4bM-induced stress granules. Collectively, these results demonstrate that

4b expression alone can induce and colocalise with stress granule but cannot inhibit or colocalise with sodium arsenite-induced stress granules.

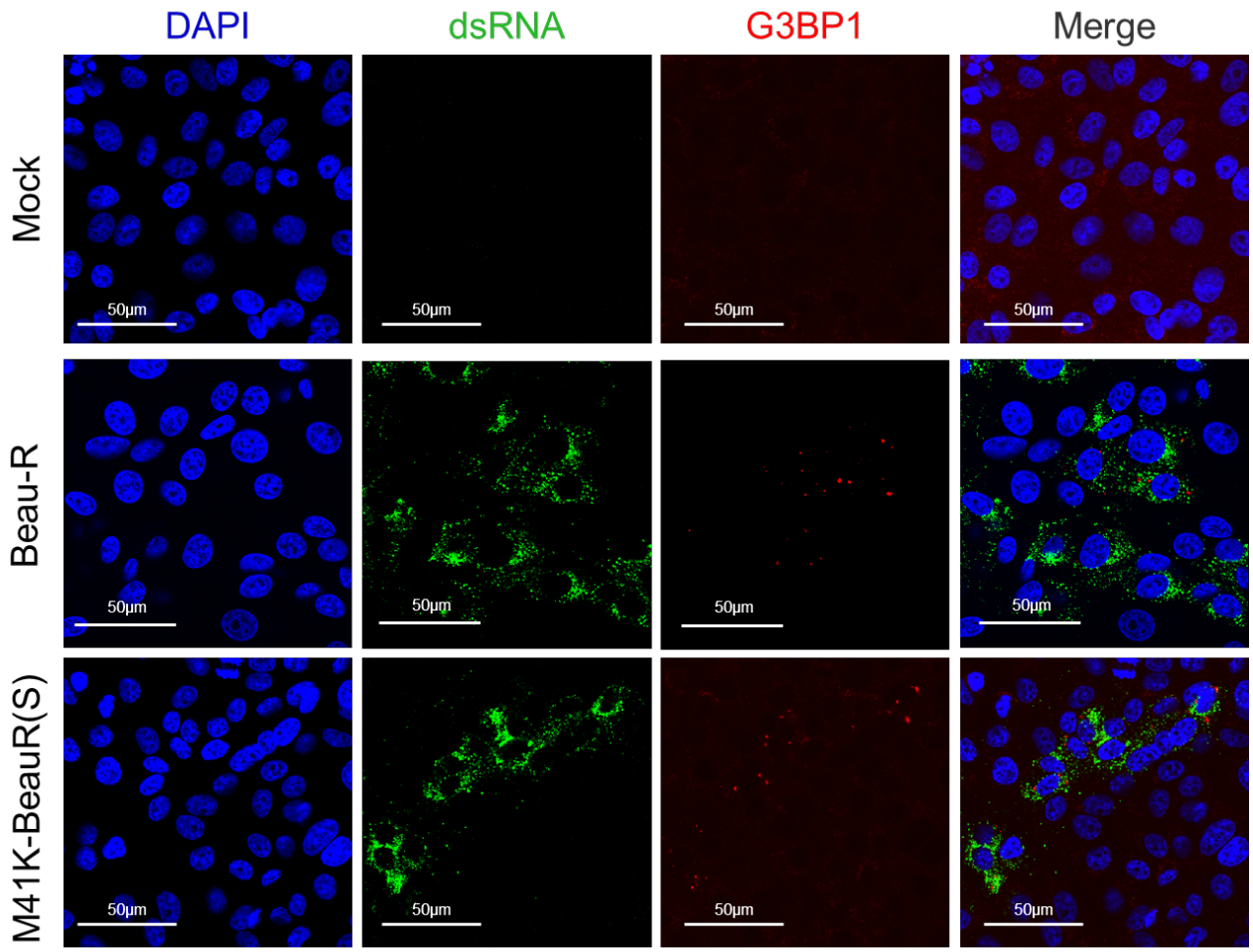

Figure 5.15 IBV induces stress granule assembly.

Vero cells were infected with Beau-R, M41K-BeauR(S) or mock infected. After 24 hours, cells were fixed, permeabilised and labelled with anti-dsRNA, anti-G3BP1. The nucleus was stained with DAPI.

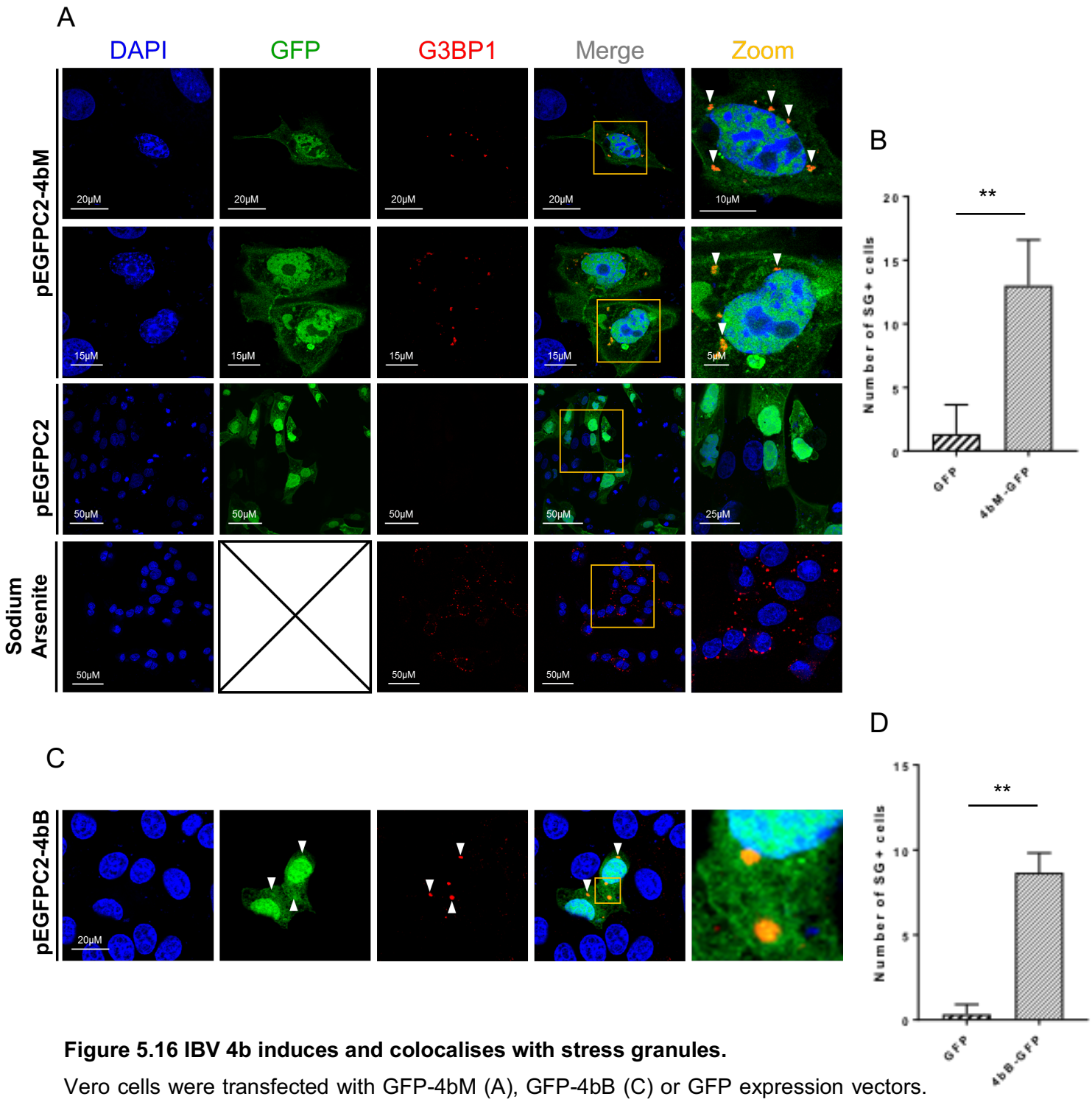

Figure 5.16 IBV 4b induces and colocalises with stress granules.

Vero cells were transfected with GFP-4bM (A), GFP-4bB (C) or GFP expression vectors. After 24 hours, cells were fixed, permeabilised and labelled with anti-G3BP1. For each transfection, 20 GFP-4bM (B), GFP-4bB (D) or GFP expressing cells were counted for the presence of stress granules as labelled with anti-G3BP1. The results are representative of three biological replicates. White arrows indicate stress granules that colocalise with GFP-tagged 4b expression. ** significant $p < 0.01$.

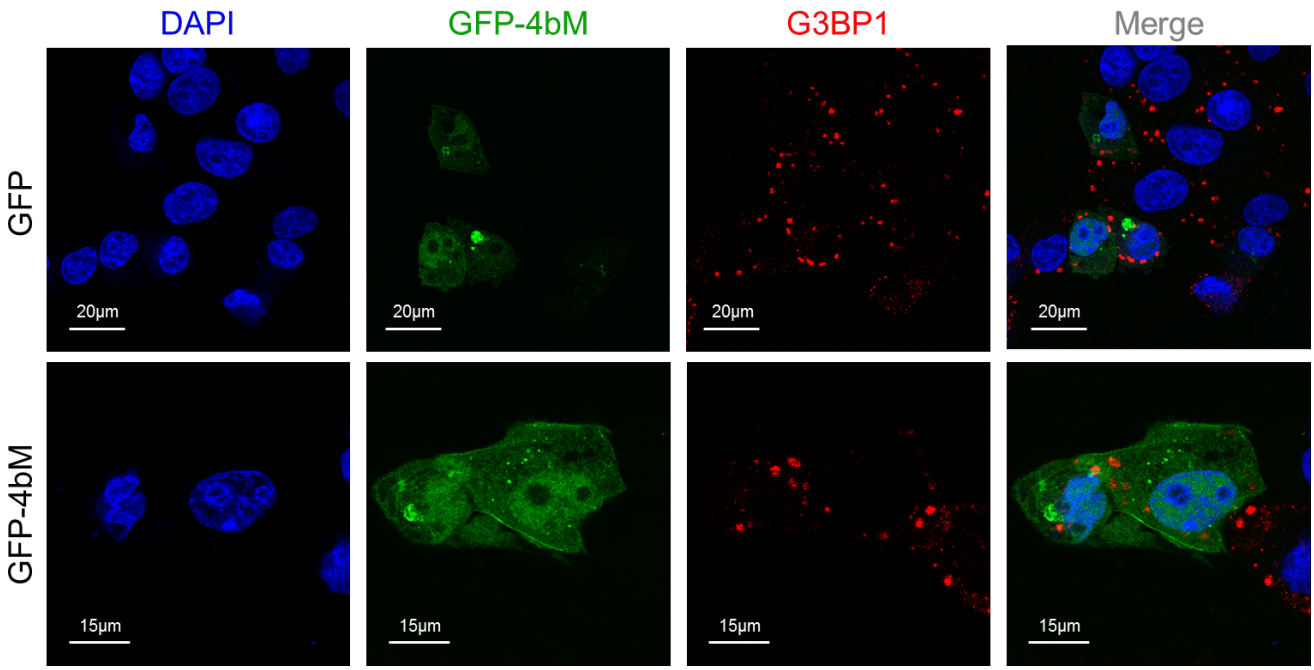

Figure 5.17 GFP-4bM does not colocalise or inhibit sodium arsenite-induced stress granules.

Vero cells were transfected with pEGFPC2-4b or pEGFPC2. Vero cells were treated with sodium arsenite for 1 hour before fixing. After 18 hours, cells were fixed and labelled with anti-G3BP1. The nucleus was stained with DAPI.

5.9. Effect of 4b on cellular translation

IBV 4b induces stress granule formation when overexpressed in Vero cells. Stress granules are formed by aggregation of stalled translation initiation complexes (Beckham et al. 2008). For this reason, the effect of GFP-4bM/GFP-4bB expression on cellular translation was measured. DF-1 cells were transfected with increasing levels of GFP-4bM or GFP-4bB expression vector, made up to 2 µg with pEGFPC2, along with a Renilla luciferase expression vector. A plasmid expressing NS1 (IAV-PR8) was transfected as a positive control, NS1 has been shown to enhance cellular translation, through eIF2α phosphorylation (Lu et al. 1995, Salvatore et al. 2002). After 16 hours, cells were lysed, and Renilla luciferase activity measured as a proxy for the cellular translational rate. Expression of GFP-4bM or GFP-4bB had a dose-dependent effect on Renilla luciferase expression with increasing levels of 4b resulting in higher levels of Renilla luciferase expression. This result suggests that 4b expression increased cellular translation (**Figure 5.18**).

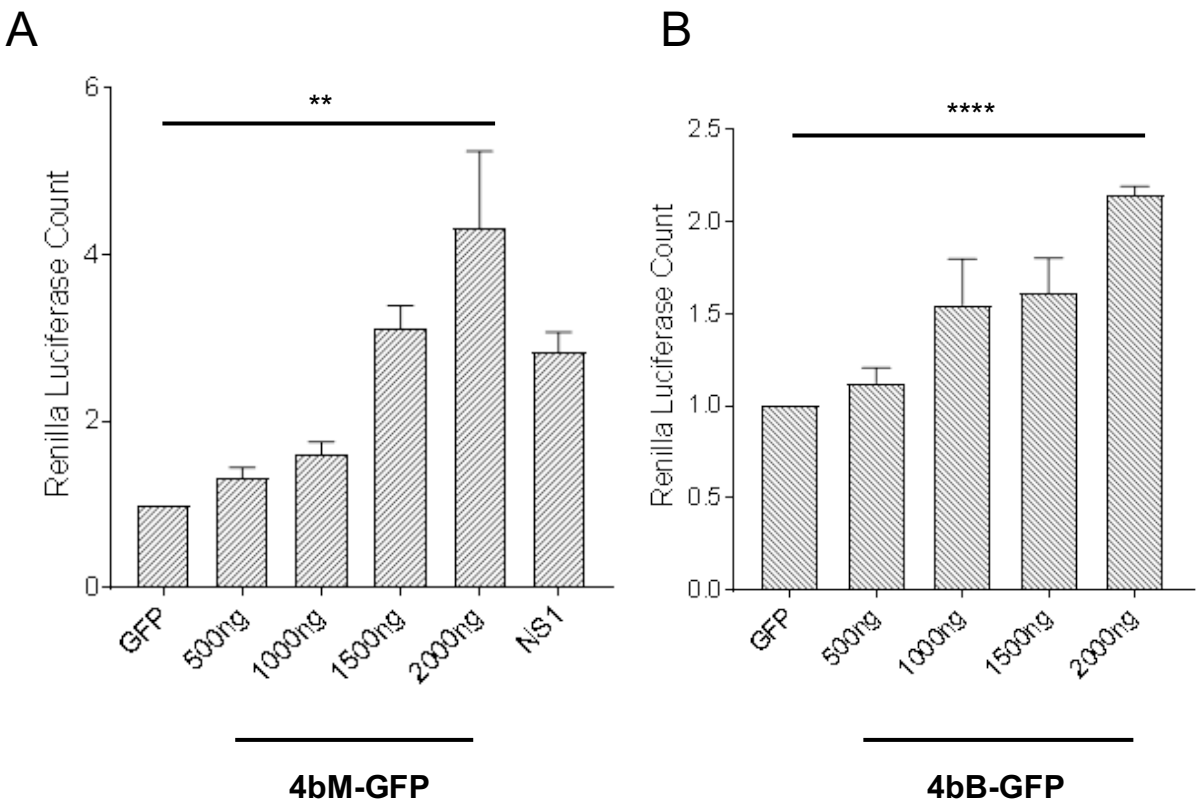

Figure 5.18 IBV 4b increases cellular translation.

DF-1 cells were transfected with increasing levels of GFP-4bM expression, made up with the GFP-4bB expression vector to 2 μg. Cells were also transfected with a Renilla luciferase expression vector. After 16 hours cells were lysed and Renilla luciferase activity measured. Results are shown as fold-change compared to the GFP control. ** significant $p < 0.01$, **** significant $p < 0.0005$.

5.10. Role of RVxF and SILK on 4b function

Bioinformatic analysis of the 4b peptide sequence identified two domains; RVxF and SILK, in the highly conserved N-terminal end (**Table 5.2**). Individually these domains mediate PP1c binding but together provide higher affinity binding to PP1c (Hendrickx et al. 2009). PP1c is a multi-functional protein involved in dephosphorylation of a range of signalling proteins including the translational

regulatory protein, eIF2α and PKR (Garcia-Bonilla et al. 2007). The cell can respond to infection by phosphorylating eIF2α and PKR, to limit cellular translation and thus inhibit viral replication (Dauber et al. 2009). To determine the significance of these motifs on the function of 4bB, the RVxF and SILK motifs were deleted both individually and together in the 4b expression vectors by site-directed mutagenesis. Mutagenesis only succeeded for the 4bB vector and due to time constraints was not repeated with the 4bM vector. Vero cells were transfected with either GFP, 4bB-GFP, 4bBGFP-delSILK, 4bBGFP-delRVxF or 4bBGFP-delSILK/RVxF expression vectors along with a Renilla luciferase expression vector. After 16 hours, cells were lysed, Renilla luciferase expression measured and plotted as fold-change compared to the GFP control (**Figure 5.19A**). Expression levels of each protein were quantified by western blot to ensure consistent levels of expression. Lysed cells were separated by SDS-PAGE, transferred to a membrane and labelled with anti-GFP (**Figure 5.19B**). Deletion of SILK, RVxF or both abrogated the effect of 4bB on increased Renilla luciferase expression. This preliminary result suggests that these motifs, are in part, responsible for the effect of 4bB on increased rates of cellular translation.

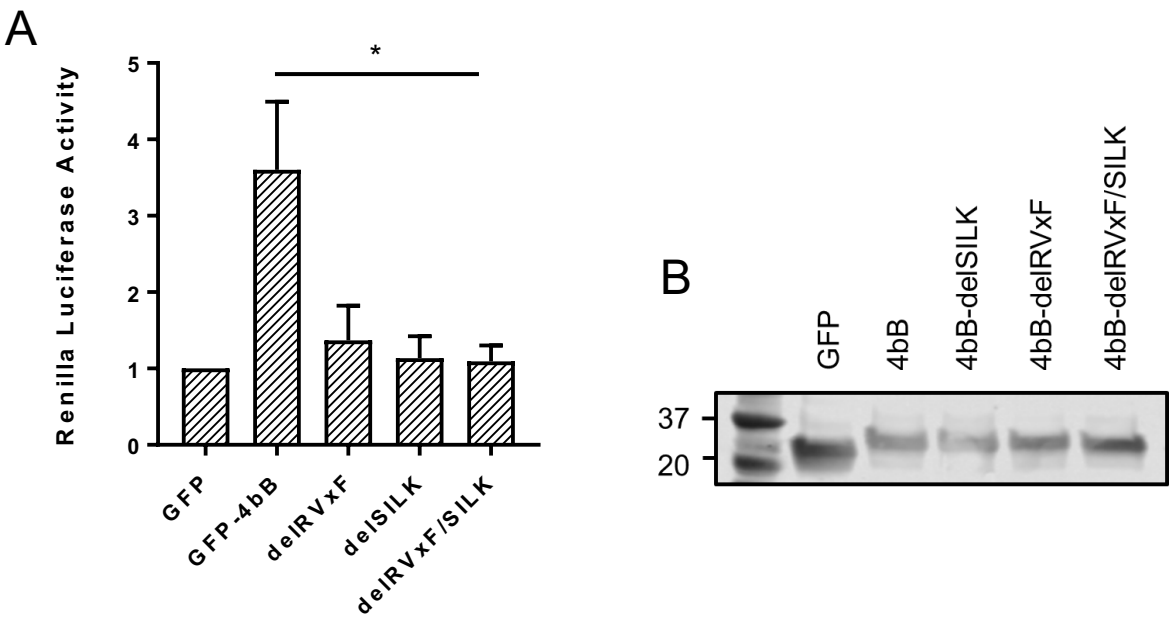

Figure 5.19 Protein 4b effect on cellular translation is dependent on SILK and/or RVxF.

(A) Vero cells were transfected with GFP-4bB, GFP4bB-delRVxF, GFP4bB-delSILK, GFP4bB-delRVxF/SILK or GFP expression vectors. After 16 hours, cells were lysed, and Renilla luciferase activity measured. (B) Lysed cells were separated by SDS-PAGE, transferred to a membrane and labelled with anti-GFP. *significance $p < 0.05$.

5.11. Discussion

Bioinformatic analysis of the IBV and TCoV strain database showed that 78% of strains contain ORF4b as well as the upstream non-canonical TRS (**Table** 5.1). Sequence conservation is lower compared to the other accessory proteins (Britton 2007). However, the strains with ORF4b have a sequence similarity of 81%, which is as high as the most conserved accessory protein, 3a (Britton et al. 2006, Britton 2007). RNA viruses tend not to express unessential sgRNA/ proteins, so although not all strains have ORF4b and because it is highly conserved when present, this suggests an essential role for this protein. The TRS for ORF4b (CAA) is also highly conserved, possibly suggesting an important role for the non-canonical TRS and the low expression levels of 4b. Sequence alignment identified a range of 4b isoforms, with truncations at the C-terminal end (**Figure 5.1**). The most common 4b isoform was 94 amino acids long, with 69% of IBV/TCoV strains encoding this length, including M41-CK and QX. The apathogenic lab strain, Beau-R, encodes a truncated form of 4b which is only 50 amino acids. Beau-R was the only strain with the truncated50 4b isoform, although two field strains encode a smaller 4b isoform at 40 amino acids.

ORF4b was previously thought to be a pseudogene. Bentley *et al.* (2013) showed; through northern blotting, that ORF4b is transcribed during infection and further concluded that the non-canonical TRS upstream of ORF4b is responsible for regulating transcription (Bentley et al. 2013). Furthermore, they showed that insertion of a GFP gene in place of ORF4b resulted in transcription and translation

of GFP (Bentley et al. 2013), suggesting the sgRNA produced by IBV can lead to the expression of a protein. Nonetheless, it was not known if transcript 4b was translated during infection. Utilising an antibody raised against the predicted 4b peptide sequence, 4b transcript translation has been confirmed and 4b protein is detectable during infection (**Figure 5.5**)**.** Anti-4b can only be used to detect 4b during M41-CK infection, as the antibody was raised against a C-terminal epitope not present in Beau-R 4b. Therefore, it has not been possible to verify that Beau-R 4b is also translated. Although truncated, Beau-R 4b is only 50 amino acids, IBV accessory protein 3a, which is similar in size is translated, suggesting Beau-R could express the smaller isoform of 4b too (Britton et al. 2006). Nonetheless, confirmation of Beau-R 4b expression is still required to say that Beau-R also expresses 4b definitively. It has been confirmed with viral growth curves comparing M41-CK, M41-K, and two rIBV-M41-K lacking ORF4b that 4b is an accessory protein (**Figure 5.7**). M41-K and both M41K-del4b viral isolates grew to similar titres suggesting this protein is dispensable for *in vitro* replication and is thus the fifth accessory protein to be identified for IBV.

Mass spectrometry was utilised to identify any cellular proteins that may interact with 4b. For this assay, HEK-293T cells were transfected with GFP-4bM or 4b-GFPM expression vectors along with a GFP control. LC-MS/MS was used to identify cellular proteins that were co-immunoprecipitated in the GFP and 4b-GFP/GFP-4b eluate. Due to the incomplete characterisation of the chicken genome, this assay was performed in HEK-293T cells; a human cell line as

opposed to a more relevant chicken cell line. Performing the assay in a human cell line increased the chance of characterising the cellular proteins by mass spectrometry but due to the differences in chicken and human cell biology may affect the interacting partners identified for 4b. Furthermore, these IPs were performed using transfected cells overexpressing 4b as opposed to M41-CK infected cells, further impacting interpretation of these results. To minimise the effect of the GFP-tag on 4b cellular interactions, 4b was tagged at either the N- or C- terminus, this increased the likelihood of detecting cellular proteins that interact with the C- or N- terminus of 4b, respectively. Furthermore, a GFP control was used to remove proteins that interact with the GFP-tag rather than 4b from the mass spectrometry data. M41-CK 4b was used for the GFP co-IPs, as M41-CK is a pathogenic strain and contains the full-length 4b sequence, as opposed to Beau-R. In the future, it would be interesting to perform GFP-tagged 4bB co-IPs to determine if Beau-R 4b interacts with similar cellular proteins. Furthermore, it may also be used to identify cellular proteins that specifically interact with the C- terminus of 4bM. As Beau-R is apathogenic and M41-CK is pathogenic, this could have implications for the role of the full-length 4b in pathogenicity.

In total 154 unique proteins were identified in higher amounts in GFP-tagged 4b IPs compared to the GFP control, with 72 appearing in both GFP-4bM and 4bM-GFP eluates (**Appendix Table 7.4, 7.5**). In total 23 proteins were identified as significant for either GFP-4b and/or 4b-GFP, with eight of these detected in both GFP-4b and 4b-GFP eluates (**Table** 5.5). The IP was repeated three times to

determine the significance of the data. For an unknown reason, the third replicate failed to align with the first and second replicate (**Appendix Table 7.4, 7.5**), with a higher proportion of cellular proteins detected, 197 for GFP-4bM and 180 for 4bM-GFP, with only 65 and 73 of these proteins appearing in the first two replicates, respectively. A higher yield of proteins could have occurred due to a more efficient transfection rate or a less stringent wash step during the co-IP, although there was no discernible difference in 4b volume in the third eluate compared to the first two (**Figure 5.8**). Nonetheless, 90% and 82% of proteins identified in the first two GFP-4bM and 4bM-GFP replicates did appear in the third, suggesting the data is reliable if not comparable. While repeats are an essential tool to determine the significance of the mass spectrometry data, the decision was made to validate the data from replicate one and two by co-IP and immunofluorescence to save time and cost. A high proportion of proteins identified were ribosomal and are involved in both translation and stress granule assembly (**Table** 5.5). Cellular translation machinery is highly conserved among eukaryotes (Sonenberg et al. 2009), reducing the risk that proteins identified as interacting partners are artefacts for 4bM. Ribosomal proteins regularly appear in mass spectrometry data and can be considered a background contaminant, therefore to validate 4b interacts with the ribosome, RPS25 was studied first (Mellacheruvu et al. 2013). RPS25 was a highly significant protein in the mass spectrometry data and has a high sequence similarity between the chicken and human isoforms. RPS25 is a ribosomal protein which has been shown to mediate cellular IRES expression and has previously been shown to play a role in viral translation during

Hepatitis C virus, poliovirus and adenovirus replication (Hertz et al. 2013). Furthermore, knockout of this protein had minimal effect on global cellular translation during homeostasis leading to the suggestion that RPS25 plays a role in viral translation (Landry et al. 2009). Immunofluorescence confirmed that GFP-4bM colocalises with RPS25 in DF-1 cells (**Figure 5.12**). Furthermore, co-IP of 4b from M41-CK infected CK cells also confirms that 4bM interacts with RPS25 during infection (**Figure 5.14**). Detection of RPS25 in the 4b co-IP further validates the mass spectrometry data and suggests a role for 4b in translation. RPS25 is a ribosomal protein but can also be present in stress granules as part of the stalled 40S ribosome complex (Kedersha et al. 2016). Three stress granule regulatory proteins were also identified by mass spectrometry including, LS14A, ATXL2, and PABP4. LS14A is present in p-bodies and stress granules and may have a role in shuttling mRNAs between the two structures (Yang et al. 2006). ATXL2 is a regulator of both p-bodies and stress granules while PABP4 relocates from the cytoplasm to stress granules during cellular stress (Kaehler et al. 2012) (Burgess et al. 2011). Expression of GFP-4bM alone induced stress granules in Vero cells; this was not seen with GFP expression (**Figure 5.16A,C**). Furthermore, GFP-4bM colocalised with these stress granules. The same effect was seen with GFP-4bB (**Figure 5.16B,D**). Stress granules are present during Beau-R and M41-K infection (**Figure 5.15**), and it has been previously shown that IBV also expresses a protein that can inhibit sodium arsenite-induced stress granule formation (Kint 2015). Overexpression of 4b failed to inhibit sodium arsenite-induced stress granules, suggesting 4b is not responsible for this previously

observed phenotype (**Figure 5.17**). As 4b can induce stress granules, it was assumed that 4b would also inhibit cellular translation, as stress granules are translationally silent (Buchan et al. 2009). Renilla luciferase expression, a proxy for gene expression and cellular translation, was measured in the presence of GFP-4bM or GFP-4bB. Interestingly, IBV 4b increased Renilla luciferase expression in a dose-dependent manner, suggesting 4b increased gene expression (**Figure 5.18**). This result implies that 4b-induced stress granules may not be canonical and may not have a role in arresting cellular translation. Alternatively, these stress granules may be a cellular response as the cell aims to curtail increased translation to preserve resources and energy (Kedersha et al. 2005). This theory is further supported by the fact that not all GFP-4b expressing cells were positive for stress granules, suggesting a possible dose-dependent effect on stress granule assembly (**Figure 5.16**). Stress granules are separated into sub-families representing their structural and functional diversity. While stress granules play a role in the silencing and storing of mRNAs, they are not required by themselves for global translational repression (Mokas et al. 2009). Thus, the role of stress granules cannot be simplistically categorised. Indeed, stress granules can represent focal points for a range of signalling pathways, including interferon and apoptosis signalling (Kedersha et al. 2013). While many viruses encode proteins to inhibit stress granule assembly, other viruses have been shown to modulate stress granules for their benefit. Indeed, stress granules are present throughout the life-cycle of respiratory syncytial virus (RSV) infection and appear beneficial for the virus, with knockdown of G3BP1 and stress granule

assembly causing a reduction in RSV translation (Lindquist et al. 2010). Vaccinia virus has been shown to co-opt canonical stress granule assembly into novel aggregates that lack silenced cellular mRNAs (Simpson-Holley et al. 2011). Furthermore, HCV recruits stress granule proteins such as G3BP1 and ataxin-2 to replication factories, which resemble stress granules but are indeed replication sites (Ariumi et al. 2011). Thus, the assembly of stress granules during infection cannot be suggested as solely negative for the virus. Future work should aim to categorise stress granule composition during IBV infection, and to determine if they have a beneficial or detrimental effect on viral replication.

The observation that both 4b from M41-CK and Beau-R can induce and colocalise with stress granules and can increase cellular translation suggests that the domains required for this effect are in the N-terminal end of 4b (**Figure 5.16B, D**). Beau-R and M41-CK are lab strains which have been passaged extensively and are thus highly cell culture adapted viruses. Beau-CK was first isolated in 1937 and has been passaged considerably more compared to M41-CK (Beaudette 1937, Cunningham et al. 1947). A high passage number could explain the acquisition of a C-terminal truncation in Beau-R 4b. This observation has been suggested before as the reason why lab strains of HCoV-229E have a truncated isoform of protein 4, while clinical strains do not, and could suggest that the C-terminal end of IBV 4b is not required for *in vitro* function (Farsani et al. 2012). This is further supported by the sequence identity of 89% between the truncated50 and FL 4b isoforms. Indeed, sequence similarity is much higher at

the N-terminal end and more divergent at the C-terminal end between the 4b isoforms suggesting the N-terminal end performs an important function (**Figure 5.1**). This result could be further validated by deleting the C-terminal end of M41 4b, to determine if function remains. Further functional analysis could look at the truncated40 4b identified in 2 field strains or even delete C-terminal or N-terminal amino acids until a stress granule phenotype is no longer detectable.

Bioinformatic analysis of 4b failed to identify any transmembrane domains or signal peptides (data not shown). Although an ELM search of 4bM did identify two motifs in the highly-conserved N-terminus, which potentially relates to cellular translation and stress granule assembly, PP1c_RVxK and PP1c_SILK (**Table 5.2**). PP1c is the catalytic subunit of PP1, a ubiquitous protein that has a role in many cellular pathways including glycogen metabolism, cell cycle and cellular translation (Hartshorne et al. 2004, Mochida et al. 2012, Walsh et al. 2013). PP1 regulates these pathways by dephosphorylating cellular proteins and can reinitiate cellular translation by dephosphorylating eIF2α (Garcia-Bonilla et al. 2007). RVxF and SILK motif are regularly found together in cellular proteins, and while individually they can mediate binding to phosphatase protein 1c (PP1c), their presence together is thought to enhance this interaction (Hendrickx et al. 2009). They have no role in stimulation or inhibition of PP1c activity, and are thought to bind to PP1 to promote interaction with a secondary site (Wakula et al. 2003). The SILK motif (SILR) appears in 93% of 4b sequences, while RVxF appears in 93.7% of 4b appearing as either KLxF or RLxF. Nonetheless, PP1c

was not identified in any of the mass spectrometry data. This fact alone does not confirm that 4b cannot interact with PP1c as the interaction may be weak and/or transient. Furthermore, the 4b/PP1c interaction may be dependent on a cellular antiviral state. As the co-IP was performed with cells overexpressing GFP-tagged 4b, the PKR/eIF2α pathway would not be activated, and subsequent PP1 activity would be lower. If the mass spectrometry co-IP was repeated cells could be treated with the dsRNA analogue, poly(I:C), to induce an antiviral state and activate the PKR pathway. Alternatively, as anti-4b can immunoprecipitate 4b during infection (**Figure 5.14A**), infected cells could be used instead, although low levels of 4b may make this technically difficult. Interestingly, two PP1c interacting proteins were detected, eIF2α and PKR, although not significantly (**Appendix Table 7.5, 7.6**) (Szyszka et al. 1989, Garcia-Bonilla et al. 2007). During IBV infection, eIF2α phosphorylation is suppressed, which has been linked with increased GADD34 expression, a protein that interacts with PP1, through an RVxF domain, to dephosphorylate eIF2α (Wang et al. 2009). Furthermore, auto-phosphorylation of PKR is also suppressed during IBV infection; this has been linked, in part, with the activity of IBV nsp2 (Wang et al. 2009). The RVxF motif has been identified and is functionally important in accessory protein 7 of TGEV, which has been shown to mediate dephosphorylation of eIF2α (Cruz et al. 2011). Although PP1c was not identified in the 4b mass spectrometry data, the presence of these two motifs along with the incidence of RVxF in another coronavirus accessory protein means these motifs warrants further investigation. To determine the importance of RVxF and SILK on 4b function, these motifs were

deleted individually and collectively from 4bB. Deletion of these motifs together and individually abrogated the effect of 4bB on cellular translation (**Figure 5.19**). Interestingly, deletion of a single motif had a similar effect as deletion together. This result could suggest that 4b function is dependent on the presence of both motifs, although these motifs have been shown to function independently of each other, especially RVxF which is shown to mediate strong PP1c binding alone (Wakula et al. 2003, Hendrickx et al. 2009). Deletion of these motifs, especially in a relatively small protein, may have had a deleterious effect on 4b structure or effect neighbouring motifs that could affect the 4b function independent of SILK/RVxF presence. Future work should aim to mutate these motifs instead of deleting them (SILK > SAAA, RVxF > RKAGA) to abrogate PP1c protein interaction while aiming to maintain 4b structure (Hendrickx et al. 2009).

The non-canonical TRS is highly conserved for ORF4b (**Table** 5.1). The M41-K vaccinia reverse genetic system was used to mutate the ORF4b non-canonical TRS to a canonical TRS (canTRS4b-M41K) to investigate the importance of it. Due to time constraints, the rIBV was not generated. Nonetheless, the mutation has been successfully inserted into the M41-K genome within the vaccinia virus backbone (data not shown). Future work will aim to express M41K-canTRS4b from within the vaccinia virus backbone to generate this recombinant IBV. M41K-canTRS4b is expected to express 4b at a higher level compared to the wild-type virus (Bentley et al. 2013). Comparing viral growth levels between M41K-canTRS4b and wild-type M41-K will help to determine the effect of higher 4b

levels on viral replication. Deletion of 4b from M41-K did not affect viral replication (**Figure 5.7**), possibly suggesting that higher levels of 4b may not affect replication either. Nonetheless, the non-canonical TRS is highly conserved, possibly suggesting a requirement for lower levels of 4b expression (**Table** 5.1). TGEV accessory protein 7b, which also increases cellular translation during infection, has a deleterious effect on TGEV pathogenicity, possibly suggesting 4b may act similarly (Cruz et al. 2011). Therefore, there may be a requirement for lower levels of 4b, as higher levels may impact pathogenicity and negatively affect *in vivo* replication and/or transmission.

Protein 4b is the fifth accessory protein to be identified for IBV. Mass spectrometry data suggests 4b can interact with multiple parts of the cellular translational machinery, including but not limited to, ribosomes, PKR, stress granule and p-body regulatory proteins. The exact mechanism of how 4b increases cellular translation or induces stress granule assembly is not known but two motifs, which are highly conserved, SILK and RVxF, suggests this protein can interact with PP1c, a protein known to dephosphorylate PKR and eIF2α (Szyszka et al. 1989, Garcia-Bonilla et al. 2007). Future work should aim to confirm the effect of 4b on translation during infection and determine the exact mechanism of 4b interaction with stress granules, p-bodies, and translation.

6. Discussion

The first aim of this project was to identify host-cell interaction partners for IBV accessory proteins 3a and 3b that may allude to function. The second aim was to determine if sgRNA 4b is translated and detectable during infection, and if so, determine the role of this protein.

6.1. Accessory protein 3a

The cellular antiviral response offers a considerable barrier for viral replication. The continuing evolutionary arms race between coronavirus and host has generated a set of accessory proteins which play an increasingly multi-functional role in controlling and modulating cell signalling pathways. These host-cell interactions often have significant impacts on disease progression and outcome (Knodler et al. 2001). The role of coronavirus accessory proteins is diverse and complex, with almost constant research finding new avenues for how these proteins function. This is best represented by the most researched area of virus host-cell interaction, the IFN signalling pathway. The type I IFN response is crucial for the control of coronaviruses and offers a significant challenge to infection (Ireland et al. 2008, Li et al. 2010). Previous work has shown that IBV accessory proteins 3a, 3b, and 5b all play a role in modulating the IFN response (Kint et al. 2015, Kint et al. 2016). Here, using mass spectrometry and *in vitro* IFNβ assays, a mechanism of action for 3a is proposed, by which 3a modulates the levels of IFN signalling proteins, MAVS and IRF7, through interaction with the IFN regulatory proteins, RNF5 and CAND1. These interactions can, in part, explain

the dual effect of 3a on IFNβ signalling. Low levels of 3a has an agnostic effect on IFNβ expression while higher levels have an overall inhibitory effect. This is an interesting observation, and while cellular proteins such as LGP2 have been shown to have opposite effects on IFN expression depending on dose, this is the first instance of this phenotype in a viral protein (Rodriguez et al. 2014). This allows 3a to have a more dynamic relationship with IFNβ expression, wherein 3a can inhibit IFNβ expression during peak viral replication but can also stimulate IFNβ expression later in infection, possibly to prevent excessive host damage. It has been shown that the decrease in 3a levels 36 h.p.i coincides with increased IFNβ expression and that 3a is responsible for this. More work is still required to determine if this is due to the role of 3a in increasing levels of MAVS during infection. A proposed mechanism of action is that 3a can affect IFN signalling by interacting with the cellular proteins, RNF5 and CAND1. More work is required to link these interactions with increased or decreased IFN expression both *in vitro* and *in vivo*. Work here mainly focused on the IFN pathway, but 3a most likely has additional roles during infection, highlighted by the range of interacting partners identified in the mass spectrometry data. Future work would be encouraged to look at the other highly significant proteins identified, including FNDC3a, SUCGL2, and DAAF5, all which appear to play a role in pathways other than IFN expression. Alternatively, anti-3a; which can immunoprecipitate 3a from infected CK cells (data not shown), could be used to gather more relevant mass spectrometry data from virus infected cells. This would help to reduce false positives that may occur

in the current dataset. Future work should also focus on the effect of 3a in combination with 3b, which may also interact with a MAVS regulatory protein.

6.2. Accessory protein 3b

The role of IBV accessory protein 3b was a difficult protein to investigate. IBV 3b is quickly turned over in cells and can localise to two cellular compartments based on whether it is expressed in avian or mammalian cells (Pendleton et al. 2006). Mass spectrometry data suggested that 3b interacts with proteins that regulate mitochondrial membrane permeabilisation and thus may have a role in apoptosis. HEK-293T cells were used for the GFP co-IP to characterise and identify interacting partners for IBV accessory proteins. This cell line has limitations, as mammalian cell biology can differ from avian cells, potentially affecting the function of 3b. This limitation is most apparent for 3b, which when overexpressed in mammalian and chicken cells colocalises differently. Due to time constraints and the lack of a 3b antibody, these interactions were not confirmed by IP or immunofluorescence. Nonetheless, recombinant IBV that lack 3b induced less caspase-dependent apoptosis, suggesting 3b is involved in apoptosis in some manner, whether this response is a cellular or viral response is unknown. The apoptotic pathway is closely linked to the IFN pathway, with both cascades proceeding through the mitochondria (Barber 2001). Protein 3b has already been shown to antagonise IFN expression, which could lead to increased pro-apoptotic signalling (Kint et al. 2015) (Randall et al. 2008). Whether apoptosis is a consequence of inhibiting IFN expression or is actively induced by 3b is unknown

and warrants further investigation. The apoptosis assays established here should be used to qualify transient 3b apoptotic activity, this should include looking at 3b from different strains of IBV including a truncated form of 3b from a Beau-R strain. Future work should also investigate how 3b inhibits IFN expression and should utilise the chIFNβ-luciferase assay used for 3a to determine at which point 3b can affect the IFN cascade.

6.3. Accessory protein 4b

Sub-genomic RNA 4b was first identified by Bentley *et al.* and work completed here confirms that this sgRNA is translated into a detectable protein during infection and is referred to as 4b. Protein 4b is an 11 kDa protein and is the fifth accessory protein to be identified for IBV along with 3a, 3b, 5a, and 5b. Protein 4b interacts with cellular proteins which are involved in translation, as well as stress granule (SG) and p-body assembly. Previous work has shown that IBV can both induce SG assembly and inhibit sodium arsenite-induced SG assembly (Kint 2015). Whether these SGs inhibit viral replication and are indeed a cellular response to infection is unknown. IBV induced SGs do not disassemble when treated with cycloheximide, supporting the idea that these SGs are non-canonical (Kint 2015). Here we show that 4b can induce SG assembly when expressed alone, while simultaneously increasing rates of cellular translation. This result supports the idea that these SGs are non-canonical and may not be coupled with cellular translational arrest. Future work needs to determine the structural composition of these SGs and determine if they are indeed translationally silent.

Neither antibody targeting G3BP1 nor TIA-1 worked in avian cells, so future work should look at different SG antibodies for use in avian cells or focus on Beau-R which can replicate in Vero cells. Interestingly, the two viral proteins that have been shown to play a role in regulating cellular translation, 5b and 4b, were unable to inhibit sodium arsenite-induced SG formation, even though IBV can (Kint 2015). This suggests that another IBV viral protein may be responsible for inhibiting these canonical SGs during infection. To confirm this is the case for 4b, cells should be infected with M41K-del4b or BeauR-delIR and then treated with sodium arsenite to determine if IBV can still inhibit SG assembly as seen with 5b (Kint 2015). While IBV 5b has been shown to regulate cellular translation, there is no proposed mechanism of action. Furthermore, the interplay between how 4b and 5b function together is unknown, especially considering they appear to have opposite roles in regulating cellular translation (Kint 2015, Kint et al. 2016). Future work should also investigate the role of 4b in the assembly of p-bodies, as proteins that play a role in SG assembly, LS14A and ATXL2, also regulate p-body assembly (Yang et al. 2006, Kaehler et al. 2012). Previous work has shown that p-body assembly is modulated during IBV infection and may be responsible for decreased cellular mRNA decay seen during infection (Kint 2015).

Sub-genomic RNA 4b is expressed under the control of a non-canonical TRS (Bentley et al. 2013). This is the first sgRNA identified; which is regulated by a non-canonical TRS, that is translated into a detectable protein. This non-canonical TRS results in lower levels of sgRNA 4b than is expected for its genome

location and raises questions as to the role of this non-canonical TRS (van der Most et al. 1995). As this non-canonical TRS is highly conserved, it suggests there is a reason why 4b is expressed at lower levels, and that higher levels may not be beneficial for the virus. Work here has started to examine these questions by synthesising a recombinant M41-K virus containing a canonical TRS upstream of ORF4b (data not shown). Work should continue to generate this rIBV and examine the effect of increased 4b expression levels on replication and pathogenicity. The effect of this non-canonical TRS should be investigated in IBV and highlights the range of mechanisms coronaviruses could employ to regulate levels of sgRNA and protein during infection.

6.4. IBV accessory proteins

Current knowledge as to the role of coronavirus accessory proteins varies between genera, with SARS-CoV and MHV accessory proteins amongst the best characterised, and IBV amongst the least (Liu et al. 2014). Regardless, more functional and structural work is required across the board to determine the pathogenic significance of these small proteins. While the function of some coronavirus accessory proteins has been determined, this most likely represents just the tip of the iceberg. While small, these proteins are usually multi-functional. The best example of this is SARS 7a which so far has been shown to inhibit cellular translation, activate the MAPK signalling pathway, suppress cell cycle progression and induce apoptosis (Liu et al. 2014). The function of this accessory protein is still only partially understood and continues to be investigated. This

feature is common for coronavirus accessory proteins and implies that IBV accessory proteins 3a, 3b, and 4b most likely play multiple roles during infection too. Future work should look at the other interacting partners identified by mass spectrometry. Due to time constraints, these interacting partners were not investigated, but they could be used to identify additional functions for these accessory proteins. The mechanism of action for 5a or 5b has yet to be determined; future work would be encouraged to use mass spectrometry to investigate these accessory proteins further.

Results shown here have predominantly relied on using 3a, 3b, and 4b expression vectors. These vectors have helped to determine interacting partners for these proteins and potential mechanism of actions. Nonetheless, these observed results need to be validated in the context of viral infection to determine their clinical significance. This can be difficult as the roles of accessory proteins can often overlap. For example, 3a, 3b, and 5b all play a role in inhibiting IFN expression, with 3a also able to stimulate IFN expression (Kint et al. 2015, Kint et al. 2016), while 4b and 5b appear to have opposite effects on cellular translation. The function of these proteins needs to be compared in the context of other accessory proteins to gain a complete picture of the complex relationship between IBV and host. Deletion of TGEV, SARS-CoV, and MHV accessory proteins leads to attenuation of the virus in the host (Paul et al. 1997, de Haan et al. 2002, Zhao et al. 2009, Liu et al. 2014). Recombinant M41 viruses lacking 3a, 3b, or 4b should be used for *in vivo* experiments to determine their role in pathogenicity. This

experiment should be complemented with recombinant viruses lacking accessory proteins in different combinations and include 5a and 5b. Discerning the role of these accessory proteins during infection is further complicated by the fact that IBV potentially expresses more, as yet unidentified, accessory proteins. ORF4b was first identified in 1980, and it was not confirmed as a sgRNA until recently (Stern et al. 1980, Bentley et al. 2013). Here we have shown that 4b is translated and detectable during IBV infection. This ORF was believed not to encode a sgRNA as it lacked a canonical TRS, highlighting the potential for IBV to express additional sgRNA under the control of a non-canonical TRS or indeed alternative expression systems. Considering coronaviruses have the largest positive-sense RNA genome, the potential to encode additional accessory proteins is highly probable if not certain (Hussain et al. 2005, Han Di et al. 2017). Indeed, an additional sgRNA has recently been detected during Beau-R infection expressed from the 3′-end of the genome and referred to as sgRNA 7 (Keep *et al*, Unpublished). Whether this sgRNA is translated into a protein during infection is unknown as is the function of this putative protein. The full repertoire of IBV accessory proteins needs to be identified, and their function determined to gain a better understanding of how IBV causes infectious bronchitis in domestic fowl. While northern blotting has helped to identify both sgRNA 4b and 7 (Keep *et al*. Unpublished) (Bentley et al. 2013), future work should use the development of next-generation sequencing and RNA-seq to identify the full range of novel sgRNAs (Bentley et al. 2013) (Han Di et al. 2017).

While 3a, 3b, and 4b are highly conserved between M41-CK and Beau-R strains, there is the potential for them; in the context of infection, to function differently. Functional differences between accessory proteins may explain the differences seen in pathogenicity between Beau-R and M41-CK. Furthermore, while M41-CK is a pathogenic strain of IBV, it is still a lab-adapted strain and therefore is not a reliable reflection of a field strain of IBV. Although accessory proteins 3a and 3b are highly conserved between Beau-R and M41-CK, they are less conserved with the clinically important field strain, Qx. Qx and Qx-like IBV strains are highly pathogenic and were first isolated in 1998 in China (ShuShuang 1998). These strains cause severe nephrotoxicity and are the biggest risk to the poultry industry (Beato et al. 2005, Valastro et al. 2010). It is not known why Qx is highly pathogenic but could be due to the differences in accessory protein peptide sequences, which are lower at 80.9% and 61.9% for 3a and 3b, respectively. Another field strain, recently identified in Australia, contained a single unrelated X1 gene in place of 3a and 3b, and deletion of 5a altogether, the significance of these deletions is not known but does show the potential for IBV to mutate these accessory proteins in the field (Mardani et al. 2008). Future work should aim to repeat assays, established here, with a panel of accessory proteins from a range of IBV strains to determine the significance of these proteins in disease outcome. Alternatively, determining the functional conservation of these accessory proteins between IBV strains could make them more attractive as cross-protective targets for vaccines and/or therapies.

6.5. Implications for vaccine design and novel therapies

Currently, domestic fowl are vaccinated against IBV using inactivated and live attenuated viruses (Box et al. 1980). For the generation of attenuated vaccines, clinical field strains of IBV are isolated and attenuated by serially passaging them in embryonated eggs. This process aims to create a vaccine that strikes a balance between attenuation and immunogenicity. This requires a process of trial and error and therefore can be labour intensive, costly and will not necessarily confer protection against different IBV serotypes (Davelaar et al. 1984, Jordan 2017). Furthermore, there is a danger that these vaccines can revert to virulence when used *in vivo,* either through mutations or recombination with field strains (Hopkins et al. 1986). There is thus a growing need for vaccines which are rationally designed that are attenuated but maintain immunogenicity. This would require a better understanding of how to introduce attenuating mutations. This could include mutating or indeed deleting accessory protein ORFs, as has been adapted for the generation of feline infectious peritonitis virus (FIPV) attenuated vaccines (Haijema et al. 2004). Deletion of accessory proteins, compared to deletion of nsps or structural proteins, is better tolerated by coronaviruses as they are non-essential for replication and assembly (Cavanagh et al. 2007). Furthermore, these deletions are less likely to revert to a virulent state compared to mutations and are therefore considered a safer way to prevent viral reversions. Determining which accessory proteins or combination of accessory proteins could be targeted for vaccine design will require a better understanding of the role of these proteins and determine how essential they are *in vivo.* These deletions

could lead to the creation of safer, more stable vaccines that can be generated quickly in response to a range of current and emerging IBV strains.

7. Appendix

Table 7.1 Cellular proteins identified my LC-MS/MS that significantly interact with GFP-3aM.

Protein ID	Unique peptides	Confidence	Relative Protein Abundance						*p* Value (-Log10)	Fold Change (Log2) GFP-3aM/GFP
			pEGFPC2-3aM			pEGFPC2				
			1	2	3	1	2	3		
SUCB2	2	51.8	34391.31213	56821.77764	41196.20091	0	0	0	15.42968233	6.777403376
FND3A	2	34.79	74980.93704	24630.06568	33157.9421	0	0	0	15.43359571	5.344140575
GCP2	2	197.65	235809.9946	105676.1593	110856.7974	0	345.0779654	89.30009403	10.02425004	1.897724605
PLCD	2	67.93	84058.48747	29179.2505	55446.0788	337.888514	0	0	8.963558546	1.888070933
RNF5	3	65.41	40010.10628	41698.36451	40304.88571	23.67064605	0.851848723	533.6542995	7.772101223	1.847905735
SYIM	2	166.85	5264.343093	38673.28811	35924.49767	272.9815635	348.4995779	0	7.005657106	1.313803241
DAAF5	6	260.95	185725.9629	107943.9298	164079.893	1605.611852	2255.546652	1306.758243	6.468832572	4.399280401
CAND1	3	99.7	26745.14688	119865.8145	61450.09147	1327.312472	803.21403	283.1585313	6.429625692	2.681942232
DRS7B	2	69.99	73008.75546	24830.37773	40296.64166	0	2227.736805	0	5.954364395	1.410611949
ODR4	2	83.56	94227.5916	30091.39846	43740.62521	0	3355.46799	20.37944099	5.637579572	1.332618828
SAAL1	2	59.11	224746.8404	137702.9975	147900.2826	3261.366937	7876.208585	2769.976351	5.197546941	3.298068207
STX18	2	108.09	107680.8457	55375.96374	76556.75843	763.3016918	4024.461995	2021.70543	5.137023465	2.704016395
NENF	2	40.87	32215.33579	110626.9175	56483.8135	2249.998017	0	3817.127125	5.037973511	0.943901617
HEAT3	2	61.68	264681.0087	126284.1501	164801.5922	0	9178.051879	7830.600162	5.030138812	0.900741473
REEP5	5	390.12	749915.828	305879.2859	410196.8144	18877.25139	19977.9151	8195.371688	4.961522125	3.037728514
NTF2	2	121.86	29436.05641	315620.5138	198763.9562	11592.76449	0	5969.017607	4.95261945	0.826531151
AL9A1	2	67.04	4154.176253	40434.74772	21783.00598	708.3351856	1021.334608	754.4832324	4.739747273	1.885859908
F134C	4	272.76	1141784.237	364034.8883	527764.8573	11166.44445	44095.2193	28322.67335	4.604648142	2.442071003
CLCC1	5	219	168918.3877	94932.29125	125618.1712	4675.755832	7539.017183	4068.684829	4.580028948	3.658382062
WLS	3	121.35	299226.2514	122157.0627	191376.7091	3018.354566	14975.83988	9071.20919	4.500800369	2.417495595
TRABD	3	258.46	356891.6626	151716.4333	245364.0152	13656.55863	13034.83679	9349.082979	4.386821094	3.395254749
MA1A2	2	66.59	215645.5795	96319.35766	62781.13751	1646.540633	14837.10708	1696.101165	4.36550919	1.879797504
COQ9	2	60.35	110354.4636	76056.90201	122233.2208	7079.981262	2429.067748	5573.197655	4.355023232	3.020661266
ERGI1	3	88.57	184876.8847	77101.71274	100338.6505	8938.181852	4635.605864	4641.070818	4.314065791	3.029781331
IPO8	2	119.01	127020.6783	69452.4371	88508.53162	3149.79612	8148.584352	3345.938955	4.282455959	2.995663854
CHCH9	2	160.86	67572.62096	360826.731	302878.3555	15159.59511	20122.69634	5962.35567	4.148140585	1.893115032
ABHGA	4	127.54	189095.1787	78592.56183	128659.5804	9674.639923	9766.763034	4021.874744	4.078288755	2.729636927
PM34	2	87.79	57197.3547	34254.4407	10667.73784	0	5332.612201	983.0557967	4.015179705	0.850035226

UCHL1	3	186.42	25494.22872	252579.1275	157222.2642	884.5261098	27887.49564	0	3.919257	0.855370301
ALG1	4	151.32	170129.9637	82346.94547	107946.4187	8060.06312	15773.06095	58.78622242	3.915098275	1.07826702
EMD	6	265.85	354469.7995	237282.4663	259536.9101	42448.24268	5526.157523	9727.697304	3.882953619	2.103879379
PSMD9	2	85.09	97466.21523	109471.8329	93926.33154	8888.832258	4863.059305	6760.611141	3.874537882	3.944032605
TOIP2	3	84.63	77623.31948	39297.2789	53983.44755	4152.550815	3693.52834	3819.042182	3.872913332	3.727616163
NU205	3	209.73	165607.2579	73567.56396	88393.00183	12717.15794	3246.093207	7151.734314	3.824893291	2.375776447
UBQL2	2	205.45	156916.6578	90090.28071	134626.7302	2436.664802	12446.06126	12506.86639	3.800488751	2.122942277
HSBP1	3	258.09	1069888.163	432952.447	680367.7133	55457.68021	64433.27794	39498.43168	3.775822299	2.999605956
GPAT4	3	108.01	96599.88757	37275.85499	79000.39059	1881.336243	14054.51056	0	3.739666621	0.829059527
ETFB	4	185.54	41798.71172	207835.8111	108182.2776	7522.672393	17400.36104	2073.603152	3.728369544	1.607173674
COG6	2	71.11	180632.3455	78810.92161	115020.1304	16867.94446	9927.445399	2235.819871	3.689148112	1.89616613
RAB18	2	117.45	243256.9894	169447.9014	189251.4121	21479.72484	6982.005359	18221.40531	3.688685394	2.713937351
ADCK4	2	85.8	94351.38794	124276.4933	169895.0733	9743.372986	5945.63161	14697.11473	3.676515496	2.93702803
NU188	2	84.14	95331.89597	53360.69943	64829.48226	13794.7404	3787.279944	72.7493266	3.596255344	1.123306796
ERGI3	2	53.68	219301.3449	102332.5309	127577.4655	6756.005925	21309.44446	9099.654538	3.595373766	2.468726847
BAG6	15	916.5	1063956.239	530962.658	711738.9269	42002.06133	91895.37871	63409.09066	3.547293393	2.908753429
TMX3	3	184.24	177673.0447	90569.12216	113261.9522	17618.31514	12170.97451	3153.771662	3.533652102	2.034140564
UB2V1	2	100.47	27592.55046	130924.2247	72665.3887	12104.53234	6519.486272	1478.853929	3.523556524	1.538065097
MPU1	2	108.56	206718.9505	115636.736	154836.9192	11968.55877	16688.87392	13403.17914	3.504029947	3.617445411
UCHL5	2	38.07	92429.56	63525.80973	72599.37128	7537.009138	7284.613162	5715.556648	3.476229818	4.170116506
TNPO3	2	71.37	144621.9199	89592.6772	120392.315	338.2526679	21920.99861	10189.34018	3.449992898	1.206894959
HSDL1	3	128.07	238412.8931	138049.5039	165886.3749	9517.300629	9194.526284	34139.25141	3.359216101	2.255200215
DHC24	7	401.81	1051291.496	339981.1588	610383.6646	68147.61699	62371.05979	66381.60123	3.345657234	2.60705999
ASNS	4	218.18	27236.7698	171430.9769	107043.9983	14413.26977	13620.8357	3076.178357	3.296708518	1.39532784
CY1	2	175.68	390624.129	223018.99	286975.9681	28300.7047	61543.82476	3119.625862	3.276170592	1.4398207
SODM	3	202.75	16683.22434	386429.2848	167136.3902	1116.735273	3051.20702	55062.56807	3.267179335	0.897462498
FACD2	10	514.36	595535.0484	319918.416	363208.044	28414.5887	51827.93688	54517.52588	3.24616961	2.873840686
NUP93	7	300.43	423476.3608	274439.1391	353048.6688	0	41416.03572	69362.66653	3.245961035	0.671846092
MSH2	3	173.35	111077.8734	99696.44018	134385.7525	0	31144.80963	6206.07863	3.208051101	0.734164784
OLA1	3	84.02	6739.60173	96279.51464	45580.26839	1905.775694	11890.49948	2289.52478	3.207568554	1.010022552
AFG32	2	87.66	266218.8291	69763.81298	129982.134	29522.17136	10236.30475	12436.5197	3.1582375	1.884998623
NCLN	3	110.84	151810.5306	118798.335	51161.51211	4026.983579	5593.222541	27600.09858	3.111869746	1.635810305
TM109	3	193.95	2128557.196	741617.905	1571766.115	116270.3236	309108.138	91861.27652	3.102285278	1.979519337
VATA	2	129.7	167583.1096	159772.5775	145135.6368	82.06007278	27494.21844	27481.07532	3.10128066	0.884954229
ABCE1	2	100.28	180280.4528	228714.1151	176016.8733	5853.351265	15469.80009	47476.7658	3.087986108	1.812994348
APT	2	69.2	81678.52251	294963.2647	132224.1422	10003.55635	31941.67625	18455.73939	3.074641929	1.85368189
TMX2	2	106.81	371290.2604	164004.6936	155805.9568	30719.98496	41544.65033	9831.420076	3.073511572	1.87689274

PIGS	2	107.23	138516.2391	42629.73737	87801.7788	4391.904365	26815.13072	1538.305236	3.037964418	1.372564613
OPA1	4	134.56	130650.4255	74911.63272	80284.10455	3403.949867	28348.88231	3080.573341	3.036695492	1.614628993
VAPB	4	268.94	416506.9089	248489.2161	232945.3183	7744.79615	68440.53099	34218.44871	3.023831853	1.637538183
RN126	3	251.08	525994.1889	280502.4686	334225.2035	67045.77592	49805.14736	23678.40168	3.021003945	2.392041083
RAC2	2	102.54	80460.41231	167604.9329	103378.7411	12685.50953	15828.63451	14877.31877	3.017812051	3.091374769
THEM6	3	179.98	302460.6286	180902.6637	221584.6424	21322.33488	46595.37978	20573.93694	2.993903447	2.650100687
DCAKD	3	114	153464.2264	83490.88646	117275.0733	15636.9141	17987.39211	11058.22892	2.986904211	3.081243797
SRPRB	13	1168.22	2356606.499	1252445.881	1772697.713	158027.6169	300604.9945	235622.8531	2.954536867	2.842057521
MPRD	2	63.4	403758.5618	189455.7616	276185.7067	69385.26371	22423.46862	22296.68755	2.929652826	2.094753638
VDAC2	2	165.53	185298.4981	63587.4718	71200.78036	12150.61983	26309.77203	3554.436452	2.929492465	1.509309944
XPOT	5	315.05	192152.0222	87834.0223	111134.1342	18165.44461	22238.0125	11344.55236	2.918036695	2.552757573
CB047	2	115.34	284719.5493	130033.8812	190940.3121	8955.553702	55631.74442	15759.10915	2.914283087	1.746291063
LAT1	3	283.6	534554.2065	250774.0012	333575.6027	27904.31074	80223.30157	42965.13305	2.88857972	2.250548912
EI24	3	79.84	198309.5484	94782.3236	94516.17662	7846.197007	26812.32063	19324.82657	2.84401227	1.992223219
UCK2	4	351.21	631346.4811	332289.1155	395077.2849	65389.18535	73917.666	50587.2553	2.838973586	3.02699373
VATH	2	90.98	456719.8086	188749.7682	292946.563	46618.49369	49388.45914	38127.75768	2.80654521	2.675757196
AAAS	5	212.77	362041.0814	157400.2565	256438.8803	25003.63463	43440.29387	42638.97024	2.804197213	2.502024053
FUND2	3	170.07	155872.4144	66284.67575	81778.76974	789.0479602	2925.884841	40106.34656	2.794063392	1.207379135
SC61B	3	258.61	869805.8076	438596.665	524439.0833	17462.80943	148948.4918	98268.19402	2.791763736	1.495266895
PSD13	5	257.79	277050.6305	256645.2022	295326.395	32953.82472	64093.08353	22728.28042	2.791081698	2.569841114
RDH11	7	463.66	850810.1228	437694.0325	614862.5361	85815.05262	120185.5841	69154.65644	2.790235542	2.811724745
PSD11	5	162	444330.9905	280377.2573	290097.3742	31561.4464	94631.09858	21669.9923	2.778874937	1.972596832
AMFR	7	463.85	533332.3635	261206.8513	292356.2496	23102.56658	85447.40766	50282.16974	2.774638376	1.985911313
DDRGK	3	267.52	191321.119	126482.1814	121025.2369	24844.11805	34792.27865	5121.311773	2.760533508	1.626837608
NTPCR	4	209.44	224270.7179	168624.377	238995.4131	14326.87493	46072.97841	33918.06515	2.74407081	2.264501734
DJB12	2	137.64	357081.3372	141342.3714	266288.1612	77299.67567	20968.1364	18545.99923	2.710705409	1.726837144
CERS2	4	176.44	588705.7071	301052.9363	440293.7639	51635.83294	96843.20871	54830.06952	2.709736317	2.600350873
HM13	2	130.39	383225.6361	102529.1486	156671.5571	23272.99079	59221.12809	19069.04482	2.661153809	1.59629211
SAE1	2	72.69	3890.241389	36693.09155	21523.55023	2610.669668	4297.940906	3084.428027	2.635757835	1.013332855
CND1	6	200.77	257381.7777	128069.9417	154547.4966	20634.99669	47027.58195	19621.23527	2.629171265	2.214347347
PTN1	4	183.41	264518.1559	108556.2263	131336.4813	11256.64812	52480.40639	18327.22862	2.619772988	1.677121747
PLCA	2	193.64	441886.5586	180590.0349	272120.6475	54541.70239	41216.35918	50904.62574	2.60873643	2.521353275
DHRS7	4	237.89	401883.9402	226211.3298	335157.6891	49773.69627	69167.30762	39677.61297	2.602352605	2.815173693
AT2B4	3	154.72	257229.1241	140766.591	216913.1939	27902.04311	46870.77667	26887.84526	2.596611135	2.683630362
DPM3	2	151.82	578373.8828	313474.5882	356597.4686	35643.24243	63884.25145	107629.4208	2.591337469	2.133913771
FANCI	7	434.1	395294.5467	231748.3048	266809.9435	23677.31952	100412.6155	24300.87146	2.590635546	1.794114836
RTN4	6	613.34	2121249.96	1560747.279	2014244.737	159811.5296	493862.9157	303631.4221	2.572958576	2.277626803

RBM4B	2	98.18	61416.63114	33119.93986	38152.43033	4916.94302	8950.836281	8663.772401	2.558030212	2.556655045
PSMD3	2	245.18	114804.9216	146011.2766	98208.84142	10785.86589	37228.27732	13231.40081	2.551407678	2.055153907
PEX19	3	111.31	256611.5387	124402.0876	204015.0439	36221.04114	34849.66186	29990.88899	2.533272516	2.826869318
PIGT	2	48.14	39631.64016	16687.27352	21902.80234	3557.777583	6985.109388	2970.958715	2.5331309	2.071575356
MTX1	2	107.82	199779.0345	56382.52488	205912.0841	29400.98041	29975.51966	21267.56121	2.5184826	1.658718923
ARF4	2	414.66	83496.06429	106467.4647	86529.65113	5987.003745	24529.6364	17948.45289	2.51222597	1.917368162
ETFD	2	146.39	254740.0909	81643.01257	124750.6509	20051.33662	39664.18429	22563.43741	2.486589839	1.869501809
STX12	4	147.51	307407.5334	145356.9347	210470.3903	61214.81117	28791.95736	31703.75157	2.446065961	2.223126199
RAB21	4	383.93	430263.783	217757.6447	316930.8193	83941.37533	71040.20029	23516.33662	2.434550349	1.795960819
6PGD	2	202.65	10499.64748	181438.9582	125112.9789	656.0449376	46718.1316	11398.14584	2.431508775	0.636587868
STX7	3	183.19	149866.5358	72172.90691	81657.27117	11483.51137	31535.27042	13658.48211	2.421789279	1.961911663
LCLT1	3	168.03	200207.5912	111411.7384	119419.2734	5447.028811	55163.06776	21584.71025	2.39069793	1.34525365
UBAC2	5	251.41	668492.4328	174492.2968	234308.6343	93470.15552	68910.54127	44404.09217	2.381209202	1.521798462
ECI1	2	152.4	44721.30075	325787.7461	203058.5391	91157.88129	15060.8219	4655.904244	2.371034499	0.907516206
PCH2	7	370.58	274138.1814	148990.0612	178754.7844	87842.22272	8037.414571	27574.76832	2.285504812	1.297333141
MPRI	2	67.67	61257.91371	35037.66052	57683.06477	5967.373519	0	25714.99018	2.280978345	0.630583361
SURF4	3	450.51	2326733.372	836510.7474	1029086.667	144164.5799	454369.4798	265216.8944	2.279065249	1.593777903
COPB	4	332.27	296998.3826	236737.9807	266841.8865	35332.90626	98141.41381	31800.93454	2.276171684	2.02700218
FACR1	9	593.27	1131804.623	441702.1667	696066.4254	213096.4901	103756.5821	154503.4005	2.267530585	1.966736971
STX5	2	93.65	326547.1604	161188.8443	221641.6748	44161.93164	35794.55173	67578.96681	2.265492286	2.316270349
RAB14	3	338.45	524554.0248	288185.7662	361188.4104	50150.38516	130743.0036	65390.84296	2.252948007	2.071224371
MET7A	2	139.31	229386.7968	112371.5828	151099.6361	13528.88939	27408.65651	62597.17065	2.251057486	1.601637099
PA1B2	2	71.19	19435.50139	226748.5071	113624.075	32622.97839	30395.61155	14075.2522	2.222540064	0.697874191
SMN	4	207.52	262084.9768	233184.8888	193074.1244	48302.97518	76662.02219	24690.24407	2.201486903	2.048564816
RFT1	2	140.05	324282.9051	121907.1591	149878.7574	45844.43004	46461.21891	37649.44843	2.197465689	2.029915184
CHIP	2	65.87	28242.34548	61483.79093	58918.28396	6133.876898	12710.07019	13884.49323	2.183248553	1.860971788
F10A1	10	779.1	3605670.176	2452277.739	3487307.46	679652.1486	888615.1282	546578.9523	2.174231028	2.896366525
ABCD3	2	88.1	222127.9399	164279.1518	123607.2643	5461.72324	48391.36376	59235.48518	2.173084707	1.135779148
RDH10	3	163.73	658740.3396	289840.3984	429233.7152	90977.6557	181422.7298	33755.62092	2.170042724	1.426778706
DIC	3	191.4	355047.2263	153114.2225	218580.3995	62962.51284	45317.41289	55214.31943	2.152203129	2.274592668
PO210	7	264.46	224424.012	183069.182	169095.6943	34828.00755	54028.21941	44162.32255	2.11591559	3.19640142
P5CR2	2	362.2	165490.5299	197684.6675	178764.2287	25452.9813	54442.29878	46460.18873	2.1006435	2.497937846
PRRC1	2	121.83	191405.489	114688.5823	129522.4701	15714.16825	35294.36761	51502.05182	2.087285813	1.794921878
S23IP	4	265.91	333884.4498	232062.4698	223640.2458	29033.73614	102326.7892	54677.72385	2.085499271	1.806077084
T161A	2	63.17	108825.4657	61651.22554	68263.3478	15846.4006	18637.01003	22077.70179	2.077558141	2.683946144
TMED9	5	363.38	1253653.149	578157.0519	672913.3144	183378.6419	264903.5635	149474.1244	2.067021953	2.074456562
AR6P1	3	131.23	489285.9693	288949.3972	338721.8629	92220.09666	40426.1019	138925.167	2.040170668	1.726018494

RAB5B	2	287.25	209507.8602	128353.7983	178747.3835	41129.10539	41887.6554	43006.70038	2.035380556	3.181315249
ATD3A	6	832.07	2174020.325	732954.0369	1057578.753	370243.8775	219969.4182	378111.5939	2.033595172	1.663259947
SUCB1	2	224.49	125568.8631	179226.2471	151200.0127	25714.07654	69586.44793	16196.27991	2.032016032	1.639898078
TMM33	7	354.95	1913965.496	630100.331	842094.0235	229505.3295	316503.1442	283805.0703	2.02879097	1.702447933
RCN1	4	328.55	114844.7278	393001.1036	246926.7618	47442.28536	74828.6619	63206.94519	2.024794799	1.565444115
MARE1	3	164.79	14586.43427	194809.063	93146.59853	0	45259.61522	29212.05129	2.022372346	0.491568553
MPCP	11	551.93	1519012.27	599678.7053	776219.856	211155.7967	436821.1525	65996.64336	2.019576291	1.208816589
SCO1	3	135.25	267182.7672	158740.3064	192179.9676	39971.35238	73570.49852	38950.57203	2.019109804	2.279390498
HAT1	2	70.98	176300.8231	231910.0048	138430.4227	15584.79959	56372.4518	63386.10531	2.013970258	1.504908034
Mar-01	3	233.52	285533.5531	147277.7749	223659.877	82800.02608	21974.86641	58031.0013	2.011578803	1.561397873
SRP68	3	193.7	247354.2736	223401.8082	249725.8688	58556.49659	51674.64419	69666.83771	2.001783313	3.925192934
C1TM	6	282.73	76445.7557	135918.569	77561.71409	7132.805171	51015.37847	14870.90373	1.989339368	1.293398868
QSOX2	3	87.06	181515.4228	80955.29865	85893.66218	35056.65314	19863.34026	33935.7694	1.97105988	1.850552396
CLIC1	3	147.11	159679.7802	313173.0779	171506.3469	48473.37817	85632.60667	31100.87375	1.963591577	1.739869388
K1C16	6	896.75	634148.1226	13902.34101	24385.96719	111394.6317	47460.89166	14533.60633	1.955384434	0.091986338
GLOD4	2	47.07	39042.4188	65764.11851	34278.01425	5813.640626	19941.26068	10213.71309	1.951151696	1.611385842
MDHC	3	188.47	44062.47206	316729.3776	198180.2147	40452.67279	61326.46933	42895.40497	1.949965056	0.82642353
S27A4	2	159.47	686536.1367	313250.2675	284714.1313	32305.10326	155840.4444	152453.3628	1.915061766	1.16176331
TX264	4	283.77	353600.9702	188089.7761	286604.1717	71557.47008	69826.86624	79845.60829	1.904597862	2.607115396
HACD3	5	192.05	2044158.665	889978.6587	1527204.912	345115.9435	453076.6049	397519.4028	1.89960794	2.109669028
LMAN1	5	278.39	532350.6678	289643.012	380234.2629	223574.4598	61841.85617	37485.39674	1.896543459	1.317443261
DOPD	2	43.58	78154.66967	346456.4452	193534.5437	66388.66515	90274.04708	11232.00161	1.880390024	0.864746575
TADBP	7	362.24	677673.5068	438401.1665	484921.5147	55745.611	235724.2106	143394.4233	1.880332874	1.509162043
TOIP1	5	362.25	724970.0886	346455.229	428759.7917	127589.2426	211457.7701	68716.24068	1.879336853	1.585176227
PGRC1	8	544.74	7190611.276	2337724.334	4210640.402	964713.607	1820666.496	952562.9378	1.877957992	1.487841993
CLPX	5	256.97	372370.7867	253158.8082	271319.9362	183007.2748	31220.11911	32347.98074	1.862837232	1.293285518
CLP1L	6	462.89	1099057.754	496726.4984	854324.3089	188434.0715	292772.8666	192777.0209	1.862059514	1.99511794
1433E	8	755.39	485224.7279	2058266.75	1723499.87	241864.9486	564152.1879	371147.5666	1.857902996	1.069537988
MCM7	5	233.53	54755.89475	299819.6128	144540.0737	0	60105.84541	79376.93784	1.839286885	0.506607224
ATLA3	4	177.86	607014.2984	208716.3727	461729.2732	81660.84858	135913.3665	143169.649	1.824231294	1.514220802
NB5R3	11	1068.11	2942457.748	1437941.474	2413545.359	538991.948	891941.9006	498781.2555	1.815861581	1.950931001
AL3A2	10	467.97	954358.9097	385144.8805	610034.3343	344528.1103	140600.6936	74382.36965	1.80089352	1.25249498
LYRIC	3	186.64	204017.8462	144055.0502	165197.6785	45816.76736	54301.91846	49752.51657	1.775996358	3.391480078
AIMP2	2	157.35	434221.3218	370577.2195	338611.3064	0	249441.5843	93244.44265	1.738383349	0.535017138
AAAT	5	291.91	1035868.958	555266.2629	570492.1298	138892.6747	358594.5269	152214.7086	1.734267982	1.583465991
COA3	3	90.72	152857.2877	79127.61545	81604.82339	14629.23177	41341.30971	38984.80021	1.72355723	1.447967598
RABL3	2	62.67	362113.092	115814.1364	176064.3707	92861.54616	44960.15419	60477.42249	1.721593808	1.336400677

MLEC	2	69.02	473668.1593	191265.2603	198548.7865	33126.35612	172313.686	58781.39574	1.708418923	1.10090919
MOT1	3	146.7	262953.6356	163721.5827	159043.8462	27194.3385	117157.2269	35338.33316	1.704699545	1.33936514
TM9S3	3	99.86	338322.1774	177693.1647	189739.7425	67423.70282	94448.82684	55605.75846	1.698296241	1.969450349
CISD2	3	225.16	891771.3081	370908.0438	536969.8582	179108.8401	263083.3578	116092.319	1.688643271	1.54087933
BZW1	15	742.34	2082286.572	982767.3991	1540951.792	287899.0364	562926.9626	582413.5114	1.684236496	1.679138974
PSB2	2	62.44	162932.3471	150762.5455	205339.2152	25772.3858	68556.80197	67306.81466	1.68308077	1.687266397
NU155	3	89.74	153929.5525	105056.7851	84231.93582	6827.48093	88566.4508	12346.79293	1.671562692	1.025695612
ABCB7	3	91.37	154525.1627	40750.40382	66118.21038	58378.47615	3143.301558	20851.2607	1.665980685	0.765280749
COX41	5	230.12	876093.7553	465518.8491	528809.5859	211474.0377	243425.3455	136143.3299	1.662029652	1.92641881
SYG	4	210.8	21967.63963	179390.3839	94800.49705	22808.47813	42736.53556	28556.81676	1.654074902	0.597483651
ARL8B	4	134.79	440315.1427	229372.949	370445.8304	34708.77127	187437.9255	113579.0373	1.631414262	1.146229705
RB11B	8	323.76	1530218.068	878446.6758	1058369.56	379861.7182	451136.2005	292623.2257	1.625546432	2.248657426
VINC	2	84.65	3345.126868	212383.3075	114565.2532	69962.0515	33709.62884	3811.269505	1.619641576	0.178833765
GBF1	5	121.6	185959.1285	82336.92752	118426.2366	78409.7636	35977.26594	11866.82963	1.614970444	1.048263066
GNAI3	5	266.06	239421.2769	186974.3089	205171.6687	70119.78593	85618.8583	52542.95687	1.60040097	2.674630023
U520	3	164.77	90113.60304	101838.5995	113086.1379	29203.21014	46442.22281	25084.23022	1.598501992	2.356230587
DHE3	12	673.63	687612.2038	872286.9386	917710.729	133782.9743	246992.5144	457464.9272	1.563513048	1.513627344
CLPB	6	314.67	210800.2161	131792.8405	151873.5535	96298.76651	45419.83482	25905.36126	1.5606447	1.388848329
NDUF3	4	357.93	243018.7106	142320.9362	245046.3478	80827.66237	62144.55298	72883.65345	1.546167164	2.233636649
GSTK1	2	55.05	16186.65559	49072.87397	35273.9776	20390.09965	9507.719796	4542.317582	1.545513634	0.994113742
PNPH	3	138.47	9702.505813	145714.8472	97089.07334	38225.82388	25422.83534	23286.39825	1.538310124	0.282328629
HYEP	12	547.03	1372311.943	901331.626	1305449.206	223539.6003	527736.482	481596.2703	1.537570505	1.674760666
PSMD8	3	116.53	306319.4431	189560.0919	235292.1162	20733.99124	199433.1	32111.78966	1.535190697	1.02569642
LETM1	13	911.56	1606282.621	886615.3141	1131003.296	399721.7827	543982.8929	310013.3385	1.531330742	1.953405366
NDUS8	2	193.31	321679.1571	157515.6666	173571.1649	57596.6143	107197.6796	61069.88053	1.531110434	1.609709118
SRP54	8	247.58	528591.6526	293390.7552	412996.565	123348.4084	167904.587	136242.0212	1.530506971	2.239598887
ILVBL	8	656.25	1472221.812	720810.5337	1089549.18	368946.029	406868.9636	367779.1521	1.521255704	2.074617222
NDUF4	3	119.91	124740.3488	78569.69299	93558.83118	12492.34591	46493.73947	44563.05895	1.519510201	1.236263746
GCN1L	121	10375.8	5895202.577	2226907.642	3263971.792	1562425.343	1005354.823	1407304.586	1.518213871	1.465515292
SYAC	2	173.36	34320.99991	366576.268	119129.6625	7341.458533	19895.2853	156422.2191	1.501557033	0.545026245
CD2A1	3	286.37	87745.79875	246640.0294	177071.5025	20587.49041	95310.6342	65464.0572	1.495740233	0.958786916
AT2A2	24	1467.59	1778927.097	859507.2756	1068048.307	468296.9351	472341.9496	377840.7699	1.491175461	1.916192624
IPO7	12	965.9	1116931.437	521663.0254	1047887.537	302960.0548	465510.9681	187392.2424	1.490842009	1.363860225
PSD10	4	180.62	79991.54839	93818.79211	83696.04723	20685.85927	38271.69437	32902.75394	1.487094701	2.288148413
GDIR1	2	105.79	3170.350911	124517.907	83407.79658	30546.4226	15669.44096	29094.65572	1.486976316	0.086066969
BAP31	10	577.54	2291410.52	1429632.517	1512410.174	596362.0988	653427.3093	619999.4871	1.484887805	2.579340767
AL1B1	5	317.51	411460.3247	332036.5343	329549.836	133641.2194	154431.3339	96625.96352	1.479912686	2.572432775

EAA1	2	187.43	430500.2778	226703.2967	274984.9166	32915.84049	60470.77371	240986.4838	1.479162921	1.01742804
FKBP8	4	232.19	590142.5363	275906.1035	368821.632	207003.9766	182722.709	54920.41138	1.473626817	1.104271982
TM9S4	2	162.23	284882.0947	139804.7569	154051.7407	87930.54206	59928.40971	61043.46346	1.470082679	1.736446809
TFR1	19	1190.91	2168178.845	1274930.322	1645592.346	774360.8119	683518.0254	403658.9368	1.450802679	1.810301541
PSME3	4	235.53	521798.3829	367699.7702	342213.2525	122035.9927	217235.0521	114435.0454	1.440834336	1.876338062
IDH3A	2	75.12	155516.7764	533529.2882	402876.1937	136485.4715	110449.1696	158821.62	1.428184882	1.065520622
EFTU	24	2192.81	3905735.67	3965093.829	4506906.656	1147125.977	2124340.895	1338229.307	1.425003902	2.232183863
SNAA	2	162.58	181120.8422	209308.6055	191973.7508	44424.16917	125066.045	49239.17666	1.412871189	1.521955328
AT1B3	7	643.05	3139642.155	1242591.416	2138248.773	1252242.664	800640.4564	413953.8404	1.402316322	1.12233299
GEMI4	4	294.07	274903.3574	130324.3349	184886.9627	99941.27524	47457.62964	76206.78278	1.400038401	1.468076706
TBB6	4	1150.6	598193.7179	390685.6512	565640.8254	132904.5126	194456.1174	262699.4631	1.397535564	1.847623874
MDHM	18	1482.55	910235.0751	7358641.984	6736036.133	1320686.564	2527258.562	1852802.016	1.396212056	0.395540615
SPTC1	11	767.37	1421792.087	723673.5128	1322641.441	394584.7973	502548.9611	421266.5573	1.395359934	1.834235761
AATM	14	970.45	200015.2001	952970.3618	635898.7173	185427.6634	211800.2424	284138.329	1.392557703	0.754192474
RAB2A	4	881.65	1205941.943	651203.375	795920.1916	333761.2038	417720.6856	259842.0618	1.391415098	1.85439654
TMED7	4	244.45	408779.0298	183217.7753	192591.0853	75490.9057	145432.819	79686.30824	1.384041908	1.310237668
VAPA	6	250.1	1125602.634	554339.9794	757009.0141	410010.4702	310155.6507	215013.3216	1.381762493	1.57378653
TBCA	4	220.12	19178.59606	370565.4222	197778.8563	66035.78554	77584.17745	83322.29339	1.37231976	0.165651983
IF4G1	2	129.65	5677.800046	72204.19231	13643.12553	35290.74368	0	71.59678173	1.371953964	0.701952557
KBL	3	120.93	193259.8619	126266.6932	148053.4603	36138.45205	59940.63531	84741.12397	1.370657325	1.638008385
PFD3	2	47.14	45845.52154	120793.7861	82397.23112	30861.14486	14130.45438	51472.66174	1.368290988	1.00271753
ACTN4	3	412.41	124455.7895	345418.42	186536.1784	29110.64029	170284.1771	55414.92167	1.36517765	0.879748629
ASNA	7	439.65	439297.6567	299152.9703	357424.1467	156833.078	179470.0913	89566.05185	1.363600579	1.814683643
PLAP	7	269.72	386204.0236	229618.6268	244659.0182	151708.0158	79882.3715	103523.2044	1.360494257	1.730256655
ADCK3	10	707.53	608309.0884	342008.0546	404590.1944	212906.8425	169263.4487	146143.0012	1.358728575	1.982367263
PDS5A	3	279.77	211896.9084	122719.6186	142935.8149	79206.78187	76878.55821	30723.28423	1.354097807	1.329087926
CNBP	4	328.11	60248.64378	199398.3688	109177.2924	35269.88575	69965.31422	39385.09469	1.35066371	1.003518584
HCDH	5	222.14	93217.39025	862927.2814	540448.2836	117342.1566	202441.3493	267722.3432	1.349006769	0.373186466
PPIF	4	393.48	32946.19881	588177.2244	283495.5339	97298.85428	33885.87558	224461.3715	1.346867881	0.260041582
CTR1	3	188.63	369793.9078	177136.6536	264975.6049	90610.02876	66829.98003	165065.8094	1.331987814	1.309561085
S61A1	6	637.7	1677526.015	651454.3851	1495493.004	496845.6598	659248.7179	364916.649	1.330230503	1.193156719
SRPR	6	475.78	600685.112	364426.8105	464079.7002	104557.5548	210653.875	255256.0686	1.324982764	1.457925283
TELO2	9	677.19	416870.4428	224747.2763	361160.2477	82217.51598	159866.9753	158875.5917	1.322471679	1.487936823
SFXN1	7	571	1193346.878	487650.6005	594971.9734	169943.8703	442910.0073	297234.8664	1.322402058	1.105747226
PGRC2	2	224.32	1088122.379	443144.4146	583886.0527	220557.0256	352907.1811	274925.9823	1.317962077	1.346205823
SYMC	13	896.62	896067.5845	683683.1103	800239.6508	231911.2753	432630.1125	291929.2315	1.315163163	2.043403994
DHB12	17	1526.96	5888141.653	3277256.845	5619004.362	2064644.99	2098850.702	1790411.911	1.312167236	1.971053456

COMT	9	1240.17	2079569.651	1360594.402	2338929.715	759047.0294	958490.3313	614635.2221	1.309168725	1.899638107
TBA1C	2	3750.23	15873295.3	9735732.725	12331964.27	4526137.186	6522285.72	4374908.495	1.298642994	2.034912601
ATX10	4	309.47	305451.3559	180250.1068	268872.7557	122938.6814	83042.30817	101175.8589	1.296687258	1.981736603
QCR2	8	586.67	631909.0204	440327.5588	522236.9523	314113.0692	171748.396	164241.3618	1.294340316	1.78885544
ZW10	4	174.41	526511.8836	219559.8645	293437.3906	165493.3701	136582.542	127807.3155	1.273885713	1.422623542
TXD17	3	223.52	77980.95667	237897.4885	169102.1787	56889.45266	105275.5897	39666.62939	1.264774527	0.921735123
XPO7	6	349.47	368682.4445	192788.4607	238310.0207	194675.1855	73638.32886	67214.51703	1.253171574	1.151763913
AT5F1	8	592.7	550607.7617	209850.3752	260201.7685	184077.6707	147662.8301	97323.64003	1.250236988	1.097885086
PTH2	3	214.75	488315.3521	303695.2336	395715.167	135385.6454	283261.3479	82102.34076	1.246041252	1.190431754
ACOD	5	379.7	1120723.771	450404.5745	680353.101	256986.3232	494685.9463	206854.0846	1.231984586	1.083395995
DYLT1	2	103.27	321685.4535	163855.4819	178872.8872	74625.82382	120412.9159	89755.39212	1.222162668	1.496544208
RS21	3	200.84	142635.8547	367550.1747	289800.5127	65903.07973	245484.4864	33324.02357	1.214585925	0.788550507
UN45A	6	328.98	431416.4797	322853.6093	439257.5935	144138.2411	221955.307	153560.8365	1.199607699	2.130974659
TMM43	5	458.38	759311.711	300612.1309	371029.3274	336798.3542	197340.6922	91071.28675	1.19456293	0.866878146
TBA1B	2	4168.03	51143902.05	30010676.04	38189816.15	16270883.92	21366087.04	14553404.46	1.193275118	1.883943209
CND2	4	215.78	174262.3347	95068.63389	128773.5422	27755.41836	96282.99122	50375.62827	1.190631057	1.083785898
F213A	2	51.16	734908.1847	310550.6617	504888.5382	382450.5351	115614.4672	183237.9476	1.186223156	0.967488504
SGMR1	2	244.26	1136693.475	239539.1218	1671511.053	61342.10757	907700.56	372922.3507	1.183394496	0.44677714
NCDN	2	172.08	311948.9831	139614.3877	166608.7221	87686.50449	148167.0145	37535.10257	1.177055326	0.895713877
MTDC	4	174.31	316615.889	500154.487	618222.5092	133262.4804	290656.2731	210730.4863	1.177012221	1.2926771
DHB4	11	940.57	423752.8909	867612.4217	754285.9516	191437.1813	359746.913	355106.3457	1.174514849	1.256543478
LPPRC	51	3205.68	2475215.978	1928022.939	2337486.028	953677.5506	1200347.849	842341.4045	1.169689513	2.503576655
4F2	13	1114.62	2435845.108	1435589.575	1842864.303	578517.3379	1473616.897	500016.1943	1.162863157	1.146171888
MOGS	8	448.54	468532.9264	290970.0936	381442.6553	116628.0577	222035.8677	171277.196	1.161827515	1.615985596
UBL4A	9	402.5	630074.1917	308538.4966	477521.6944	175424.9339	385013.4299	82133.79237	1.140027802	0.889597858
UBQL1	3	403.15	726627.1763	437932.0304	558872.3245	325991.4622	268941.3402	187273.8139	1.13966234	1.655668334
COPA	8	331.5	446233.2552	362885.3051	354885.0857	133405.7633	218566.9576	176543.694	1.139075392	2.129037044
DJB11	2	207.7	352007.8113	269196.5148	302200.0621	101231.9964	140626.2628	177721.3957	1.138017864	1.957124446
RPN1	22	2078.12	4503030.428	1890188.829	3814516.142	1543207.726	2336413.762	764092.1443	1.136311926	0.911953879
RENR	2	82.93	225864.8593	92722.14731	63745.20206	95613.79645	68226.02186	10850.76181	1.130024926	0.561931937
RCN2	4	304.03	724176.9814	584155.2591	472636.9754	345129.7583	244036.2786	226114.3355	1.127294391	1.923360102
FAM3C	4	213.32	202597.4044	86685.37756	118472.125	40297.59484	93243.33005	53421.12134	1.12495681	1.047547175
PDIA3	23	1803.71	440808.0713	1931468.654	2248285.7	432829.4145	883580.6169	804387.2385	1.123461752	0.465846338
BAG2	4	277.87	270105.668	84814.98164	337061.4924	86516.58315	187420.3529	44460.55165	1.119905854	0.592120142
ETFA	8	426.2	649445.0457	619035.64	663214.0686	250379.8764	392632.1983	247856.0925	1.116583279	2.189343165
UCRIL	2	113	216874.2228	107670.6205	163200.9986	120703.7548	37577.63311	68205.30124	1.106703309	0.997724783
SC22B	6	909.07	913494.0006	396451.1644	566084.6783	291931.517	316460.1257	266635.3806	1.100283301	1.338573236

LMAN2	5	369.86	1565619.565	611088.4881	1250799.023	441646.7675	778882.7436	380758.8348	1.097926525	0.965185292
PPT1	7	647.21	904416.326	627832.2952	960099.8642	234437.2806	444817.1925	486006.2537	1.096853009	1.392083565
PREB	2	205.87	431340.9647	252090.6128	315427.04	184606.3898	121262.3915	164876.799	1.085332938	1.686573967
GRPE1	4	147.53	145660.5861	329383.8949	360388.7218	122338.2641	194830.7625	77252.12258	1.08278757	0.885419493
K2C6A	2	985.81	608473.8189	394028.1239	144317.0086	184679.6456	149182.1043	210770.1443	1.074284275	0.609456191
KAD2	13	1026.54	407025.9826	1598078.699	1527803.65	402176.3687	690704.3235	586474.7896	1.072948668	0.56162922
STML2	10	885.96	1797565.531	1036292.854	1362745.351	619718.5724	826773.0221	553369.4586	1.069322476	1.671064393
TIM8B	2	97.62	95010.8299	172077.0448	158448.8148	65239.57565	82260.57253	55313.51051	1.06912871	1.525626449
TIM50	8	616.52	1557407.42	608050.0514	979278.34	637061.9893	486899.524	384332.4861	1.060021153	1.041945307
RIR1	2	93.72	23414.55646	94828.03362	65098.87237	45295.00333	22511.09439	20571.67618	1.052777589	0.590587142
APMAP	15	1045.31	2663882.832	1631034.368	2323781.454	729200.1271	1413408.357	1061254.34	1.046735208	1.430037949
RAB1A	4	966.58	2048671.831	1085437.392	1625079.977	622046.8375	1020849.914	667969.9537	1.042281764	1.379733089
ATP5L	4	331.73	902899.9839	409387.5845	430215.6655	364007.0254	315908.3374	166951.7829	1.040953767	0.940241788
TMED2	5	385.44	751831.2913	301720.019	752857.691	250055.6273	363646.9478	266041.2931	1.037969122	0.934673829
ADT3	5	929.59	2075770.092	988898.2336	1396818.772	802549.9606	778297.2517	596089.7574	1.035225031	1.358218843
PRS6A	11	676.03	1063031.4	625901.5297	996878.1399	337575.5328	575041.8302	405179.2891	1.027230057	1.444606987
MBB1A	5	160.72	69671.89106	60143.14046	65892.52985	14638.63957	67257.27865	14710.03086	1.018515558	0.899961723
RAB1B	4	1094.16	4765184.488	2552392.601	3700725.227	1382974.4	2060475.519	2008167.978	1.0151456	1.437282409
TRAP1	19	1871.94	919438.2359	1027955.136	979284.9527	410036.2323	412575.3711	626546.484	1.0140492	2.130724274
CH60	58	7652.33	86186971.87	35453853.17	75345308.91	33228319.12	28515924.18	35919788.95	1.012194832	1.051912965
SCPDL	2	105.04	413639.6579	249191.7228	418034.4101	8233.232308	117318.2096	411872.7864	1.008054129	0.599524027
SSRA	4	304.72	1231518.759	549688.0062	748274.9035	381673.201	537663.6516	338485.5245	1.007913577	1.141512342
AN32A	2	189.77	25542.71163	312839.4815	137349.9582	81572.97965	102151.0951	53378.72572	1.004636827	0.147078067

Shown are cellular proteins identified by label-free mass spectrometry/mass spectrometry that interact with GFP-3aM. Protein identifier (ID) and number of unique peptides used to identify proteins are indicated. Relative abundance score for each protein are shown. Confidence score (-Log2) is the score of the probability of the peptide sequence occurring randomly, added together for each unique peptide. The higher the confidence score, the higher the confidence in protein identification. The p value (-Log10) is a comparison of the cellular protein abundance between GFP-3aM and GFP. The higher the p value, the higher the probability the protein interacts with 3aM. The fold-change (Log2) is the change in the relative abundance of the cellular protein detected between GFP-3aM and GFP

Table 7.2 Panther GO Cellular component of GFP-3aM interacting partner

GO cellular component complete	Expected	Actual	Fold Enrichment	*p* value
proteasome regulatory particle	0.14	4	27.67	2.07E-02
cytoplasm	74.29	122	1.64	3.44E-15
endoplasmic reticulum	11.68	53	4.54	7.13E-19
nuclear pore	0.49	6	12.18	1.59E-02
nuclear envelope	2.88	16	5.55	5.31E-05
membrane	62.63	104	1.66	1.01E-09
nuclear membrane	1.99	10	5.02	4.81E-02
endoplasmic reticulum membrane	6.68	43	6.44	4.10E-20
endoplasmic reticulum-Golgi intermediate compartment	0.76	7	9.18	1.80E-02
mitochondrial membrane	4.63	17	3.68	5.71E-03
mitochondrion	11.33	27	2.38	2.67E-02
Golgi membrane	4.63	17	3.67	5.82E-03
Golgi apparatus	9.79	26	2.66	5.88E-03

Table 7.3 Cellular proteins that have a higher chance of interacting with GFP-3bM

Name	Unique Peptides	Confidence Score	Relative Protein Abundance						*p* Value (-Log10)	Fold Change (Log2) GFP-3bM/GFP
			pEGFPC2-3bM			pEGFPC2				
			1	2	3	1	2	3		
BAG6	7	43.529	16470945.06	28858040.37	24418986.71	4865916.052	3169799.154	4398407.984	2.906321357	2.487846495
VDAC2	3	20.668	25898945.09	14765020.26	15152998.83	3653834.859	3770985.049	5317622.748	2.576106121	2.131061799
COX5B	4	23.644	30800063.72	19350935.8	16642052.05	7956320.71	4038701.248	4591550.556	2.136701975	2.009682233
HSPB1	2	14.253	10848031.97	39054893.75	27991976.06	1997591.283	1360843.752	5366537.023	1.786641052	3.158306491
CLTB	5	34.721	82785226.63	18960977.42	18320048.67	5815815.212	2910206.307	3573954.904	1.726453339	3.287103251
RPS24	3	22.269	30267999.7	24865980.78	17672955.62	13033037.28	2198868.656	1708655.359	1.327963149	2.103594221
RPL11	5	36.951	40493864.61	52234874.32	39416053.52	32932986.23	3020215.369	5380914.677	1.090897383	1.676714625
ENO1	8	55.729	40518853.02	40645998.68	24602984.52	26007961.69	1135321.92	2932785.241	1.02136672	1.81421306
ALDOA	9	76.912	35958013.86	21848032.05	31849116.13	26253928.86	4178778.909	2107629.723	0.951639751	1.462157437
GAPDH	9	83.934	171130302.1	111709760.2	243190225	120099924.2	63961923.98	105049932.9	0.922894036	0.863518469
PCBP1	5	44.212	37269961.68	57406071.72	42436137.1	24614071.79	3328406.014	25599991.58	0.851018945	1.356601052
UBL4A	8	58.202	125140193.6	9007716.553	10411971.99	2914526.321	3665986.392	10919246.74	0.745663027	3.046260239
RPL22	5	57.219	148430260.1	44116041.23	25634972.25	64839067.2	2492980.211	4298971.156	0.740122908	1.606870919
GNB2L1	4	24.287	7630678.961	14685000.71	28960034.79	13102420.32	4413831.119	4327792.804	0.7371529	1.231035705
HSPE1	6	46.846	75512911.11	14169052.98	6707482.71	6977796.051	6770307.827	4959385.7	0.720658975	2.36525923
HSP90AA1	7	47.26	31104931.64	42325976	33364024.8	19387050.55	3033748.375	28180033.68	0.718304409	1.077610162
PCBP2	4	32.484	50025141.25	61691996.49	58589954.75	80057875.75	2657816.369	7516918.858	0.713260623	0.91641768
RPLP2	6	89.327	856572428.9	47936126.49	54482138.63	69639861.6	2412604.496	25154967.68	0.69553017	3.302378265
HSPA8	29	323.31	2720604315	974468290.8	716921541	1732994584	43409877.03	160749610.4	0.663120241	1.187492174
CCT3	15	144.17	259350875.7	15856049.11	64914165.49	64944769.35	3368278.502	6371051.196	0.656284213	2.18717545
RPL24	5	33.803	34827896.37	21167976.07	33097983.79	45133020.58	2783599.07	4470795.11	0.64945998	0.76610568
C1QBP	7	82.756	315369959	77766743.98	99174783.01	135999867	2543458.281	40128113.55	0.617040337	1.462262365
SLC25A5	7	48.22	130199620.3	51523954.87	208150242.7	154280448.1	12145007.12	23440987.31	0.59610664	1.038022331
TCP1	15	100.96	65977921.79	49299852.69	83975200.54	97941027.79	6493163.02	17490036.93	0.590161309	0.708616431
HSP90AB1	17	198.43	288360836.8	152319984.9	424020860	290979041.1	66742852	121930178	0.588899506	0.850214209
RPL7	8	99.725	53487928.66	35588061.13	32100000.86	81394050.01	2662167.655	5493522.175	0.552533088	0.436342731
ATP5A1	18	323.31	693139262.2	71439071.8	445549351.3	286849746.1	2954515.22	95303112.76	0.533759295	1.651826627
RPS2	7	44.332	33112899.3	32597093.56	50521004.9	43501143.82	3518770.521	23261003.48	0.519218588	0.725789937
RPL37A	3	22.295	36240009.56	20856012.26	17812047.15	33788992.55	5132534.538	9967152.697	0.50528658	0.615620685
RPS3	20	164.96	284450031.5	46227884.27	140190174.7	173550466.2	682509.6884	38619067.68	0.503678416	1.145472017
CCT7	13	84.011	128840417.5	4089463.056	16403950.96	16184954.79	3191669.862	3780197.027	0.488085111	2.689031885

RAB10	3	24.12	17148986.73	3197560	7812917.773	6456585.584	2101925.347	4701892.095	0.466134277	1.086495275
LDHA	4	24.612	25278017.77	18828960.26	152299926	13528044.74	2944456.644	61489212.74	0.443430598	1.333007928
SLC25A6	7	138.16	512028899.9	36062098.11	211230072.1	342590522.5	2486887.819	30642910.57	0.441749443	1.015050895
ATP5B	14	121.09	217340229.5	34229099.44	40732019.24	60009184.98	7295725.405	45613893.98	0.438886149	1.372170725
DCD	4	40.945	210040166	422029907.7	720248744.7	178949838.4	327441059.7	338420096	0.399830386	0.678734802
HSPA1B	21	323.31	4728088847	731209716.2	773888242.3	3594390480	94285984.75	269969278.1	0.380221451	0.654962983
RPL28	9	63.733	107079717.7	12259017.3	30229001.71	59295118.36	1475773.618	15536950.15	0.377905449	0.97089577
RPS4X	10	84.556	61880005.96	21130008.33	17233949.19	38562894.3	2434256.899	20082979.68	0.375717945	0.714740304
EEF1D	7	52.266	54011002.85	17853950.56	10885014.55	27112973.36	2331844.25	15586028.24	0.375388394	0.877845176
CCT4	17	122.27	285129090.9	10445006.11	15065967.64	94276835.63	1356568.06	4416003.852	0.37226896	1.634531289
RPL7A	9	57.804	208160342.5	15482015.9	31323020.42	79352921.32	2270816.974	19874014.68	0.358651391	1.328853572
HNRNPC	4	28.411	15176965.19	23045951.54	17630010.52	11213007.91	2217972.427	36528014.46	0.31845376	0.160888445
ATP1A1	18	151.71	227709619.8	4445394.426	28149969.04	64693166.79	1751828.361	7058694.734	0.314572863	1.824314351
RPS27	3	66.714	75105748.59	14693044.22	26253928.86	56846965.34	6235353.836	12682976.26	0.314427662	0.615171284
RPS11	13	90.247	197819581.5	22030974.87	36710005.63	103519692.8	1659066.173	37976931.34	0.308383886	0.841714402
LDHB	4	34.963	26433974.08	30655019.79	160180135	13110051.34	25753050.56	73397113.94	0.292202513	0.952636463
PHB2	9	76.913	99024350.65	8556918.98	24550005.3	38402050.21	1210935.003	33513058	0.257541681	0.853514781
RPL34	3	17.891	25620050.79	2019210.658	19790983.88	14628008.15	1270046.598	6872768.813	0.254392527	1.05862086
RPL12	5	47.468	69413839.72	27741068.09	20321027.28	36089854.72	2951342.658	55366116.66	0.254088651	0.315394712
RPS3A	12	79.644	167730522	19298026.73	33039991.96	100059991.9	2748017.955	37325027.82	0.246384444	0.651155799
TUFM	9	84.826	74189927.77	4556738.028	34198032.74	74931032.75	1624517.664	7340871.919	0.242185378	0.428935359
RPL26	6	39.845	56135885.92	4402556.231	13354012.87	29710921.17	3067389.623	6169875.725	0.232220766	0.923870906
RPS16	6	38.53	168720495.9	5775041.967	67640781.85	88210679.81	1980522.966	31428933.91	0.211873354	0.99343738
RPL4	6	47	13958978.16	3769338.685	26386926.82	30469025.02	2390780.085	3930196.46	0.211039364	0.261963516
SLC25A3	9	65.634	113820091.2	3865195.617	22063066.71	47687902.73	5203424.58	5376366.286	0.209870788	1.262063175
MIF	2	46.843	265320332.9	4183693452	56046851.72	274859670.8	2444004846	2544939.625	0.192490377	0.727192487
KHSRP	11	88.777	118049770.8	5152210.118	15253954.86	73652951.3	4842162.28	4710895.83	0.165857618	0.734667272
YBX1	6	77.296	114010384.8	6191896.819	42681868.53	65750111.26	3111567.257	31068085.38	0.154573755	0.704859875
PARK7	9	77.879	234009198.5	16129965.31	6881205.985	72174206.23	24767072.25	4559012.708	0.104450203	1.340398837
CCT5	7	54.548	10863984.57	9423816.391	12799019.88	16536951.84	7242016.334	8969710.551	0.089702967	0.014819975
DSP	13	80.915	39931114.41	131689949.2	162899846.1	19591981.76	171760136.3	141300369.8	0.084795112	0.008080568
PCNA	6	42.685	47957063.94	5940405.566	41911999.09	42224880.37	4393349.979	32751099.39	0.080844818	0.271586618
DSG1	4	27.711	7532983.82	51825184.08	27228987.47	13790008.4	17466049.52	29728019.14	0.075830193	0.505720422
PHGDH	10	63.859	62223232.11	1654128.634	81199077.43	46335994.48	892331.3494	76330166.37	0.059627628	0.23161906
PHB	6	39.758	27628999.8	2891807.323	18688014.98	8769906.313	4528368.711	25139977.1	0.053963238	0.356374248

HSPD1	19	164.46	201929997	44284853.18	110039786.1	208719478	33247902.66	111249992.7	0.0394662	0.012352485
TUBB	5	105.4	584359114.3	65052898.35	684459529.5	900380767.7	92133980	227720668.6	0.035846679	0.128460226
RPS18	11	109.93	315179836.3	5330058.734	49098989.6	128080002.5	20083954.14	45776061.33	0.030857672	0.930388914
RPL13	8	75.412	140759787.5	2346078.734	37921954.84	126529627.7	2236978.562	29139039.76	0.027698281	0.197148676

Shown are cellular proteins identified by label-free mass spectrometry/mass spectrometry that interact with GFP-3bM. Protein identifier (ID), protein name and number of unique peptides used to identify proteins are indicated. Relative abundance score for each protein is indicated. Confidence score (-Log2) is the score of the probability of the unique peptide sequence occurring randomly, added together for each unique peptide. The higher the confidence score, the higher the confidence in protein identification. The p value (-Log10) is a comparison of the cellular protein abundance between GFP-3bM and GFP. The higher the p value, the higher the probability the protein interacts with 3b. The fold-change is the change in the abundance of the cellular protein between GFP-3bM and GFP. Cellular proteins which appear in both GFP-3bM and 3bM-GFP data are labelled with an asterisk (*).

Table 7.4 Cellular proteins that have a higher chance of interacting with 3bM-GFP

Name	Unique Peptides	Confidence Score	Relative Protein Abundance						*p* Value (-Log10)	Fold Change (Log2) 3bM-GFP/GFP
			pEGFPN1-3bM			pEGFPC2				
			1	2	3	1	2	3		
VDAC2	3	20.668	7499120.63	17683984.02	17660954.73	3653834.859	3770985.049	5317622.748	1.690929301	1.749453318
GNB2L1	4	24.287	13319993.11	28875047.82	16578038.7	13102420.32	4413831.119	4327792.804	1.173502982	1.427915511
RAB10	3	24.12	7248896.703	7734089.345	10889995.33	6456585.584	2101925.347	4701892.095	0.988435436	0.964321683
RPL34	3	17.891	33095001.49	21090939.12	19311006.17	14628008.15	1270046.598	6872768.813	0.981830341	1.690497848
ENO1	8	55.729	43553037.39	23601905.43	30798996.29	26007961.69	1135321.92	2932785.241	0.976636643	1.703487501
UBL4A	8	58.202	11586969.89	13873707.14	9620563.714	2914526.321	3665986.392	10919246.74	0.958133267	1.003364682
RPL4	6	47	22745061.5	54760033.75	31838962.73	30469025.02	2390780.085	3930196.46	0.937528239	1.57148918
COX5B	4	23.644	29899955.47	5815533.034	17579004.05	7956320.71	4038701.248	4591550.556	0.897123299	1.683970657
CCT7	13	84.011	12852983.96	18792973.26	16677041.01	16184954.79	3191669.862	3780197.027	0.891818962	1.061272716
PCBP1	5	44.212	39500018.69	62620860.61	40698999.68	24614071.79	3328406.014	25599991.58	0.870506088	1.415441218
TXN	8	74.762	65599887.28	71818889.02	73566213.45	68024919.1	35628045.36	16483965.35	0.810331678	0.812460664
RPL11	5	36.951	35840067.03	29110978.55	22231932.14	32932986.23	3020215.369	5380914.677	0.791499813	1.076713437
RPS24	3	22.269	28521964.15	29375905.76	4223711.897	13033037.28	2198868.656	1708655.359	0.720477986	1.874612889
BAG6	7	43.529	9586813.925	6962480.736	3957176.544	4865916.052	3169799.154	4398407.984	0.716080118	0.721774474
RPS16	6	38.53	121419929.5	126850151.4	72148196.7	88210679.81	1980522.966	31428933.91	0.703601776	1.39757433
HSP90AA1	7	47.26	18661996.48	54775977.91	46738885.59	19387050.55	3033748.375	28180033.68	0.662310619	1.247926103
CLTB	5	34.721	31371039.53	12264031.74	3230799.969	5815815.212	2910206.307	3573954.904	0.660787232	1.929882152
HSPB1	2	14.253	3245524.014	6800974.256	4806149.184	1997591.283	1360843.752	5366537.023	0.64804722	0.767497695
RPL22	5	57.219	82947203.1	39254099.67	20849941.5	64839067.2	2492980.211	4298971.156	0.635298036	0.997875685
RPS2	7	44.332	35329010.33	75877036.64	35783967.07	43501143.82	3518770.521	23261003.48	0.619112475	1.06451321
RPL28	9	63.733	63371902.86	61155122.01	23688934.93	59295118.36	1475773.618	15536950.15	0.551876405	0.957797569
RPL7A	9	57.804	101970033.4	53656886.23	34927983.06	79352921.32	2270816.974	19874014.68	0.542206142	0.908758939
RPL26	6	39.845	43033892.35	13976017.65	13896998.65	29710921.17	3067389.623	6169875.725	0.512512157	0.864370044
RPS3	20	164.96	210330087.5	146929617.8	45108000.46	173550466.2	682509.6884	38619067.68	0.482430135	0.918663577
RPL37A	3	22.295	52213154.97	18019054.8	16098020.93	33788992.55	5132534.538	9967152.697	0.469591309	0.820365397
DCD	4	40.945	315479276.9	289109344.7	547308871.1	178949838.4	327441059.7	338420096	0.462019381	0.447311822
LDHA	4	24.612	12178980.21	78696710.67	73145207.21	13528044.74	2944456.644	61489212.74	0.45041621	1.073041926
PHB	6	39.758	10957991.09	19369051.89	27157926.53	8769906.313	4528368.711	25139977.1	0.444406619	0.580642051
RPS4X	10	84.556	35733898.95	62386044.31	14313964.79	38562894.3	2434256.899	20082979.68	0.430064416	0.880302133
HSPE1	6	46.846	126960106.3	5443639.13	6455287.859	6977796.051	6770307.827	4959385.7	0.404933041	2.891933156
PHB2	9	76.913	42219027.17	29566087.35	30126923.09	38402050.21	1210935.003	33513058	0.394505515	0.478867263

KHSRP	11	88.777	171449683.5	20313985.77	13315008.37	73652951.3	4842162.28	4710895.83	0.385739356	1.301417867
ATP5A1	18	323.31	145590401.1	130969896.1	167809598.8	286849746.1	2954515.22	95303112.76	0.3720535	0.206500336
PHGDH	10	63.859	29555022.85	65835847.18	70886128.38	46335994.48	892331.3494	76330166.37	0.366807771	0.428394439
ATP1A1	18	151.71	30875945.92	13915987.96	30131935.28	64693166.79	1751828.361	7058694.734	0.35678092	0.027608729
RPS11	13	90.247	168190385.9	57429155.06	18702010.05	103519692.8	1659066.173	37976931.34	0.325650392	0.771196109
RPL13	8	75.412	252260660.9	33398963.61	25278017.77	126529627.7	2236978.562	29139039.76	0.321100985	0.977562524
LDHB	4	34.963	16333039.97	110460092.5	83594228.29	13110051.34	25753050.56	73397113.94	0.316356266	0.906201298
RPS18	11	109.93	299070423.2	72505143.13	36085102.08	128080002.5	20083954.14	45776061.33	0.314351283	1.071758248
ALDOA	9	76.912	36116881.67	2661927.78	31965891.63	26253928.86	4178778.909	2107629.723	0.309970216	1.120392877
EEF2	16	104.18	19693961.4	241520431.7	44248033.39	101549648.1	18015058.49	12268963.18	0.30937431	1.212276056
TCP1	15	100.96	27152091.58	58804776.14	45061125.1	97941027.79	6493163.02	17490036.93	0.30767216	0.103780117
HSP90AB1	17	198.43	85717711.65	290720990.7	366409076.3	290979041.1	66742852	121930178	0.293327236	0.631078323
EEF1A1P5	17	173.88	762731477.9	540698832.4	87211194.7	1126000249	27094937.81	79071803.79	0.279504582	0.174552762
RPL24	5	33.803	24584062.43	28537982.28	5507896.427	45133020.58	2783599.07	4470795.11	0.253060155	0.16241734
YBX1	6	77.296	183950199.5	18471017.43	14940033.01	65750111.26	3111567.257	31068085.38	0.221402004	1.121108416
RPL7	8	99.725	42467916.64	64667163.73	3869726.033	81394050.01	2662167.655	5493522.175	0.207443344	0.309860999
HSPD1	19	164.46	103660426.9	141919737	123030434.2	208719478	33247902.66	111249992.7	0.200133559	0.061541246
RPS3A	12	79.644	95219914.65	52581064	6527096.779	100059991.9	2748017.955	37325027.82	0.103238136	0.139203417
PCBP2	4	32.484	45361971.26	61706964.88	1571052.542	80057875.75	2657816.369	7516918.858	0.076608235	0.267834397
CCT8	9	75.209	19055973.81	37274095.28	26072037.56	45174021	17755959.66	18759005.37	0.067203462	0.012539646
PKM	6	48.927	34480085.12	169249930.4	4917214.979	35247070.02	13881979.81	32662004.56	0.063649946	1.351050804
PARK7	9	77.879	76991188.2	19776036.84	8359411.79	72174206.23	24767072.25	4559012.708	0.049432133	0.050644397
DSG1	4	27.711	22170070.16	4975085.883	56796945.15	13790008.4	17466049.52	29728019.14	0.019923738	0.460961972

Shown are cellular proteins identified by label-free mass spectrometry/mass spectrometry that interact with 3bM-GFP. Protein identifier (ID), protein name and number of unique peptides used to identify proteins are indicated. Relative abundance score for each protein is indicated. Confidence score (-Log2) is the score of the probability of the unique peptide sequence occurring randomly, added together for each unique peptide. The higher the confidence score, the higher the confidence in protein identification. The p value (-Log10) is a comparison of the cellular protein abundance between 3bM-GFP and GFP. The higher the p value, the higher the probability the protein interacts with 3b. The fold-change is the change in the abundance of the cellular protein between GFP-3bM and GFP. Cellular proteins which appear in both GFP-3bM and 3bM-GFP data are labelled with an asterisk (*).

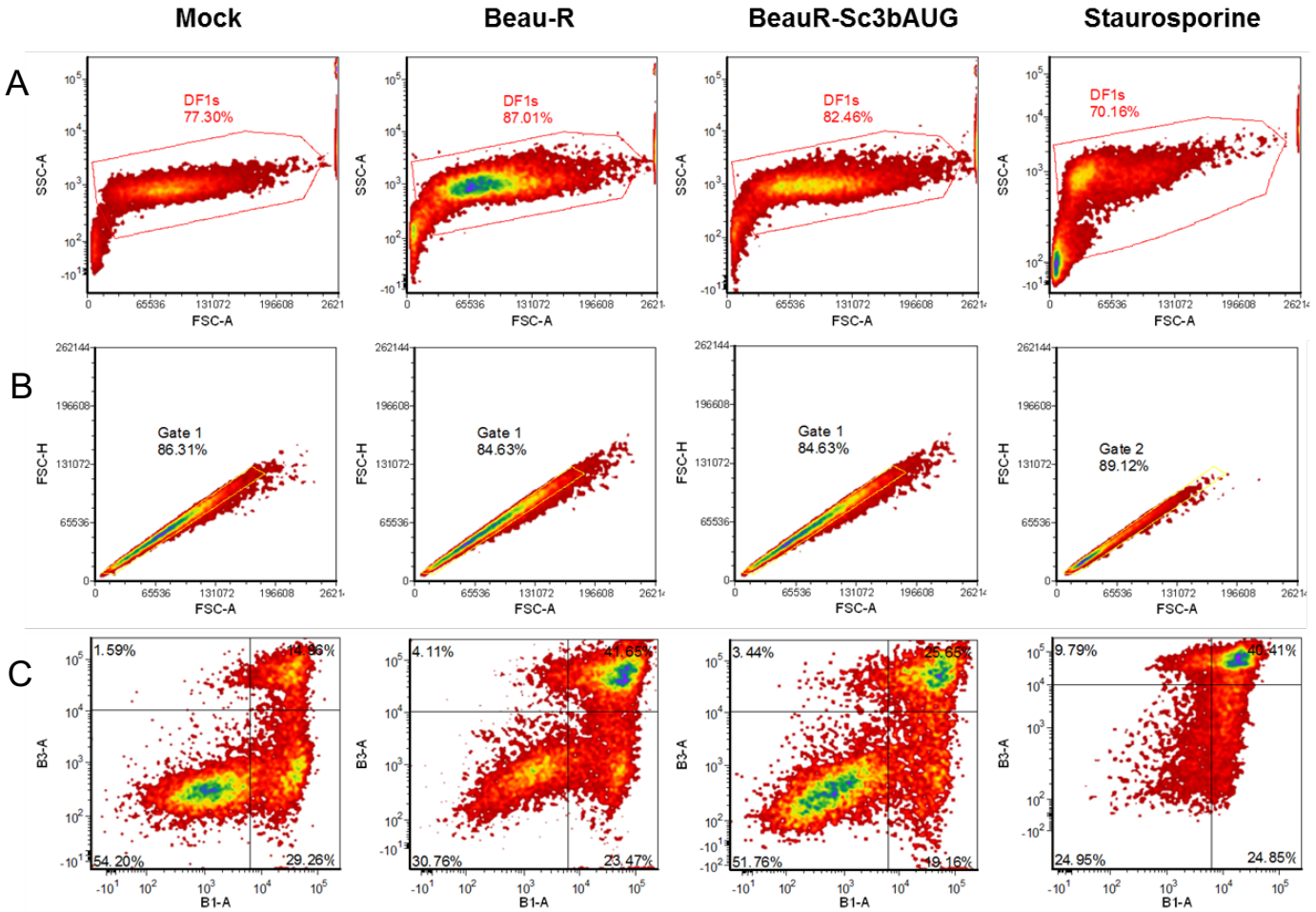

Figure 7.1 IBV 3b induces apoptosis.

DF-1 cells were mock infected or infected with Beau-R or BeauR-Sc3bAUG at an MOI of 4 for 24 hours. As a positive control, cells were treated with (D) staurosporine for 6 hours. Cells were harvested, washed with PBS and labelled with anti-PS and propidium iodide. (A) Cells were sorted by forward scatter area (FSC-A), and side scatter area (SSC-A) to gate DF-1 cells. (B) DF-1 cells were then sorted by forward scatter area (FSC-A) and forward scatter height (FSC-H) to gate single cell populations. (C) Single DF-1 cells were then sorted by annexin V (FITC) and propidium iodide (PI) fluorescence and shown as a density plot. Cells were separated into three gates, representing cells that are viable (dark green), viable cells undergoing apoptosis (light green) and cells which are dead from apoptosis (red).

Table 7.5 Cellular proteins identified by LC-MS/MS that interact with 4bM-GFP

Name	Unique Peptide	Confidence Score	Relative Protein Abundance						*p* Value (-Log2)	Fold Change (Log10) 4bM-GFP/GFP
			pEGFPN1-4bM			pEGFPN1				
			1	2	3	1	2	3		
LAP2B	3	367.06	308301.4581	308630.484	721836.6619	80902.72867	92397.04123	24409.89257	1.748856032	2.759451338
RL34	3	189.71	528427.6891	282680.832	1578712.974	164306.7962	75411.48874	42751.15199	1.480517467	3.08073618
TCPH	2	214.33	3341.124075	8993.922182	41135.24955	921.0552625	1101.108238	2917.09935	1.163171647	3.436370007
DESP	10	621.61	585581.0348	113195.1917	1417524.335	37282.9971	122572.7351	8009.798482	1.136799303	3.656166612
DSG1	4	380.4	255888.2483	128315.5368	739277.6606	78286.60921	117522.5949	51076.30009	1.097646584	2.186062262
PRDX6	2	389.29	3837.703586	12580.77905	59278.77169	2581.596323	1076.176879	3524.981782	1.023050489	3.397631763
RS2	6	290.56	56730.16038	179024.2354	150958.2496	60416.24602	58061.0729	16145.7868	0.91312853	1.522335896
POP7	2	134.3	911.8707526	1588.670511	647618.2754	0	0	3480.976415	0.892347224	7.545067562
LRC59	3	385.18	5635.367448	926780.8934	180529.2952	2806.613199	3906.844135	12404.58578	0.873895322	5.86330435
RL11	2	168.39	1168.419944	0	148438.3374	0	0	0	0.859694832	10
K1C17	3	513.47	316032.344	16713.1404	284010.8027	19824.06716	34851.66881	4060.045856	0.83919468	3.392388951
CASK_BOVIN	2	162.13	124675.5449	12799.90292	7020.604791	8038.580892	3360.13759	172.4779952	0.826040607	3.642420127
TIM14	3	302.16	4537.983877	32298.5626	782860.5011	1437.734931	1329.487708	15095.84856	0.746353508	5.520038752
RM43	3	236.52	47539.26502	2638.642934	149635.5899	987.1212169	3179.171192	10525.4074	0.697187968	3.765580815
PRDX2	3	263.01	2194.851774	75765.74001	1463.378974	1287.62327	855.4837881	0	0.694090889	5.211798663
HDGF	2	178.65	44.57430193	0	379734.0245	0	0	0	0.686747809	10
NHRF2	6	658.58	123937.8009	87441.99072	780723.0634	42755.90333	19697.35678	165598.1996	0.674666623	2.121130294
EIF2A	4	360.96	26191.1189	43491.86927	1841034.114	91.64032414	34015.52374	25612.43638	0.653694747	4.999765867
RS28	12	1010.4	9335907.542	1561375.14	348358602.1	1327670.645	2829222.062	1312178.327	0.648898822	6.037572178
K1C10;1::sp	31	5728.78	189782196.9	23099693.88	258417835	33932067.03	40516832.58	31209457.17	0.646420393	2.157237964
HDGR3	2	164.41	1445.063931	10798.94118	820505.6078	3324.502837	2512.857452	310.4074153	0.634102218	7.081676315
NDUS3	2	412.34	20629.71799	1999.259114	50514.42269	1347.559789	33.79957874	11929.76846	0.630852132	2.458094874
K1C14;1::sp	6	1961.58	4821928.186	952135.7381	5343121.205	1102543.308	2382982.831	250710.1779	0.627316243	1.573133931
ANXA2	3	192.23	2800.499492	2048.317129	510901.443	6.097818185	403.7181974	11178.20336	0.61532189	5.475966735
UBL4A	2	109.74	4.670518648	0	11585.8507	0	0	0	0.602751727	10
K2C1;1::sp	32	4927.35	340676833.2	30965711.8	340741933.4	49839413.71	95306169.77	16717900.51	0.600757635	2.137878529
CKAP2	2	60.97	10499.23545	0	265646.9065	248.7785753	0	0	0.559263271	10.11635401

RS15A	2	128.47	20261.0697	2371.321675	1547851.233	291.7003083	6161.207923	10836.00181	0.549973469	6.50521817
PSIP1	9	699.4	297264.6488	187054.7042	4652998.681	152311.7922	153462.2957	250435.4747	0.549866111	3.207314935
LBR	3	264.33	60858.39061	50330.00959	276069.6311	33390.01468	85903.10905	26381.32755	0.549275387	1.410547283
CRIPT	2	112.35	3088.452999	3208.453899	708960.0249	0	957.8799199	20052.40092	0.548269363	5.089294223
K2C5	14	2081.41	13074916.38	726923.1183	12272841	1414399.585	2952717.418	496617.2506	0.548066484	2.422513265
PLAK	3	327.34	4818.853753	8284.501143	1048185.416	1074.73093	3788.566625	11982.52712	0.537782351	5.977282393
F207A	3	125.74	2665.674085	24716.52682	436914.6617	1544.690352	1371.284639	24661.12907	0.52864817	4.073504663
K1C16	9	1889.28	9008377.583	741193.6442	4929766.083	1359080.113	2244486.942	443015.7484	0.524458609	1.859010818
RRBP1	4	255.74	13264.28431	1920.542701	394072.296	100.8331958	80.90184734	74288.45556	0.522041875	2.458272572
K22E	24	4408.38	48444035.36	5049567.12	69356896.11	10055459.69	13549305.94	5999830.284	0.519990389	2.053010646
RT18C	2	58.65	2883.006852	555.2213157	77469.25066	127.0382721	0	15768.68076	0.515541976	2.34763479
KNOP1	3	344.24	7699.489829	10379.41236	243852.3416	1375.459289	3321.386324	29970.67561	0.503323516	2.917531568
ALBU	3	1068.08	125050.4352	16386.09102	241384.1391	75783.41164	32564.13499	477.5206335	0.498310502	1.814657799
FETUA	2	117.82	901.5507811	0	209905.5078	272.9358479	0	0	0.475440062	9.593145566
RS18	7	637.21	872335.419	95302.95698	4363039.16	58917.7636	444318.8968	254097.6107	0.455576846	2.815316792
ECHB	3	237.82	5651.63785	1349.749736	103377.5059	0	4140.803886	9516.751654	0.446184338	3.014693133
COA3	3	155.7	182997.7145	3890.780845	45583.77057	7180.032985	337.0304998	46960.17009	0.44311373	2.093333264
DCD	4	554.6	7741768.006	915169.5098	7449578.338	2143771.519	2293672.703	1233108.336	0.419749597	1.506083217
LS14A	3	206.55	11842.01799	177278.6436	323990.9499	10689.58084	15915.39419	112936.5305	0.402397647	1.87857837
FRG1;1::sp	3	402.12	7309.775246	14467.08766	925237.035	6127.762579	15927.57922	13340.0076	0.3947007	4.741753876
RS5	5	711.7	20612.23866	120821.6199	7483139.053	92099.47641	63118.72208	20555.59642	0.394149962	5.438864619
TCPZ	2	179.73	1199.589166	1297.870216	201008.7171	29.93943986	1038.618996	12706.84516	0.383667311	3.884906088
NOL7	2	63.6	98.80464168	35238.41465	85286.30717	0	7009.940392	3269.580222	0.382212751	3.552666427
CYTA	2	72.13	35086.67208	13102.29212	633011.4202	43598.46219	29109.56956	6829.090441	0.380777752	3.098378981
PTBP1;1::sp	17	2384.54	1359942.816	669208.1566	7918979.31	316431.2917	593615.2138	2734783.841	0.379470209	1.448573738
ILF3	6	362.57	19295.6386	747.6190726	683302.3509	1383.82142	1.110636144	148921.5051	0.375319674	2.226326975
SMD3	8	1276.85	3983972.397	823151.9969	19107583.45	672201.0136	356235.5355	7850347.088	0.374320526	1.429464215
RM11	9	867.54	326613.254	207668.7433	3917107.051	90138.53586	182371.7422	813028.4955	0.372844298	2.035844339
MZT2B;1::sp	2	174.18	120976.7424	2216.960967	128355.4955	1795.271526	6879.219477	38154.61604	0.372612496	2.425363161
RT18A	2	140.61	0.708102515	1513.809318	191815.2413	0	0	4575.837512	0.370734063	5.400884091
DNJC9	2	205.6	5799.140826	3132.524111	542057.7279	92003.45981	76080.78194	104154.1123	0.368786989	1.017154211

CH059	2	80.34	14425.65752	439.037194	507501.4148	0	20303.50923	8805.629401	0.368527127	4.165517245
K1C9	35	4527.82	202871229	23664448.74	177687456.6	34449667.34	119938769.7	21831498.89	0.362688523	1.197774745
MO4L2	5	426.83	178194.1	81147.25623	2345399.322	45786.37813	112930.1598	327320.9936	0.357437546	2.422000121
RS3	11	665.84	1042603.38	397058.0176	9900319.723	103965.8704	1582205.053	973210.7352	0.354198918	2.092255494
RLA0L	3	321.82	14062.81281	101583.8782	924632.1616	26880.82039	27883.76908	72081.77094	0.354120705	3.035816273
RS25	8	820.46	737016.6507	450290.2693	114415617	96942.49295	143057.6572	9122771.33	0.343777923	3.626098432
CALM	7	841	159297.0479	235917.7982	7479835.884	36906.94512	42441.29678	2164486.043	0.335778308	1.811323085
RL40;1::sp	4	1272.81	55522.90208	273535.8095	1239132.52	36265.8443	28315.76306	676364.1166	0.334203973	1.081661728
ATX2L	6	366.47	41675.76547	23737.19591	995318.3981	10275.79864	5527.036502	301483.3553	0.326191135	1.74120269
RPAB4	2	53.62	5902.929403	11104.92896	1849652.16	0	43353.01395	156093.6491	0.325461146	3.226384297
RM33	4	577.42	37947.07336	204204.1302	2648419.034	2369.810485	39473.18832	1278996.567	0.319695314	1.129898886
CLCB	5	237	1421826.711	95529.78205	1743416.526	66432.62061	876560.7064	275393.0336	0.305347598	1.420242323
HNRPU	2	354.96	1883.362992	4543.78438	294555.4664	2367.458807	6860.563168	4501.213468	0.302043876	4.45435696
ETFB	6	621.65	537566.5881	39224.24334	84346.52153	36946.0763	13725.35752	276247.706	0.291320832	1.016016183
YMEL1	2	243.81	0	4327.831587	227468.7478	7605.080226	5223.752685	55348.95324	0.288371908	1.765485618
FA32A	3	147.74	32040.06876	5639.276833	2171594.494	191390.6031	36055.59699	164.0759761	0.283824066	3.278934654
RT23	5	384.75	77119.10118	43852.63677	1400043.349	74024.30344	12153.41793	273335.9389	0.28342201	2.080915969
RS11	20	1847.17	2266909.351	423529.4725	31007174.35	453840.1356	463438.894	6099591.553	0.277446056	2.263746749
RS30	5	469.49	1550201.705	792446.3427	152466671.4	258417.5316	307780.9791	23915915.66	0.276968678	2.66069227
RRS1	2	77.67	1500.306172	0	9446.452205	0	0	4917.172274	0.268245905	1.154602907
CCD86	6	497.8	114831.6293	1812.880952	1430282.907	1216.727289	11919.17867	175319.1642	0.261830714	3.037112992
FUS	14	1831.48	3685606.117	1901792.793	84521950.29	1774477.653	2654482.073	10201056.15	0.25969758	2.622745465
HORN	7	600.98	451844.8349	16814.55612	753363.6645	120053.8168	154355.9794	22895.11619	0.258969095	2.039256298
CHTOP	11	1048.35	494204.2965	229409.3663	52691335.7	128674.1111	105193.5423	7056342.969	0.250384887	2.873211168
FBRL	9	591.73	149097.126	33877.92389	1191823.115	39266.9082	144545.3401	129949.4515	0.248774545	2.131478669
MTDC	6	539.87	267619.8633	23832.71905	216758.5335	117326.4233	24942.54693	85693.52994	0.248578431	1.15663141
RS16	7	465.83	90375.31989	155875.0319	7133250.092	186493.7407	112231.4964	343970.578	0.246060433	3.521315173
RL24	11	735.49	186124.5488	1364066.5	3426832.923	339789.1816	411618.8524	1093529.538	0.245603837	1.431711336
HMGB3	3	116.21	15275.19571	0	100871.2016	22324.78987	6399.830654	6646.368224	0.245597984	1.715305951
MRP	2	234.67	539268.976	57135.97328	728363.9282	81540.9579	265998.1235	203925.6753	0.243048783	1.264400092
BCL7C	2	133.69	2843.926801	13014.84444	448795.5628	27292.18599	6785.680799	4781.96392	0.242390916	3.579806344

MAZ	9	523.58	301425.3047	37373.40311	929345.6964	25748.2669	82879.28831	485751.5684	0.238895259	1.093263685
PDIP3	18	1732.04	111313.3434	167835.0644	16015118.17	46234.96748	37622.19365	3447699.524	0.236334138	2.205988258
RL37A	3	286.14	18872.78109	28081.80356	3542375.425	13141.21064	21390.57544	226225.8851	0.233428072	3.782932972
RM53	7	576.9	215644.0538	70550.38238	9864277.45	40524.17816	70774.87065	1764249.682	0.233165503	2.436162146
ERH	4	533.05	19087.59523	25014.06553	2091441.896	146133.4181	291599.2943	348179.9428	0.227869972	1.442162436
RL23	8	549.21	416720.2986	267180.3389	13197825.93	148440.2075	358869.2129	2200608.289	0.22465744	2.357931214
IF2B1	13	1681.43	240192.9464	148950.8683	11976948.72	86125.40777	94522.56675	2482918.57	0.223943585	2.214958477
PABP2	3	335.01	490984.8964	113121.8831	3894622.923	127658.3143	529656.8577	471806.2036	0.221545811	1.99431711
MAP4	13	1275.28	141843.7498	112704.6698	3787402.89	114820.4676	83991.45317	696461.5392	0.217255543	2.174651619
RL12	11	1709.04	5890951.431	2630862.224	627869609.2	3988049.059	4123285.319	27927923	0.217132568	4.142273203
RRP12	2	62.27	0	27.67559495	65632.78339	2531.035433	0	0	0.209627149	4.697225225
RL7A	15	1180.14	230822.9384	144452.4731	34160736.52	69729.70612	170777.4276	3382447.501	0.204221562	3.25286285
E5D0B6_9GAMC	3	117.1	130.2404694	11466.89289	146326.7442	39765.17175	14715.27896	10325.91359	0.204185828	1.285021914
L10K	5	221.39	5819.620125	12646.90678	839885.9265	4182.273806	2801.669346	207490.8138	0.2011596	2.000762307
1433Z	2	308.14	146755.8069	14913.4842	665318.761	30435.37785	171632.8661	40993.69135	0.200767745	1.766542508
RL30	12	1719.29	7585014.161	5873825.376	989329524.8	2701626.283	4122333.545	149841185.3	0.200288293	2.678261011
RL26	4	1766.26	62263.57059	177318.1504	7865708.783	31796.40626	70558.9224	1943503.322	0.198191512	1.986157423
CWC15	7	434.62	7093.990711	100114.652	1299288.702	10788.52486	9493.688533	436629.6537	0.198110699	1.62211901
RS21	5	485.38	269379.2183	191815.7883	13047394.55	451410.6962	404269.1472	468423.1361	0.195186247	3.350789815
HNRDL	4	368.42	332247.258	150297.052	1911459.774	388242.0993	310276.938	250778.5932	0.193061221	1.334493226
NUSAP	5	334.48	17574.56615	52926.25375	769067.4886	10487.81278	55465.93703	158336.4305	0.190649329	1.904281251
CC124	16	1589.84	2302422.256	830571.7663	30171142.28	712281.6558	1188905.201	9389635.706	0.190440768	1.560550774
RL37	4	142.19	125528.0227	7785.044418	1347916.311	6422.829873	48712.27439	272993.5739	0.189442607	2.174461474
RL28	4	235.96	354718.8173	17717.60424	445788.0212	75476.4273	143707.9318	52440.66559	0.188121122	1.590880235
RS24	2	151.09	0	1716.515544	1183436.443	2029.27008	942.1790308	527665.9861	0.187420484	1.159274905
RL13	17	1569.04	991969.6281	380053.7402	34942005.32	729911.902	334565.6869	5157816.964	0.187083862	2.545008396
SZRD1	3	175.07	211339.5013	0	168579.6382	6074.83052	9951.534515	167850.4229	0.183004466	1.046953024
RT26	2	38.15	101.6085717	0	22612.51317	0	0	9691.778787	0.172034071	1.228756142
RL35A	9	587.59	892990.314	154422.7912	4991964.88	1280536.245	618383.6547	180886.2548	0.171414474	1.537950899
RL38	5	531.73	191737.0547	6346.397575	841612.6169	26002.27603	19062.068	223392.2068	0.170835678	1.953401337
HMGN1	3	301.28	119367.8722	88466.94361	5043852.448	173670.2558	112414.645	480691.5641	0.158355656	2.775903045

CETN2	3	279.76	2596.234633	5508.59917	2694501.9	15542.4189	68017.29577	803870.9601	0.155355146	1.606645268
SRP14	11	1902.3	470648.7836	588968.9287	120041637.9	205603.9915	238126.7524	32758311.32	0.153466867	1.866869943
RS20	6	646.42	48568.27576	66534.66659	32962481.28	33027.11146	56765.547	2557110.729	0.152844397	3.643476431
RPA34	6	937.12	65034.92821	9500.081215	2265385.055	95456.03659	25346.56721	76091.10377	0.152574401	3.570970335
RS19	16	2106.63	6072377.988	1436218.848	124408594.8	2328065.063	1635694.791	39755743.05	0.147339645	1.593283689
NOP2	2	121.91	715.5481332	1102.455414	193045.1975	17744.20132	23400.36736	3475.464117	0.147227409	2.126698192
RM48	3	222.52	8647.711693	0	655025.9875	22513.51431	628.6164117	35253.1409	0.147205338	3.506550642
PKRI1	2	223.75	0	0	223775.1307	687.1336117	0	0	0.144319273	8.34724334
RM46	2	276.75	0	1419.281255	215864.1344	676.3158918	1491.544303	13891.12799	0.143825305	3.758125161
RSMN	8	525.57	152110.2384	6862.185751	5264192.57	14275.12229	12569.84025	1746605.611	0.140607577	1.612575941
RL31	18	1625.83	3475783.08	1423298.398	127244635.8	865097.856	1901116.778	47510818.7	0.139829391	1.394136405
MK	3	268.4	1669.769088	451.0793763	1100645.657	22071.67427	8086.723512	78100.71386	0.139232058	3.348566994
PAIRB	24	2871.75	7108699.273	1867869.803	101775713.7	2494203.573	3702862.006	30336214.87	0.137642792	1.600053226
TIM8A	3	301.21	100457.1189	5091.888431	3566709.941	340422.874	102067.1445	458823.6708	0.136913153	2.026566586
ZN593	3	330.28	22916.63454	143922.7836	2534149.793	77958.43994	58463.07347	368618.5152	0.132669822	2.419018234
HNRPK	4	339.4	13995.07057	54228.85377	1007292.794	84895.48846	225235.1203	159391.5682	0.131007942	1.195764744
NEP1	4	478.6	9534.470493	26897.47359	602157.3189	121230.6922	57320.30354	82806.68287	0.127151183	1.28886275
RT11	5	484.85	16122.88633	13072.18186	6884427.525	9643.404158	9827.465578	1092768.889	0.12438029	2.635974036
RPC4	4	104.04	29340.11681	1261.029451	195719.8984	48379.81885	16775.21623	38193.96134	0.117108167	1.130846362
EIF3H	2	226.03	160210.0843	0	722802.4756	7819.19591	43733.59049	8868.019343	0.104902888	3.86931663
HAP28	8	824.87	48086.67152	108091.3055	6431567.793	716774.141	587601.6983	288821.1269	0.10036107	2.047860243
WIBG	13	1490.01	854812.0337	362479.1405	27446536.58	2741224.612	1434374.308	6889740.55	0.098992933	1.373183568
RT28	10	960.77	572563.4129	341231.3667	51783055.87	357757.7044	437990.456	12646131.1	0.098921718	1.970981893
YBOX3	12	2360.52	1308101.733	286131.5555	30274649.44	267691.4365	696462.0599	14016588.76	0.096220899	1.089039334
RLA2	9	1508.17	719002.5153	142946.6191	34053119.28	343859.3744	366183.183	6278885.994	0.093935785	2.320706596
EAF6	2	402.41	0	2193.109264	302222.4249	49.0997585	1772.162761	130588.2683	0.093347265	1.201035009
NDUV2	4	169.89	5554.830323	0	357544.2354	285.4170822	1061.773122	82364.44795	0.08805109	2.116863103
H3C	2	90.68	19007.83797	1999.537284	175388.5561	19841.47068	15686.18473	8083.351098	0.08743598	2.17100085
RL29	11	1005.06	8280277.127	618713.1613	89179397.32	1663107.619	3195759.42	27629947.79	0.080055565	1.593992145
HMGB1	4	285.97	62070.03667	606.4103879	980015.9015	170790.8233	21926.71075	42904.18307	0.077129849	2.145769123
TCPQ	8	664.98	20087.20782	46872.97716	1022357.655	9917.601685	152123.0448	234553.0973	0.075588752	1.457691138

RL23A	17	1998.62	2046355.297	1578772.213	140167606.5	1486114.806	1741380.808	56082298.4	0.070780949	1.27764851
CA131	4	362.08	459731.4611	15051.1954	16756665.08	99766.45913	892420.6533	384973.2718	0.066713788	3.645275427
NUCL	52	6666.07	20655585	3969742.9	304259397.9	20190215.49	25811243.31	104216125.2	0.066270243	1.130528307
DECR	4	267.39	3493.079249	2515.371366	861658.316	25400.05935	11591.77791	9504.368047	0.059985099	4.221956189
ROA0	6	567.61	5310.197463	8049.069985	2775666.031	6305.350453	21785.60862	270761.9985	0.058067968	3.222253295
HNRPD	12	1555.33	2288197.773	1117668.4	42471276.81	2053883.709	2351566.019	12031312.97	0.057727515	1.480849369
THOC4	18	2330.74	3857522.939	3678987.063	285424879.5	4165126.592	3140828.475	125899034.7	0.055429719	1.137062413
EWS	7	1114.34	1655726.492	189900.5331	18806231.84	493942.7959	991388.4464	5850920.347	0.054890393	1.493156623
G3BP1	7	594.99	325165.4507	45272.80342	2414039.973	50080.29734	419927.0561	856727.9917	0.054597056	1.069526399
RS14	11	1595.96	1586713.923	148163.0609	25844232.71	429167.9847	643343.6462	9801358.507	0.051916487	1.342710381
RS12	6	452.39	234743.6266	89243.02432	5399182.6	245987.1872	600323.9956	450951.943	0.047788919	2.141343139
CIRBP	7	1010.7	301462.8121	191576.3568	33565447.84	168205.6521	346443.8233	14018436.6	0.045904084	1.228673258
CASB_BOVIN	2	179.48	1461.097548	0	0	182.9677614	0.936170805	0	0.04364592	2.990028268
PRKRA	5	236.56	43453.73027	128.3210948	1293701.806	22012.38653	56772.79106	16137.75078	0.042986775	3.816405312
NDUS6	5	651.41	32760.80297	74364.94617	4499347.454	125019.4178	175997.0266	912573.3627	0.041860702	1.924381747
NONO	16	1722.95	317896.4586	279029.2546	15338559.43	1641369.257	816026.2927	1623510.44	0.03980941	1.96528156
MIC19	7	558.58	3203945.583	598900.4602	56267.82814	263868.8608	1082840.91	579598.4311	0.039006405	1.002431067
SNRPA	6	804.38	126445.7763	34111.81477	4360441.333	75577.47981	93475.17815	1466573.78	0.038896311	1.466798287
RL9	7	795.67	189311.452	35896.22632	14064785.9	302323.3695	206117.4148	2805090.428	0.034783903	2.108563854
NOP14	2	36.91	0	91.44264821	171179.8779	861.6157942	0	4371.227858	0.034637051	5.032544627
RL8	10	1196.15	244364.6875	17929.41347	10229554.57	78889.61242	68729.43924	4627639.92	0.028220677	1.135618024
NHP2	2	177.1	4794.475394	1888.813934	907653.4755	1001.516656	10545.74179	423773.2698	0.026058204	1.070647577
RBMS1	3	108.49	33276.06663	271.1406131	1081505.053	7771.861959	6960.848232	104765.05	0.02363382	3.222055845
NPM	21	2584.33	2138165.19	425655.7154	82239342.26	2301441.784	3118133.218	14234363.52	0.020867636	2.10929963
CNBP	5	426.62	0	99701.70041	3436597.754	6406.292553	1599.38971	6987.023579	0.020216508	7.881835857
RM49	2	346.44	10442.8254	4826.936918	615923.529	18549.26459	7197.301219	173381.0573	0.018324597	1.664388505
RS10	19	1734.35	2316955.501	682417.5391	91912186.2	4433699.334	3217941.789	12732761.27	0.016115574	2.219118141
HMGN2	4	665.01	113578.5992	73192.77361	4412319.132	287263.9221	290059.0693	515910.0116	0.01331153	2.07274767
NDUA2	3	385.82	160660.238	31527.50832	5156504.787	52944.47059	174939.1792	2332862.53	0.011132515	1.062622013
H1X	15	2059.49	203904.6256	320615.4861	34081282.06	411600.2731	625863.7488	10120116.11	0.008972496	1.63298978
RM18	2	99.17	368498.06	209.0801653	50987.72505	9315.364779	4369.201246	105298.4192	0.003901826	1.818585533

CALL5	5	829.63	33304.24203	28017.56083	5130793.884	88099.63343	39461.05163	1282412.538	0.003872097	1.880654765
SRP09	9	871.03	428266.3847	196934.1396	82898179.62	751013.074	1077451.01	8220552.917	0.002660748	3.055125715
HNRPR	2	425.57	2568.370477	24264.21788	584576.6189	23793.93311	17731.20257	88379.63916	0.001531502	2.234683818

Shown are cellular proteins identified by label-free mass spectrometry/mass spectrometry that interact with 4bM-GFP. Protein identifier (ID), protein name and number of unique peptides used to identify proteins are indicated. Confidence score is the score of the probability of the unique peptide sequence occurring randomly, added together for each unique peptide. The higher the confidence score, the higher the confidence in protein identification. The -Log2 p value is a comparison of the cellular protein abundance between 4bM-GFP and GFP. The higher the p value, the higher the probability the protein interacts with 4bM. The fold-change is the change in the abundance of the cellular protein between GFP-4bM and GFP. Cellular proteins which appear in both GFP-4bM and 4bM-GFP data are labelled with an asterisk (*). Proteins which appear in the third replicate are labelled (*).

Table 7.6 Cellular proteins identified by LC-MS/MS that interact with GFP-4bM.

Name	Unique Peptide	Confidence Score	Relative Protein Abundance						*p* Value (-Log10)	Fold Change (Log2) GFP-4bM/GFP
			pEGFPC2-4bM			pEGFPN1				
			1	2	3	1	2	3		
LAP2B	3	367.06	136685.3054	216452.7164	392330.6564	80902.72867	92397.04123	24409.89257	1.245425587	1.914764357
RRS1	2	77.67	1556.740123	20216.67469	30394.43262	0	0	4917.172274	0.999504058	3.407260099
PRDX2	3	263.01	5215.96236	16505.10114	227062.8667	1287.62327	855.4837881	0	0.974611688	6.859045568
LS14A	3	206.55	69195.71256	265077.3598	172551.0425	10689.58084	15915.39419	112936.5305	0.960634287	1.860790867
RLA0L	3	321.82	90613.70622	120295.2302	1395195.765	26880.82039	27883.76908	72081.77094	0.949946223	3.662411915
RRP12	2	62.27	790.2868236	1826.565518	73865.67688	2531.035433	0	0	0.932141673	4.917330623
RT18A	2	140.61	745.3216979	6387.487721	249956.4255	0	0	4575.837512	0.928848462	5.812089569
HDGR3	2	164.41	3768.138364	14764.81383	6398.227269	3324.502837	2512.857452	310.4074153	0.903562663	2.019816578
POP7	2	134.3	2829.72501	359.3812335	82829.75435	0	0	3480.976415	0.850293596	4.627089077
PSIP1	9	699.4	228268.3059	315697.4688	1063818.038	152311.7922	153462.2957	250435.4747	0.797961412	1.531372977
UBL4A	2	109.74	0	219.5166039	125234.708	0	0	0	0.79426677	12
RM43	3	236.52	13414.7761	10110.47499	952572.9486	987.1212169	3179.171192	10525.4074	0.78451836	6.053953068
RS2	6	290.56	79362.52455	81137.98086	1036934.237	60416.24602	58061.0729	16145.7868	0.764722498	3.152949084
IF2B2	2	497.86	0	127.7464791	172821.5504	0	0	0	0.759702539	12
PHB2	8	713.88	99289.62987	116778.3876	3589120.913	73490.16727	28103.76015	53308.46372	0.75561545	4.618536767
TIM14	3	302.16	4293.606251	25456.40159	993963.807	1437.734931	1329.487708	15095.84856	0.698949446	5.840688503
NHRF2	6	658.58	117581.3879	96626.84277	801436.7071	42755.90333	19697.35678	165598.1996	0.690956883	2.154964825
ALBU	3	1068.08	140779.9275	48159.22437	149265.0735	75783.41164	32564.13499	477.5206335	0.629963575	1.635883773
RT18C	2	58.65	7589.78398	874.8109784	163755.5698	127.0382721	0	15768.68076	0.620578817	3.437543891
RL14	8	582.74	41072.21332	106616.499	2877863.98	4213.913143	5345.27756	278459.7082	0.607136322	3.392963325
YMEL1	2	243.81	10916.3814	101042.6663	213454.43	7605.080226	5223.752685	55348.95324	0.604443908	2.254900346
CL065	2	118.03	0	0	468076.6922	13299.32869	64294.07444	11433.41851	0.588077695	2.394432972
CRIPT	2	112.35	7897.1543	3704.151862	190778.6196	0	957.8799199	20052.40092	0.584978943	3.267898843
RL40	4	1272.81	192391.0279	309618.5155	980663.2205	36265.8443	28315.76306	676364.1166	0.584319447	1.000760449

RM39	5	426.25	41849.98436	51265.52214	1333620.066	20181.15531	14832.39725	78911.87357	0.577354535	3.646556302
G3P	5	316.53	48448.80105	25205.89476	872362.8818	40284.75983	20077.36409	21757.11279	0.544102432	3.526074867
P5CR2	2	150.76	14844.08324	5525.250762	225259.0594	3799.352065	11599.55541	6430.221355	0.53129773	3.492150878
COA3	3	155.7	354180.8467	2338.813523	351670.5033	7180.032985	337.0304998	46960.17009	0.521099172	3.700411457
HSPB1	2	186.59	70909.68319	117303.671	172438.5174	0	19071.62716	150223.0021	0.516249351	1.091070705
CASB_BOVIN	2	179.48	0	2311.715856	108136.046	182.9677614	0.936170805	0	0.500474228	9.230196141
RS15A	2	128.47	4213.299073	6073.555598	714339.7386	291.7003083	6161.207923	10836.00181	0.498461298	5.389318928
ETFB	6	621.65	101866.9631	79344.66573	1105203.696	36946.0763	13725.35752	276247.706	0.496031274	1.97635075
H4	3	190.69	2359.894419	67538.96573	174918.591	0	3631.896338	50381.02264	0.4930372	2.180329979
RL38	5	531.73	263926.3563	26451.87981	1959954.348	26002.27603	19062.068	223392.2068	0.475453235	3.067377723
RS15	4	605.86	28492.70436	40025.40123	702125.6639	5617.555967	12556.24725	126239.8159	0.470972528	2.415857324
FRG1	3	402.12	3985.391534	142906.1815	103972.7796	6127.762579	15927.57922	13340.0076	0.46611044	2.825275759
ILF3	6	362.57	16120.7154	3600.479751	687434.6158	1383.82142	1.110636144	148921.5051	0.459895443	2.234121329
CKAP2	2	60.97	6911.654187	0	1803.961137	248.7785753	0	0	0.456293235	5.130668371
FETUA	2	117.82	2208.743297	3476.771502	0	272.9358479	0	0	0.439040652	4.380657186
F207A	3	125.74	1680.31623	23144.90107	330384.9932	1544.690352	1371.284639	24661.12907	0.438921911	3.687130183
ANXA2	3	192.23	375.7952171	1829.758816	464823.7678	6.097818185	403.7181974	11178.20336	0.436321194	5.332807223
RL11	2	168.39	0	0	84580.01029	0	0	0	0.427243412	12
ECHB	3	237.82	1314.561067	3076.313885	170197.1485	0	4140.803886	9516.751654	0.426338798	3.6761834
EIF2A	4	360.96	36264.45686	10181.8508	93962.19191	91.64032414	34015.52374	25612.43638	0.425624087	1.233353853
CG050	10	711.38	794322.3343	372768.1185	11004238.87	209786.5088	188270.1	1863209.117	0.42516845	2.428284303
SF3B2	3	284.5	25368.78841	2277.64473	275343.0038	0	5449.38623	66843.73706	0.420083879	2.067337172
SF3A2	5	496.49	177611.4362	11138.48437	849549.523	2967.731071	105296.2257	43477.51588	0.410907832	2.774535224
RRBP1	4	255.74	1889.294019	3590.533721	191498.4704	100.8331958	80.90184734	74288.45556	0.407230414	1.403301736
UBP2L	2	197.76	4101.430355	4264.351672	204759.573	2740.664026	6.342555383	52407.68854	0.394260448	1.95014663
EF2	3	213.09	0	851.485626	129169.6	3854.229012	11827.57435	18527.84178	0.368150971	1.92627056
MTDC	6	539.87	516719.0503	13645.57736	1727321.669	117326.4233	24942.54693	85693.52994	0.351522593	3.307976613
RL32	3	182.78	7649.564981	442.9076681	1811133.166	64373.88596	233600.9704	212847.3643	0.349840182	1.832431303

IF2G	10	1075.97	61705.9887	241988.4221	4755076.513	28920.04337	59192.69474	718805.9276	0.348247374	2.648291743
TCPE	4	479.39	7624.936222	11029.49369	462145.2232	7913.166364	5119.823646	27894.47236	0.347914411	3.554294732
CHCH1	3	189.97	399.1320538	32.41494431	481406.1776	0	0	98705.09468	0.345033146	2.287350894
TCPG	3	344.99	0	4237.347796	419807.7582	7373.887538	51589.47409	55827.39829	0.342445785	1.885211217
GSCR2	4	165.26	4304.367806	1442.353144	134910.3399	2792.694824	21.04425417	28039.63671	0.340324426	2.188681722
RL24	11	735.49	322207.7208	870325.5528	4100636.399	339789.1816	411618.8524	1093529.538	0.337055123	1.520559901
ATX2L	6	366.47	56290.80765	23285.8282	621618.7474	10275.79864	5527.036502	301483.3553	0.335570862	1.144031766
DLDH	2	130.21	38606.73861	17238.20966	575061.6371	7456.063811	15038.39415	143364.5582	0.311381842	1.92746897
CWC15	7	434.62	24204.19489	67123.52447	1271211.916	10788.52486	9493.688533	436629.6537	0.300368039	1.57631038
NOP16	3	386.64	19371.29931	22854.07835	965287.9179	12177.78038	20450.8859	78377.44787	0.300342876	3.182087831
HNRPU	2	354.96	649.47959	0	97546.96571	2367.458807	6860.563168	4501.213468	0.294807484	2.838419514
ECI2	3	469.71	194.1740958	860.2587756	258254.6821	3655.253638	0	7198.008297	0.288019994	4.578472306
RL23	8	549.21	600629.2195	280155.1907	13566230.99	148440.2075	358869.2129	2200608.289	0.278729798	2.415515675
CH059	2	80.34	336.4611986	2965.761671	330159.8157	0	20303.50923	8805.629401	0.277260919	3.51797848
H3C	2	90.68	21267.88252	4789.607341	337836.6671	19841.47068	15686.18473	8083.351098	0.274274978	3.060754694
TCEA1	2	251.28	1204.013257	6864.717137	225171.9324	98016.39855	9892.807824	0	0.272811081	1.112001373
CN166	4	198.09	40351.51631	822.3364252	473604.4353	93.58354826	4509.741244	133500.1636	0.268408505	1.898201444
RS16	7	465.83	166659.8425	134988.7258	2104096.111	186493.7407	112231.4964	343970.578	0.266968404	1.904275554
LDHB	3	177.52	1434.260544	19903.32299	252108.0739	1765.863782	12880.13092	12466.00142	0.263880376	3.33425091
RAE1L	8	533.54	30294.66842	47083.29105	1111146.725	51069.9901	26732.04131	107661.6265	0.262668387	2.679963447
BAG2	2	171.7	15301.32256	12834.40149	327885.901	583.2792941	38700.06828	77082.89526	0.258447345	1.613292273
NUSAP	5	334.48	28289.23015	57971.48438	585885.6145	10487.81278	55465.93703	158336.4305	0.257229082	1.583408889
RT26	2	38.15	35.39387216	2.945639484	211523.3691	0	0	9691.778787	0.256805061	4.448173246
RS29	2	245.64	19791.90463	306784.1052	2814437.076	47131.58672	19786.94775	618071.5964	0.253818138	2.197074846
PLRG1	3	328.31	0	13962.73989	381210.9995	9227.299327	38475.67275	18611.04607	0.252269433	2.575101299
RUSD3	3	326.92	794.8369688	3441.612958	441008.9106	812.4205472	1109.279448	21806.29013	0.249577409	4.229938771
MAZ	9	523.58	253968.0702	37526.16321	1297036.04	25748.2669	82879.28831	485751.5684	0.24491254	1.418237234
RS18	7	637.21	351602.7786	63098.84191	3319981.788	58917.7636	444318.8968	254097.6107	0.244333109	2.30198383

RM18	2	99.17	292707.9472	1560.239305	414562.4967	9315.364779	4369.201246	105298.4192	0.243890301	2.574685775
TCPZ	2	179.73	785.6225366	504.4722431	78017.5312	29.93943986	1038.618996	12706.84516	0.240406334	2.52536501
TCPD	10	2004.09	73509.01231	121405.2856	7121766.719	26200.93356	207936.7472	534836.9716	0.237912575	3.250181415
ILF2	7	1103.26	135824.0916	23319.32383	4189817.889	34286.65927	18589.86583	700783.9112	0.234754336	2.528684307
PABP4	9	2074.35	24056.19916	75291.47456	1655879.319	16367.35231	9263.514578	733881.2503	0.230750875	1.208512731
UBC12	2	44.93	0	832.2905385	146969.4232	0	0	27653.27328	0.230224934	2.418140832
RM11	9	867.54	151125.3728	209190.2615	3127413.518	90138.53586	182371.7422	813028.4955	0.224984376	1.683876751
H13	5	1500.85	29034.78708	47858.47094	996634.6588	12962.57495	15205.84947	476442.9093	0.216204222	1.089115193
LRC59	3	385.18	2308.410025	1436.621264	2248647.759	2806.613199	3906.844135	12404.58578	0.214311399	6.880379768
ANXA5	4	524.61	9319.635153	4423.553482	756678.2026	4425.706093	2934.680728	102253.474	0.208025046	2.81321752
RL39	4	156.19	1182920.235	29542.99612	5443035.607	539746.1887	21356.66003	747627.7105	0.207916684	2.346378695
TCPB	6	1005.82	6187.943111	123018.3045	1018627.197	3151.074685	171763.2511	69939.57323	0.203037301	2.228920242
RS5	5	711.7	43686.74395	18559.91698	1241139.393	92099.47641	63118.72208	20555.59642	0.201451414	2.890472554
NUP50	2	130.82	0	290.045336	125613.1616	836.9350926	311.755658	27784.65194	0.200177589	2.121510117
PUR6	3	414.37	0	1379.463089	363458.0133	3917.621284	773.9031583	48035.2728	0.199423584	2.79064566
RM16	2	130.3	1258.118524	0	385862.7039	20158.34559	524.1948198	11621.5325	0.194813116	3.582995932
RT17	5	514.22	31384.02708	31368.68112	5675358.482	115014.6319	559427.7922	1438319.943	0.190255218	1.441445415
FBRL	9	591.73	56038.10845	44233.65465	2114030.434	39266.9082	144545.3401	129949.4515	0.189567846	2.819110966
WBP11	3	128.54	190.4402564	39436.97706	212852.958	27180.56644	21265.07384	66364.76136	0.189037215	1.136917901
RL36	5	324.02	16893.69453	21957.30289	2159382.515	20107.06041	4595.047123	416151.9453	0.187903782	2.31797162
RL6	12	1215.91	89194.67067	130598.4888	6744180.292	26359.6608	61646.17888	2701052.268	0.184910139	1.320132711
RS6	5	577.24	21935.78239	19563.13094	1098232.569	2039.149188	65734.97938	225429.7413	0.18016579	1.958717919
NDUS3	2	412.34	82.00785534	1308.376665	336075.4959	1347.559789	33.79957874	11929.76846	0.177919829	4.664036927
PRC2A	8	601.51	54077.99927	49269.27377	2182502.024	43741.65679	29699.57999	532443.6898	0.174453324	1.915614573
PRDX6	2	389.29	5824.340736	111.3381708	414853.7558	2581.596323	1076.176879	3524.981782	0.174310921	5.872417368
RS25	8	820.46	288740.1475	318635.3012	19656627.9	96942.49295	143057.6572	9122771.33	0.166049349	1.113911669
CCD86	6	497.8	82941.98936	813.8838954	907277.9591	1216.727289	11919.17867	175319.1642	0.158360819	2.3947137
SLIRP	5	668.2	310784.3238	479724.4919	5915759.285	272630.6668	469694.333	1770659.321	0.158128141	1.41610849

RPC4	4	104.04	11139.45825	858.1228715	348395.3874	48379.81885	16775.21623	38193.96134	0.157458402	1.802046484
RS27	3	274.5	991.927907	13671.51179	2260848.945	15463.82479	75866.09265	605444.2587	0.156517214	1.707428378
RL19	4	433.41	62435.78477	45337.5899	807403.8942	13225.46156	102706.4427	334549.4187	0.153334319	1.022583926
RS11	20	1847.17	1041608.405	287012.4994	32962019.51	453840.1356	463438.894	6099591.553	0.153094092	2.288915189
HNRPR	2	425.57	15066.98252	27719.90786	328680.6884	23793.93311	17731.20257	88379.63916	0.152454428	1.51578184
PPIB	6	454.8	2537.129537	1021660.158	1691987.663	239815.8839	458290.2208	521903.225	0.152171828	1.154689538
NDUV2	4	169.89	1047.149669	0	299957.7591	285.4170822	1061.773122	82364.44795	0.149214841	1.846286899
TPP1	2	250.38	251.9888728	12388.1215	665143.3869	36496.12138	7205.344898	143031.2791	0.147697288	1.85984957
CNBP	5	426.62	0	78869.13605	20485.00854	6406.292553	1599.38971	6987.023579	0.145592045	2.728319371
RL34	3	189.71	20753.54309	399229.7033	199775.3846	164306.7962	75411.48874	42751.15199	0.144733685	1.133611681
TCPH	2	214.33	54.15194008	5736.654566	142023.8674	921.0552625	1101.108238	2917.09935	0.144590569	4.903349941
DHB4	3	330.81	4432.67773	1416.267286	584326.227	21480.8691	17822.31852	85931.85094	0.141677606	2.23650497
RM33	4	577.42	6716.397905	97896.38463	3042663.647	2369.810485	39473.18832	1278996.567	0.136544646	1.252648656
ATPO	4	454.17	55259.28899	24711.84198	9426964.058	23943.06679	14640.81302	2377041.832	0.136457386	1.976583391
TCPQ	8	664.98	14219.49543	85381.03168	1975596.814	9917.601685	152123.0448	234553.0973	0.13441194	2.387514712
MZT2B	2	174.18	63937.87193	261.8027504	365858.108	1795.271526	6879.219477	38154.61604	0.133750456	3.19905308
HSP7C	14	2842.54	2231284.922	1898931.789	36935884.08	1382029.798	2623007.2	12907186.78	0.125958971	1.279881599
ODP2	8	954.55	21889.34142	42846.02153	4381255.937	9885.771108	136902.8334	389142.9612	0.125900378	3.052384429
NOL7	2	63.6	0	15320.24048	252236.2454	0	7009.940392	3269.580222	0.124224849	4.701998611
NEP1	4	478.6	6757.192113	38007.10654	591549.5441	121230.6922	57320.30354	82806.68287	0.122895923	1.283712961
RT22	4	259.98	19373.56347	8107.176561	345618.2378	10297.82793	14053.97568	99163.7614	0.121008225	1.594865551
TIM13	5	542.38	7314.087445	97593.34525	1583209.303	83956.37464	130971.5206	506560.136	0.117710769	1.226367305
NOP2	2	121.91	645.1354719	4160.317795	113036.3068	17744.20132	23400.36736	3475.464117	0.116435222	1.401087404
RM46	2	276.75	1542.36332	0	397124.6368	676.3158918	1491.544303	13891.12799	0.114346153	4.633731288
RM12	5	506.56	21264.83129	99372.11731	27610590.42	4687.77731	176572.5054	4493041.101	0.112954707	2.568688808
PRDX1	9	725.53	75631.01433	104877.3735	3393229.781	44546.75383	139521.1036	1041372.327	0.112843159	1.544133873
RL26;1::sp	4	1766.26	65028.31624	63582.71303	6607550.977	31796.40626	70558.9224	1943503.322	0.11116462	1.719220364
PSMD9	5	429.31	16907.85817	19955.68764	692347.5956	23889.02085	12581.65858	205283.1679	0.108646953	1.592797755

GAMC	3	117.1	49.74049152	6144.805299	1359371.841	39765.17175	14715.27896	10325.91359	0.108249959	4.397220143
ATPA	5	585.69	22500.50375	85899.59422	1153686.376	36845.40491	150572.8055	132825.1752	0.107445195	1.978570084
RS20	6	646.42	579.0077153	61612.4528	9176648.32	33027.11146	56765.547	2557110.729	0.103553661	1.803406151
ALDOA_RABIT	8	942.64	79905.08116	234720.4892	3842447.884	613761.5173	464878.2043	612779.3888	0.090882038	1.297334056
RRP1B	14	1122.6	84469.21361	45163.02797	6040654.025	24206.46652	69612.39399	2827096.248	0.088549589	1.078916995
ODO2	2	222.64	255.2390504	5412.387	296529.0073	998.9872516	8353.036221	10118.87445	0.085880124	3.956096266
RL29	11	1005.06	1678668.57	332188.2173	73744298.86	1663107.619	3195759.42	27629947.79	0.082831186	1.221400961
L10K	5	221.39	619.5363638	29177.75714	754418.3965	4182.273806	2801.669346	207490.8138	0.082275413	1.87044265
H2A1	3	263.47	61890.04989	183868.0189	7943892.775	120160.0035	91195.4997	2397912.99	0.080541121	1.650156541
RM30	3	339.08	20136.18048	36137.62977	4936378.793	12693.45351	49342.48046	1260720.449	0.080497665	1.916259146
RL10A	4	222.81	32340.1257	663.2119757	695842.5463	69347.15917	17371.20699	2766.563627	0.079456668	3.025897143
RRP15	2	43.27	0	0	52726.49102	0	0	2270.837328	0.077392675	4.537231721
RM53	7	576.9	48897.61312	68747.74905	5282086.136	40524.17816	70774.87065	1764249.682	0.07704076	1.525574923
RM49	2	346.44	8400.430176	13178.89384	616933.3299	18549.26459	7197.301219	173381.0573	0.076539001	1.681021845
K1M1_SHEEP	2	97.03	823322.0116	1884.450008	2466.076575	56985.25759	2087.991099	8080.454361	0.07330154	3.623521229
RADI	3	292.8	1276.820321	2793.724434	344340.7173	11824.21741	3608.911776	9552.921937	0.072069053	3.801596442
RL26L	2	1535.13	147.2170475	0	581751.2698	0	52.82109283	64025.16671	0.071104375	3.182866745
CETN2	3	279.76	1488.701207	61705.01624	2249022	15542.4189	68017.29577	803870.9601	0.068420337	1.381569673
CALL5	5	829.63	31663.57775	137455.319	2712466.561	88099.63343	39461.05163	1282412.538	0.067430128	1.031195042
AIFM1	8	791.58	12785.04357	53534.93217	1619764.06	41086.60702	27209.24747	383046.1809	0.066844612	1.901383389
RM50	4	308.15	22802.22121	9684.061411	2314162.59	106489.0868	32849.50774	53959.06661	0.066743098	3.601705903
HSP71	13	4839.79	313937.9202	549129.7105	39993281.67	331431.4626	769334.5772	9476648.281	0.066488475	1.949573299
RBM42	4	714.33	3431.925232	2611.17898	2383359.171	5091.92704	16166.33982	1135716.613	0.061696366	1.046292222
SZRD1	3	175.07	46765.84424	1532.137108	357323.342	6074.83052	9951.534515	167850.4229	0.056155024	1.141394126
NDUF3	2	168.47	3905.438277	2252.612087	232103.678	7094.32273	2380.497681	52372.59143	0.056003722	1.945762104
PKRI1	2	223.75	4018.840649	0	0	687.1336117	0	0	0.052702406	2.548116814
EAF6	2	402.41	0	6108.586332	463840.9979	49.0997585	1772.162761	130588.2683	0.051275839	1.827499023
RUVB1	3	277.01	7454.966311	61580.10777	497283.4449	89259.21614	40186.13658	108876.1436	0.049103582	1.248704621

RSMN	8	525.57	52909.06267	4783.536683	3587504.42	14275.12229	12569.84025	1746605.611	0.048103374	1.03943767
SMD2	9	815.58	161202.6051	423803.4386	13700545.07	184768.7434	404060.9541	6118897.468	0.04773414	1.090660781
RT23	5	384.75	18086.71816	26934.47996	959249.5559	74024.30344	12153.41793	273335.9389	0.047215049	1.482029782
RS4X	12	1341.34	266787.3504	703801.3498	10555095.59	1237808.613	861814.4661	2931704.002	0.044819997	1.195841521
RM40	11	1137.06	59202.59249	74669.1711	30088552.55	204598.2707	154716.5644	10926309.05	0.044214512	1.421133218
MO4L2	5	426.83	70121.64595	39704.88898	879517.1858	45786.37813	112930.1598	327320.9936	0.037661068	1.025404111
MAP4	13	1275.28	31002.13332	155975.338	2199883.516	114820.4676	83991.45317	696461.5392	0.036938333	1.414714221
MIC25	5	232.22	17325.64742	28300.04572	585606.8654	51499.58727	83650.97443	46465.28194	0.036516693	1.797281556
CN142	2	377.38	574.8183629	1769.320016	767076.025	898.6720897	7774.952562	241464.5037	0.031330256	1.621046654
RS30	5	469.49	196217.0826	317834.8634	54553256.91	258417.5316	307780.9791	23915915.66	0.027913362	1.169467957
ATPB	8	1084.52	32882.6668	88180.54767	2741527.691	185303.1278	118448.3316	261451.0331	0.026790133	2.340481776
RM48	3	222.52	1013.053001	1892.257122	448590.4172	22513.51431	628.6164117	35253.1409	0.026255291	2.950788874
RT11	5	484.85	19862.43716	3045.230341	3134389.963	9643.404158	9827.465578	1092768.889	0.025965265	1.505222451
RL8	10	1196.15	156599.4109	24340.62926	11167457.57	78889.61242	68729.43924	4627639.92	0.02589878	1.248837724
DECR	4	267.39	1095.17304	711.6874345	1986432.575	25400.05935	11591.77791	9504.368047	0.025484544	5.418234717
RL18A	5	284.29	9569.732586	0	601877.4624	113761.2116	173063.6648	0	0.023227164	1.092057757
NDUS6	5	651.41	45356.58798	94302.96016	3628291.079	125019.4178	175997.0266	912573.3627	0.01920719	1.634499187
HMGB3	3	116.21	2764.822217	630.1648205	391238.2569	22324.78987	6399.830654	6646.368224	0.018486765	3.479874041
RM27	8	804.78	53202.57721	30865.51652	4353742.211	104427.6979	92983.44477	973617.1645	0.017748165	1.92207205
TFAM	8	619.58	33084.36566	109513.1919	3542728.364	334309.849	37371.65836	1353183.432	0.017443821	1.095308813
CH60	16	2119.53	50512.22841	177118.5022	5617752.563	152843.9592	313216.8359	1329032.963	0.016878314	1.70323843
RL7A	15	1180.14	46470.00832	68067.1145	16977133.87	69729.70612	170777.4276	3382447.501	0.014170616	2.238054805
NDUA7	4	489.3	6003.177168	7257.224809	1348364.958	16934.16481	18553.40545	238632.5962	0.013622064	2.312449439
FUBP2	3	281.69	1646.485024	0	271445.8257	0	14524.55348	58941.32457	0.013460215	1.894242457
KNOP1	3	344.24	99.55676848	9264.101378	192975.5358	1375.459289	3321.386324	29970.67561	0.012118014	2.545119212
CDC5L	6	394.93	257127.5667	2033.469535	894909.265	140662.539	199278.5544	20700.49781	0.011926849	1.678093418
RS27A	2	1136.52	55.97676721	6643.764464	2996064.962	3483.214521	717.7935609	666214.0282	0.011739125	2.163165018
C1QBP	12	2532.82	4663150.473	5149154.641	301925543.4	4611073.482	10128748.46	130502771.6	0.011188956	1.101868728

LBR	3	264.33	2865.734436	31862.5971	720113.4792	33390.01468	85903.10905	26381.32755	0.009399217	2.37342646
RL31	18	1625.83	990674.5097	563983.9765	165393276.8	865097.856	1901116.778	47510818.7	0.008421317	1.731426822
RS13	7	342.94	165566.696	108891.8948	13040581.44	338274.9795	258954.6147	2980815.153	0.00669407	1.895813431
RPA34	6	937.12	158510.8674	537.1006512	2492325.787	95456.03659	25346.56721	76091.10377	0.006162489	3.751251146
GRPE1	5	398.86	18479.01281	184233.9991	2632336.844	375444.5525	45112.63794	563577.9351	0.004216963	1.526445784
PRDX3	4	412.73	8725.855792	329610.5264	5731049.364	65251.36328	144651.8569	1764526.44	0.000529848	1.620114544

Shown are cellular proteins identified by label-free mass spectrometry/mass spectrometry that interact with GFP-4bM. Protein identifier (ID), protein name and number of unique peptides used to identify proteins are indicated. Confidence score is the score of the probability of the unique peptide sequence occurring randomly, added together for each unique peptide. The higher the confidence score, the higher the confidence in protein identification. The -Log2 p value is a comparison of the cellular protein abundance between GFP-4bM and GFP. The higher the p value, the higher the probability the protein interacts with 4bM. The fold-change is the change in the abundance of the cellular protein between GFP-4bM and GFP. Cellular proteins which appear in both GFP-4bM and 4bM-GFP data are labelled with an asterisk (*).

8. References

Abraham, S., T. E. Kienzle, W. Lapps and D. A. Brian (1990). "Deduced Sequence of the Bovine Coronavirus Spike Protein and Identification of the Internal Proteolytic Cleavage Site." Virology **176**(1): 296-301.

Adam Balint, A. F., Akos Hornyak, Laszlo Dencso, Fernando Almazan, Luis Enjuanes, Sandor Beak, Zoltan Zadori (2014). "Invesigation of the role of ORF3abc in the in vitro and in vivo tropism of FCoV." Salamanca Nidovirus 2014 Poster S7.P-04.

Alcami, A. and U. H. Koszinowski (2000). "Viral mechanisms of immune evasion." Trends in Microbiology **8**(9): 410-418.

Annelike Dedeurwaerder, D. D. A., Dominique A. J. Olslaegaers, Lowiese M. B. Desmarets, inge D. M. Roukaerts, Sebastiaan Theuns and Hans J. Nauwynck (2014). "ORF7-Encoded accessory protein 7a of feline infectious peritonitis virus as a counteragent against IFN-alpha-induced antiviral reponse."

Ariumi, Y., M. Kuroki, Y. Kushima, K. Osugi, M. Hijikata, M. Maki, M. Ikeda and N. Kato (2011). "Hepatitis C Virus Hijacks P-Body and Stress Granule Components around Lipid Droplets." Journal of Virology **85**(14): 6882-6892.

Asif, M., J. W. Lowenthal, M. E. Ford, K. A. Schat, W. G. Kimpton and A. G. Bean (2007). "Interleukin-6 expression after infectious bronchitis virus infection in chickens." Viral Immunol **20**(3): 479-486.

Balagopal, V. and R. Parker (2009). "Polysomes, P bodies and stress granules: states and fates of eukaryotic mRNAs." Curr Opin Cell Biol **21**(3): 403-408.

Barber, G. N. (2001). "Host defense, viruses and apoptosis." Cell Death Differ **8**(2): 113-126.

Barber, M. R. W., J. R. Aldridge, R. G. Webster and K. E. Magor (2013). "Association of RIG-I with innate immunity of ducks to influenza (vol 107,pg 5913,2010)." Proceedings of the National Academy of Sciences of the United States of America **110**(19): 7958-7958.

Beato, M. S., C. De Battisti, C. Terregino, A. Drago, I. Capua and G. Ortali (2005). "Evidence of circulation of a Chinese strain of infectious bronchitis virus (QXIBV) in Italy." Vet Rec **156**(22): 720.

Beaudette, R. H., C (1937). "Cultivation of the virus of infectious bronchitis." J. Am. Vet. Med. Assoc **90**: 51-60.

Beckham, C. J. and R. Parker (2008). "P bodies, stress granules, and viral life cycles." Cell Host & Microbe **3**(4): 206-212.

Belmokhtar, C. A., J. Hillion and E. Segal-Bendirdjian (2001). "Staurosporine induces apoptosis through both caspase-dependent and caspase-independent mechanisms." Oncogene **20**(26): 3354-3362.

Belouzard, S., J. K. Millet, B. N. Licitra and G. R. Whittaker (2012). "Mechanisms of Coronavirus Cell Entry Mediated by the Viral Spike Protein." Viruses-Basel **4**(6): 1011-1033.

Benedict, C. A., P. S. Norris and C. F. Ware (2002). "To kill or be killed: viral evasion of apoptosis." Nature Immunology **3**(11): 1013-1018.

Bentley, K., S. M. Keep, M. Armesto and P. Britton (2013). "Identification of a noncanonically transcribed subgenomic mRNA of infectious bronchitis virus and other gammacoronaviruses." J Virol **87**(4): 2128-2136.

Bergmann, M., A. Garcia-Sastre, E. Carnero, H. Pehamberger, K. Wolff, P. Palese and T. Muster (2000). "Influenza virus NS1 protein counteracts PKR-mediated inhibition of replication." J Virol **74**(13): 6203-6206.

Bertram, R., M. G. Pedersen, D. S. Luciani and A. Sherman (2006). "A simplified model for mitochondrial ATP production." Journal of Theoretical Biology **243**(4): 575-586.

Bhardwaj, K., P. H. Liu, J. L. Leibowitz and C. C. Kao (2012). "The Coronavirus Endoribonuclease Nsp15 Interacts with Retinoblastoma Tumor Suppressor Protein." Journal of Virology **86**(8): 4294-4304.

Boscarino, J. A., H. L. Logan, J. J. Lacny and T. M. Gallagher (2008). "Envelope protein palmitoylations are crucial for murine coronavirus assembly." Journal of Virology **82**(6): 2989-2999.

Bosch, B. J., R. van der Zee, C. A. M. de Haan and P. J. M. Rottier (2003). "The coronavirus spike protein is a class I virus fusion protein: Structural and functional characterization of the fusion core complex." Journal of Virology **77**(16): 8801-8811.

Box, P. G., A. V. Beresford and B. Roberts (1980). "Protection of Laying Hens against Infectious-Bronchitis with Inactivated Emulsion Vaccines." Veterinary Record **106**(12): 264-268.

Brierley, I., M. E. Boursnell, M. M. Binns, B. Bilimoria, V. C. Blok, T. D. Brown and S. C. Inglis (1987). "An efficient ribosomal frame-shifting signal in the polymerase-encoding region of the coronavirus IBV." EMBO J **6**(12): 3779-3785.

Brierley, I., P. Digard and S. C. Inglis (1989). "Characterization of an Efficient Coronavirus Ribosomal Frameshifting Signal - Requirement for an Rna Pseudoknot." Cell **57**(4): 537-547.

Britton, P., R. Casais, T. Hodgson, M. Davis and D. Cavanagh (2006). "Genes 3 and 5 of infectious bronchitis virus are accessory protein genes." Adv Exp Med Biol **581**: 363-368.

Britton, P., P. Green, S. Kottier, K. L. Mawditt, Z. Penzes, D. Cavanagh and M. A. Skinner (1996). "Expression of bacteriophage T7 RNA polymerase in avian and mammalian cells by a recombinant fowlpox virus." J Gen Virol **77 (Pt 5)**: 963-967.

Britton, P. C., D. (2007). Avian coronavirus diseases and infectious bronchitis vaccine development. Coronaviruses: molecular and cellular biology. Norfolk, United Kingdom, Caister Academic Press**:** p 161–181.

Bruey, J. M., C. Ducasse, P. Bonniaud, L. Ravagnan, S. A. Susin, C. Diaz-Latoud, S. Gurbuxani, A. P. Arrigo, G. Kroemer, E. Solary and C. Garrido (2000). "Hsp27 negatively regulates cell death by interacting with cytochrome c." Nature Cell Biology **2**(9): 645-652.

Bryantsev, A. L., S. Y. Kurchashova, S. A. Golyshev, V. Y. Polyakov, H. F. Wunderink, B. Kanon, K. R. Budagova, A. E. Kabakov and H. H. Kampinga (2007). "Regulation of stress-induced intracellular sorting and chaperone function of Hsp27 (HspB1) in mammalian cells." Biochem J **407**(3): 407-417.

Buchan, J. R. and R. Parker (2009). "Eukaryotic stress granules: the ins and outs of translation." Mol Cell **36**(6): 932-941.

Burgess, H. M., W. A. Richardson, R. C. Anderson, C. Salaun, S. V. Graham and N. K. Gray (2011). "Nuclear relocalisation of cytoplasmic poly(A)-binding proteins PABP1 and PABP4 in response to UV irradiation reveals mRNA-dependent export of metazoan PABPs." J Cell Sci **124**(Pt 19): 3344-3355.

Calvo, E., D. Escors, J. A. Lopez, J. M. Gonzalez, A. Alvarez, E. Arza and L. Enjuanes (2005). "Phosphorylation and subcellular localization of transmissible gastroenteritis virus nucleocapsid protein in infected cells." Journal of General Virology **86**: 2255-2267.

Campisi, L., R. J. Cummings and J. M. Blander (2014). "Death-Defining Immune Responses After Apoptosis." American Journal of Transplantation **14**(7): 1488-1498.

Cande, C., N. Vahsen, C. Garrido and G. Kroemer (2004). "Apoptosis-inducing factor (AIF): caspase-independent after all." Cell Death and Differentiation **11**(6): 591-595.

Casais, R., M. Davies, D. Cavanagh and P. Britton (2005). "Gene 5 of the avian coronavirus infectious bronchitis virus is not essential for replication." J Virol **79**(13): 8065-8078.

Casais, R., B. Dove, D. Cavanagh and P. Britton (2003). "Recombinant avian infectious bronchitis virus expressing a heterologous spike gene demonstrates that the spike protein is a determinant of cell tropism." Journal of Virology **77**(16): 9084-9089.

Casais, R., V. Thiel, S. G. Siddell, D. Cavanagh and P. Britton (2001). "Reverse genetics system for the avian coronavirus infectious bronchitis virus." Journal of Virology **75**(24): 12359-12369.

Castanier, C., D. Garcin, A. Vazquez and D. Arnoult (2010). "Mitochondrial dynamics regulate the RIG-I-like receptor antiviral pathway." EMBO Rep **11**(2): 133-138.

Castanier, C., N. Zemirli, A. Portier, D. Garcin, N. Bidere, A. Vazquez and D. Arnoult (2012). "MAVS ubiquitination by the E3 ligase TRIM25 and degradation by the proteasome is involved in type I interferon production after activation of the antiviral RIG-I-like receptors." Bmc Biology **10**.

Cavanagh, D. (1983). "Coronavirus Ibv Glycopolypeptides - Size of Their Polypeptide Moieties and Nature of Their Oligosaccharides." Journal of General Virology **64**(May): 1187-1191.

Cavanagh, D., and Naqi, S (2003). Infectious bronchitis. In Diseases of Poultry, Iowa State University Press**:** p 101-119.

Cavanagh, D., R. Casais, M. Armesto, T. Hodgson, S. Izadkhasti, M. Davies, F. Lin, I. Tarpey and P. Britton (2007). "Manipulation of the infectious bronchitis coronavirus genome for vaccine development and analysis of the accessory proteins." Vaccine **25**(30): 5558-5562.

Cavanagh, D., R. Casais, M. Armesto, T. Hodgson, S. Izadkhasti, D. Marc, F. Lin, I. Tarpey and P. Britton (2007). "Manipulation of the infectious bronchitis coronavirus genome for vaccine development and analysis of the accessory proteins." Vaccine **25**(30): 5558-5562.

Cavanagh, D., K. Mawditt, D. D. Welchman, P. Britton and R. E. Gough (2002). "Coronaviruses from pheasants (Phasianus colchicus) are genetically closely related to coronaviruses of domestic fowl (infectious bronchitis virus) and turkeys." Avian Pathology **31**(1): 81-93.

Chalfie, M. (2001). Cell Markers: Green Fluorescent Protein (GFP) A2 - Brenner, Sydney. Encyclopedia of Genetics. J. H. Miller. New York, Academic Press**:** 311-313.

Chen, B. Y., S. Hosi, T. Nunoya and C. Itakura (1996). "Histopathology and immunohistochemistry of renal lesions due to infectious bronchitis virus in chicks." Avian Pathology **25**(2): 269-283.

Chen, C. C., J. Kruger, I. Sramala, H. J. Hsu, P. Henklein, Y. M. A. Chen and W. B. Fischer (2011). "ORF8a of SARS-CoV forms an ion channel: Experiments and molecular dynamics simulations." Biochimica Et Biophysica Acta-Biomembranes **1808**(2): 572-579.

Chen, Y., H. Cai, J. Pan, N. Xiang, P. Tien, T. Ahola and D. Y. Guo (2009). "Functional screen reveals SARS coronavirus nonstructural protein nsp14 as a novel cap N7 methyltransferase." Proceedings of the National Academy of Sciences of the United States of America **106**(9): 3484-3489.

Chen, Y., C. Y. Su, M. Ke, X. Jin, L. R. Xu, Z. Zhang, A. D. Wu, Y. Sun, Z. N. Yang, P. Tien, T. Ahola, Y. Liang, X. Q. Liu and D. Y. Guo (2011). "Biochemical and Structural Insights into the Mechanisms of SARS Coronavirus RNA Ribose 2 '-O-Methylation by nsp16/nsp10 Protein Complex." Plos Pathogens **7**(10).

Cheng, E. H. Y., T. V. Sheiko, J. K. Fisher, W. J. Craigen and S. J. Korsmeyer (2003). "VDAC2 inhibits BAK activation and mitochondrial apoptosis." Science **301**(5632): 513-517.

Cheng, E. H. Y., T. V. Sheiko, J. K. Fisher, W. J. Craigen and S. J. Korsmeyer (2004). "VDAC2 inhibits BAK activation and mitochondrial apoptosis." Biophysical Journal **86**(1): 516a-516a.

Chhabra, R., J. Chantrey and K. Ganapathy (2015). "Immune Responses to Virulent and Vaccine Strains of Infectious Bronchitis Viruses in Chickens." Viral Immunol **28**(9): 478-488.

Choesmel, V., S. Fribourg, A. H. Aguissa-Toure, N. Pinaud, P. Legrand, H. T. Gazda and P. E. Gleizes (2008). "Mutation of ribosomal protein RPS24 in Diamond-Blackfan anemia results in a ribosome biogenesis disorder." Hum Mol Genet **17**(9): 1253-1263.

Clementz, M. A., Z. B. Chen, B. S. Banach, Y. H. Wang, L. Sun, K. Ratia, Y. M. Baez-Santos, J. Wang, J. Takayama, A. K. Ghosh, K. Li, A. D. Mesecar and S. C. Baker (2010). "Deubiquitinating and Interferon Antagonism Activities of Coronavirus Papain-Like Proteases." Journal of Virology **84**(9): 4619-4629.

Cohen, G. M. (1997). "Caspases: the executioners of apoptosis." Biochemical Journal **326**: 1-16.

Concannon, C. G., S. Orrenius and A. Samali (2001). "Hsp27 inhibits cytochrome c-mediated caspase activation by sequestering both pro-caspase-3 and cytochrome c." Gene Expression **9**(4-5): 195-201.

Cormican, P., A. T. Lloyd, T. Downing, S. J. Connell, D. Bradley and C. O'Farrelly (2009). "The avian Toll-Like receptor pathway-Subtle differences amidst general conformity." Developmental and Comparative Immunology **33**(9): 967-973.

Corse, E. and C. E. Machamer (2000). "Infectious bronchitis virus E protein is targeted to the Golgi complex and directs release of virus-like particles." Journal of Virology **74**(9): 4319-4326.

Corse, E. and C. E. Machamer (2002). "The cytoplasmic tail of infectious bronchitis virus E protein directs Golgi targeting." Journal of Virology **76**(3): 1273-1284.

Corse, E. and C. E. Machamer (2003). "The cytoplasmic tails of infectious bronchitis virus E and M proteins mediate their interaction." Virology **312**(1): 25-34.

Cruz, J. L. G., I. Sola, M. Becares, B. Alberca, J. Plana, L. Enjuanes and S. Zuniga (2011). "Coronavirus Gene 7 Counteracts Host Defenses and Modulates Virus Virulence." Plos Pathogens **7**(6).

Cunningham, C. H. and H. O. Stuart (1947). "Cultivation of the Virus of Infectious Bronchitis of Chickens in Embryonated Chicken Eggs." American Journal of Veterinary Research **8**(27): 209-212.

Dalton, K., R. Casais, K. Shaw, K. Stirrups, S. Evans, P. Britton, T. D. Brown and D. Cavanagh (2001). "cis-acting sequences required for coronavirus infectious bronchitis virus defective-RNA replication and packaging." J Virol **75**(1): 125-133.

Dauber, B. and T. Wolff (2009). "Activation of the Antiviral Kinase PKR and Viral Countermeasures." Viruses-Basel **1**(3): 523-544.

Davelaar, F. G., B. Kouwenhoven and A. G. Burger (1984). "Occurrence and significance of infectious bronchitis virus variant strains in egg and broiler production in the Netherlands." Vet Q **6**(3): 114-120.

Davies, M. (2009). "Subcellular location and protein interactions of the infectious bronchitis virus gene 3 and 5 accessory proteins." University of Warwick.

Davies, M. T. (2009). Subcellular location and protein interactions of the infectious bronchitis virus gene 3 and 5 accessory proteins. PhD thesis, University of Warwick.

de Haan, C. A., P. S. Masters, X. Shen, S. Weiss and P. J. Rottier (2002). "The group-specific murine coronavirus genes are not essential, but their deletion, by reverse genetics, is attenuating in the natural host." Virology **296**(1): 177-189.

Decker, C. J. and R. Parker (2012). "P-Bodies and Stress Granules: Possible Roles in the Control of Translation and mRNA Degradation." Cold Spring Harbor Perspectives in Biology **4**(9).

Decroly, E., I. Imbert, B. Coutard, M. L. Bouvet, B. Selisko, K. Alvarez, A. E. Gorbalenya, E. J. Snijder and B. Canard (2008). "Coronavirus nonstructural

protein 16 is a cap-0 binding enzyme possessing (nucleoside-2'O)-methyltransferase activity." Journal of Virology **82**(16): 8071-8084.

Dedeurwaerder, A., L. M. Desmarets, D. A. J. Olyslaegers, B. L. Vermeulen, H. L. Dewerchin and H. J. Nauwynck (2013). "The role of accessory proteins in the replication of feline infectious peritonitis virus in peripheral blood monocytes." Veterinary Microbiology **162**(2-4): 447-455.

Defra (2002). Economic assessment of livestock diseases in Great Britain, University of Reading.

Degroot, R. J., W. Luytjes, M. C. Horzinek, B. A. M. Vanderzeijst, W. J. M. Spaan and J. A. Lenstra (1987). "Evidence for a Coiled-Coil Structure in the Spike Proteins of Coronaviruses." Journal of Molecular Biology **196**(4): 963-966.

Delmas, B. and H. Laude (1990). "Assembly of Coronavirus Spike Protein into Trimers and Its Role in Epitope Expression." Journal of Virology **64**(11): 5367-5375.

Denison, M. R. (2008). "Seeking membranes: positive-strand RNA virus replication complexes." PLoS Biol **6**(10): e270.

Denison, M. R., W. J. M. Spaan, Y. van der Meer, C. A. Gibson, A. C. Sims, E. Prentice and X. T. Lu (1999). "The putative helicase of the coronavirus mouse hepatitis virus is processed from the replicase gene polyprotein and localizes in complexes that are active in viral RNA synthesis." Journal of Virology **73**(8): 6862-6871.

Desmots, F., H. R. Russell, D. Michel and P. J. McKinnon (2008). "Scythe regulates apoptosis-inducing factor stability during endoplasmic reticulum stress-induced apoptosis." Journal of Biological Chemistry **283**(6): 3264-3271.

Edeling, M. A., C. Smith and D. Owen (2006). "Life of a clathrin coat: insights from clathrin and AP structures." Nature Reviews Molecular Cell Biology **7**(1): 32-44.

Egloff, M. P., F. Ferron, V. Campanacci, S. Longhi, C. Rancurel, H. Dutartre, E. J. Snijder, A. E. Gorbalenya, C. Cambillau and B. Canard (2004). "The severe acute respiratory syndrome-coronavirus replicative protein nsp9 is a single-stranded RNA-binding subunit unique in the RNA virus world." Proceedings of the National Academy of Sciences of the United States of America **101**(11): 3792-3796.

Emmott, E., D. Munday, E. Bickerton, P. Britton, M. A. Rodgers, A. Whitehouse, E. M. Zhou and J. A. Hiscox (2013). "The cellular interactome of the coronavirus infectious bronchitis virus nucleocapsid protein and functional implications for virus biology." J Virol **87**(17): 9486-9500.

Fan, H., A. Ooi, Y. W. Tan, S. F. Wang, S. G. Fang, D. X. Liu and J. Lescar (2005). "The nucleocapsid protein of coronavirus infectious bronchitis virus: Crystal

structure of its N-terminal domain and multimerization properties." Structure **13**(12): 1859-1868.

Fang, P. X., L. R. Fang, Y. Y. Hong, X. R. Liu, N. Dong, P. P. Ma, J. Bi, D. Wang and S. B. Xiao (2017). "Discovery of a novel accessory protein NS7a encoded by porcine deltacoronavirus." Journal of General Virology **98**(2): 173-178.

Fang, P. X., L. R. Fang, X. R. Liu, Y. Y. Hong, Y. L. Wang, N. Dong, P. P. Ma, J. Bi, D. Wang and S. B. Xiao (2016). "Identification and subcellular localization of porcine deltacoronavirus accessory protein NS6." Virology **499**: 170-177.

Farsani, S. M. J., R. Dijkman, M. F. Jebbink, H. Goossens, M. Ieven, M. Deijs, R. Molenkamp and L. van der Hoek (2012). "The first complete genome sequences of clinical isolates of human coronavirus 229E." Virus Genes **45**(3): 433-439.

Fischer, F., C. F. Stegen, C. A. Koetzner and P. S. Masters (1997). "Analysis of a recombinant mouse hepatitis virus expressing a foreign gene reveals a novel aspect of coronavirus transcription." Journal of Virology **71**(7): 5148-5160.

Fischer, F., C. F. Stegen, P. S. Masters and W. A. Samsonoff (1998). "Analysis of constructed E gene mutants of mouse hepatitis virus confirms a pivotal role for E protein in coronavirus assembly." J Virol **72**(10): 7885-7894.

Freundt, E. C., L. Yu, E. Park, M. J. Lenardo and X. N. Xu (2009). "Molecular determinants for subcellular localization of the severe acute respiratory syndrome coronavirus open reading frame 3b protein." J Virol **83**(13): 6631-6640.

Fuchs, S. Y. (2012). "Ubiquitination-mediated regulation of interferon responses." Growth Factors **30**(3): 141-148.

Fuentes-Gonzalez, A. M., A. Contreras-Paredes, J. Manzo-Merino and M. Lizano (2013). "The modulation of apoptosis by oncogenic viruses." Virology Journal **10**.

Fung, T. S., Y. Liao and D. X. Liu (2014). "The Endoplasmic Reticulum Stress Sensor IRE1 alpha Protects Cells from Apoptosis Induced by the Coronavirus Infectious Bronchitis Virus." Journal of Virology **88**(21): 12752-12764.

Fung, T. S. and D. X. Liu (2014). "Coronavirus infection, ER stress, apoptosis and innate immunity." Front Microbiol **5**: 296.

Gack, M. U., R. A. Albrecht, T. Urano, K. S. Inn, I. C. Huang, E. Carnero, M. Farzan, S. Inoue, J. U. Jung and A. Garcia-Sastre (2009). "Influenza A Virus NS1 Targets the Ubiquitin Ligase TRIM25 to Evade Recognition by the Host Viral RNA Sensor RIG-I." Cell Host & Microbe **5**(5): 439-449.

Galan, C., I. Sola, A. Nogales, B. Thomas, A. Akoulitchev, L. Enjuanes and F. Almazan (2009). "Host cell proteins interacting with the 3 ' end of TGEV coronavirus genome influence virus replication." Virology **391**(2): 304-314.

Galati, D., S. Srinivasan, H. Raza, S. K. Prabu, M. Hardy, K. Chandran, M. Lopez, B. Kalyanaraman and N. G. Avadhani (2009). "Role of nuclear-encoded subunit Vb in the assembly and stability of cytochrome c oxidase complex: implications in mitochondrial dysfunction and ROS production." Biochem J **420**(3): 439-449.

Garcia-Bonilla, L., C. Cid, A. Alcazar, J. Burda, I. Ayuso and M. Salinas (2007). "Regulatory proteins of eukaryotic initiation factor 2-alpha subunit (eIF2 alpha) phosphatase, under ischemic reperfusion and tolerance." J Neurochem **103**(4): 1368-1380.

Geng, H., Y. M. Liu, W. S. Chan, A. W. Lo, D. M. Au, M. M. Waye and Y. Y. Ho (2005). "The putative protein 6 of the severe acute respiratory syndrome-associated coronavirus: expression and functional characterization." FEBS Lett **579**(30): 6763-6768.

Goldsmith, C. S., K. M. Tatti, T. G. Ksiazek, P. E. Rollin, J. A. Comer, W. W. Lee, P. A. Rota, B. Bankamp, W. J. Bellini and S. R. Zaki (2004). "Ultrastructural characterization of SARS coronavirus." Emerging Infectious Diseases **10**(2): 320-326.

Gosert, R., A. Kanjanahaluethai, D. Egger, K. Bienz and S. C. Baker (2002). "RNA replication of mouse hepatitis virus takes place at double-membrane vesicles." J Virol **76**(8): 3697-3708.

Graham, R. L., A. C. Sims, S. M. Brockway, R. S. Baric and M. R. Denison (2005). "The nsp2 replicase proteins of murine hepatitis virus and severe acute respiratory syndrome coronavirus are dispensable for viral replication." Journal of Virology **79**(21): 13399-13411.

Grant, C. E., M. Z. Vasa and R. G. Deeley (1995). "Cirf-3, a New Member of the Interferon Regulatory Factor (Irf) Family That Is Rapidly and Transiently Induced by Dsrna." Nucleic Acids Research **23**(12): 2137-2146.

Guy, J. S. (2000). "Turkey coronavirus is more closely related to avian infectious bronchitis virus than to mammalian coronaviruses: a review." Avian Pathology **29**(3): 207-212.

Hagemeijer, M. C., A. M. Vonk, I. Monastyrska, P. J. M. Rottier and C. A. M. de Haan (2012). "Visualizing Coronavirus RNA Synthesis in Time by Using Click Chemistry." Journal of Virology **86**(10): 5808-5816.

Haijema, B. J., H. Volders and P. J. M. Rottier (2004). "Live, attenuated coronavirus vaccines through the directed deletion of group-specific genes provide protection against feline infectious peritonitis." Journal of Virology **78**(8): 3863-3871.

Haller, O. and G. Kochs (2011). "Human MxA protein: an interferon-induced dynamin-like GTPase with broad antiviral activity." J Interferon Cytokine Res **31**(1): 79-87.

Han Di, J. C. M., Esther K. Morantz, Rachel Graham, and S. B. Ralph, M. A. Brinton (2017). Identification of functional transcription regulatory sequences (TRS) in the SHFV genome by next generation sequencing. Georgia State University, Atlanta, GA, Nidovirus Conference 2017.

Hartshorne, D. J., M. Ito and F. Erdodi (2004). "Role of protein phosphatase type 1 in contractile functions: myosin phosphatase." J Biol Chem **279**(36): 37211-37214.

Hatada, E. and R. Fukuda (1992). "Binding of Influenza-a Virus Ns1 Protein to Dsrna Invitro." Journal of General Virology **73**: 3325-3329.

Havasi, A., Z. J. Li, Z. Y. Wang, J. L. Martin, V. Botla, K. Ruchalski, J. H. Schwartz and S. C. Borkan (2008). "Hsp27 inhibits Bax activation and apoptosis via a phosphatidylinositol 3-kinase-dependent mechanism." Journal of Biological Chemistry **283**(18): 12305-12313.

Hendrickx, A., M. Beullens, H. Ceulemans, T. Den Abt, A. Van Eynde, E. Nicolaescu, B. Lesage and M. Bollen (2009). "Docking Motif-Guided Mapping of the Interactome of Protein Phosphatase-1." Chemistry & Biology **16**(4): 365-371.

Hertz, M. I., D. M. Landry, A. E. Willis, G. X. Luo and S. R. Thompson (2013). "Ribosomal Protein S25 Dependency Reveals a Common Mechanism for Diverse Internal Ribosome Entry Sites and Ribosome Shunting." Molecular and Cellular Biology **33**(5): 1016-1026.

Himly, M., D. N. Foster, I. Bottoli, J. S. Iacovoni and P. K. Vogt (1998). "The DF-1 chicken fibroblast cell line: Transformation induced by diverse oncogenes and cell death resulting from infection by avian leukosis viruses." Virology **248**(2): 295-304.

Hiscox, J. A., K. L. Mawditt, D. Cavanagh and P. Britton (1995). "Investigation of the control of coronavirus subgenomic mRNA transcription by using T7-generated negative-sense RNA transcripts." J Virol **69**(10): 6219-6227.

Hodgson, T., P. Britton and D. Cavanagh (2006). "Neither the RNA nor the proteins of open reading frames 3a and 3b of the coronavirus infectious bronchitis virus are essential for replication." J Virol **80**(1): 296-305.

Hopkins, S. R. and H. W. Yoder, Jr. (1986). "Reversion to virulence of chicken-passaged infectious bronchitis vaccine virus." Avian Dis **30**(1): 221-223.

Hu, H. and S. C. Sun (2016). "Ubiquitin signaling in immune responses." Cell Res **26**(4): 457-483.

Hu, Y., W. Li, T. Gao, Y. Cui, Y. Jin, P. Li, Q. Ma, X. Liu and C. Cao (2017). "SARS Coronavirus Nucleocapsid Inhibits Type I Interferon Production by Interfering with TRIM25-Mediated RIG-I Ubiquitination." J Virol.

Huang, C., K. G. Lokugamage, J. M. Rozovics, K. Narayanan, B. L. Semler and S. Makino (2011). "Alphacoronavirus transmissible gastroenteritis virus nsp1 protein suppresses protein translation in mammalian cells and in cell-free HeLa cell extracts but not in rabbit reticulocyte lysate." J Virol **85**(1): 638-643.

Hurst, K. R., L. L. Kuo, C. A. Koetzner, R. Ye, B. Hsuej and P. S. Masters (2005). "A major determinant for membrane protein interaction localizes to the carboxy-terminal domain of the mouse coronavirus nucleocapsid protein." Journal of Virology **79**(21): 13285-13297.

Hussain, S., J. Pan, Y. Chen, Y. L. Yang, J. Xu, Y. Peng, Y. Wu, Z. Y. Li, Y. Zhu, P. Tien and D. Y. Guo (2005). "Identification of novel subgenomic RNAs and noncanonical transcription initiation signals of severe acute respiratory syndrome coronavirus." Journal of Virology **79**(9): 5288-5295.

Imbert, I., J. C. Guillemot, J. M. Bourhis, C. Bussetta, B. Coutard, M. P. Egloff, F. Ferron, A. E. Gorbalenya and B. Canard (2006). "A second, non-canonical RNA-dependent RNA polymerase in SARS coronavirus." Embo Journal **25**(20): 4933-4942.

Inglis, S. C., N. Rolley and I. Brierley (1990). The Ribosomal Frame-Shift Signal of Infectious Bronchitis Virus. Post-Transcriptional Control of Gene Expression. J. E. G. McCarthy and M. F. Tuite. Berlin, Heidelberg, Springer Berlin Heidelberg**:** 603-610.

Ireland, D. D. C., S. A. Stohlman, D. R. Hinton, R. Atkinson and C. C. Bergmann (2008). "Type I interferons are essential in controlling neurotropic coronavirus infection irrespective of functional CD8 T cells." Journal of Virology **82**(1): 300-310.

Iseni, F., D. Garcin, M. Nishio, N. Kedersha, P. Anderson and D. Kolakofsky (2002). "Sendai virus trailer RNA binds TIAR, a cellular protein involved in virus-induced apoptosis." Embo Journal **21**(19): 5141-5150.

Ito, N., E. C. Mossel, K. Narayanan, V. L. Popov, C. Huang, T. Inoue, C. J. Peters and S. Makino (2005). "Severe acute respiratory syndrome coronavirus 3a protein is a viral structural protein." Journal of Virology **79**(5): 3182-3186.

Ivanov, K. A., V. Thiel, J. C. Dobbe, Y. van der Meer, E. J. Snijder and J. Ziebuhr (2004). "Multiple enzymatic activities associated with Severe acute respiratory syndrome coronavirus helicase." Journal of Virology **78**(11): 5619-5632.

Ivanov, K. A. and J. Ziebuhr (2004). "Human coronavirus 229E nonstructural protein 13: Characterization of duplex-unwinding, nucleoside triphosphatase, and RNA 5 '-triphosphatase activities." Journal of Virology **78**(14): 7833-7838.

Jacobs, J. L. and C. B. Coyne (2013). "Mechanisms of MAVS Regulation at the Mitochondrial Membrane." Journal of Molecular Biology **425**(24): 5009-5019.

Jacobs, J. L., J. Zhu, S. N. Sarkar and C. B. Coyne (2014). "Regulation of mitochondrial antiviral signaling (MAVS) expression and signaling by the mitochondria-associated endoplasmic reticulum membrane (MAM) protein Gp78." J Biol Chem **289**(3): 1604-1616.

Jia, W. and S. A. Naqi (1997). "Sequence analysis of gene 3, gene 4 and gene 5 of avian infectious bronchitis virus strain CU-T2." Gene **189**(2): 189-193.

Jordan, B. (2017). "Vaccination against infectious bronchitis virus: A continuous challenge." Veterinary Microbiology **206**: 137-143.

Kaehler, C., J. Isensee, U. Nonhoff, M. Terrey, T. Hucho, H. Lehrach and S. Krobitsch (2012). "Ataxin-2-Like Is a Regulator of Stress Granules and Processing Bodies." Plos One **7**(11).

Kameka, A. M., S. Haddadi, D. S. Kim, S. C. Cork and M. F. Abdul-Careem (2014). "Induction of innate immune response following infectious bronchitis corona virus infection in the respiratory tract of chickens." Virology **450-451**: 114-121.

Kamitani, W., K. Narayanan, C. Huang, K. Lokugamage, T. Ikegami, N. Ito, H. Kubo and S. Makino (2006). "Severe acute respiratory syndrome coronavirus nsp1 protein suppresses host gene expression by promoting host mRNA degradation." Proceedings of the National Academy of Sciences of the United States of America **103**(34): 12885-12890.

Kannaki, T. R., M. R. Reddy, M. Shanmugam, P. C. Verma and R. P. Sharma (2010). "Chicken toll-like receptors and their role in immunity." Worlds Poultry Science Journal **66**(4): 727-738.

Kawai, T., K. Takahashi, S. Sato, C. Coban, H. Kumar, H. Kato, K. J. Ishii, O. Takeuchi and S. Akira (2005). "IPS-1, an adaptor triggering RIG-I- and Mda5-mediated type I interferon induction." Nat Immunol **6**(10): 981-988.

Kedersha, N., M. R. Cho, W. Li, P. W. Yacono, S. Chen, N. Gilks, D. E. Golan and P. Anderson (2000). "Dynamic shuttling of TIA-1 accompanies the recruitment of mRNA to mammalian stress granules." J Cell Biol **151**(6): 1257-1268.

Kedersha, N., P. Ivanov and P. Anderson (2013). "Stress granules and cell signaling: more than just a passing phase?" Trends in Biochemical Sciences **38**(10): 494-506.

Kedersha, N., M. D. Panas, C. A. Achorn, S. Lyons, S. Tisdale, T. Hickman, M. Thomas, J. Lieberman, G. M. McInerney, P. Ivanov and P. Anderson (2016). "G3BP-Caprin1-USP10 complexes mediate stress granule condensation and associate with 40S subunits." J Cell Biol **212**(7): 845-860.

Kedersha, N., G. Stoecklin, M. Ayodele, P. Yacono, J. Lykke-Andersen, M. J. Fritzler, D. Scheuner, R. J. Kaufman, D. E. Golan and P. Anderson (2005). "Stress granules and processing bodies are dynamically linked sites of mRNP remodeling." J Cell Biol **169**(6): 871-884.

Kedersha, N. L., M. Gupta, W. Li, I. Miller and P. Anderson (1999). "RNA-binding proteins TIA-1 and TIAR link the phosphorylation of eIF-2 alpha to the assembly of mammalian stress granules." J Cell Biol **147**(7): 1431-1442.

Khan, S., B. C. Fielding, T. H. P. Tan, C. F. Chou, S. Shen, S. G. Lim, W. Hong and Y. J. Tan (2006). "Over-expression of severe acute respiratory syndrome coronavirus 3b protein induces both apoptosis and necrosis in Vero E6 cells." Virus Research **122**(1-2): 20-27.

Kim, L., J. Hayes, P. Lewis, A. V. Parwani, K. O. Chang and L. J. Saif (2000). "Molecular characterization and pathogenesis of transmissible gastroenteritis coronavirus (TGEV) and porcine respiratory coronavirus (PRCV) field isolates co-circulating in a swine herd." Arch Virol **145**(6): 1133-1147.

Kint, J. (2015). Activation and Evasion of the type I Interferon Response by Infectious Bronchitis Virus. PhD, Wageningen University.

Kint, J., M. Fernandez-Gutierrez, H. J. Maier, P. Britton, M. A. Langereis, J. Koumans, G. F. Wiegertjes and M. Forlenza (2015). "Activation of the chicken type I interferon response by infectious bronchitis coronavirus." J Virol **89**(2): 1156-1167.

Kint, J., M. A. Langereis, H. J. Maier, P. Britton, F. J. van Kuppeveld, J. Koumans, G. F. Wiegertjes and M. Forlenza (2016). "Infectious Bronchitis Coronavirus Limits Interferon Production by Inducing a Host Shutoff That Requires Accessory Protein 5b." Journal of Virology **90**(16): 7519-7528.

Klumperman, J., J. K. Locker, A. Meijer, M. C. Horzinek, H. J. Geuze and P. J. Rottier (1994). "Coronavirus M proteins accumulate in the Golgi complex beyond the site of virion budding." J Virol **68**(10): 6523-6534.

Klumperman, J., J. K. Locker, A. Meijer, M. C. Horzinek, H. J. Geuze and P. J. M. Rottier (1994). "Coronavirus M-Proteins Accumulate in the Golgi-Complex Beyond the Site of Virion Budding." Journal of Virology **68**(10): 6523-6534.

Knodler, L. A., J. Celli and B. B. Finlay (2001). "Pathogenic trickery: Deception of host cell processes." Nature Reviews Molecular Cell Biology **2**(8): 578-588.

Knoops, K., M. Kikkert, S. H. E. van den Worm, J. C. Zevenhoven-Dobbe, Y. van der Meer, A. J. Koster, A. M. Mommaas and E. J. Snijder (2008). "SARS-coronavirus replication is supported by a reticulovesicular network of modified endoplasmic reticulum." Plos Biology **6**(9): 1957-1974.

Knoops, K., M. Kikkert, S. H. Worm, J. C. Zevenhoven-Dobbe, Y. van der Meer, A. J. Koster, A. M. Mommaas and E. J. Snijder (2008). "SARS-coronavirus replication is supported by a reticulovesicular network of modified endoplasmic reticulum." PLoS Biol **6**(9): e226.

Koch, G., L. Hartog, A. Kant and D. J. Vanroozelaar (1990). "Antigenic Domains on the Peplomer Protein of Avian Infectious-Bronchitis Virus - Correlation with Biological Functions." Journal of General Virology **71**: 1929-1935.

Koetzner, C. A., L. Kuo, S. J. Goebel, A. B. Dean, M. M. Parker and P. S. Masters (2010). "Accessory protein 5a is a major antagonist of the antiviral action of interferon against murine coronavirus." J Virol **84**(16): 8262-8274.

Kopecky-Bromberg, S. A., L. Martinez-Sobrido, M. Frieman, R. A. Baric and P. Palese (2007). "Severe acute respiratory syndrome coronavirus open reading frame (ORF) 3b, ORF 6, and nucleocapsid proteins function as interferon antagonists." Journal of Virology **81**(2): 548-557.

Kopecky-Bromberg, S. A., L. Martinez-Sobrido and P. Palese (2006). "7a protein of severe acute respiratory syndrome coronavirus inhibits cellular protein synthesis and activates p38 mitogen-activated protein kinase." Journal of Virology **80**(2): 785-793.

Koyama, A. H., H. Irie, T. Fukumori, S. Hata, S. Iida, H. Akari and A. Adachi (1998). "Role of virus-induced apoptosis in a host defense mechanism against virus infection." J Med Invest **45**(1-4): 37-45.

Krijnselocker, J., M. Ericsson, P. J. M. Rottier and G. Griffiths (1994). "Characterization of the Budding Compartment of Mouse Hepatitis-Virus - Evidence That Transport from the Rer to the Golgi-Complex Requires Only One Vesicular Transport Step." Journal of Cell Biology **124**(1-2): 55-70.

Kroemer, G., L. Galluzzi and C. Brenner (2007). "Mitochondrial membrane permeabilization in cell death." Physiological Reviews **87**(1): 99-163.

Kubo, H., Y. K. Yamada and F. Taguchi (1994). "Localization of Neutralizing Epitopes and the Receptor-Binding Site within the Amino-Terminal 330 Amino-Acids of the Murine Coronavirus Spike Protein." Journal of Virology **68**(9): 5403-5410.

Kvansakul, M., A. H. Wei, J. I. Fletcher, S. N. Willis, L. Chen, A. W. Roberts, D. C. S. Huang and P. M. Colman (2010). "Structural Basis for Apoptosis Inhibition by Epstein-Barr Virus BHRF1." Plos Pathogens **6**(12).

Landry, D. M., M. I. Hertz and S. R. Thompson (2009). "RPS25 is essential for translation initiation by the Dicistroviridae and hepatitis C viral IRESs." Genes & Development **23**(23): 2753-2764.

Law, P. T. W., C. H. Wong, T. C. C. Au, C. P. Chuck, S. K. Kong, P. K. S. Chan, K. F. To, A. W. I. Lo, J. Y. W. Chan, Y. K. Suen, H. Y. E. Chan, K. P. Fung, M. M. Y. Waye, J. J. Y. Sung, Y. M. D. Lo and S. K. W. Tsui (2005). "The 3a protein of severe acute respiratory syndrome-associated coronavirus induces apoptosis in Vero E6 cells." Journal of General Virology **86**: 1921-1930.

Le, S. Y., N. Sonenberg and J. V. Maizel, Jr. (1994). "Distinct structural elements and internal entry of ribosomes in mRNA3 encoded by infectious bronchitis virus." Virology **198**(1): 405-411.

Lecoeur, H., A. Borgne-Sanchez, O. Chaloin, R. El-Khoury, M. Brabant, A. Langonne, M. Porceddu, J. J. Briere, N. Buron, D. Rebouillat, C. Pechoux, A. Deniaud, C. Brenner, J. P. Briand, S. Muller, P. Rustin and E. Jacotot (2012). "HIV-1 Tat protein directly induces mitochondrial membrane permeabilization and inactivates cytochrome c oxidase." Cell Death Dis **3**: e282.

Lesage, B., M. Beullens, M. Nuytten, A. Van Eynde, S. Keppens, B. Himpens and M. Bollen (2004). "Interactor-mediated nuclear translocation and retention of protein phosphatase-1." J Biol Chem **279**(53): 55978-55984.

Li, F. Q., J. P. Tam and D. X. Liu (2007). "Cell cycle arrest and apoptosis induced by the coronavirus infectious bronchitis virus in the absence of p53." Virology **365**(2): 435-445.

Li, J. F., Y. Liu and X. M. Zhang (2010). "Murine Coronavirus Induces Type I Interferon in Oligodendrocytes through Recognition by RIG-I and MDA5." Journal of Virology **84**(13): 6472-6482.

Li, L. Y., L. Luo and X. D. Wang (2001). "Endonuclease G is an apoptotic DNase when released from mitochondria." Nature **412**(6842): 95-99.

Li, Z., Y. Wang, Y. Xue, X. Li, H. Cao and S. J. Zheng (2012). "Critical role for voltage-dependent anion channel 2 in infectious bursal disease virus-induced apoptosis in host cells via interaction with VP5." J Virol **86**(3): 1328-1338.

Lian, X. J. and I. E. Gallouzi (2009). "Oxidative Stress Increases the Number of Stress Granules in Senescent Cells and Triggers a Rapid Decrease in p21waf1/cip1 Translation." J Biol Chem **284**(13): 8877-8887.

Liao, Y., T. S. Fung, M. Huang, S. G. Fang, Y. Zhong and D. X. Liu (2013). "Upregulation of CHOP/GADD153 during coronavirus infectious bronchitis virus infection modulates apoptosis by restricting activation of the extracellular signal-regulated kinase pathway." J Virol **87**(14): 8124-8134.

Lim, K. P. and D. X. Liu (1998). "Characterisation of a papain-like proteinase domain encoded by ORF1a of the coronavirus IBV and determination of the C-terminal cleavage site of an 87 kDa protein." Adv Exp Med Biol **440**: 173-184.

Lim, K. P. and D. X. Liu (1998). "Characterization of the two overlapping papain-like proteinase domains encoded in gene 1 of the coronavirus infectious bronchitis virus and determination of the C-terminal cleavage site of an 87-kDa protein." Virology **245**(2): 303-312.

Lin, R. T., L. Yang, P. Nakhaei, Q. Sun, E. Sharif-Askari, I. Julkunen and J. Hiscott (2006). "Negative regulation of the retinoic acid-inducible gene I-induced antiviral state by the ubiquitin-editing protein A20." Journal of Biological Chemistry **281**(4): 2095-2103.

Lindquist, M. E., A. W. Lifland, T. J. Utley, P. J. Santangelo and J. E. Crowe (2010). "Respiratory Syncytial Virus Induces Host RNA Stress Granules To Facilitate Viral Replication." Journal of Virology **84**(23): 12274-12284.

Lissenberg, A., M. M. Vrolijk, A. L. W. van Vliet, M. A. Langereis, J. D. F. de Groot-Mijnes, P. J. M. Rottier and R. J. de Groot (2005). "Luxury at a cost? Recombinant mouse hepatitis viruses expressing the accessory hemagglutinin esterase protein display reduced fitness in vitro." Journal of Virology **79**(24): 15054-15063.

Liu, C., H. Y. Xu and D. X. Liu (2001). "Induction of caspase-dependent apoptosis in cultured cells by the avian coronavirus infectious bronchitis virus." J Virol **75**(14): 6402-6409.

Liu, D. X., D. Cavanagh, P. Green and S. C. Inglis (1991). "A polycistronic mRNA specified by the coronavirus infectious bronchitis virus." Virology **184**(2): 531-544.

Liu, D. X., T. S. Fung, K. K. Chong, A. Shukla and R. Hilgenfeld (2014). "Accessory proteins of SARS-CoV and other coronaviruses." Antiviral Res **109**: 97-109.

Liu, D. X. and S. C. Inglis (1992). "Identification of two new polypeptides encoded by mRNA5 of the coronavirus infectious bronchitis virus." Virology **186**(1): 342-347.

Liu, D. X. and S. C. Inglis (1992). "Internal entry of ribosomes on a tricistronic mRNA encoded by infectious bronchitis virus." J Virol **66**(10): 6143-6154.

Lomniczi, B. and J. Morser (1981). "Polypeptides of infectious bronchitis virus. I. Polypeptides of the virion." J Gen Virol **55**(Pt 1): 155-164.

Lu, X. L., J. Pan, J. L. Tao and D. Y. Guo (2011). "SARS-CoV nucleocapsid protein antagonizes IFN-beta response by targeting initial step of IFN-beta induction pathway, and its C-terminal region is critical for the antagonism." Virus Genes **42**(1): 37-45.

Lu, X. T., Y. Q. Lu and M. R. Denison (1996). "Intracellular and in vitro-translated 27-kDa proteins contain the 3C-like proteinase activity of the coronavirus MHV-A59." Virology **222**(2): 375-382.

Lu, Y., M. Wambach, M. G. Katze and R. M. Krug (1995). "Binding of the Influenza Virus NS1 Protein to Double-Stranded RNA Inhibits the Activation of the Protein Kinase That Phosphorylates the eIF-2 Translation Initiation Factor." Virology **214**(1): 222-228.

Lui, P. Y., L. Y. Wong, C. L. Fung, K. L. Siu, M. L. Yeung, K. S. Yuen, C. P. Chan, P. C. Woo, K. Y. Yuen and D. Y. Jin (2016). "Middle East respiratory syndrome coronavirus M protein suppresses type I interferon expression through the inhibition of TBK1-dependent phosphorylation of IRF3." Emerg Microbes Infect **5**: e39.

Luytjes, W., L. S. Sturman, P. J. Bredenbeek, J. Charite, B. A. M. Vanderzeijst, M. C. Horzinek and W. J. M. Spaan (1987). "Primary Structure of the Glycoprotein-E2 of Coronavirus Mhv-A59 and Identification of the Trypsin Cleavage Site." Virology **161**(2): 479-487.

Ma, Y. M., Y. Zhang, X. Y. Liang, F. F. Lou, M. Oglesbee, S. Krakowka and J. R. Li (2015). "Origin, Evolution, and Virulence of Porcine Deltacoronaviruses in the United States." Mbio **6**(2).

Madu, I. G., V. C. Chu, H. Lee, A. D. Regan, B. E. Bauman and G. R. Whittaker (2007). "Heparan sulfate is a selective attachment factor for the avian coronavirus infectious bronchitis virus beaudette." Avian Diseases **51**(1): 45-51.

Maier, H. J., E. Bickerton and P. Britton (2015). "Preface. Coronaviruses." Methods Mol Biol **1282**: v.

Maier, H. J., E. M. Cottam, P. Stevenson-Leggett, J. A. Wilkinson, C. J. Harte, T. Wileman and P. Britton (2013). "Visualizing the autophagy pathway in avian cells and its application to studying infectious bronchitis virus." Autophagy **9**(4): 496-509.

Maier, H. J., P. C. Hawes, E. M. Cottam, J. Mantell, P. Verkade, P. Monaghan, T. Wileman and P. Britton (2013). "Infectious bronchitis virus generates spherules from zippered endoplasmic reticulum membranes." MBio **4**(5).

Maier, H. J., B. W. Neuman, E. Bickerton, S. M. Keep, H. Alrashedi, R. Hall and P. Britton (2016). "Extensive coronavirus-induced membrane rearrangements are not a determinant of pathogenicity." Scientific Reports **6**: 27126.

Mardani, K., A. H. Noormohammadi, P. Hooper, J. Ignjatovic and G. F. Browning (2008). "Infectious bronchitis viruses with a novel genomic organization." Journal of Virology **82**(4): 2013-2024.

Masters, P. S. (2006). "The molecular biology of coronaviruses." Adv Virus Res **66**: 193-292.

Masters, P. S. (2006). "The molecular biology of coronaviruses." Advances in Virus Research, Vol 66 **66**: 193-292.

Matsuki, H., M. Takahashi, M. Higuchi, G. N. Makokha, M. Oie and M. Fujii (2013). "Both G3BP1 and G3BP2 contribute to stress granule formation." Genes to Cells **18**(2): 135-146.

McBride, C. E., J. Li and C. E. Machamer (2007). "The cytoplasmic tail of the severe acute respiratory syndrome coronavirus spike protein contains a novel endoplasmic reticulum retrieval signal that binds COPI and promotes interaction with membrane protein." Journal of Virology **81**(5): 2418-2428.

McBride, R. and B. C. Fielding (2012). "The role of severe acute respiratory syndrome (SARS)-coronavirus accessory proteins in virus pathogenesis." Viruses **4**(11): 2902-2923.

McBride, R., M. van Zyl and B. C. Fielding (2014). "The Coronavirus Nucleocapsid Is a Multifunctional Protein." Viruses-Basel **6**(8): 2991-3018.

McLean, J. E., A. Ruck, A. Shirazian, F. Pooyaei-Mehr and Z. F. Zakeri (2008). "Viral manipulation of cell death." Curr Pharm Des **14**(3): 198-220.

Meager, A., R. Nairn and R. C. Hughes (1977). "Properties of a Baby-Hamster-Kidney Cell Line with Increased Resistance to 2-Deoxy-D-Glucose." European Journal of Biochemistry **72**(2): 275-281.

Mellacheruvu, D., Z. Wright, A. L. Couzens, J. P. Lambert, N. A. St-Denis, T. Li, Y. V. Miteva, S. Hauri, M. E. Sardiu, T. Y. Low, V. A. Halim, R. D. Bagshaw, N. C. Hubner, A. Al-Hakim, A. Bouchard, D. Faubert, D. Fermin, W. H. Dunham, M. Goudreault, Z. Y. Lin, B. G. Badillo, T. Pawson, D. Durocher, B. Coulombe, R. Aebersold, G. Superti-Furga, J. Colinge, A. J. Heck, H. Choi, M. Gstaiger, S. Mohammed, I. M. Cristea, K. L. Bennett, M. P. Washburn, B. Raught, R. M. Ewing, A. C. Gingras and A. I. Nesvizhskii (2013). "The CRAPome: a contaminant repository for affinity purification-mass spectrometry data." Nat Methods **10**(8): 730-736.

Minakshi, R., K. Padhan, M. Rani, N. Khan, F. Ahmad and S. Jameel (2009). "The SARS Coronavirus 3a protein causes endoplasmic reticulum stress and induces ligand-independent downregulation of the type 1 interferon receptor." PLoS One **4**(12): e8342.

Mizutani, T., S. Fukushi, M. Saijo, I. Kurane and S. Morikawa (2004). "Importance of Akt signaling pathway for apoptosis in SARS-CoV-infected Vero E6 cells." Virology **327**(2): 169-174.

Mochida, S. and T. Hunt (2012). "Protein phosphatases and their regulation in the control of mitosis." Embo Reports **13**(3): 197-203.

Mokas, S., J. R. Mills, C. Garreau, M. J. Fournier, F. Robert, P. Arya, R. J. Kaufman, J. Pelletier and R. Mazroui (2009). "Uncoupling Stress Granule Assembly and Translation Initiation Inhibition." Molecular Biology of the Cell **20**(11): 2673-2683.

Mollet, S., N. Cougot, A. Wilczynska, F. Dautry, M. Kress, E. Bertrand and D. Weil (2008). "Translationally Repressed mRNA Transiently Cycles through Stress Granules during Stress." Molecular Biology of the Cell **19**(10): 4469-4479.

Moutaoufik, M. T., R. El Fatimy, H. Nassour, C. Gareau, J. Lang, R. M. Tanguay, R. Mazroui and E. W. Khandjian (2014). "UVC-Induced Stress Granules in Mammalian Cells." Plos One **9**(11).

Nakagawa, K., K. G. Lokugamage and S. Makino (2016). "Viral and Cellular mRNA Translation in Coronavirus-Infected Cells." Adv Virus Res **96**: 165-192.

Nanduri, S., F. Rahman, B. R. G. Williams and J. Qin (2000). "A dynamically tuned double-stranded RNA binding mechanism for the activation of antiviral kinase PKR." Embo Journal **19**(20): 5567-5574.

Narayanan, K., C. Huang and S. Makino (2008). "SARS coronavirus accessory proteins." Virus Research **133**(1): 113-121.

Narayanan, K., A. Maeda, J. Maeda and S. Makino (2000). "Characterization of the coronavirus M protein and nucleocapsid interaction in infected cells." Journal of Virology **74**(17): 8127-8134.

Narayanaswamy, R., M. Levy, M. Tsechansky, G. M. Stovall, J. D. O'Connell, J. Mirrielees, A. D. Ellington and E. M. Marcotte (2009). "Widespread reorganization of metabolic enzymes into reversible assemblies upon nutrient starvation." Proceedings of the National Academy of Sciences of the United States of America **106**(25): 10147-10152.

Niemeyer, D., T. Zillinger, D. Muth, F. Zielecki, G. Horvath, T. Suliman, W. Barchet, F. Weber, C. Drosten and M. A. Muller (2013). "Middle East respiratory syndrome coronavirus accessory protein 4a is a type I interferon antagonist." J Virol **87**(22): 12489-12495.

Okino, C. H., I. L. dos Santos, F. S. Fernando, A. C. Alessi, X. Wang and H. J. Montassier (2014). "Inflammatory and cell-mediated immune responses in the respiratory tract of chickens to infection with avian infectious bronchitis virus." Viral Immunol **27**(8): 383-391.

Okino, C. H., M. A. Mores, I. M. Trevisol, A. Coldebella, H. J. Montassier and L. Brentano (2017). "Early immune responses and development of pathogenesis of

avian infectious bronchitis viruses with different virulence profiles." PLoS One **12**(2): e0172275.

Oostra, M., M. C. Hagemeijer, M. van Gent, C. P. J. Bekker, E. G. T. Lintelo, P. J. M. Rottier and C. A. M. de Haan (2008). "Topology and Membrane Anchoring of the Coronavirus Replication Complex: Not All Hydrophobic Domains of nsp3 and nsp6 Are Membrane Spanning." Journal of Virology **82**(24): 12392-12405.

Oostra, M., E. G. te Lintelo, M. Deijs, M. H. Verheije, P. J. M. Rottier and C. A. M. de Haan (2007). "Localization and membrane topology of coronavirus nonstructural protein 4: Involvement of the early secretory pathway in replication." Journal of Virology **81**(22): 12323-12336.

Ortego, J., I. Sola, F. Almazan, J. E. Ceriani, C. Riquelme, M. Balasch, J. Plana and L. Enjuanes (2003). "Transmissible gastroenteritis coronavirus gene 7 is not essential but influences in vivo virus replication and virulence." Virology **308**(1): 13-22.

Pasternak, A. O., E. van den Born, W. J. Spaan and E. J. Snijder (2001). "Sequence requirements for RNA strand transfer during nidovirus discontinuous subgenomic RNA synthesis." EMBO J **20**(24): 7220-7228.

Paul, P. S., E. M. Vaughn and P. G. Halbur (1997). "Pathogenicity and sequence analysis studies suggest potential role of gene 3 in virulence of swine enteric and respiratory coronaviruses." Mechanisms in the Pathogenesis of Enteric Diseases **412**: 317-321.

Pekosz, A., S. R. Schaecher, M. S. Diamond, D. H. Fremont, A. C. Sims and R. S. Baric (2006). "Structure, expression, and intracellular localization of the SARS-CoV accessory proteins 7a and 7b." Nidoviruses: Toward Control of Sars and Other Nidovirus Diseases **581**: 115-120.

Pendleton, A. R. and C. E. Machamer (2005). "Infectious bronchitis virus 3a protein localizes to a novel domain of the smooth endoplasmic reticulum." J Virol **79**(10): 6142-6151.

Pendleton, A. R. and C. E. Machamer (2006). "Differential localization and turnover of infectious bronchitis virus 3b protein in mammalian versus avian cells." Virology **345**(2): 337-345.

Pewe, L., H. Zhou, J. Netland, C. Tangudu, H. Olivares, L. Shi, D. Look, T. Gallagher and S. Perlman (2005). "A severe acute respiratory syndrome-associated coronavirus-specific protein enhances virulence of an attenuated murine coronavirus." J Virol **79**(17): 11335-11342.

Pfefferle, S., V. Krahling, V. Ditt, K. Grywna, E. Muhlberger and C. Drosten (2009). "Reverse genetic characterization of the natural genomic deletion in SARS-

Coronavirus strain Frankfurt-1 open reading frame 7b reveals an attenuating function of the 7b protein in-vitro and in-vivo." Virology Journal **6**.

Prakash, A. and D. E. Levy (2006). "Regulation of IRF7 through cell type-specific protein stability." Biochemical and Biophysical Research Communications **342**(1): 50-56.

Prinz, W. A. (2014). "Bridging the gap: Membrane contact sites in signaling, metabolism, and organelle dynamics." Journal of Cell Biology **205**(6): 759-769.

Promkuntod, N., R. E. van Eijndhoven, G. de Vrieze, A. Grone and M. H. Verheije (2014). "Mapping of the receptor-binding domain and amino acids critical for attachment in the spike protein of avian coronavirus infectious bronchitis virus." Virology **448**: 26-32.

Putics, A., W. Filipowicz, J. Hall, A. E. Gorbalenya and J. Ziebuhr (2005). "ADP-ribose-1 "-monophosphatase: That is dispensable for viral a conserved coronavirus enzyme replication in tissue culture." Journal of Virology **79**(20): 12721-12731.

Qin, Q. S., K. Carroll, C. Hastings and C. L. Miller (2011). "Mammalian Orthoreovirus Escape from Host Translational Shutoff Correlates with Stress Granule Disruption and Is Independent of eIF2 alpha Phosphorylation and PKR." Journal of Virology **85**(17): 8798-8810.

Qin, Q. S., C. Hastings and C. L. Miller (2009). "Mammalian Orthoreovirus Particles Induce and Are Recruited into Stress Granules at Early Times Postinfection." Journal of Virology **83**(21): 11090-11101.

Raaben, M., M. J. Groot Koerkamp, P. J. Rottier and C. A. de Haan (2007). "Mouse hepatitis coronavirus replication induces host translational shutoff and mRNA decay, with concomitant formation of stress granules and processing bodies." Cell Microbiol **9**(9): 2218-2229.

Raamsman, M. J., J. K. Locker, A. de Hooge, A. A. de Vries, G. Griffiths, H. Vennema and P. J. Rottier (2000). "Characterization of the coronavirus mouse hepatitis virus strain A59 small membrane protein E." J Virol **74**(5): 2333-2342.

Rabouw, H. H., M. A. Langereis, R. C. Knaap, T. J. Dalebout, J. Canton, I. Sola, L. Enjuanes, P. J. Bredenbeek, M. Kikkert, R. J. de Groot and F. J. van Kuppeveld (2016). "Middle East Respiratory Coronavirus Accessory Protein 4a Inhibits PKR-Mediated Antiviral Stress Responses." PLoS Pathog **12**(10): e1005982.

Raj, V. S., A. D. M. E. Osterhaus, R. A. M. Fouchier and B. L. Haagmans (2014). "MERS: emergence of a novel human coronavirus." Current Opinion in Virology **5**: 58-62.

Rajsbaum, R., R. A. Albrecht, M. K. Wang, N. P. Maharaj, G. A. Versteeg, E. Nistal-Villan, A. Garcia-Sastre and M. U. Gack (2012). "Species-Specific Inhibition of RIG-I Ubiquitination and IFN Induction by the Influenza A Virus NS1 Protein." Plos Pathogens **8**(11).

Randall, R. E. and S. Goodbourn (2008). "Interferons and viruses: an interplay between induction, signalling, antiviral responses and virus countermeasures." J Gen Virol **89**(Pt 1): 1-47.

Rodriguez, K. R., A. M. Bruns and C. M. Horvath (2014). "MDA5 and LGP2: Accomplices and Antagonists of Antiviral Signal Transduction." Journal of Virology **88**(15): 8194-8200.

Rottier, P., D. Brandenburg, J. Armstrong, B. Vanderzeijst and G. Warren (1984). "Assembly Invitro of a Spanning Membrane-Protein of the Endoplasmic-Reticulum - the E1 Glycoprotein of Coronavirus Mouse Hepatitis-Virus A59." Proceedings of the National Academy of Sciences of the United States of America-Biological Sciences **81**(5): 1421-1425.

Ruch, T. R. and C. E. Machamer (2011). "The hydrophobic domain of infectious bronchitis virus E protein alters the host secretory pathway and is important for release of infectious virus." J Virol **85**(2): 675-685.

Saffarian, S., E. Cocucci and T. Kirchhausen (2009). "Distinct dynamics of endocytic clathrin-coated pits and coated plaques." PLoS Biol **7**(9): e1000191.

Salvatore, M., C. F. Basler, J. P. Parisien, C. M. Horvath, S. Bourmakina, H. Zheng, T. Muster, P. Palese and A. Garcia-Sastre (2002). "Effects of influenza A virus NS1 protein on protein expression: the NS1 protein enhances translation and is not required for shutoff of host protein synthesis." J Virol **76**(3): 1206-1212.

Sawicki, S. G. and D. L. Sawicki (1995). "Coronaviruses use discontinuous extension for synthesis of subgenome-length negative strands." Adv Exp Med Biol **380**: 499-506.

Sawicki, S. G., D. L. Sawicki and S. G. Siddell (2007). "A contemporary view of coronavirus transcription." J Virol **81**(1): 20-29.

Schaecher, S. R., E. Touchette, J. Schriewer, R. M. Buller and A. Pekosz (2007). "Severe acute respiratory syndrome coronavirus gene 7 products contribute to virus-induced apoptosis." Journal of Virology **81**(20): 11054-11068.

Schultze, B., D. Cavanagh and G. Herrler (1992). "Neuraminidase Treatment of Avian Infectious-Bronchitis Coronavirus Reveals a Hemagglutinating Activity That Is Dependent on Sialic Acid-Containing Receptors on Erythrocytes." Virology **189**(2): 792-794.

Schwarz, H., O. Harlin, A. Ohnemus, B. Kaspers and P. Staeheli (2004). "Synthesis of IFN-gamma by virus-infected chicken embryo cells demonstrated with specific antisera and a new bioassay." Journal of Interferon and Cytokine Research **24**(3): 179-184.

Seth, R. B., L. J. Sun, C. K. Ea and Z. J. J. Chen (2005). "Identification and characterization of MAVS, a mitochondrial antiviral signaling protein that activates NF-kappa B and IRF3." Cell **122**(5): 669-682.

Shaw, G., S. Morse, M. Ararat and F. L. Graham (2002). "Preferential transformation of human neuronal cells by human adenoviruses and the origin of HEK 293 cells." FASEB J **16**(8): 869-871.

Shen, S., Z. L. Wen and D. X. Liu (2003). "Emergence of a coronavirus infectious bronchitis virus mutant with a truncated 3b gene: functional characterization of the 3b protein in pathogenesis and replication." Virology **311**(1): 16-27.

ShuShuang, W. Y. W. Y. Z. Z. F. G. J. Y. L. X. D. J. W. (1998). "Isolation and identification of glandular stomach type IBV (QX IBV) in chickens." Chinese Journal of Animal Quarantine **15**(1): 1-3.

Siddell, S., H. Wege and V. Termeulen (1983). "The Biology of Coronaviruses." Journal of General Virology **64**(Apr): 761-776.

Simpson-Holley, M., N. Kedersha, K. Dower, K. H. Rubins, P. Anderson, L. E. Hensley and J. H. Connor (2011). "Formation of Antiviral Cytoplasmic Granules during Orthopoxvirus Infection." Journal of Virology **85**(4): 1581-1593.

Siu, K. L., M. L. Yeung, K. H. Kok, K. S. Yuen, C. Kew, P. Y. Lui, C. P. Chan, H. Tse, P. C. Woo, K. Y. Yuen and D. Y. Jin (2014). "Middle east respiratory syndrome coronavirus 4a protein is a double-stranded RNA-binding protein that suppresses PACT-induced activation of RIG-I and MDA5 in the innate antiviral response." J Virol **88**(9): 4866-4876.

Siu, Y. L., K. T. Teoh, J. Lo, C. M. Chan, F. Kien, N. Escriou, S. W. Tsao, J. M. Nicholls, R. Altmeyer, J. S. M. Peiris, R. Bruzzone and B. Nal (2008). "The M, E, and N Structural Proteins of the Severe Acute Respiratory Syndrome Coronavirus Are Required for Efficient Assembly, Trafficking, and Release of Virus-Like Particles." Journal of Virology **82**(22): 11318-11330.

Smith, J., J. R. Sadeyen, D. Cavanagh, P. Kaiser and D. W. Burt (2015). "The early immune response to infection of chickens with Infectious Bronchitis Virus (IBV) in susceptible and resistant birds." BMC Vet Res **11**: 256.

Sola, I., C. Galan, P. A. Mateos-Gomez, L. Palacio, S. Zuniga, J. L. Cruz, F. Almazan and L. Enjuanes (2011). "The polypyrimidine tract-binding protein affects coronavirus RNA accumulation levels and relocalizes viral RNAs to novel

cytoplasmic domains different from replication-transcription sites." J Virol **85**(10): 5136-5149.

Sonenberg, N. and A. G. Hinnebusch (2009). "Regulation of Translation Initiation in Eukaryotes: Mechanisms and Biological Targets." Cell **136**(4): 731-745.

Spiegel, M., A. Pichlmair, L. Martinez-Sobrido, J. Cros, A. Garcia-Sastre, O. Haller and F. Weber (2005). "Inhibition of Beta interferon induction by severe acute respiratory syndrome coronavirus suggests a two-step model for activation of interferon regulatory factor 3." J Virol **79**(4): 2079-2086.

Stark, G. R. and J. E. Darnell (2012). "The JAK-STAT Pathway at Twenty." Immunity **36**(4): 503-514.

Steinkamp, J. A., B. E. Lehnert and N. M. Lehnert (1999). "Discrimination of damaged/dead cells by propidium iodide uptake in immunofluorescently labeled populations analyzed by phase-sensitive flow cytometry." J Immunol Methods **226**(1-2): 59-70.

Stern, D. F., L. Burgess and B. M. Sefton (1982). "Structural-Analysis of Virion Proteins of the Avian Coronavirus Infectious-Bronchitis Virus." Journal of Virology **42**(1): 208-219.

Stern, D. F. and S. I. T. Kennedy (1980). "Coronavirus Multiplication Strategy .1. Identification and Characterization of Virus-Specified Rna." Journal of Virology **34**(3): 665-674.

Sturman, L. S., K. V. Holmes and J. Behnke (1980). "Isolation of coronavirus envelope glycoproteins and interaction with the viral nucleocapsid." J Virol **33**(1): 449-462.

Sun, L., Y. L. Xing, X. J. Chen, Y. Zheng, Y. D. Yang, D. B. Nichols, M. A. Clementz, B. S. Banach, K. Li, S. C. Baker and Z. B. Chen (2012). "Coronavirus Papain-like Proteases Negatively Regulate Antiviral Innate Immune Response through Disruption of STING-Mediated Signaling." Plos One **7**(2).

Sun, Y., L. Dong, S. Yu, X. Wang, H. Zheng, P. Zhang, C. Meng, Y. Zhan, L. Tan, C. Song, X. Qiu, G. Wang, Y. Liao and C. Ding (2017). "Newcastle disease virus induces stable formation of bona fide stress granules to facilitate viral replication through manipulating host protein translation." FASEB J **31**(4): 1337-1353.

Sutton, G., E. Fry, L. Carter, S. Sainsbury, T. Walter, J. Nettleship, N. Berrow, R. Owens, R. Gilbert, A. Davidson, S. Siddell, L. L. M. Poon, J. Diprose, D. Alderton, M. Walsh, J. M. Grimes and D. I. Stuart (2004). "The nsp9 replicase protein of SARS-coronavirus, structure and functional insights." Structure **12**(2): 341-353.

Szyszka, R., W. Kudlicki, G. Kramer, B. Hardesty, J. Galabru and A. Hovanessian (1989). "A type 1 phosphoprotein phosphatase active with phosphorylated Mr = 68,000 initiation factor 2 kinase." J Biol Chem **264**(7): 3827-3831.

Tahara, S. M., T. A. Dietlin, C. C. Bergmann, G. W. Nelson, S. Kyuwa, R. P. Anthony and S. A. Stohlman (1994). "Coronavirus translational regulation: leader affects mRNA efficiency." Virology **202**(2): 621-630.

Tan, Y. J., B. C. Fielding, P. Y. Goh, S. Shen, T. H. P. Tan, S. G. Lim and W. J. Hong (2004). "Overexpression of 7a, a protein specifically encoded by the severe acute respiratory syndrome coronavirus, induces apoptosis via a caspase-dependent pathway." Journal of Virology **78**(24): 14043-14047.

Tan, Y. X., T. H. P. Tan, M. J. R. Lee, P. Y. Tham, V. Gunalan, J. Druce, C. Birch, M. Catton, N. Y. Fu, V. C. Yu and Y. J. Tan (2007). "Induction of apoptosis by the severe acute respiratory syndrome coronavirus 7a protein is dependent on its interaction with the Bcl-X-L protein." Journal of Virology **81**(12): 6346-6355.

Taylor, R. C., S. P. Cullen and S. J. Martin (2008). "Apoptosis: controlled demolition at the cellular level." Nature Reviews Molecular Cell Biology **9**(3): 231-241.

Thompson, M. R., J. J. Kaminski, E. A. Kurt-Jones and K. A. Fitzgerald (2011). "Pattern recognition receptors and the innate immune response to viral infection." Viruses **3**(6): 920-940.

Thorburn, A. (2004). "Death receptor-induced cell killing." Cellular Signalling **16**(2): 139-144.

To, K. K., I. F. Hung, J. F. Chan and K. Y. Yuen (2013). "From SARS coronavirus to novel animal and human coronaviruses." J Thorac Dis **5 Suppl 2**: S103-108.

Tohya, Y., K. Narayanan, W. Kamitani, C. Huang, K. Lokugamage and S. Makino (2009). "Suppression of host gene expression by nsp1 proteins of group 2 bat coronaviruses." J Virol **83**(10): 5282-5288.

Tomley, F. M., A. P. Mockett, M. E. Boursnell, M. M. Binns, J. K. Cook, T. D. Brown and G. L. Smith (1987). "Expression of the infectious bronchitis virus spike protein by recombinant vaccinia virus and induction of neutralizing antibodies in vaccinated mice." J Gen Virol **68 (Pt 9)**: 2291-2298.

Tooze, J., S. A. Tooze and S. D. Fuller (1987). "Sorting of Progeny Coronavirus from Condensed Secretory Proteins at the Exit from the Trans-Golgi Network of Att20 Cells." Journal of Cell Biology **105**(3): 1215-1226.

Tourriere, H., K. Chebli, L. Zekri, B. Courselaud, J. M. Blanchard, E. Bertrand and J. Tazi (2003). "The RasGAP-associated endoribonuclease G3BP assembles stress granules." J Cell Biol **160**(6): 823-831.

Tung, F. Y. T., S. Abraham, M. Sethna, S. L. Hung, P. Sethna, B. G. Hogue and D. A. Brian (1992). "The 9-Kda Hydrophobic Protein Encoded at the 3' End of the Porcine Transmissible Gastroenteritis Coronavirus Genome Is Membrane-Associated." Virology **186**(2): 676-683.

Valastro, V., I. Monne, M. Fasolato, K. Cecchettin, D. Parker, C. Terregino and G. Cattoli (2010). "QX-type infectious bronchitis virus in commercial flocks in the UK." Vet Rec **167**(22): 865-866.

van Boheemen, S., M. de Graaf, C. Lauber, T. M. Bestebroer, V. S. Raj, A. M. Zaki, A. D. M. E. Osterhaus, B. L. Haagmans, A. E. Gorbalenya, E. J. Snijder and R. A. M. Fouchier (2012). "Genomic Characterization of a Newly Discovered Coronavirus Associated with Acute Respiratory Distress Syndrome in Humans." Mbio **3**(6).

van der Most, R. G. and W. J. M. Spaan (1995). Coronavirus Replication, Transcription, and RNA Recombination. The Coronaviridae. S. G. Siddell. Boston, MA, Springer US**:** 11-31.

van Hemert, M. J., S. H. van den Worm, K. Knoops, A. M. Mommaas, A. E. Gorbalenya and E. J. Snijder (2008). "SARS-coronavirus replication/transcription complexes are membrane-protected and need a host factor for activity in vitro." PLoS Pathog **4**(5): e1000054.

van Marle, G., J. C. Dobbe, A. P. Gultyaev, W. Luytjes, W. J. M. Spaan and E. J. Snijder (1999). "Arterivirus discontinuous mRNA transcription is guided by base pairing between sense and antisense transcription-regulating sequences." Proceedings of the National Academy of Sciences of the United States of America **96**(21): 12056-12061.

Van Roekel, H., Bullis, K. L., Clarke, M. K., Olesiuk, O, N, Sperling, F. G. (1950). "Infectious Bronchitis." Bulletin of the Massachusetts Agricultural Experiment Station **460**: 1-47.

Varshavsky, A. (2011). "The N-end rule pathway and regulation by proteolysis." Protein Science **20**(8): 1298-1345.

Velthuis, A. J. W. T., S. H. E. van den Worm and E. J. Snijder (2012). "The SARS-coronavirus nsp7+nsp8 complex is a unique multimeric RNA polymerase capable of both de novo initiation and primer extension." Nucleic Acids Research **40**(4): 1737-1747.

Vennema, H., G. J. Godeke, J. W. A. Rossen, W. F. Voorhout, M. C. Horzinek, D. J. E. Opstelten and P. J. M. Rottier (1996). "Nucleocapsid-independent assembly of coronavirus-like particles by co-expression of viral envelope protein genes." Embo Journal **15**(8): 2020-2028.

Wakula, P., M. Beullens, H. Ceulemans, W. Stalmans and M. Bollen (2003). "Degeneracy and function of the ubiquitous RVXF motif that mediates binding to protein phosphatase-1." Journal of Biological Chemistry **278**(21): 18817-18823.

Walsh, D., M. B. Mathews and I. Mohr (2013). "Tinkering with Translation: Protein Synthesis in Virus-Infected Cells." Cold Spring Harbor Perspectives in Biology **5**(1).

Wang, X., Y. Liao, P. L. Yap, K. J. Png, J. P. Tam and D. X. Liu (2009). "Inhibition of protein kinase R activation and upregulation of GADD34 expression play a synergistic role in facilitating coronavirus replication by maintaining de novo protein synthesis in virus-infected cells." J Virol **83**(23): 12462-12472.

Wang, Y., H. Shi, P. Rigolet, N. Wu, L. Zhu, X. G. Xi, A. Vabret, X. Wang and T. Wang (2010). "Nsp1 proteins of group I and SARS coronaviruses share structural and functional similarities." Infect Genet Evol **10**(7): 919-924.

Wei, C. W., C. F. Ni, T. Song, Y. Liu, X. L. Yang, Z. R. Zheng, Y. X. Jia, Y. A. Yuan, K. Guan, Y. Xu, X. Z. Cheng, Y. H. Zhang, X. A. Yang, Y. L. Wang, C. Y. Wen, Q. Wu, W. Shi and H. Zhong (2010). "The Hepatitis B Virus X Protein Disrupts Innate Immunity by Downregulating Mitochondrial Antiviral Signaling Protein." Journal of Immunology **185**(2): 1158-1168.

White, J. P., A. M. Cardenas, W. E. Marissen and R. E. Lloyd (2007). "Inhibition of cytoplasmic mRNA stress granule formation by a viral proteinase." Cell Host & Microbe **2**(5): 295-305.

Wilson, L., P. Gage and G. Ewart (2006). "Hexamethylene amiloride blocks E protein ion channels and inhibits coronavirus replication." Virology **353**(2): 294-306.

Wilson, L., C. McKinlay, P. Gage and G. Ewart (2004). "SARS coronavirus E protein forms cation-selective ion channels." Virology **330**(1): 322-331.

Winter, C., C. Schwegmann-Wessels, D. Cavanagh, U. Neumann and G. Herrler (2006). "Sialic acid is a receptor determinant for infection of cells by avian Infectious bronchitis virus." Journal of General Virology **87**: 1209-1216.

Woo, P. C. Y., S. K. P. Lau, C. S. F. Lam, C. C. Y. Lau, A. K. L. Tsang, J. H. N. Lau, R. Bai, J. L. L. Teng, C. C. C. Tsang, M. Wang, B. J. Zheng, K. H. Chan and K. Y. Yuen (2012). "Discovery of Seven Novel Mammalian and Avian Coronaviruses in the Genus Deltacoronavirus Supports Bat Coronaviruses as the Gene Source of Alphacoronavirus and Betacoronavirus and Avian Coronaviruses as the Gene Source of Gammacoronavirus and Deltacoronavirus." Journal of Virology **86**(7): 3995-4008.

Wu, J. and Z. J. Chen (2014). "Innate immune sensing and signaling of cytosolic nucleic acids." Annu Rev Immunol **32**: 461-488.

Wurm, T., H. Y. Chen, T. Hodgson, P. Britton, G. Brooks and J. A. Hiscox (2001). "Localization to the nucleolus is a common feature of coronavirus nucleoproteins, and the protein may disrupt host cell division." Journal of Virology **75**(19): 9345-9356.

Yamada, Y. and D. X. Liu (2009). "Proteolytic Activation of the Spike Protein at a Novel RRRR/S Motif Is Implicated in Furin-Dependent Entry, Syncytium Formation, and Infectivity of Coronavirus Infectious Bronchitis Virus in Cultured Cells." Journal of Virology **83**(17): 8744-8758.

Yang, W. H., J. H. Yu, T. Gulick, K. D. Bloch and D. B. Bloch (2006). "RNA-associated protein 55 (RAP55) localizes to mRNA processing bodies and stress granules." RNA **12**(4): 547-554.

Yang, Y., F. Ye, N. Zhu, W. L. Wang, Y. Deng, Z. D. Zhao and W. J. Tan (2015). "Middle East respiratory syndrome coronavirus ORF4b protein inhibits type I interferon production through both cytoplasmic and nuclear targets." Scientific Reports **5**.

Yang, Y., L. Zhang, H. Y. Geng, Y. Deng, B. Y. Huang, Y. Guo, Z. D. Zhao and W. J. Tan (2013). "The structural and accessory proteins M, ORF 4a, ORF 4b, and ORF 5 of Middle East respiratory syndrome coronavirus (MERS-CoV) are potent interferon antagonists." Protein & Cell **4**(12): 951-961.

Yasumura, Y. K., Y. (1963). "Studies on SV40 in tissue culture: preliminary step for cancer reserach in vitro (in Japanese) " Nihon Rinsho **21**: 1201–1215.

Youn, S., E. W. Collisson and C. E. Machamer (2005). "Contribution of trafficking signals in the cytoplasmic tail of the infectious bronchitis virus spike protein to virus infection." Journal of Virology **79**(21): 13209-13217.

Yount, B., R. S. Roberts, A. C. Sims, D. Deming, M. B. Frieman, J. Sparks, M. R. Denison, N. Davis and R. S. Baric (2005). "Severe acute respiratory syndrome coronavirus group-specific open reading frames encode nonessential functions for replication in cell cultures and mice." J Virol **79**(23): 14909-14922.

Yu, G. Y., G. B. He, C. Y. Li, M. Tang, S. Grivennikov, W. T. Tsai, M. S. Wu, C. W. Hsu, Y. Tsai, L. H. C. Wang and M. Karin (2012). "Hepatic Expression of HCV RNA-Dependent RNA Polymerase Triggers Innate Immune Signaling and Cytokine Production." Molecular Cell **48**(2): 313-321.

Yu, I. M., M. L. Oldham, J. Q. Zhang and J. Chen (2006). "Crystal structure of the severe acute respiratory syndrome (SARS) coronavirus nucleocapsid protein dimerization domain reveals evolutionary linkage between Corona- and Arteriviridae." Journal of Biological Chemistry **281**(25): 17134-17139.

Yu, Y. X. and G. S. Hayward (2010). "The Ubiquitin E3 Ligase RAUL Negatively Regulates Type I Interferon through Ubiquitination of the Transcription Factors IRF7 and IRF3." Immunity **33**(6): 863-877.

Zamarin, D., A. Garcia-Sastre, X. Xiao, R. Wang and P. Palese (2005). "Influenza virus PB1-F2 protein induces cell death through mitochondrial ANT3 and VDAC1." PLoS Pathog **1**(1): e4.

Zhang, F. Q., A. Moon, K. Childs, S. Goodbourn and L. K. Dixon (2010). "The African Swine Fever Virus DP71L Protein Recruits the Protein Phosphatase 1 Catalytic Subunit To Dephosphorylate eIF2 alpha and Inhibits CHOP Induction but Is Dispensable for These Activities during Virus Infection." Journal of Virology **84**(20): 10681-10689.

Zhang, L. K., Q. L. Xin, S. L. Zhu, W. W. Wan, W. Wang and G. F. Xiao (2016). "Activation of the RLR/MAVS Signaling Pathway by the L Protein of Mopeia Virus." Journal of Virology **90**(22): 10259-10270.

Zhang, R. H., K. Wang, W. Lv, W. J. Yu, S. Q. Xie, K. Xu, W. Schwarz, S. D. Xiong and B. Sun (2014). "The ORF4a protein of human coronavirus 229E functions as a viroporin that regulates viral production." Biochimica Et Biophysica Acta-Biomembranes **1838**(4): 1088-1095.

Zhao, J., A. Falcon, H. Zhou, J. Netland, L. Enjuanes, P. P. Brena and S. Perlman (2009). "Severe Acute Respiratory Syndrome Coronavirus Protein 6 Is Required for Optimal Replication." Journal of Virology **83**(5): 2368-2373.

Zhao, L., B. K. Jha, A. Wu, R. Elliott, J. Ziebuhr, A. E. Gorbalenya, R. H. Silverman and S. R. Weiss (2012). "Antagonism of the Interferon-Induced OAS-RNase L Pathway by Murine Coronavirus ns2 Protein Is Required for Virus Replication and Liver Pathology." Cell Host & Microbe **11**(6): 607-616.

Zhao, Y. Y., X. F. Sun, X. L. Nie, L. W. Sun, T. S. Tang, D. H. Chen and Q. M. Sun (2012). "COX5B Regulates MAVS-mediated Antiviral Signaling through Interaction with ATG5 and Repressing ROS Production." Plos Pathogens **8**(12).

Zheng, J. Y., X. M. Yang, J. M. Harrell, S. Ryzhikov, E. H. Shim, K. Lykke-Andersen, N. Wei, H. Sun, R. Kobayashi and H. Zhang (2002). "CAND1 binds to unneddylated CUL1 and regulates the formation of SCF ubiquitin E3 ligase complex." Molecular Cell **10**(6): 1519-1526.

Zhong, B., Y. Zhang, B. Tan, T. T. Liu, Y. Y. Wang and H. B. Shu (2010). "The E3 Ubiquitin Ligase RNF5 Targets Virus-Induced Signaling Adaptor for Ubiquitination and Degradation." Journal of Immunology **184**(11): 6249-6255.

Zhong, Y., Y. W. Tan and D. X. Liu (2012). "Recent progress in studies of arterivirus- and coronavirus-host interactions." Viruses **4**(6): 980-1010.

Zhong, Y. X., Y. Liao, S. G. Fang, J. P. Tam and D. X. Liu (2012). "Up-Regulation of Mcl-1 and Bak by Coronavirus Infection of Human, Avian and Animal Cells Modulates Apoptosis and Viral Replication." Plos One **7**(1).

Zhou, B., J. L. Liu, Q. Wang, X. Liu, X. R. Li, P. Li, Q. J. Ma and C. Cao (2008). "The nucleocapsid protein of severe acute respiratory syndrome coronavirus inhibits cell cytokinesis and proliferation by interacting with translation elongation factor 1 alpha." Journal of Virology **82**(14): 6962-6971.

Zhou, M. and E. W. Collisson (2000). "The amino and carboxyl domains of the infectious bronchitis virus nucleocapsid protein interact with 3' genomic RNA." Virus Res **67**(1): 31-39.

Zhou, M. L., A. K. Williams, S. I. Chung, L. Wang and E. W. Collisson (1996). "Infectious bronchitis virus nucleocapsid protein binds RNA sequences in the 3' terminus of the genome." Virology **217**(1): 191-199.

Ziebuhr, J., E. J. Snijder and A. E. Gorbalenya (2000). "Virus-encoded proteinases and proteolytic processing in the Nidovirales." J Gen Virol **81**(Pt 4): 853-879.

Ziebuhr, J., V. Thiel and A. E. Gorbalenya (2001). "The autocatalytic release of a putative RNA virus transcription factor from its polyprotein precursor involves two paralogous papain-like proteases that cleave the same peptide bond." J Biol Chem **276**(35): 33220-33232.

Zou, J., M. X. Chang, P. Nie and C. J. Secombes (2009). "Origin and evolution of the RIG-I like RNA helicase gene family." Bmc Evolutionary Biology **9**.

Zuniga, S., I. Sola, S. Alonso and L. Enjuanes (2004). "Sequence motifs involved in the regulation of discontinuous coronavirus subgenomic RNA synthesis." Journal of Virology **78**(2): 980-994.